Application of the Functional Renormalization Group to Bose systems with broken symmetry

Dissertation
zur Erlangung des Doktorgrades
der Naturwissenschaften

vorgelegt beim Fachbereich FB 13 Physik
der Johann Wolfgang Goethe-Universität
in Frankfurt am Main

von
Andreas Sinner
aus Kuibyschew

Frankfurt (2009)

(D 30)

vom Fachbereich FB 13 Physik der

Johann Wolfgang Goethe-Universität als Dissertation angenommen.

Dekan:	Prof. Dr. Dirk-Hermann Rischke
Gutachter:	Prof. Dr. Peter Kopietz Prof. Dr. Walter Hoffstetter
Datum der Disputation:	6. Juli 2009

Abstract

The physics of interacting bosons in the phase with broken symmetry is determined by the presence of the condensate and is very different from the physics in the symmetric phase. The Functional Renormalization Group (FRG) represents a powerful investigation method which allows the description of symmetry breaking with high efficiency. In the present thesis we apply FRG for studying the physics of two different models in the broken symmetry phase.

In the first part of this thesis we consider the classical $O(1)-$model close to the critical point of the second order phase transition. Employing a truncation scheme based on the relevance of coupling parameters we study the behavior of the RG-flow which is shown to be influenced by competition between two characteristic lengths of the system. We also calculate the momentum dependent self-energy and study its dependence on both length scales.

In the second part we apply the FRG-formalism to systems of interacting bosons in arbitrary spatial dimensions at zero temperature. We use a truncation scheme based on a new non-local potential approximation which satisfy both exact relations postulated by Hugenholtz and Pines, and Nepomnyashchy and Nepomnyashchy. We study the RG-flow of the model, discuss different scaling regimes, calculate the single-particle spectral density function of interacting bosons and extract both damping of quasi-particles and spectrum of elementary excitations from the latter.

Contents

Foreword

In the present thesis we apply the mathematical apparatus of the Functional Renormalization Group (FRG) to systems of interacting bosons. At critical temperature T_c such systems undergo a phase transition. Below T_c a new macroscopic fraction emerges in the system which is referred to as the Bose-Einstein condensate [1, 2]. The critical temperature of the phase transition depends on both external and internal quantities like pressure, strength of the magnetic and electric fields, density and mass of particles, etc. In non-interacting systems, the quantum coherence of single boson wave functions is responsible for the macroscopic population of the lowest allowed energetic state. In this case, the critical temperature is proportional to $\rho^{2/3}/m$ [3], where ρ denotes the density of bosons. Above the critical temperature quantum coherence is destroyed by thermal fluctuations and quantum effects do not play any important role anymore.

The emergence of the long-range order in interacting Bose systems is due to the interaction between particles [4]. Phenomenologically it is taken into account by introducing an order parameter representing a macroscopic quantity which is non-zero below and vanishes at and above the critical temperature. Therefore, the system is said to be in the ordered phase below the critical temperature. Since the emergence of the long-range order is always related to the reduction of the symmetry of the corresponding mathematical model [5] one often speaks about the symmetry broken phase in order to describe the phase below the critical temperature. One distinguishes between the first and second order phase transitions due to the behavior of the system at the critical temperature. In the case of the second order phase transition, the order parameter vanishes continuously as the system approaches the critical point from below. In the vicinity of the critical point several observable quantities diverge power-law-like. The powers of these divergences are called critical exponents. They are the same for systems sharing the same symmetries, even though these systems might be very different from each other. Different mathematical models with the same critical exponents are said to belong to the same universality class.

The calculation of the critical exponents used to be an agenda for the physicists for several decades. For a long time, the phenomenological Landau theory of the second-order phase transitions [5, 6] (and mean-field theories in a broader sense) was believed to provide a correct prediction for the critical exponents and thus to describe phase transitions correctly. However, the comparison with the few known exact solutions (e. g. for the Ising model in two spatial dimensions [7]) clearly demonstrated that the mean-field predictions for the critical exponents is not always correct. In general, the mean-field exponents are always false in and below some specific spatial dimension D_c which is called the upper critical dimension of the corresponding mathematical model [8], and correct in dimensions above D_c. The reason for the failure of the mean-field theory is

that it does not take fluctuations into account which become important in the vicinity of the critical point. The length scale at which this happens is determined by the Ginzburg-criterion and is referred to as the Ginzburg-scale [8]. An attempt to improve the accuracy by calculating perturbative corrections to the mean-field Hamiltonian usually does not work well, since in this case fluctuations are taken into account at all length scales simultaneously, i. e. at irrelevant ones as well. Perturbation theory itself is often plagued by non-physical divergences. Therefore, there is a necessity to go a completely different way in order to describe phase transitions correctly. This way was explored by Kenneth Wilson in the form of his Renormalization Group (RG)-approach [9, 10]. The main idea behind the Wilsonian RG-approach consists of the elimination of fluctuations scale by scale from the original microscopic model. The effective Hamiltonian which emerges at the end of this procedure yields astonishingly accurate results for the critical exponents for a number of models. Reformulated in terms of generating functionals [11, 12, 13], the Functional Renormalization Group represents a powerful and promising method, whose applicability reaches far beyond the determination of the critical exponents.

It is of significant interest to apply the Functional Renormalization Group to systems with broken symmetry. On the one hand, this is because it completes our understanding of the physics of continuous phase transitions and provides thus a unified picture of the critical phenomena. On the other hand, this is because it offers a way to look inside the ordered phase itself in order to study its physics on a higher accuracy level than that of the mean-field or perturbation theory. An appropriate reformulation of the FRG for dealing with symmetry breaking has only very recently been undertaken [14], and it still lacks on concrete applications of the formalism. Below we apply the FRG-formalism for studying two well-known models. The first one represents the classical scalar field model close to criticality. The second model describes interacting bosons at zero temperature. In both cases we do not want to restrict our consideration to the thermodynamics only. Instead we want to study the physics at finite momenta. Structurally this thesis consists of the following parts:

1. Chapter 1 deals with the formal foundations of the Functional Renormalization Group. We introduce the concept of generating functionals and derive exact RG-flow equations for these. Reexpressed in terms of power series in field variables, the RG-flow equation for the effective action functional gives rise to an infinite hierarchy of the flow equations for each one-particle irreducible vertex function. In the symmetry broken phase this hierarchy should be augmented by an additional equation which takes the RG-flow of the order parameter into account. A brief overview over the basics of the Wilsonian Renormalization Group completes this introduction and provides us with the vocabulary.

2. In chapter 2 the FRG-formalism is applied to the simple one-component scalar field model close to criticality, which is often referred to as the classical ϕ^4-model and belongs to the Ising universality class. As the discrete Z_2-symmetry is broken, the finite magnetization emerges. We derive RG-flow equations for the order parameter and for the irreducible self-energy as well. The RG-flow equation for the interaction

is extracted from the latter in the limit of zero momenta. Hence, a closed system of integro-differential equations emerges and is solved numerically. We discuss several regularization schemes and demonstrate the insufficiency of the so-called regularization scheme with the sharp cutoff-regulator. In order to describe the nearly-critical behavior of the model we have to carefully fine-tune starting values of each flowing quantity. The flow then stays sufficiently long close to the critical trajectory. The nearly-critical RG-flow is influenced by two distinct length-scales: an intrinsic interaction dependent critical Ginzburg-length, and a temperature dependent correlation length. Expressions for both scales are obtained from the flow equations. Introducing the concept of the FRG-enhanced perturbation theory we calculate the physical momentum dependent self-energy close to the critical point. The behavior of the determined self-energy is influenced by the both length scales. This fact reveals itself in the emergence of an intermediate regime at small momenta, where the nearly-critical behavior of the self-energy crosses over into the non-critical one.

3. In chapter 3 the FRG-formalism is applied to systems of interacting bosons at zero temperature. According to the Goldstone-theorem [15], the breaking of the continuous $U(1)-$symmetry leads to the emergence of a gapless spectrum of elementary excitations which has a linear phononic character at small momenta. The behavior of interacting bosons in thermodynamic limit is determined by two exact relations. On the one hand, there is the Hugenholtz-Pines equality [16] (HPE) which connects normal and anomalous self-energies at zero momentum with the chemical potential and postulates thus the absence of the energetic gap in the elementary excitation spectrum. On the other hand, there is the Nepomnyashchy-Nepomnyashchy equality [17] (NNE) which states the vanishing of the anomalous self-energy in the long wave-length limit. While the HPE follows already from the leading order in perturbative expansion, NNE cannot be reproduced by perturbation theory to any finite order. The perturbation theory itself turns out to be infrared-divergent. By resumation of the perturbative series by means of the Functional Renormalization Group, both exact relations can be simultaneously fulfilled. We use a truncation scheme of the effective action based on a new non-local potential approximation. We derive RG-flow equations for relevant coupling parameters and solve them numerically. Our results do not suffer from any infrared divergences. The RG-flow of the effective action is governed by a Ginzburg-like length scale which can be extracted from the flow of the interaction. We recover correctly the infrared asymptotic behavior of both self-energies, as well as of normal and anomalous Green functions. Finally, we calculate the single-particle spectral density function of interacting bosons and extract from this the spectrum of elementary excitations and the damping of quasi-particles. At weak interactions our calculation reproduces the perturbation theory results. However, the real power of our approach consists in the possibility of a fully controlled description of the strong interacting regime.

4. In appendix A we present an alternative parameterization for the mathematical model of interacting bosons in the real field basis. Such a transformation is always possible because of the isomorphy between the $U(1)-$ and $O(2)-$symmetry groups. This choice has some aesthetic advantages comparing to the $U(1)-$invariant representation.

1 Functional Renormalization Group

In this chapter we develop the formal framework of the Functional Renormalization Group (FRG). We introduce the concept of generating functionals and show how they can be employed in order to derive the exact Renormalization Group (RG)-flow equation for the effective action. A brief outlook about the Wilsonian Renormalization Group approach gives a formal justification for this procedure. Being a rather complicated mathematical object, the exact RG-flow equation cannot be solved in general exactly. We discuss how this equation can be treated approximately by expanding generating functionals into power series of fields and appropriately truncating one-particle irreducible vertex functions. Finally we show how the formalism can be extended to systems in the broken symmetry phase. The representation of the FRG-formalism given here is heavily influenced by the lectures on the subject given by Professor Peter Kopietz at the Goethe-Universität Frankfurt during the summer semester 2006 [18, 19].

1.1 Generalized fields and sources

The way to treat condensed matter systems in the framework of the functional integral formalism has become standard in the last decades [20, 21, 22]. Within this framework, the grand canonical partition function of a many body system can be represented as a functional integral over some abstract space spanned by the fields $\bar{\boldsymbol{\phi}}$, $\boldsymbol{\phi}$ which are adjoint to each other, i. e.

$$Z = \int \mathcal{D}\{\bar{\boldsymbol{\phi}}, \boldsymbol{\phi}\}\; e^{-S[\bar{\boldsymbol{\phi}},\boldsymbol{\phi}]} = \int \mathcal{D}\boldsymbol{\Phi}\; e^{-S[\boldsymbol{\Phi}]}, \tag{1.1}$$

where $S[\bar{\boldsymbol{\phi}}, \boldsymbol{\phi}]$ is the Euclidean action of the system. In the second equality of equation (1.1) we collected both field components into a superfield vector $\boldsymbol{\Phi} = (\bar{\boldsymbol{\phi}}, \boldsymbol{\phi})^T$. The field $\boldsymbol{\phi}$ is supposed to be a multi-component quantum vector field which may contain vector bosonic ψ, fermionic c, scalar bosonic φ, etc. components

$$\boldsymbol{\phi}_K = (\psi_{1,K}, \dots c_{1,K}, \dots \varphi_{1,K}, \dots)^T = \sum_i \phi_{i,K} \hat{e}_i, \tag{1.2}$$

and, correspondingly, for the adjoint field

$$\bar{\boldsymbol{\phi}}_K = \sum_i \bar{\phi}_{i,K} \hat{e}_i. \tag{1.3}$$

The unit vectors of the basis $\{\hat{e}_i\}$ are associated with the distinct components of the fields $\boldsymbol{\phi}$. Each of them dwells on its unique subspace of the abstract quantum field space

which is orthogonal to all others. The multi-index

$$K = \{\boldsymbol{k}, i\omega_n, \sigma\} \tag{1.4}$$

contains the D-dimensional momentum vector $\boldsymbol{k}$ and Matsubara frequency ω_n, which in turn has the form [1]

$$\begin{aligned} \omega_n &= 2n\frac{\pi}{\beta}, \qquad n \in \mathbb{Z} \text{ for bosons,} \\ \omega_n &= (2n+1)\frac{\pi}{\beta}, \quad n \in \mathbb{Z} \text{ for fermions,} \end{aligned} \tag{1.5}$$

with the inverse temperature β. Finally, the index σ is related to the spin of the particle. We define the summation over the multi-index K by

$$\int\limits_K \equiv \frac{1}{\beta V} \sum_{\sigma,\omega_n,\boldsymbol{k}} \to \sum_\sigma \int \frac{d\omega}{2\pi} \int \frac{d^D k}{(2\pi)^D}, \tag{1.6}$$

where V denotes the D-dimensional volume of the system. In the second expression we took the continuous limit $\beta \to \infty, V \to \infty$. The integration measure in equation (1.1) is defined by

$$\mathcal{D}\{\boldsymbol{\Phi}\} = \mathcal{D}\{\bar{\boldsymbol{\phi}}, \boldsymbol{\phi}\} = \prod_{i,K} d\bar{\phi}_{i,K} d\phi_{i,K} = \prod_{i,\sigma,\boldsymbol{k},\omega_n} d\bar{\phi}_{i,\sigma,\boldsymbol{k},\omega_n} d\phi_{i,\sigma,\boldsymbol{k},\omega_n}. \tag{1.7}$$

The action $S[\boldsymbol{\Phi}]$

$$S[\boldsymbol{\Phi}] = S_0[\boldsymbol{\Phi}] + S_I[\boldsymbol{\Phi}] \tag{1.8}$$

consists of the non-interacting part $S_0[\boldsymbol{\Phi}]$ and some interacting part $S_I[\boldsymbol{\Phi}]$. The former part is quadratic in the superfields

$$S_0[\boldsymbol{\Phi}] = -\frac{1}{2}\boldsymbol{\Phi} \cdot \boldsymbol{G}_0^{-1} \cdot \boldsymbol{\Phi} = -\frac{1}{2} \int\limits_\alpha \int\limits_{\alpha'} \Phi_\alpha \left[G_0^{-1}\right]_{\alpha\alpha'} \Phi_{\alpha'}, \tag{1.9}$$

where the integration over α means summation over the discrete variables like spin or sort of particles and integration over the continuous ones. The inverse free propagator matrix $\boldsymbol{G}_0^{-1}$ is non-diagonal in the two-dimensional space of the superfields $\boldsymbol{\Phi}$:

$$\boldsymbol{G}_0^{-1} = \begin{pmatrix} 0 & \hat{\boldsymbol{G}}_0^{-1} \\ \mathbb{P} \cdot \hat{\boldsymbol{G}}_0^{-1} & 0 \end{pmatrix}. \tag{1.10}$$

Matrices of inverse free propagators $\hat{\boldsymbol{G}}_0^{-1}$ for entries of the fields $\boldsymbol{\phi}$ and $\bar{\boldsymbol{\phi}}$ are diagonal in both, quantum field and multi-index space

$$[\hat{G}_0^{-1}]_{ii';KK'} = \delta_{i,i'}\delta_{K,K'} G_{0,i}^{-1}(K), \tag{1.11}$$

[1] We use a natural unit system with $\hbar = k_B = 1$ throughout the manuscript.

where the Kronecker δ-symbol in the multi-index space is defined by

$$\begin{aligned}\delta_{K,K'} &= \beta V \delta_{\sigma,\sigma'}\delta_{\omega_n,\omega_{n'}}\delta_{\boldsymbol{k},\boldsymbol{k}'} \\ &\to (2\pi)^{D+1}\delta_{\sigma,\sigma'}\delta(\omega-\omega')\delta(\boldsymbol{k}-\boldsymbol{k}') \\ &= \delta(K-K'),\end{aligned} \tag{1.12}$$

and the arrow denotes taking the continuum limit. The diagonal matrix $\mathbb{P}$ with matrix elements $\zeta = +1$ for bosons and $\zeta = -1$ for fermions is introduced in order to account their different statistics. Defining the 2×2 matrix in the space of fields $\boldsymbol{\Phi}$

$$\boldsymbol{Z} = \begin{pmatrix} \mathbb{P} & 0 \\ 0 & \mathbb{P} \end{pmatrix}, \tag{1.13}$$

with the obvious property

$$\boldsymbol{Z}\cdot\boldsymbol{Z} = \mathbb{1}, \tag{1.14}$$

we find

$$[\boldsymbol{G}_0^{-1}]^T = \boldsymbol{Z}\cdot\boldsymbol{G}_0^{-1}. \tag{1.15}$$

In contrast, the interacting part $S_I[\boldsymbol{\Phi}]$ of the Euclidean action may contain terms with any number of fields which is compatible with the symmetry properties of the particular model.

We now define the supersource vector

$$\boldsymbol{J} = (\boldsymbol{j}, \bar{\boldsymbol{j}})^T, \tag{1.16}$$

and the scalar product between both vectors $\boldsymbol{\Phi}$ and $\boldsymbol{J}$:

$$\boldsymbol{J}\cdot\boldsymbol{\Phi} = \bar{\boldsymbol{j}}\cdot\boldsymbol{\phi} + \boldsymbol{j}\cdot\bar{\boldsymbol{\phi}} = \int\limits_\alpha J_\alpha \Phi_\alpha. \tag{1.17}$$

Here, the summation is performed over all relevant degrees of freedom. The following identity will be crucial for the formalism developed below

$$\frac{\delta}{\delta J_\alpha} e^{\boldsymbol{J}\cdot\boldsymbol{\Phi}}\bigg|_{\boldsymbol{J}=0} = \int\limits_{\alpha'} \frac{\delta J_{\alpha'}}{\delta J_\alpha}\Phi_{\alpha'} = \int\limits_{\alpha'} \delta_{\alpha,\alpha'}\Phi_{\alpha'} = \Phi_\alpha. \tag{1.18}$$

Finally we define the tensor product of two vectors

$$\boldsymbol{a} = \sum_\alpha a_\alpha \hat{e}_\alpha \tag{1.19}$$

and

$$\boldsymbol{b} = \sum_\alpha b_\alpha \hat{e}_\alpha \tag{1.20}$$

as a matrix

$$\boldsymbol{ab} = \boldsymbol{a}\otimes\boldsymbol{b} = \sum_{\alpha,\alpha'} a_\alpha b_{\alpha'}\hat{e}_\alpha\otimes\hat{e}_{\alpha'} = \sum_{\alpha,\alpha'}[ab]_{\alpha\alpha'}. \tag{1.21}$$

1.2 Generating functionals

The n-point Green function $G^{(n)}_{\alpha_1\ldots\alpha_n}$ is defined as the time-ordered average over the product of n fields $\mathbf{\Phi}$, i. e.

$$\begin{aligned} G^{(n)}_{\alpha_1\ldots\alpha_n} &= \langle \Phi_{\alpha_1}\ldots\Phi_{\alpha_n}\rangle && \text{(1.22a)}\\ &= \frac{1}{Z_0}\int \mathcal{D}\mathbf{\Phi}\ \Phi_{\alpha_1}\ldots\Phi_{\alpha_n} e^{-S[\mathbf{\Phi}]} && \text{(1.22b)}\\ &= \frac{\delta^{(n)}}{\delta J_{\alpha_n}\cdots\delta J_{\alpha_1}}\frac{1}{Z_0}\int \mathcal{D}\mathbf{\Phi}\ e^{-S[\mathbf{\Phi}]+\boldsymbol{J}\cdot\mathbf{\Phi}}\Big|_{\boldsymbol{J}=0} && \text{(1.22c)}\\ &= \frac{\delta^{(n)}\mathcal{G}[\boldsymbol{J}]}{\delta J_{\alpha_n}\cdots\delta J_{\alpha_1}}\Big|_{\boldsymbol{J}=0}, && \text{(1.22d)} \end{aligned}$$

where

$$Z_0 = \int \mathcal{D}\mathbf{\Phi}\ e^{-S_0[\mathbf{\Phi}]} \tag{1.23}$$

denotes the partition function of the non-interacting system. In order to bring line (1.22b) to the form (1.22c) we used identity (1.18). Finally, in line (1.22d) we introduced the quantity

$$\mathcal{G}[\boldsymbol{J}] = \frac{1}{Z_0}\int \mathcal{D}\mathbf{\Phi}\ e^{-S[\mathbf{\Phi}]+\boldsymbol{J}\cdot\mathbf{\Phi}}, \tag{1.24}$$

which is referred to as the *generating functional of (disconnected) Green functions*.

Usually it is more convenient to work with the *generating functional of connected Green functions* $\mathcal{G}_c[\boldsymbol{J}]$ which relates to the Helmholtz free energy in the very same manner as $\mathcal{G}[\boldsymbol{J}]$ relates to the grand canonical partition function. This means that both functionals may be connected with each other through the following relation:

$$\mathcal{G}[\boldsymbol{J}] = e^{\mathcal{G}_c[\boldsymbol{J}]}. \tag{1.25}$$

A n-point connected Green function can be generated from $\mathcal{G}_c[\boldsymbol{J}]$ by taking functional derivatives with respect to the sources $\boldsymbol{J}$ at the point $\boldsymbol{J}=0$

$$G^{(n)}_{c;\alpha_1\ldots\alpha_n} = \frac{\delta^{(n)}\mathcal{G}_c[\boldsymbol{J}]}{\delta J_{\alpha_n}\cdots\delta J_{\alpha_1}}\Big|_{\boldsymbol{J}=0}. \tag{1.26}$$

In the special case $n=2$ we obtain the full propagator

$$\boldsymbol{G}_{\alpha,\alpha'} = -G^{(2)}_{c;\alpha,\alpha'}. \tag{1.27}$$

Assuming the existence of a $G^{(n)}_c$ for each positive integer n, a unique expansion of the functional $\mathcal{G}_c[\boldsymbol{J}]$ in powers of sources $\boldsymbol{J}$ should exist

$$\mathcal{G}_c[\boldsymbol{J}] = \mathcal{G}_c[0] + \sum_{n=1}^{\infty}\frac{1}{n!}\int_{\alpha_1}\cdots\int_{\alpha_n} G^{(n)}_{c;\alpha_1,\ldots,\alpha_n} J_{\alpha_1}\cdots J_{\alpha_n}, \tag{1.28}$$

where $\mathcal{G}_c[0]$ denotes the Helmholtz free energy. In practice one is more interested in working with the field-dependent quantities, rather than with the source-dependent ones. In order to restore the field-dependence we introduce a vector of averaged fields

$$\tilde{\boldsymbol{\Phi}}[\boldsymbol{J}] \equiv \langle \boldsymbol{\Phi} \rangle = \frac{\delta}{\delta \boldsymbol{J}} \mathcal{G}_c[\boldsymbol{J}], \tag{1.29}$$

and map $\mathcal{G}_c[\boldsymbol{J}]$ onto a new field-dependent functional $\mathcal{L}[\tilde{\boldsymbol{\Phi}}]$ by means of a Legendre transformation

$$\mathcal{L}[\tilde{\boldsymbol{\Phi}}[\boldsymbol{J}]] = \boldsymbol{J} \cdot \tilde{\boldsymbol{\Phi}}[\boldsymbol{J}] - \mathcal{G}_c[\boldsymbol{J}]. \tag{1.30}$$

Here, the functional $\mathcal{L}[\tilde{\boldsymbol{\Phi}}]$ is referred to as the *effective action*. It is supposed to be expandable in an infinite series in powers of averaged fields $\tilde{\boldsymbol{\Phi}}$

$$\mathcal{L}[\tilde{\boldsymbol{\Phi}}] = \mathcal{L}[0] + \sum_{n=1}^{\infty} \frac{1}{n!} \int_{\alpha_1} \cdots \int_{\alpha_n} \Gamma^{(n)}_{\alpha_1,\ldots,\alpha_n} \tilde{\Phi}_{\alpha_1} \cdots \tilde{\Phi}_{\alpha_n}. \tag{1.31}$$

Note that coefficients $\Gamma^{(n)}_{\alpha_1,\ldots,\alpha_n}$ of this expansion, which for $n > 2$ are referred to as the one-particle irreducible vertex functions, are supposed to be analytic in continuous variables entering α_i.

Taking the functional derivative with respect to the field $\tilde{\boldsymbol{\Phi}}$, using the basis change identity

$$\frac{\delta}{\delta \tilde{\boldsymbol{\Phi}}} = \left[\frac{\delta}{\delta \tilde{\boldsymbol{\Phi}}} \otimes \boldsymbol{J} \right] \cdot \boldsymbol{Z} \cdot \frac{\delta}{\delta \boldsymbol{J}} = \frac{\delta \boldsymbol{J}}{\delta \tilde{\boldsymbol{\Phi}}} \cdot \boldsymbol{Z} \cdot \frac{\delta}{\delta \boldsymbol{J}}, \tag{1.32}$$

and equation (1.29) we obtain

$$\frac{\delta}{\delta \tilde{\boldsymbol{\Phi}}} \mathcal{L}[\tilde{\boldsymbol{\Phi}}] = \boldsymbol{Z} \cdot \boldsymbol{J}. \tag{1.33}$$

It is often useful to introduce a further field-dependent functional $\Gamma[\tilde{\boldsymbol{\Phi}}]$ which is known as the *generating functional of one-particle irreducible vertex functions*. It relates to the functional $\mathcal{L}[\tilde{\boldsymbol{\Phi}}]$ via

$$\Gamma[\tilde{\boldsymbol{\Phi}}] = \mathcal{L}[\tilde{\boldsymbol{\Phi}}] - S_0[\tilde{\boldsymbol{\Phi}}] = \mathcal{L}[\tilde{\boldsymbol{\Phi}}] + \frac{1}{2} \tilde{\boldsymbol{\Phi}} \cdot \boldsymbol{G}_0^{-1} \cdot \tilde{\boldsymbol{\Phi}}. \tag{1.34}$$

Using equations (1.32), (1.29) and (1.33) we obtain an important relation

$$\mathbb{1} = \frac{\delta \tilde{\boldsymbol{\Phi}}}{\delta \tilde{\boldsymbol{\Phi}}} = \frac{\delta \boldsymbol{J}}{\delta \tilde{\boldsymbol{\Phi}}} \cdot \boldsymbol{Z} \cdot \frac{\delta \tilde{\boldsymbol{\Phi}}}{\delta \boldsymbol{J}} = \frac{\delta^{(2)} \mathcal{L}}{\delta \tilde{\boldsymbol{\Phi}} \delta \tilde{\boldsymbol{\Phi}}} \cdot \boldsymbol{Z} \cdot \frac{\delta^{(2)} \mathcal{G}_c}{\delta \boldsymbol{J} \delta \boldsymbol{J}}, \tag{1.35}$$

which can also be written in the following form

$$\frac{\delta^{(2)} \mathcal{G}_c}{\delta \boldsymbol{J} \delta \boldsymbol{J}} = \boldsymbol{Z} \cdot \left(\frac{\delta^{(2)} \mathcal{L}}{\delta \tilde{\boldsymbol{\Phi}} \delta \tilde{\boldsymbol{\Phi}}} \right)^{-1}. \tag{1.36}$$

Equation (1.36) represents a functional master-equation for the so-called *tree expansion*, a procedure which establishes connections between one-particle irreducible vertex functions and connected Green functions. In order to perform the tree expansion one has to

take functional derivatives with respect to the fields on both sides of the master-equation by exploiting the basis change identity (1.32) and setting eventually fields and sources to zero. The general representation of the tree expansion can be found in standard text books (see for instance [20, 21]), and for this reason we will not give it at this point. We restrict our considerations to the first order term in this expansion because we shall need it below. Setting fields and sources in equation (1.36) to zero and using equation (1.34) we obtain

$$-\boldsymbol{G}^T = \left(\boldsymbol{\Sigma}^T - [\boldsymbol{G}_0^{-1}]^T\right)^{-1}, \tag{1.37}$$

which is nothing but the Dyson-equation. If no spontaneous symmetry breaking occurs, the matrix representation of the full inverse propagator $\boldsymbol{G}^{-1}$ has the same structure as the matrix of the non-interacting propagator given by equation (1.10), i. e.

$$\boldsymbol{G}^{-1} = \begin{pmatrix} 0 & \hat{\boldsymbol{G}}^{-1} \\ \mathbb{P}\cdot[\hat{\boldsymbol{G}}^{-1}]^T & 0 \end{pmatrix}. \tag{1.38a}$$

The same is also valid for the self-energy matrix

$$\boldsymbol{\Sigma} = \begin{pmatrix} 0 & \hat{\boldsymbol{\Sigma}} \\ \mathbb{P}\cdot\hat{\boldsymbol{\Sigma}}^T & 0 \end{pmatrix}. \tag{1.38b}$$

Here, the quantities $\hat{\boldsymbol{G}}^{-1}$ and $\hat{\boldsymbol{\Sigma}}$ represent diagonal matrices of the inverse full propagator and self-energy in the space of the averaged fields $\tilde{\boldsymbol{\phi}}$.

In order to simplify our analysis below it is convenient to introduce the functional field dependent matrix

$$\boldsymbol{U}^T = \frac{\delta^{(2)}\Gamma}{\delta\tilde{\boldsymbol{\Phi}}\delta\tilde{\boldsymbol{\Phi}}} - \left.\frac{\delta^{(2)}\Gamma}{\delta\tilde{\boldsymbol{\Phi}}\delta\tilde{\boldsymbol{\Phi}}}\right|_{\tilde{\boldsymbol{\Phi}}=0} = \frac{\delta^{(2)}\Gamma}{\delta\tilde{\boldsymbol{\Phi}}\delta\tilde{\boldsymbol{\Phi}}} - \boldsymbol{\Sigma}^T, \tag{1.39}$$

with the matrix elements

$$[\boldsymbol{U}]_{\alpha\alpha'} = \sum_{n=1}^{\infty}\frac{1}{n!}\int_{\alpha_1}\cdots\int_{\alpha_n}\left[\boldsymbol{\Gamma}^{(n+2)}_{\alpha_1\ldots\alpha_n}\right]^T_{\alpha\alpha'}\tilde{\Phi}_{\alpha_1}\cdots\tilde{\Phi}_{\alpha_n}. \tag{1.40}$$

Equation (1.36) can thus be rewritten as follows:

$$\begin{aligned}
&\frac{\delta^{(2)}\mathcal{G}_c}{\delta\boldsymbol{J}\delta\boldsymbol{J}} = \boldsymbol{Z}\cdot\left(\frac{\delta^{(2)}\Gamma}{\delta\tilde{\boldsymbol{\Phi}}\delta\tilde{\boldsymbol{\Phi}}} - [\boldsymbol{G}_0^{-1}]^T\right)^{-1} = \boldsymbol{Z}\cdot\left(\boldsymbol{U}^T + \boldsymbol{\Sigma}^T - [\boldsymbol{G}_0^{-1}]^T\right)^{-1} \\
= \;& -\boldsymbol{Z}\cdot\left([\boldsymbol{G}^T]^{-1} - \boldsymbol{U}^T\right)^{-1} = -\boldsymbol{Z}\cdot\boldsymbol{G}^T\cdot\left(\mathbb{1} - \boldsymbol{U}^T\cdot\boldsymbol{G}^T\right)^{-1} \\
= \;& -\boldsymbol{Z}\cdot\boldsymbol{G}^T\cdot\left(\mathbb{1} + \boldsymbol{U}^T\cdot\boldsymbol{G}^T + \boldsymbol{U}^T\cdot\boldsymbol{G}^T\cdot\boldsymbol{U}^T\cdot\boldsymbol{G}^T + \cdots\right) \\
= \;& -\sum_{l=0}^{\infty}\boldsymbol{Z}\cdot\boldsymbol{G}^T\cdot\left(\boldsymbol{U}^T\cdot\boldsymbol{G}^T\right)^l,
\end{aligned} \tag{1.41}$$

where equation (1.37) has been used.

1.3 Basics of the Wilsonian RG

Nowadays, there is a large variety of excellent textbooks and reviews which introduce to the basics of the Wilsonian Renormalization Group. We do not pretend to give here an exhaustive overview of the Wilsonian RG and refer the reader to the literature. Historically, the Wilsonian RG has been developed alongside with the theory of phase transitions. Therefore, most of the books, especially those dating back to the early days of RG, treat it from the point of view of statistical physics. Besides the widely cited original works by Wilson [9, 10, 23] and by Wilson in collaboration with Fisher and Kogut [24, 25], an excellent overview was written by Ma in [26] and extended later to a book [27]. Classics on the subject are regarded books by Goldenfeld [28], Cardy [29], and Amit [30]. A nice brief introduction to the basics of the Renormalization Group theory can by found by Chaikin and Lubensky in [31]. Binney *et al.* offer in [32] their view on the Renormalization Group with the strong emphasis on the numerical methods. The representation of the Wilsonian RG given here is influenced by that given by P. Kopietz in his lectures [18, 19].

We want to summarize in a few words the main idea about the Wilsonian Renormalization Group transformation. As we have seen above, the partition function of a physical system can be written in the form of a functional integral

$$Z = \int \mathcal{D}\mathbf{\Phi}\ e^{-S[\mathbf{\Phi},\{u\}]}, \tag{1.42}$$

where the Euclidean action of the system $S[\mathbf{\Phi},\{u\}]$ is now supposed to be not only a functional of the superfields $\mathbf{\Phi}$, but also of a (usually finite) set of coupling parameters $\{u\}$. The domain of definition of fields $\mathbf{\Phi}$ covers the entire $D+1-$dimensional frequency-momentum space. Since we are interested in the physics which occurs below some specific momentum and energy Λ we may notice that the fast field modes with $|\boldsymbol{\kappa}| > \Lambda$, where

$$\boldsymbol{\kappa} = (\boldsymbol{k}, i\omega_n) \tag{1.43}$$

denote momenta and frequencies entering the multi-index K defined in equation (1.4), do not contribute significantly and thus can be integrated out. In order to perform such an integration we have to split the superfield $\mathbf{\Phi}$ into the slow and fast modes

$$\mathbf{\Phi} = \Theta(|\boldsymbol{\kappa}| \leqslant \Lambda)\mathbf{\Phi}_< + \Theta(\Lambda < |\boldsymbol{\kappa}| < \Lambda_0)\mathbf{\Phi}_>, \tag{1.44}$$

where $\Lambda_0 \gg \Lambda$ is an appropriate ultraviolet cutoff regulator which is introduced to avoid the appearance of ultraviolet divergences. As a result we can express the action in terms of the slow fields only:

$$\begin{aligned} Z &= \int \mathcal{D}\mathbf{\Phi}\ e^{-S[\mathbf{\Phi},\{u\}]} \\ &= \int \mathcal{D}\{\mathbf{\Phi}_<, \mathbf{\Phi}_>\}\ e^{-S[\mathbf{\Phi}_<,\mathbf{\Phi}_>,\{u\}]} \\ &= \int \mathcal{D}\mathbf{\Phi}_<\ e^{-S_{\text{eff}}[\mathbf{\Phi}_<,\{u'\},\boldsymbol{b}]}, \end{aligned}$$

where we introduced effective low-energy action $S_{\text{eff}}[\cdots]$ defined by

$$e^{-S_{\text{eff}}[\boldsymbol{\Phi}_<,\{u'\},\boldsymbol{b}]} = \int \mathcal{D}\boldsymbol{\Phi}_> \, e^{-S[\boldsymbol{\Phi}_<,\boldsymbol{\Phi}_>,\{u\}]}. \tag{1.45}$$

In order to guarantee the invariance of the form of the new effective action, the momentum vector $|\boldsymbol{\kappa}| < \Lambda$ should be rescaled by means of some appropriate vector $\boldsymbol{b}$, i. e.

$$\boldsymbol{\kappa} \;\rightarrow\; \boldsymbol{\kappa}\cdot\boldsymbol{b} \;=\; (\boldsymbol{k}b, i\omega_n b^z), \tag{1.46}$$

where z denotes the so-called *dynamical exponent*. In the same manner the slow field modes should also be rescaled

$$\boldsymbol{\Phi}_<(\boldsymbol{k}, i\omega_n) \rightarrow b^{-\frac{D+z-2}{2}} \boldsymbol{\Phi}_<(\boldsymbol{k}b, i\omega_n b^z), \tag{1.47}$$

as well as all entries of the new parameter set $\{u'\}$. There are only very few examples known, where the integration on the right-hand side of equation (1.45) could be carried out exactly [26]. In most physical relevant cases one is reliant on approximations.

The effective low-energy action $S_{\text{eff}}[\cdots]$ depends on the coupling parameter set $\{u'\}$ which in general differs from the initial set $\{u\}$. In order to realize this fact we have to expand the right-hand side of equation (1.45) into a power series of the slow fields $\boldsymbol{\Phi}_<$. Since such a series contains terms of all orders in $\boldsymbol{\Phi}_<$, infinitely many new coupling parameters are generated which makes the parameter set $\{u'\}$ different from the initial set $\{u\}$. Formally, we can think of the mapping of the initial parameter set $\{u\}$ onto $\{u'\}$ which can be written in the form of a non-linear equation

$$\{u'\} = \mathcal{R}_{\boldsymbol{b}}\left[\{u\}\right], \tag{1.48}$$

where $\mathcal{R}_{\boldsymbol{b}}$ denotes the mapping transformation. After repeating the whole procedure once again, a new parameter set $\{u''\}$ is generated which relates to the old ones through

$$\{u''\} = \mathcal{R}_{\boldsymbol{s}}\left[\{u'\}\right] = \mathcal{R}_{\boldsymbol{s}}\left[\mathcal{R}_{\boldsymbol{b}}\left[\{u\}\right]\right] = \mathcal{R}_{\boldsymbol{s}\circ\boldsymbol{b}}\left[\{u\}\right]. \tag{1.49}$$

Equation (1.49) represents a semi-group equation which gives the name to the whole procedure. By integrating out fast modes successively over infinitesimally thin momentum shells $\Lambda - d\Lambda < |\boldsymbol{\kappa}| < \Lambda \leqslant \Lambda_0$, the rescaling parameter b changes infinitesimally, too, which leads to the infinitesimal change in the parameter set $\{u\}$. It is then possible to rewrite equation (1.49) in the form of the first-order differential equation [11]

$$\frac{d\boldsymbol{u}}{d\ell} = \boldsymbol{G}[\boldsymbol{u}], \tag{1.50}$$

where we collected entries of the parameter set $\{u\}$ to the vector $\boldsymbol{u}$ and introduced the flowing parameter $\ell = -\ln(b)$. Equation (1.50) is referred to as the Renormalization Group (RG)-flow equation and $\boldsymbol{G}$ as the so-called RG-flow generator. In general $\boldsymbol{G}$ represents a non-linear transformation.

The great achievement of the Wilsonian theory consists in the possibility to calculate critical exponents from the microscopic ansatz. They represent a set of numbers which

characterize the non-analytic behavior of thermodynamic observables close to the critical point of continuous phase transitions [27, 28, 29, 31]. Systems which have the same critical exponents are said to belong to the same *universality class*. Wilson and Fisher managed to show [23, 24] that critical exponents can be extracted from the RG-flow in the vicinity of the fixed point, i. e. at a point, where the RG-flow stops:

$$\boldsymbol{G}[\boldsymbol{u}_\star] = 0. \tag{1.51}$$

In addition to equation (1.51) one has to assume that the parameter vector $\boldsymbol{u}$ converges to some critical vector $\boldsymbol{u}_\star$ in the limit $\ell \to \infty$, i. e.

$$\lim_{\ell\to\infty} \boldsymbol{u} = \boldsymbol{u}_\star. \tag{1.52}$$

After linearizing the operator $\boldsymbol{G}$ in the vicinity of the fixed point, critical exponents can be determined as eigenvalues of this linearized transformation. One usually combines the linearization of the RG-flow around the fixed point with the expansion in some small parameter $\epsilon = D_c - D$, where D_c denotes the so-called *upper critical dimension* of the particular model. In $D > D_c$ critical exponents of the model are correctly predicted by the the mean-field theory [8].

Usually the components of the coupling parameter vector $\boldsymbol{u}$ are classified due to their behavior in the vicinity of the fixed point [33, 34]. Close to the fixed point, the flow of each coupling parameter u_i may be approximated by

$$u_i \approx e^{-y_i \ell} \cdot u_{i,\star}. \tag{1.53}$$

The sign of the *scaling dimension* y_i enables us to classify the corresponding coupling parameters as

$$\begin{aligned} &\text{relevant} \quad \text{if} \quad y_i > 0, \\ &\text{marginal} \quad \text{if} \quad y_i = 0, \\ &\text{irrelevant} \quad \text{if} \quad y_i < 0. \end{aligned}$$

At this point we want to make some general remarks on the formalism which we briefly described above. The method is essentially non-perturbative, although the integration over the fast modes in equation (1.45) is in general very complicated to implement analytically and some form of diagrammatic expansion is needed to perform it approximately. However, these diagrams are not plagued by any divergences [35, 36], since the integration in the momentum space is performed over the finite shell $\Lambda < |\boldsymbol{\kappa}| < \Lambda_0$. Thus, the Wilsonian RG transformation offers a way to go beyond the perturbative expansion and has been successfully applied to a number of problems, for which the usual *naive* perturbative treatment fails [37].

In recent decades, several approaches have been suggested in order to reformulate the Wilsonian RG in the language of continuous functional differential equations. One of them which enjoys wide recognition due to its formal elegance and intuitive depth, was provided independently by Christof Wetterich [12] and Tim Morris [13] in the early 90's. We shall consider this approach in the next section of this thesis.

1.4 Exact RG-flow equation

The interpretation of the Renormalization Group from the quantum field theoretical point of view gained attention after Wilson's ideas could be reformulated in the formally exact way which was first done by Wegner and Houghton [11] and two decades later by Wetterich [12] and Morris [13]. For standard works introducing the Renormalization Group analysis within the field theoretical approach we can mention reviews by Berges and collaborators [38], Bagnuls and Bervillier [39], and the recent review by Delamotte [36]. However, these authors mostly restrict their consideration to the N-component classical scalar models. The generalization to the arbitrary fields was made by Schütz, Bartosch and Kopietz in [40] (see also [18, 19]).

In order to derive the exact functional RG-flow equation we have to extend the initial action of the system by an additional cutoff term

$$\Delta S_\Lambda[\boldsymbol{\Phi}] = -\frac{1}{2}\boldsymbol{\Phi}\cdot\boldsymbol{R}_\Lambda\cdot\boldsymbol{\Phi}, \tag{1.54}$$

which depends on the cutoff momentum Λ, such that the generating functional of Green functions reads

$$\mathcal{G}_\Lambda[\boldsymbol{J}] = e^{\mathcal{G}_{c,\Lambda}[\boldsymbol{J}]} = \frac{1}{Z_{0,\Lambda}}\int \mathcal{D}\boldsymbol{\Phi}\; e^{-S_\Lambda[\boldsymbol{\Phi}]+\boldsymbol{J}\cdot\boldsymbol{\Phi}}, \tag{1.55}$$

where

$$S_\Lambda[\boldsymbol{\Phi}] = S[\boldsymbol{\Phi}] + \Delta S_\Lambda[\boldsymbol{\Phi}], \tag{1.56}$$

and the renormalized non-interacting partition function

$$Z_{0,\Lambda} = \int \mathcal{D}\boldsymbol{\Phi}\; e^{-S_{0,\Lambda}[\boldsymbol{\Phi}]}, \tag{1.57}$$

with

$$S_{0,\Lambda}[\boldsymbol{\Phi}] = S_0[\boldsymbol{\Phi}] + \Delta S_\Lambda[\boldsymbol{\Phi}]. \tag{1.58}$$

The matrix $\boldsymbol{R}_\Lambda$ has the same structure in the space of the superfields as the free propagator matrix given in equation (1.10)

$$\boldsymbol{R}_\Lambda = \begin{pmatrix} 0 & \hat{\boldsymbol{R}}_\Lambda \\ \mathbb{P}\cdot\hat{\boldsymbol{R}}_\Lambda & 0 \end{pmatrix}. \tag{1.59}$$

Matrices $\hat{\boldsymbol{R}}_\Lambda$ should be diagonal in multi-indices

$$[\hat{\boldsymbol{R}}_\Lambda]_{\alpha\alpha'} = \delta_{i,i'}\delta_{K,K'}R_{i,\Lambda}(\boldsymbol{\kappa}), \tag{1.60}$$

where $R_{i,\Lambda}(\boldsymbol{\kappa})$ denotes a regulator function for the i-th entry in the field $\boldsymbol{\phi}$ which explicitly depend on the cutoff momentum $0 \leqslant \Lambda < \Lambda_0$. Here, Λ_0 is an appropriate ultraviolet cutoff momentum which is usually chosen to be much larger than some inverse characteristic length of the system. The choice of the regulator $R_{i,\Lambda}(\boldsymbol{\kappa})$ is a matter of taste but it should obey following properties [41]:

1. It has to be a positive-valued function having at least one well defined derivative with respect to the cutoff momentum Λ.

2. It should obey the condition

$$\lim_{|\boldsymbol{\kappa}|\to 0} R_{i,\Lambda}(\boldsymbol{\kappa}) > 0, \tag{1.61}$$

which ensures that the elements of the series (1.28) and (1.31) do not suffer from any infrared divergences.

3. It should become infinite in the ultraviolet limit, i. e. as $\Lambda \to \Lambda_0$

$$\lim_{\Lambda\to\Lambda_0} R_{i,\Lambda}(\boldsymbol{\kappa}) \to \infty. \tag{1.62}$$

This requirement ensures that the effective action $\mathcal{L}_\Lambda[\tilde{\boldsymbol{\Phi}}]$ approaches the microscopic action $S[\boldsymbol{\Phi}]$ in the ultraviolet limit, i. e.

$$\lim_{\Lambda>\Lambda_0} \mathcal{L}[\tilde{\boldsymbol{\Phi}}] \approx S[\boldsymbol{\Phi}]. \tag{1.63}$$

Hence, introducing the regulator corresponds to the augmenting of the initial action by a large mass-like term which effectively suppresses fluctuations for $\Lambda \leqslant \Lambda_0$ and leaves them unaffected above the cutoff. In this sense, the FRG-philosophy differs from the Wilsonian, where the initial microscopic action contains all fluctuations and the RG-flow basically describes their elimination.

4. It should vanish in the limit $\Lambda \to 0$, i. e.

$$\lim_{\Lambda\to 0} R_{i,\Lambda}(\boldsymbol{\kappa}) \to 0. \tag{1.64}$$

This property guarantees that the destined physical effective action $\mathcal{L}_{\Lambda\to 0}[\tilde{\boldsymbol{\Phi}}]$ does not depend on the particular shape of the cutoff.

A popular choice of the regulator function which led in the past to the very accurate estimation of critical exponents of the classical $O(N)$-model [12, 38] reads

$$R_\Lambda(\boldsymbol{\kappa}) = \frac{f_\Lambda |\boldsymbol{\kappa}|^2}{e^{|\boldsymbol{\kappa}|^2/\Lambda^2} - 1}, \tag{1.65}$$

where f_Λ is a Λ-dependent function which is introduced due to reasons of dimensionality. Another prominent representative of the class is the Litim-regulator [41]

$$R_\Lambda(\boldsymbol{\kappa}) = f_\Lambda(\Lambda^2 - |\boldsymbol{\kappa}|^2)\Theta(\Lambda^2 - |\boldsymbol{\kappa}|^2), \tag{1.66}$$

where

$$\Theta(x) = \begin{cases} 0 \text{ if } x < 0 \\ 1 \text{ if } x \geqslant 0 \end{cases} \tag{1.67}$$

denotes the Heaviside step function. The advantage is that the Litim-regulator enables the momentum integration to be carried out analytically. Finally, the sharp cutoff regulator [13, 40] has to be mentioned which shares advantages of the Litim-regulator, but causes some specific difficulties, if chosen to work with [42, 43, 44]. In this case, the regulator function is indistinguishable from the inverse free propagator

$$R_\Lambda(\boldsymbol{\kappa}) = \left[\Theta(|\boldsymbol{\kappa}|^2 - \Lambda_0^2) - \Theta(|\boldsymbol{\kappa}|^2 - \Lambda^2)\right] G_0^{-1}(\boldsymbol{\kappa}). \tag{1.68}$$

Taking derivative with respect to the cutoff-momentum Λ on both sides of equation (1.55) we obtain

$$\begin{aligned}
\partial_\Lambda \mathcal{G}_{c,\Lambda}[\boldsymbol{J}] &= -\partial_\Lambda \ln Z_{0,\Lambda} - \frac{\mathcal{G}_\Lambda^{-1}[\boldsymbol{J}]}{Z_{0,\Lambda}} \int \mathcal{D}\boldsymbol{\Phi}\ \partial_\Lambda \Delta S_\Lambda[\boldsymbol{\Phi}]\ e^{-S_\Lambda[\boldsymbol{\Phi}] + \boldsymbol{J}\cdot\boldsymbol{\Phi}} && \text{(1.69a)}\\
&= -\partial_\Lambda \ln Z_{0,\Lambda} - \mathcal{G}_\Lambda^{-1}[\boldsymbol{J}]\, \partial_\Lambda \Delta S_\Lambda \left[\frac{\delta}{\delta \boldsymbol{J}}\right] \mathcal{G}_\Lambda[\boldsymbol{J}] && \text{(1.69b)}\\
&= -\partial_\Lambda \ln Z_{0,\Lambda} - \partial_\Lambda \Delta S_\Lambda \left[\frac{\delta \mathcal{G}_{c,\Lambda}}{\delta \boldsymbol{J}}\right] + \frac{1}{2}\mathrm{Tr}\left\{\frac{\delta^{(2)}\mathcal{G}_{c,\Lambda}}{\delta \boldsymbol{J}\delta \boldsymbol{J}} \cdot [\partial_\Lambda \boldsymbol{R}_\Lambda]^T\right\}, && \text{(1.69c)}
\end{aligned}$$

where we used equation (1.18) in line (1.69b). The operator Tr in line (1.69c) denotes taking the trace over the field space and summation over all relevant multi-indices K:

$$\mathrm{Tr} \equiv \mathrm{Tr}_{\boldsymbol{\Phi}} \int_{\alpha_1} \cdots \int_{\alpha_n}. \tag{1.70}$$

From equation (1.30) follows that

$$\partial_\Lambda \mathcal{G}_{c,\Lambda}[\boldsymbol{J}] = -\partial_\Lambda \mathcal{L}_\Lambda[\tilde{\boldsymbol{\Phi}}[\boldsymbol{J}]] = -\partial_\Lambda \tilde{\mathcal{L}}_\Lambda[\tilde{\boldsymbol{\Phi}}[\boldsymbol{J}]] - \partial_\Lambda \Delta S_\Lambda \left[\tilde{\boldsymbol{\Phi}}[\boldsymbol{J}]\right], \tag{1.71}$$

where $\tilde{\mathcal{L}}_\Lambda[\tilde{\boldsymbol{\Phi}}] = \mathcal{L}_\Lambda[\tilde{\boldsymbol{\Phi}}] - \Delta S_\Lambda[\tilde{\boldsymbol{\Phi}}]$. Hence, under taking into account equations (1.34), (1.36) and (1.69c) we obtain the exact RG-flow equation for the effective action [12, 13]:

$$\begin{aligned}
\partial_\Lambda \tilde{\mathcal{L}}_\Lambda[\tilde{\boldsymbol{\Phi}}] &= \partial_\Lambda \ln Z_{0,\Lambda} - \frac{1}{2}\mathrm{Tr}\left\{\boldsymbol{Z} \cdot \left(\frac{\delta^{(2)}\tilde{\mathcal{L}}_\Lambda}{\delta\tilde{\boldsymbol{\Phi}}\delta\tilde{\boldsymbol{\Phi}}} - \boldsymbol{R}_\Lambda\right)^{-1} \cdot [\partial_\Lambda \boldsymbol{R}_\Lambda]^T\right\}\\
&= \partial_\Lambda \ln Z_{0,\Lambda} - \frac{1}{2}\mathrm{Tr}\left\{\boldsymbol{Z} \cdot \left(\frac{\delta^{(2)}\Gamma_\Lambda}{\delta\tilde{\boldsymbol{\Phi}}\delta\tilde{\boldsymbol{\Phi}}} - [\boldsymbol{G}_{0,\Lambda}^{-1}]^T\right)^{-1} \cdot [\partial_\Lambda \boldsymbol{R}_\Lambda]^T\right\}. \qquad \text{(1.72)}
\end{aligned}$$

Equation (1.72) represents a functional integro-differential functional equation and is a highly complex mathematical object. Although both sides of this equation are expressed in terms of the functional $\tilde{\mathcal{L}}_\Lambda$, it appears on the right-hand side as a second derivative with respect to the fields $\tilde{\boldsymbol{\Phi}}$. Due to equation (1.37) the expression within the round brackets reproduces for $\tilde{\boldsymbol{\Phi}} = 0$ the full inverse propagator. Therefore, equation (1.72) has essentially a shape of a single-closed loop.

We can further rearrange the exact RG-flow equation (1.72) by making use of expression (1.41). Plugging it into equation (1.72) we obtain

$$\begin{aligned}\partial_\Lambda \tilde{\mathcal{L}}_\Lambda[\tilde{\boldsymbol{\Phi}}] &= \partial_\Lambda \ln Z_{0,\Lambda} - \frac{1}{2}\mathrm{Tr}\left\{\boldsymbol{Z}\cdot\boldsymbol{G}_\Lambda^T\cdot[\partial_\Lambda \boldsymbol{R}_\Lambda]^T\right\} \\ &\quad -\frac{1}{2}\mathrm{Tr}\sum_{l=1}^{\infty}\left\{\boldsymbol{Z}\cdot\boldsymbol{G}_\Lambda^T\cdot\left(\boldsymbol{U}_\Lambda^T\cdot\boldsymbol{G}_\Lambda^T\right)^l\cdot[\partial_\Lambda \boldsymbol{R}_\Lambda]^T\right\} \\ &= \partial_\Lambda \ln Z_{0,\Lambda} - \frac{1}{2}\mathrm{Tr}\left\{\boldsymbol{Z}\cdot\boldsymbol{G}_\Lambda^T\cdot[\partial_\Lambda \boldsymbol{R}_\Lambda]^T\right\} \\ &\quad -\frac{1}{2}\mathrm{Tr}\sum_{l=0}^{\infty}\left\{\boldsymbol{Z}\cdot\dot{\boldsymbol{G}}_\Lambda^T\cdot\boldsymbol{U}_\Lambda^T\cdot\left(\boldsymbol{G}_\Lambda^T\cdot\boldsymbol{U}_\Lambda^T\right)^l\right\}, \end{aligned} \tag{1.73}$$

where we introduced the so-called *single-scale propagator matrix*

$$\dot{\boldsymbol{G}}_\Lambda = -\boldsymbol{G}_\Lambda\cdot[\partial_\Lambda \boldsymbol{R}_\Lambda]\cdot\boldsymbol{G}_\Lambda. \tag{1.74}$$

in the last line.

There is no general exact solution for this equation. However, several approximate approaches have been proposed in the past [13, 38, 40]. Here we consider an approach which is based on the expansion of the functional $\tilde{\mathcal{L}}_\Lambda[\tilde{\boldsymbol{\Phi}}]$ in powers of the fields $\tilde{\boldsymbol{\Phi}}$.

By using expansions (1.31) and (1.40) and comparing terms with the same number of fields on both sides of equation (1.73) one obtains the flow equation for the field independent part of the effective action [40]

$$\partial_\Lambda \tilde{\mathcal{L}}_\Lambda^{(0)} = \partial_\Lambda \ln Z_{0,\Lambda} - \frac{1}{2}\mathrm{Tr}\left\{\boldsymbol{Z}\cdot\boldsymbol{G}_\Lambda^T\cdot[\partial_\Lambda \boldsymbol{R}_\Lambda]^T\right\}, \tag{1.75}$$

which basically describes the RG-flow of the Helmholtz free energy. Quite generally, the master-equation for the functions $\Gamma^{(n)}_{\Lambda|\alpha_1,\ldots,\alpha_n}$ with $n \geqslant 1$ fields can be written in the form

$$\begin{aligned}\partial_\Lambda \Gamma^{(n)}_{\Lambda|\alpha_1,\ldots,\alpha_n} &= -\frac{1}{2}\sum_{l=1}^{\infty}\sum_{m_1,\ldots,m_l=1}^{\infty}\delta_{n,m_1+\cdots+m_l}\times \\ &\mathcal{S}_{\alpha_1,\ldots,\alpha_{m_1};\alpha_{m_1+1},\ldots\alpha_{m_1+m_2};\cdots;\alpha_{m_1+\cdots+m_{l-1}+1},\ldots,\alpha_n}\times \\ &\left\{\mathrm{Tr}\left(\boldsymbol{Z}\cdot\dot{\boldsymbol{G}}^T\cdot\left[\boldsymbol{\Gamma}^{(m_1+2)}_{\Lambda|\alpha_1,\cdots,\alpha_{m_1}}\right]^T\cdot\boldsymbol{G}^T\cdot\left[\boldsymbol{\Gamma}^{(m_2+2)}_{\Lambda|\alpha_{m_1+1},\cdots,\alpha_{m_1+m_2}}\right]^T\cdot\ldots\right.\right. \\ &\left.\left.\ldots\cdot\boldsymbol{G}^T\cdot\left[\boldsymbol{\Gamma}^{(m_l+2)}_{\Lambda|\alpha_{m_1+\cdots+m_{l-1}+1},\cdots,\alpha_n}\right]^T\right)\right\}, \end{aligned} \tag{1.76}$$

where the symmetrization operator is defined by

$$\begin{aligned}&\mathcal{S}_{\alpha_1,\ldots,\alpha_{m_1};\alpha_{m_1+1},\ldots\alpha_{m_1+m_2};\cdots;\alpha_{m_1+\cdots+m_{l-1}+1},\ldots,\alpha_n}\left\{A_{\alpha_1,\cdots,\alpha_n}\right\} \\ &\quad = \frac{1}{\prod_i m_i!}\sum_P \mathrm{sgn}_\zeta(P) A_{\alpha_{P(1)}\cdots\alpha_{P(n)}}, \end{aligned} \tag{1.77}$$

where P is a permutation of $1, \ldots, n$ and sgn_ζ is the sign created by permuting field variables according to the permutation P (+1 for each permutation in the Bose-subspace of $\tilde{\mathbf{\Phi}}$ and -1 for each permutation in the Fermi-subspace), i. e.

$$\tilde{\mathbf{\Phi}}_{\alpha_1} \cdot \ldots \cdot \tilde{\mathbf{\Phi}}_{\alpha_n} = \mathrm{sgn}_\zeta(P) \tilde{\mathbf{\Phi}}_{\alpha_{P(1)}} \cdot \ldots \cdot \tilde{\mathbf{\Phi}}_{\alpha_{P(n)}}. \tag{1.78}$$

Expression (1.76) represents the master-equation for the infinite hierarchy of the flow equations for each function $\Gamma^{(n)}$. Although not quite correct we will call functions $\Gamma^{(n)}$ the irreducible vertices below. For clarity we give here the first three equations from this hierarchy:

$$\partial_\Lambda \Gamma^{(1)}_{\Lambda|\alpha_1} = -\frac{1}{2}\mathrm{Tr}\left(\boldsymbol{Z} \cdot \dot{\boldsymbol{G}}^T \cdot \left[\mathbf{\Gamma}^{(3)}_{\Lambda|\alpha_1} \right]^T \right), \tag{1.79a}$$

$$\begin{aligned} \partial_\Lambda \Gamma^{(2)}_{\Lambda|\alpha_1\alpha_2} &= -\frac{1}{2}\mathrm{Tr}\left(\boldsymbol{Z} \cdot \dot{\boldsymbol{G}}^T \cdot \left[\mathbf{\Gamma}^{(4)}_{\Lambda|\alpha_1\alpha_2} \right]^T \right) \\ -\frac{1}{2}\mathcal{S}_{\alpha_1;\alpha_2} &\left\{ \mathrm{Tr}\left(\boldsymbol{Z} \cdot \dot{\boldsymbol{G}}^T \cdot \left[\mathbf{\Gamma}^{(3)}_{\Lambda|\alpha_1} \right]^T \cdot \boldsymbol{G}^T \cdot \left[\mathbf{\Gamma}^{(3)}_{\Lambda|\alpha_2} \right]^T \right) \right\}, \end{aligned} \tag{1.79b}$$

$$\begin{aligned} \partial_\Lambda \Gamma^{(3)}_{\Lambda|\alpha_1\alpha_2\alpha_3} &= -\frac{1}{2}\mathrm{Tr}\left(\boldsymbol{Z} \cdot \dot{\boldsymbol{G}}^T \cdot \left[\mathbf{\Gamma}^{(5)}_{\Lambda|\alpha_1\alpha_2\alpha_3} \right]^T \right) \\ -\frac{1}{2}\mathcal{S}_{\alpha_1\alpha_2;\alpha_3} &\left\{ \mathrm{Tr}\left(\boldsymbol{Z} \cdot \dot{\boldsymbol{G}}^T \cdot \left[\mathbf{\Gamma}^{(4)}_{\Lambda|\alpha_1\alpha_2} \right]^T \cdot \boldsymbol{G}^T \cdot \left[\mathbf{\Gamma}^{(3)}_{\Lambda|\alpha_3} \right]^T \right) \right\} \\ -\frac{1}{2}\mathcal{S}_{\alpha_1;\alpha_2\alpha_3} &\left\{ \mathrm{Tr}\left(\boldsymbol{Z} \cdot \dot{\boldsymbol{G}}^T \cdot \left[\mathbf{\Gamma}^{(3)}_{\Lambda|\alpha_1} \right]^T \cdot \boldsymbol{G}^T \cdot \left[\mathbf{\Gamma}^{(4)}_{\Lambda|\alpha_2\alpha_3} \right]^T \right) \right\} \\ -\frac{1}{2}\mathcal{S}_{\alpha_1;\alpha_2;\alpha_3} &\left\{ \mathrm{Tr}\left(\boldsymbol{Z} \cdot \dot{\boldsymbol{G}}^T \cdot \left[\mathbf{\Gamma}^{(3)}_{\Lambda|\alpha_1} \right]^T \cdot \boldsymbol{G}^T \cdot \left[\mathbf{\Gamma}^{(3)}_{\Lambda|\alpha_2} \right] \boldsymbol{G}^T \cdot \left[\mathbf{\Gamma}^{(3)}_{\Lambda|\alpha_3} \right]^T \right) \right\}. \end{aligned} \tag{1.79c}$$

As one can clearly see from equations (1.79a-1.79c), the hierarchy of flow equations for the irreducible vertices is not closed, i. e. the flow of each irreducible vertex function is determined by the higher-order vertices entering each equation on the right-hand side. Therefore, in practice some approximation scheme is always needed to close the hierarchy. Usually, a physical insight helps to appropriately truncate vertex functions in the flow equations. For instance, if one pursues the goal of calculating critical exponents of some second-order phase transition, one usually chooses the truncation scheme based on the relevance of vertex functions in the vicinity of the non-trivial fixed point. Within this truncation scheme one considers equations for relevant and marginal vertices only and neglects irrelevant ones. In the past this scheme has been successfully applied for studying critical behavior of weakly interacting bosons [42, 43]. This truncation scheme has also been employed for the exact solution of the Tomonaga-Luttinger model within the FRG-approach [40].

Schütz *et al.* developed in [40] a diagrammatic technique for dealing with equations (1.76) which simplifies enormously the derivation of the flow equations for each single

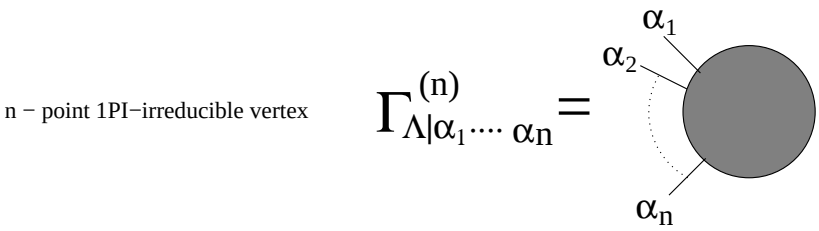

Figure 1.1: Graphical representation of propagators and vertex functions

vertex function if concrete calculations have to be done. A brief glossary of the diagrammatic language is shown in Figure 1.1. We show the diagrammatic representation of equations (1.79a), (1.79b) and (1.79c) in Figures 1.2, 1.3 and 1.4 respectively. Black dots above the vertices on the left-hand side of each equation denote taking partial derivative with respect to the flowing cutoff-parameter Λ.

1.5 Taking symmetry breaking into account

In the previous section we derived the functional RG-flow equation (1.73) in full generality, without making any assumptions about the symmetry properties of the fields $\tilde{\mathbf{\Phi}}$. It can be used without any restriction to describe the physics in the symmetric phase, i. e. if fields do not possess any finite vacuum expectation values

$$\frac{\delta}{\delta \boldsymbol{J}} \mathcal{G}_c[\boldsymbol{J}]\bigg|_{\boldsymbol{J}=0} = \tilde{\mathbf{\Phi}}[\boldsymbol{J}=0] = 0. \tag{1.80}$$

Because of equation (1.80), equation (1.79a) vanishes identically on both sides. However, this situation changes if the system is in an ordered phase, i. e. if some of the components of the field $\tilde{\mathbf{\Phi}}$ acquire a non-vanishing vacuum expectation

$$\frac{\delta}{\delta \boldsymbol{J}} \mathcal{G}_c[\boldsymbol{J}]\bigg|_{\boldsymbol{J}=0} = \tilde{\mathbf{\Phi}}[\boldsymbol{J}=0] = \tilde{\mathbf{\Phi}}^0 \neq 0. \tag{1.81}$$

Since $\tilde{\mathbf{\Phi}}^0$ correspond to a macroscopically observable quantity, it should be flowing in the RG sense. In order to build in the symmetry breaking into the hierarchy (1.76) we have to expand the effective action $\mathcal{L}_\Lambda[\tilde{\mathbf{\Phi}}]$ not around the point $\tilde{\mathbf{\Phi}} = 0$, as we did in equation (1.31), but around $\tilde{\mathbf{\Phi}} = \tilde{\mathbf{\Phi}}^0_\Lambda$. If we introduce fluctuating fields $\Delta\tilde{\mathbf{\Phi}}$ in the following way

$$\Delta\tilde{\mathbf{\Phi}}_{\Lambda|\alpha} = \tilde{\mathbf{\Phi}}_{\Lambda|\alpha} - \tilde{\mathbf{\Phi}}^0_{\Lambda|\alpha}, \tag{1.82}$$

insert them in place of $\tilde{\mathbf{\Phi}}$ in the power series (1.31) and (1.40), and then the latter into the FRG equation (1.73) and, finally, compare terms with the same number of the fields

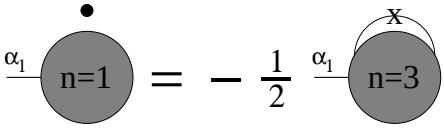

Figure 1.2: Graphical representation of the RG-flow equation (1.79a) for $n = 1-$vertex

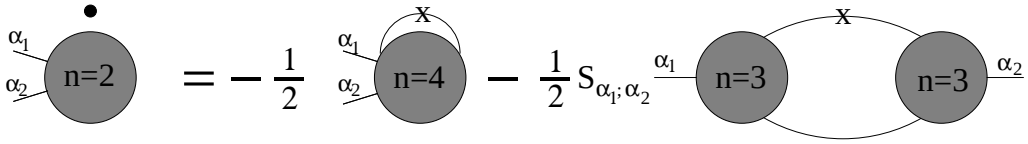

Figure 1.3: Graphical representation of the RG-flow equation (1.79b) for $n = 2-$vertex.

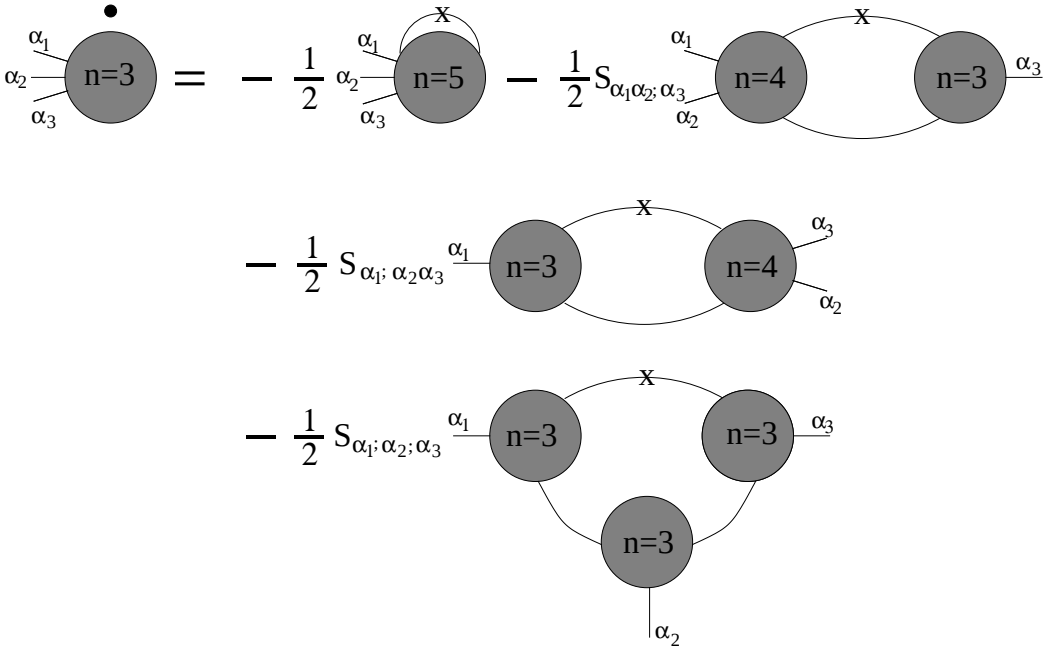

Figure 1.4: Graphical representation of the RG-flow equation (1.79c) for $n = 3-$ vertex.

on both sides, then we obtain a modified master-equation for the irreducible vertices in the symmetry broken phase [14]

$$\begin{aligned}
\partial_\Lambda \Gamma^{(n)}_{\Lambda|\alpha_1,\ldots,\alpha_n} = &\left[\boldsymbol{\Gamma}^{(n+1)}_{\Lambda|\alpha_1,\ldots,\alpha_n}\right]^T \cdot \left[\partial_\Lambda \tilde{\boldsymbol{\Phi}}^0_\Lambda\right] - \frac{1}{2}\sum_{l=1}^{\infty}\sum_{m_1,\ldots,m_l=1}^{\infty} \delta_{n,m_1+\cdots+m_l} \times \\
&\mathcal{S}_{\alpha_1,\ldots,\alpha_{m_1};\alpha_{m_1+1},\ldots\alpha_{m_1+m_2};\cdots;\alpha_{m_1+\cdots+m_{l-1}+1},\ldots,\alpha_n} \times \\
&\left\{ \mathrm{Tr}\left(\boldsymbol{Z}\cdot\dot{\boldsymbol{G}}^T \cdot \left[\boldsymbol{\Gamma}^{(m_1+2)}_{\Lambda|\alpha_1,\cdots,\alpha_{m_1}}\right]^T \cdot \boldsymbol{G}^T \cdot \left[\boldsymbol{\Gamma}^{(m_2+2)}_{\Lambda|\alpha_{m_1+1},\cdots,\alpha_{m_1+m_2}}\right]^T \cdot \ldots \right.\right. \\
&\left.\left. \ldots \cdot \boldsymbol{G}^T \cdot \left[\boldsymbol{\Gamma}^{(m_l+2)}_{\Lambda|\alpha_{m_1+\cdots+m_{l-1}+1},\cdots,\alpha_n}\right]^T \right) \right\}. \qquad (1.83)
\end{aligned}$$

With this generalization, the first three equations of the hierarchy can be rewritten as

$$\partial_\Lambda \Gamma^{(1)}_{\Lambda|\alpha_1} = \left[\mathbf{\Gamma}^{(2)}_{\Lambda|\alpha_1}\right]^T \cdot \left[\partial_\Lambda \tilde{\mathbf{\Phi}}^0_\Lambda\right] - \frac{1}{2}\mathrm{Tr}\left(\boldsymbol{Z}\cdot\dot{\boldsymbol{G}}^T\cdot\left[\mathbf{\Gamma}^{(3)}_{\Lambda|\alpha_1}\right]^T\right), \tag{1.84a}$$

$$\begin{aligned}\partial_\Lambda \Gamma^{(2)}_{\Lambda|\alpha_1\alpha_2} = &\left[\mathbf{\Gamma}^{(3)}_{\Lambda|\alpha_1\alpha_2}\right]^T \cdot \left[\partial_\Lambda \tilde{\mathbf{\Phi}}^0_\Lambda\right] - \frac{1}{2}\mathrm{Tr}\left(\boldsymbol{Z}\cdot\dot{\boldsymbol{G}}^T\cdot\left[\mathbf{\Gamma}^{(4)}_{\Lambda|\alpha_1\alpha_2}\right]^T\right)\\ &-\frac{1}{2}\mathcal{S}_{\alpha_1;\alpha_2}\left\{\mathrm{Tr}\left(\boldsymbol{Z}\cdot\dot{\boldsymbol{G}}^T\cdot\left[\mathbf{\Gamma}^{(3)}_{\Lambda|\alpha_1}\right]^T\cdot\boldsymbol{G}^T\cdot\left[\mathbf{\Gamma}^{(3)}_{\Lambda|\alpha_2}\right]^T\right)\right\},\end{aligned} \tag{1.84b}$$

$$\begin{aligned}\partial_\Lambda \Gamma^{(3)}_{\Lambda|\alpha_1\alpha_2\alpha_3} = &\left[\mathbf{\Gamma}^{(4)}_{\Lambda|\alpha_1\alpha_2\alpha_3}\right]^T \cdot \left[\partial_\Lambda \tilde{\mathbf{\Phi}}^0_\Lambda\right] - \frac{1}{2}\mathrm{Tr}\left(\boldsymbol{Z}\cdot\dot{\boldsymbol{G}}^T\cdot\left[\mathbf{\Gamma}^{(5)}_{\Lambda|\alpha_1\alpha_2\alpha_3}\right]^T\right)\\ &-\frac{1}{2}\mathcal{S}_{\alpha_1\alpha_2;\alpha_3}\left\{\mathrm{Tr}\left(\boldsymbol{Z}\cdot\dot{\boldsymbol{G}}^T\cdot\left[\mathbf{\Gamma}^{(4)}_{\Lambda|\alpha_1\alpha_2}\right]^T\cdot\boldsymbol{G}^T\cdot\left[\mathbf{\Gamma}^{(3)}_{\Lambda|\alpha_3}\right]^T\right)\right\}\\ &-\frac{1}{2}\mathcal{S}_{\alpha_1;\alpha_2\alpha_3}\left\{\mathrm{Tr}\left(\boldsymbol{Z}\cdot\dot{\boldsymbol{G}}^T\cdot\left[\mathbf{\Gamma}^{(3)}_{\Lambda|\alpha_1}\right]^T\cdot\boldsymbol{G}^T\cdot\left[\mathbf{\Gamma}^{(4)}_{\Lambda|\alpha_2\alpha_3}\right]^T\right)\right\}\\ &-\frac{1}{2}\mathcal{S}_{\alpha_1;\alpha_2;\alpha_3}\left\{\mathrm{Tr}\left(\boldsymbol{Z}\cdot\dot{\boldsymbol{G}}^T\cdot\left[\mathbf{\Gamma}^{(3)}_{\Lambda|\alpha_1}\right]^T\cdot\boldsymbol{G}^T\cdot\left[\mathbf{\Gamma}^{(3)}_{\Lambda|\alpha_2}\right]\boldsymbol{G}^T\cdot\left[\mathbf{\Gamma}^{(3)}_{\Lambda|\alpha_3}\right]^T\right)\right\}.\end{aligned} \tag{1.84c}$$

The flow equation for the field vacuum expectation value follows from equation (1.84a) by demanding its vanishing. Hence,

$$\left[\mathbf{\Gamma}^{(2)}_{\Lambda|\alpha_1}\right]^T \cdot \left[\partial_\Lambda \tilde{\mathbf{\Phi}}^0_\Lambda\right] = \frac{1}{2}\mathrm{Tr}\left(\boldsymbol{Z}\cdot\dot{\boldsymbol{G}}^T\cdot\left[\mathbf{\Gamma}^{(3)}_{\Lambda|\alpha_1}\right]^T\right). \tag{1.85}$$

The modified diagrammatic approach to systems displaying a broken symmetry was developed by Schütz and Kopietz in [14]. The necessary modification of the diagrammatic glossary which accounts the additional term with coupled condensate is shown in Figure 1.5.

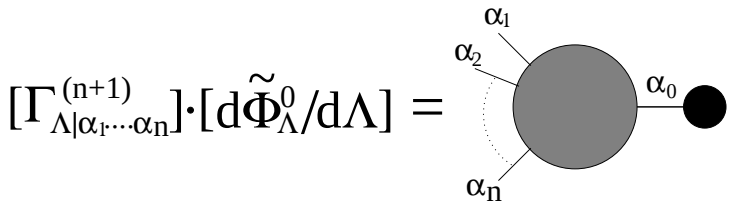

Figure 1.5: Graphical representation of the condensate coupled term.

In Figures 1.6, 1.7 and 1.8, the diagrammatic representations of equations (1.84b), (1.84c) and (1.85) are demonstrated.

The functional RG-flow equation derived in this chapter, provides us with the formal framework. Of course, this representation is very general and therefore lacks on clarity. To make ourselves familiar with the formalism we will proceed with concrete calculations in the next chapters.

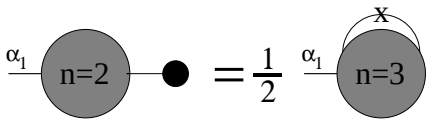

Figure 1.6: Graphical representation of the RG-flow equation (1.85) for the condensate.

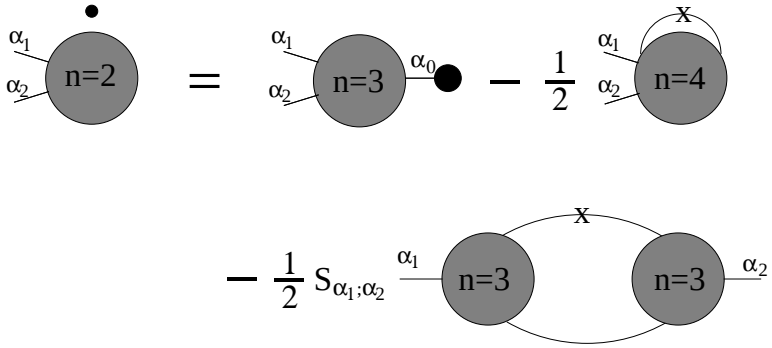

Figure 1.7: Graphical representation of the RG-flow equation (1.84b) for $n = 2-$vertex in symmetry broken phase.

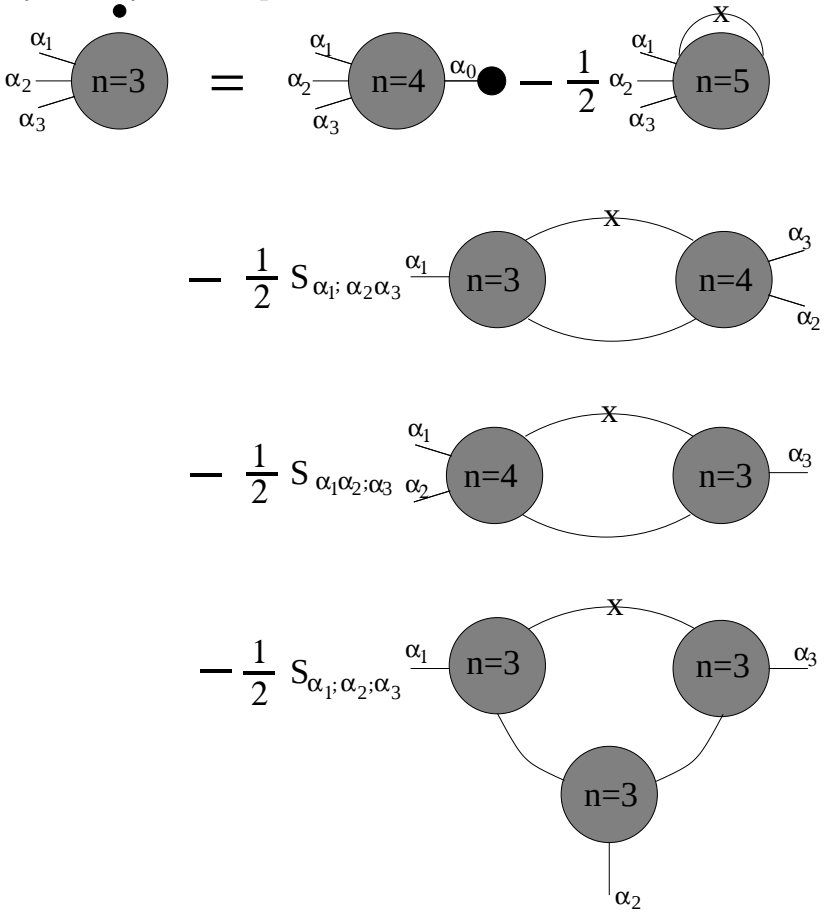

Figure 1.8: Graphical representation of the RG-flow equation (1.84c) for $n = 3-$ vertex in symmetry broken phase.

2 Classical ϕ^4-model close to criticality

In this chapter, the FRG-formalism is applied to the classical one-component scalar model which is often referred to as the ϕ^4-model. The model belongs to the Ising universality class and is thus one of the best studied ever. Following the guideline described in the previous chapter, RG-flow equations for the order parameter and irreducible self-energy are derived. By employing the local potential approximation (LPA)-related truncation scheme we are able to close the hierarchy of the flow equations and solve them numerically. We discuss different regularization schemes. In order to investigate the near critical behavior of the model we have to carefully adjust initial values of each relevant flowing parameter. The near critical RG-flow is affected by the interplay between two characteristic length scales: the interaction-dependent Ginzburg scale and the temperature-dependent correlation length. Finally we calculate the near critical momentum dependent self-energy and study the influence of both length-scales on this. Parts of this chapter were published in [44, 45, 46].

2.1 RG-flow equations in the broken symmetry phase

The classical ϕ^4-model remains a standard for probing newly developed techniques before applying them to more complicated models. It has been studied for several decades and is commonly believed to be well understood. The action of the ϕ^4-model is given by

$$S[\phi] = \int d^D r \left[\frac{1}{2} (\boldsymbol{\nabla}\phi)^2 + \frac{r_{\Lambda_0}}{2}\phi^2 + \frac{u_{\Lambda_0}}{4!}\phi^4 \right], \tag{2.1}$$

where ϕ is a real one-component scalar field, r_{Λ_0} denotes the distance to the critical point,

$$r_{\Lambda_0} = \frac{1}{a^2} \frac{T - T_c^{MF}}{T_c^{MF}} \tag{2.2}$$

with the lattice spacing a, the mean-field estimation for the critical temperature T_c^{MF}, and u_{Λ_0} denoting some local four-point interaction. The spatial integration in equation (2.1) is regularized by means of an appropriate ultraviolet cutoff Λ_0^{-1} which is related to the lattice spacing a. The action (2.1) belongs to the Ising universality class [47], i. e. it remains invariant under mirroring the sign of the fields $\phi \to -\phi$. Such a symmetry is known as Z_2-symmetry. It is known that the model undergoes the second-order phase transition in all dimensions $D \geqslant 2$. The ϕ^4-model is the only known model with exactly calculated critical exponents in $D = 2$ [7, 48, 49, 50]. In $D > 2$ critical exponents of the model are calculated with the highest accuracy (see for instance chapter 4 in [38]).

The first application of the modern RG−approach to the ϕ^4-model from the disordered phase was done by Kenneth Wilson himself [9, 10]. Therefore, it appears naturally first to apply the formalism represented in the previous chapter to this model.

In the broken symmetry phase, the Fourier transformed fields $\phi_{\boldsymbol{k}}$ acquire a finite vacuum expectation value

$$\phi_{\boldsymbol{k}} = \phi^0_{\boldsymbol{k}} + \Delta\phi_{\boldsymbol{k}}, \tag{2.3}$$

where $\phi^0_{\boldsymbol{k}} = (2\pi)^D \delta(\boldsymbol{k}) M$ and M denotes the quantity related to the magnetization in the corresponding Ising model. Note that in this case a discrete symmetry is broken. By substituting this expression into equation (2.1) and expanding in powers of $\Delta\phi_{\boldsymbol{k}}$ we generate terms involving one and three powers of $\Delta\phi_{\boldsymbol{k}}$. Demanding the vanishing of the vertex $\Gamma^{(1)}_{\Lambda_0}$, associated with the term linear in $\Delta\phi_{\boldsymbol{k}}$, we obtain the magnetization in the Landau approximation,

$$M_{\Lambda_0} = \begin{cases} 0 & \text{for } r_{\Lambda_0} > 0, \\ \sqrt{-\dfrac{6 r_{\Lambda_0}}{u_{\Lambda_0}}} & \text{for } r_{\Lambda_0} < 0. \end{cases} \tag{2.4}$$

This expression will serve as the initial condition for the flow equation of the order parameter in our functional RG approach.

In order to derive an exact hierarchy of flow equations for the vertices of our model we introduce a momentum cutoff Λ into the free propagator separating fluctuations with small momenta $|\boldsymbol{k}| \lesssim \Lambda$ from those with large momenta $|\boldsymbol{k}| \gtrsim \Lambda$.

We would like to calculate the true order parameter $M = \lim_{\Lambda\to 0} M_\Lambda$ and the true momentum dependent single-particle Green function $G(\boldsymbol{k}) = \lim_{\Lambda\to 0} G_\Lambda(\boldsymbol{k})$ which we parameterize in terms of an irreducible self-energy $\Sigma(\boldsymbol{k})$,

$$G(\boldsymbol{k}) = \frac{1}{\boldsymbol{k}^2 + \Sigma(\boldsymbol{k})}. \tag{2.5}$$

In the broken symmetry phase, the initial condition for the self-energy at scale $\Lambda = \Lambda_0$ is given by

$$\Sigma_{\Lambda_0}(\boldsymbol{k}) = r_{\Lambda_0} + \frac{u_{\Lambda_0}}{2} M^2_{\Lambda_0} = \frac{u_{\Lambda_0}}{3} M^2_{\Lambda_0} = -2 r_{\Lambda_0}, \tag{2.6}$$

with M_{Λ_0} defined in equation (2.4). Following the formalism presented in chapter 1 and noticing that

$$\partial_\Lambda \Gamma^{(2)}_\Lambda(\boldsymbol{k}) = \partial_\Lambda \Sigma_\Lambda(\boldsymbol{k}), \tag{2.7a}$$

as well as

$$\Gamma^{(2)}_\Lambda(0) = \Sigma_\Lambda(0), \tag{2.7b}$$

we derive the RG-flow equation for the self-energy

$$\begin{aligned}\partial_\Lambda \Sigma_\Lambda(\boldsymbol{k}) &= (\partial_\Lambda M_\Lambda)\Gamma^{(3)}_\Lambda(\boldsymbol{k},-\boldsymbol{k},0) \\ &\quad -\frac{1}{2}\int \frac{d^Dk'}{(2\pi)^D}\dot{G}_\Lambda(\boldsymbol{k}')\Gamma^{(4)}_\Lambda(\boldsymbol{k}',-\boldsymbol{k}',\boldsymbol{k},-\boldsymbol{k}) \\ &\quad -\int \frac{d^Dk'}{(2\pi)^D}\dot{G}_\Lambda(\boldsymbol{k}')\Gamma^{(3)}_\Lambda(\boldsymbol{k},-\boldsymbol{k}-\boldsymbol{k}',\boldsymbol{k}') \\ &\quad \times G_\Lambda(\boldsymbol{k}'+\boldsymbol{k})\Gamma^{(3)}_\Lambda(-\boldsymbol{k}',\boldsymbol{k}+\boldsymbol{k}',-\boldsymbol{k}), \end{aligned} \tag{2.8}$$

where the single-scale propagator is defined by

$$\dot{G}_\Lambda(\boldsymbol{k}) = -\partial_\Lambda R_\Lambda(\boldsymbol{k}) G^2_\Lambda(\boldsymbol{k}) \ , \tag{2.9}$$

with the regulator $R_\Lambda(\boldsymbol{k})$ which should have the dimensionality of the inverse Green function and will be specified below. On the other hand, the flowing order parameter M_Λ satisfies the following RG-flow equation

$$(\partial_\Lambda M_\Lambda)\Sigma_\Lambda(0) = \frac{1}{2}\int \frac{d^Dk}{(2\pi)^D}\dot{G}_\Lambda(\boldsymbol{k})\Gamma^{(3)}_\Lambda(\boldsymbol{k},-\boldsymbol{k},0) \ . \tag{2.10}$$

Expressed in corresponding diagrams, equations (2.8) and (2.10) are shown in Figures 1.6 and 1.7. The subscripts α_1 and α_2 should be replaced by $\boldsymbol{k}$ and $-\boldsymbol{k}$, respectively, and the symmetrizer $S_{\alpha_1,\alpha_2} = 2!/(1!1!) = 2$.

The right-hand side of equation (2.8) depends on the vertices $\Gamma^{(3)}_\Lambda$ and $\Gamma^{(4)}_\Lambda$ with three and four fields, which satisfy more complicated flow equations [14, 40] involving higher order vertices. Keeping in line with the derivative expansion for the effective action [38] we truncate the hierarchy as follows [14],

$$\Sigma_\Lambda(0) \approx \frac{u_\Lambda}{3}M^2_\Lambda \ , \tag{2.11a}$$

$$\Gamma^{(3)}_\Lambda(\boldsymbol{k}_1,\boldsymbol{k}_2,\boldsymbol{k}_3) \approx u_\Lambda M_\Lambda \ , \tag{2.11b}$$

$$\Gamma^{(4)}_\Lambda(\boldsymbol{k}_1,\boldsymbol{k}_2,\boldsymbol{k}_3,\boldsymbol{k}_4) \approx u_\Lambda \ . \tag{2.11c}$$

This truncation of the field expansion is motivated by the local potential approximation (LPA) [38], where one approximates the generating functional Γ by [38]

$$\Gamma[\tilde{\phi}] \approx \int d^Dr \ U_{\text{eff}}[\tilde{\phi}^2(\boldsymbol{r})], \tag{2.12}$$

with the effective potential U_{eff}. In our approximation we truncate U_{eff} to the quartic order in the fields

$$U_{\text{eff}}[\tilde{\phi}] \approx \frac{u_\Lambda}{4!}\left[\tilde{\phi}^2 - M^2_\Lambda\right]^2, \tag{2.13}$$

where $\tilde{\phi}$ means an averaged field in the sense of definitions of chapter 1.2. The completely local character of all correlations in the LPA is known to be a surprisingly good approximation in the scaling regime close to criticality [38]. Outside the critical regime, the LPA

does not fare that well and in general cannot reproduce the structure known from perturbation theory (in the case considered here, only the leading order from perturbation theory will be reproduced). The LPA combined with a derivative expansion converges best, if one expands around the local minimum of U_{eff}, see [51]. The condition that M_Λ is the flowing minimum leads to a flow equation for M_Λ, which in the field expansion leads to equations (2.11a–2.11c). In this truncation, the exact flow equation (2.10) for the order parameter reduces to

$$\partial_\Lambda M_\Lambda^2 = 3 \int \frac{d^D k}{(2\pi)^D} \dot{G}_\Lambda(\boldsymbol{k}), \tag{2.14}$$

while our flow equation (2.8) for the self-energy becomes

$$\begin{aligned} \partial_\Lambda \Sigma_\Lambda(\boldsymbol{k}) &= \frac{u_\Lambda}{2} \partial_\Lambda M_\Lambda^2 - \frac{u_\Lambda}{2} \int \frac{d^D k'}{(2\pi)^D} \dot{G}_\Lambda(\boldsymbol{k}') - u_\Lambda^2 M_\Lambda^2 \int \frac{d^D k'}{(2\pi)^D} \dot{G}_\Lambda(\boldsymbol{k}') G_\Lambda(\boldsymbol{k}' + \boldsymbol{k}) \\ &= u_\Lambda \int \frac{d^D k'}{(2\pi)^D} \dot{G}_\Lambda(\boldsymbol{k}') - u_\Lambda^2 M_\Lambda^2 \int \frac{d^D k'}{(2\pi)^D} \dot{G}_\Lambda(\boldsymbol{k}') G_\Lambda(\boldsymbol{k}' + \boldsymbol{k}) \; . \end{aligned} \tag{2.15}$$

By demanding that the flow of $\Sigma_\Lambda(0)$ is consistent with our truncation (2.11a) we obtain the flow equation for the effective interaction,

$$\partial_\Lambda u_\Lambda = -3 u_\Lambda^2 \int \frac{d^D k}{(2\pi)^D} \dot{G}_\Lambda(\boldsymbol{k}) G_\Lambda(\boldsymbol{k}) \; . \tag{2.16}$$

The above equations (2.14–2.16) form a closed system of coupled integro-differential equations for the order parameter M_Λ, the effective interaction u_Λ, and the momentum dependent self-energy $\Sigma_\Lambda(\boldsymbol{k})$. In contrast to the LPA, these equations can be used to calculate the full momentum-dependence of $\Sigma(\boldsymbol{k})$. Our truncation is similar in spirit but not identical to the truncation proposed by Blaizot *et al.* [52, 53, 54, 55, 56], who also used the LPA as a guide to propose a truncation of the hierarchy of flow equations for the momentum dependent vertices generated in the field expansion. However, unlike our equation (2.8), the flow equation for the self-energy proposed by Blaizot *et al.* does not involve the flowing order parameter, because these authors approach the critical point using an expansion around the symmetric state.

The self-energy $\Sigma_\Lambda(\boldsymbol{k})$ is supposed to have the low-momentum asymptotic behavior given by

$$\begin{aligned} \Sigma_\Lambda(\boldsymbol{k}) &\approx \Sigma_\Lambda(0) + \frac{\boldsymbol{k}^2}{2} \left. \frac{\partial^2 \Sigma_\Lambda(\boldsymbol{k})}{\partial \boldsymbol{k}^2} \right|_{\boldsymbol{k}=0} \\ &= \frac{1}{3} u_\Lambda M_\Lambda^2 + \boldsymbol{k}^2 \left(Z_\ell^{-1} - 1 \right) , \end{aligned} \tag{2.17}$$

where the inverse of the flowing wave-function renormalization factor is given by

$$Z_\ell^{-1} = 1 + \frac{1}{2} \left. \frac{\partial^2 \Sigma_\Lambda(\boldsymbol{k})}{\partial \boldsymbol{k}^2} \right|_{\boldsymbol{k}^2=0} , \tag{2.18}$$

and $\ell = \ln(\Lambda_0/\Lambda)$.

It is convenient to rescale all quantities in order to reveal their scaling dimensions. We define dimensionless momenta $\boldsymbol{q} = \boldsymbol{k}/\Lambda$. The dimensionless coupling parameters $\tilde{u}_\ell$ and $\tilde{M}^2_\ell$ are defined as follows:

$$u_\Lambda = \frac{\Lambda^{4-D}}{K_D Z_\ell^2}\, \tilde{u}_\ell \,, \tag{2.19}$$

$$M^2_\Lambda = Z_\ell K_D \Lambda^{D-2} \tilde{M}^2_\ell \,, \tag{2.20}$$

where K_D is defined by

$$K_D = \frac{\Omega_D}{(2\pi)^D} = \frac{2^{1-D}}{\pi^{D/2}\Gamma(D/2)} \,, \tag{2.21}$$

and Ω_D is the surface area of the D-dimensional unit sphere. Recalling definitions of chapter 1.3, the RG-flow of both coupling parameters in the vicinity of the fixed point should obey

$$u_{\Lambda\to 0} \approx e^{-(4-D)\ell}\, \tilde{u}_\star, \tag{2.22}$$

$$M^2_{\Lambda\to 0} \approx e^{-(D-2)\ell}\, \tilde{M}^2_\star, \tag{2.23}$$

where $\tilde{u}_\star$ and $\tilde{M}^2_\star$ denote the expected fixed point values of both quantities. Thus, the interaction is a relevant parameter in $D < 4$, marginal in $D = 4$ and irrelevant in dimensions higher than 4, while the order parameter is relevant in all dimensions larger than 2, marginal in $D = 2$ and irrelevant for $D < 2$. Therefore, $D = 2$ is the lower critical dimension of the model, $D = 4$ is the upper critical dimension and the Wilsonian small expansion parameter should be chosen as $\epsilon = 4 - D$. Thus, our truncation takes all relevant and marginal coupling parameters in dimensions $2 < D < 4$ into account which arise from the truncated effective potential (2.13) and is sufficient to describe critical physics of the model. This fact provides the formal justification for the truncation of the flowing self-energy given by equation (2.17).

Furthermore, we define the rescaled flowing propagator,

$$\mathcal{G}_\ell(\boldsymbol{q}) = \frac{\Lambda^2}{Z_\ell} G_\Lambda(\boldsymbol{k}), \tag{2.24}$$

and the corresponding single-scale propagator

$$\dot{\mathcal{G}}_\ell(\boldsymbol{q}) = \dot{R}_\ell(\boldsymbol{q}) \mathcal{G}^2_\ell(\boldsymbol{q}), \tag{2.25}$$

where

$$\dot{R}_\ell(\boldsymbol{q}) = -\frac{Z_\ell}{\Lambda} \partial_\Lambda R_\Lambda(\boldsymbol{k}). \tag{2.26}$$

Here, the quantity

$$\eta_\ell = -\partial_\ell \ln Z_\ell \tag{2.27}$$

denotes the flowing anomalous dimension.

The rescaled propagator (2.24) depends on the rescaled irreducible self-energy,

$$\Gamma^{(2)}_\ell(\boldsymbol{q}) = \frac{Z_\ell}{\Lambda^2}\Sigma_\Lambda(\boldsymbol{k})\,. \tag{2.28}$$

By construction, the constant part of the rescaled self-energy is given by

$$\Gamma^{(2)}_\ell(0) = \frac{\tilde{u}_\ell}{3}\tilde{M}^2_\ell = \frac{Z_\ell}{\Lambda^2}\frac{u_\Lambda}{3}M^2_\Lambda\,. \tag{2.29}$$

The flow of $\Gamma^{(2)}_\ell(0)$ is thus determined by the flow of $\tilde{M}^2_\ell$ and $\tilde{u}_\ell$, which in our truncation is given by

$$\partial_\ell \tilde{M}^2_\ell = (D-2+\eta_\ell)\tilde{M}^2_\ell + 3\int_{\boldsymbol{q}} \dot{\mathcal{G}}_\ell(\boldsymbol{q}), \tag{2.30}$$

$$\partial_\ell \tilde{u}_\ell = (4-D-2\eta_\ell)\tilde{u}_\ell + 3\tilde{u}^2_\ell \int_{\boldsymbol{q}} \dot{\mathcal{G}}_\ell(\boldsymbol{q})\mathcal{G}_\ell(\boldsymbol{q})\,, \tag{2.31}$$

where

$$\int_{\boldsymbol{q}} = \frac{1}{\Omega_D}\int d^D q. \tag{2.32}$$

In order to calculate the anomalous dimension η_ℓ we need the momentum dependent part of the rescaled self-energy,

$$\gamma_\ell(\boldsymbol{k}) = \Gamma^{(2)}_\ell(\boldsymbol{k}) - \Gamma^{(2)}_\ell(0), \tag{2.33}$$

which satisfies the flow equations

$$\partial_\ell \gamma_\ell(\boldsymbol{k}) = (2-\eta_\ell - \boldsymbol{k}\cdot\nabla_{\boldsymbol{k}})\gamma_\ell(\boldsymbol{k}) + \dot{\gamma}_\ell(\boldsymbol{k}), \tag{2.34}$$

where

$$\dot{\gamma}_\ell(\boldsymbol{k}) = \tilde{u}^2_\ell \tilde{M}^2_\ell \int_{\boldsymbol{q}} \dot{\mathcal{G}}_\ell(\boldsymbol{q})[\mathcal{G}_\ell(\boldsymbol{k}+\boldsymbol{q}) - \mathcal{G}_\ell(\boldsymbol{q})]\,. \tag{2.35}$$

In accordance with equation (2.17), the low-momentum behavior of the rescaled self-energy $\Gamma_\ell(\boldsymbol{q})$ is given by expansion

$$\Gamma_\ell(\boldsymbol{k}) \approx \tilde{r}_\ell + \boldsymbol{k}^2(1-Z_\ell) \tag{2.36}$$

with $\tilde{r}_\ell = \frac{1}{3}\tilde{u}_\ell\tilde{M}^2_\ell$. By expanding both sides of equation (2.34) to the second order in $\boldsymbol{k}$, the flowing anomalous dimension can be expressed in terms of the rescaled self-energy

$$\eta_\ell = \frac{1}{2}\left.\frac{\partial^2\dot{\gamma}_\ell(\boldsymbol{k})}{\partial\boldsymbol{k}^2}\right|_{\boldsymbol{k}=0}. \tag{2.37}$$

Flow equations (2.30) and (2.31) of relevant coupling parameters and expression (2.37) for the anomalous dimension form a closed system of integro-differential equations. In order to solve them we need to specify the regularization scheme. Below, we shall consider two main schemes. The first scheme employes a sharp momentum cutoff regulator function, while the second one uses a smooth additive regulator.

2.2 Probing sharp-cutoff regularization scheme

Within the sharp-cutoff regularization scheme, the Green function of interacting system at momenta $|\boldsymbol{k}| < \Lambda_0 \to \infty$ is given by [13]

$$G_\Lambda(\boldsymbol{k}) = \frac{\Theta(|\boldsymbol{k}| - \Lambda)}{\boldsymbol{k}^2 + \Sigma_\Lambda(\boldsymbol{k})}, \tag{2.38}$$

and the corresponding single-scale propagator by

$$\dot{G}_\Lambda(\boldsymbol{k}) = -\frac{\delta(|\boldsymbol{k}| - \Lambda)}{\Lambda^2 + \Sigma_\Lambda(\boldsymbol{k})}. \tag{2.39}$$

After rescaling all quantities we obtain for the propagators

$$\mathcal{G}_\ell(\boldsymbol{q}) = \frac{\Theta(|\boldsymbol{q}| - 1)}{Z_\ell \boldsymbol{q}^2 + \Gamma_\ell(\boldsymbol{q})}, \tag{2.40}$$

$$\dot{\mathcal{G}}_\ell(\boldsymbol{q}) = -\frac{\delta(1 - |\boldsymbol{q}|)}{Z_\ell + \Gamma_\ell(\hat{\boldsymbol{q}})}, \tag{2.41}$$

where $\hat{\boldsymbol{q}}$ denotes a unit vector. The momentum integrals in equations (2.30) and (2.31) can be carried out analytically and we obtain

$$\partial_\ell \tilde{M}_\ell^2 = (D - 2 + \eta_\ell)\tilde{M}_\ell^2 - \frac{3}{Z_\ell + \Gamma_\ell(1)}, \tag{2.42}$$

$$\partial_\ell \tilde{u}_\ell = (4 - D - 2\eta_\ell)\tilde{u}_\ell - \frac{3}{2}\frac{\tilde{u}_\ell^2}{(Z_\ell + \Gamma_\ell(1))^2}, \tag{2.43}$$

where we used the Morris lemma [13]

$$\delta(x) f(\Theta(x)) = \delta(x) \int_0^1 dt f(t). \tag{2.44}$$

Furthermore, we used the following identity for the angular integration

$$\frac{\Omega_{D-1}}{\Omega_D} \int_0^\pi d\theta \left(\sin(\theta)\right)^{D-2} = S_0 \int_{-1}^1 dy \left(1 - y^2\right)^{\frac{1}{2}(D-3)} = 1, \tag{2.45}$$

with $y = \cos(\theta)$ and

$$S_0 = \frac{\Omega_{D-1}}{\Omega_D}. \tag{2.46}$$

It turns out that the truncation (2.36) for the rescaled self-energy is not sufficient once the sharp-cutoff regulator is chosen. In fact, the leading order in the expansion of $\dot{\gamma}_\ell(\boldsymbol{k})$ is proportional to $|\boldsymbol{k}| = k$, as it can be seen from the following calculation in $D > 1$:

$$\tilde{u}_\ell^2 \tilde{M}_\ell^2 \frac{\partial}{\partial k} \int\limits_{\boldsymbol{q}} \dot{\mathcal{G}}_\ell(\boldsymbol{q}) \mathcal{G}_\ell(\boldsymbol{k}+\boldsymbol{q}) \Bigg|_{k=0} = \tag{2.47a}$$

$$-\tilde{u}_\ell^2 \tilde{M}_\ell^2 \frac{\partial}{\partial k} \int\limits_{\boldsymbol{q}} \frac{\delta(1-|\boldsymbol{q}|)}{1+\tilde{r}_\ell} \frac{\Theta(|\boldsymbol{k}+\boldsymbol{q}|-1)}{(\boldsymbol{k}+\boldsymbol{q})^2+\tilde{r}_\ell} \Bigg|_{k=0} = \tag{2.47b}$$

$$-\frac{\tilde{u}_\ell^2 \tilde{M}_\ell^2}{1+\tilde{r}_\ell} S_0 \int\limits_0^\infty dq\; q^{D-1}\; \delta(1-q) \;\times$$

$$\frac{\partial}{\partial k} \int\limits_{-1}^{1} dy\; (1-y^2)^{\frac{1}{2}(D-3)}\; \frac{\Theta((\boldsymbol{k}+\boldsymbol{q})^2-1)}{(\boldsymbol{k}+\boldsymbol{q})^2+\tilde{r}_\ell} \Bigg|_{k=0} = \tag{2.47c}$$

$$-\frac{2\tilde{u}_\ell^2 \tilde{M}_\ell^2}{1+\tilde{r}_\ell} S_0 \int\limits_{-1}^{1} dy\; (1-y^2)^{\frac{1}{2}(D-3)} (k+y) \;\times$$

$$\left\{ \frac{\delta(1-(\boldsymbol{k}+\hat{\boldsymbol{q}})^2)}{(\boldsymbol{k}+\hat{\boldsymbol{q}})^2+\tilde{r}_\ell} - \frac{\Theta((\boldsymbol{k}+\hat{\boldsymbol{q}})^2-1)}{((\boldsymbol{k}+\hat{\boldsymbol{q}})^2+\tilde{r}_\ell)^2} \right\} \Bigg|_{k=0} = \tag{2.47d}$$

$$-\frac{\tilde{u}_\ell^2 \tilde{M}_\ell^2}{(1+\tilde{r}_\ell)^2} S_0 \int\limits_{-1}^{1} dy\; (1-y^2)^{\frac{1}{2}(D-3)} \left(1+\frac{y}{k}\right) \delta\left(y+\frac{k}{2}\right) \Bigg|_{k=0} +$$

$$\frac{2\tilde{u}_\ell^2 \tilde{M}_\ell^2}{1+\tilde{r}_\ell} S_0 \int\limits_{-1}^{1} dy\; (1-y^2)^{\frac{1}{2}(D-3)} (k+y) \frac{\Theta\left(y+\frac{k}{2}\right)}{((\hat{\boldsymbol{q}}+\boldsymbol{k})^2+\tilde{r}_\ell)^2} \Bigg|_{k=0} = \tag{2.47e}$$

$$-\frac{1}{2} \frac{\tilde{u}_\ell^2 \tilde{M}_\ell^2}{(1+\tilde{r}_\ell)^2} \left\{ S_0 - \frac{4S_1}{1+\tilde{r}_\ell} \right\} \neq 0, \tag{2.47f}$$

where $S_1 = \dfrac{S_0}{D-1}$. Note that vertices $\Gamma_\ell(\boldsymbol{k})$ entering propagators $\mathcal{G}_\ell(\boldsymbol{k})$ and $\dot{\mathcal{G}}_\ell(\boldsymbol{k})$ are approximated by means of the truncation (2.36). In the line (2.47c) we replaced $\Theta(|\boldsymbol{k}+\boldsymbol{q}|-1)$ by $\Theta((\boldsymbol{k}+\boldsymbol{q})^2-1)$, which is allowed by condition $|\boldsymbol{k}+\boldsymbol{q}| \geqslant 0$ and in the line (2.47e) $\Theta(k^2+2ky)$ by $\Theta\,(y+k/2)$, which does not change anything in the logic.

The coupling parameter of the linear term x_Λ has the scaling dimension 1 and is relevant in all dimensions. Therefore, it must be taken into account in the low-momentum truncation of the self-energy which thus becomes non-analytic,

$$\Gamma_\ell(\boldsymbol{k}) \approx \tilde{r}_\ell + \tilde{x}_\ell |\boldsymbol{k}| + \boldsymbol{k}^2 (1-Z_\ell). \tag{2.48}$$

The RG-flow equation for the parameter $\tilde{x}_\ell$ is as follows:

$$\begin{aligned}\partial_\ell \tilde{x}_\ell &= (1-\eta_\ell)\tilde{x}_\ell + \tilde{u}_\ell^2 \tilde{M}_\ell^2 \frac{\partial}{\partial k} \int\limits_{\boldsymbol{q}} \dot{\mathcal{G}}_\ell(\boldsymbol{q}) \mathcal{G}_\ell(\boldsymbol{k}+\boldsymbol{q}) \Bigg|_{k=0} \\ &= (1-\eta_\ell)\tilde{x}_\ell - \frac{1}{2} \frac{\tilde{u}_\ell^2 \tilde{M}_\ell^2}{(1+\tilde{x}_\ell+\tilde{r}_\ell)^2} \left\{ S_0 - S_1 \frac{2(2+\tilde{x}_\ell)}{1+\tilde{x}_\ell+\tilde{r}_\ell} \right\}, \end{aligned} \tag{2.49}$$

where we followed the path sketched by equations (2.47a)-(2.47f) while deriving inhomogeneous part. In order to close the system of ordinary differential equations (2.42), (2.43) and (2.49) we need an explicit expression for the flowing anomalous dimension η_ℓ. It can be found by using definition (2.37). Following the guideline given by equations (2.47a)-(2.47f) we find after laborious calculations

$$\eta_\ell = \frac{1}{4} \frac{\tilde{u}_\ell^2 \tilde{M}_\ell^2}{(1+\tilde{x}_\ell+\tilde{r}_\ell)^3} \left\{ 2 + \tilde{x}_\ell - \frac{1}{D} \left(\tilde{x}_\ell + \frac{2(2+\tilde{x}_\ell)^2}{1+\tilde{x}_\ell+\tilde{r}_\ell} \right) \right\}. \tag{2.50}$$

There are two fixed points in the physical relevant octant of the parameter space delimited by the non-negative valued $\tilde{M}_\ell^2$, $\tilde{u}_\ell$ and $\tilde{x}_\ell$: the Gaussian fixed point at vanishing interaction $\tilde{u}$ and $\tilde{x}$ and finite magnetization $\tilde{M}_G^2$, and the Wilson-Fisher fixed point at finite positive $\tilde{M}_\star^2$, $\tilde{u}_\star$ and $\tilde{x}_\star$. Below we list these values for different dimensions D:

	$D=2$	$D=3$	$D=4-\epsilon$
$\tilde{M}_\star^2$	0.1322	1.19495	$\frac{3}{2}+\frac{\epsilon}{4}+\mathcal{O}(\epsilon^2)$
$\tilde{u}_\star$	533.901	2.56502	$\frac{2\epsilon}{3}+\mathcal{O}(\epsilon^2)$
$\tilde{x}_\star$	9.822	0.22329	$\sim \epsilon^2$
$\eta_\star$	0.66	0.118	$\frac{\epsilon^3}{36}+\mathcal{O}(\epsilon^4)$

Since in the vicinity of the fixed point and for small ϵ we have $\partial_\ell \tilde{x}_\ell \sim \tilde{u}_\ell^2 \tilde{M}_\ell^2$, it can be omitted in ϵ-expansion. The value of the anomalous dimension $\eta_\star$ at the Wilson-Fisher fixed point may be taken as a control parameter of how good our approximation is. The established values for $O(1)$-universality class are: $\eta_\star = 0.25$ in $D=2$ (exact Osanger solution [7]), $\eta_\star = 0.0334 - 0.0374$ in $D=3$ (field theoretical 7-loop calculation and Monte-Carlo simulations [38]) and $\eta_\star = \frac{\epsilon^2}{54}$ for $D=4-\epsilon$ (calculated by Wilson and Fisher in [24, 23]). While in $D=2$ and $D=3$ our results are at least of the same order with established ones and compare well with results obtained by different authors in the

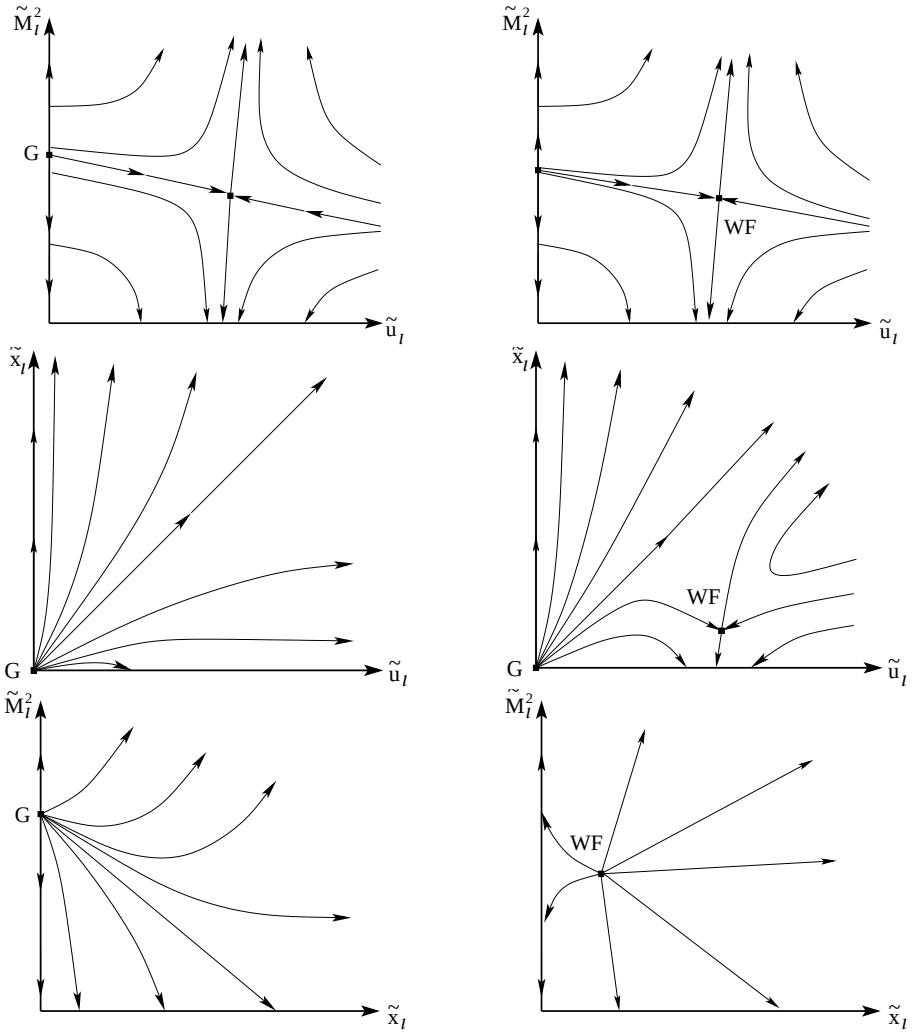

Figure 2.1: Qualitative visualization of the RG-flow in the three dimensional parameter space for $2 < D < 4$. The figures in the left column show the flow projections onto the planes $\{\hat{e}_{\tilde{M}^2}, \hat{e}_{\tilde{u}}, 0\}$, $\left\{\tilde{M}^2_G, \hat{e}_{\tilde{u}}, \hat{e}_{\tilde{x}}\right\}$ and $\{\hat{e}_{\tilde{M}^2}, 0, \hat{e}_{\tilde{x}}\}$ respectively, where $\hat{e}_i$ represents a unit vector pointing in the i-th direction. The figures in the right column show flow projections onto the planes $\left\{\hat{e}_{\tilde{M}^2}, \hat{e}_{\tilde{u}}, \tilde{x}_{WF}\right\}$, $\{\tilde{u}_{WF}, \hat{e}_{\tilde{u}}, \hat{e}_{\tilde{x}}, \}$ and $\left\{\hat{e}_{\tilde{M}^2}, \tilde{u}_{WF}, \hat{e}_{\tilde{x}}\right\}$, respectively. Subscripts G and WF denote the Gaussian and Wilson-Fisher fixed points.

lowest order local potential approximation [62, 63], our calculation predicts an entirely different behavior for $D \lesssim 4$. However, as we will see later, this unsatisfactory result is just an artefact of the sharp-cutoff regularization scheme.

Let us explore the stability properties of the fixed points. The key quantity for such an investigation is the Lyapunov dynamical or stability matrix (see for instance [57, 58]). Due to the Lyapunov stability criterion, a fixed point is stable or attractive, if real parts of eigenvalues of the dynamical matrix taken at the fixed point are negative. In this case, the direction of the flow is toward the fixed point. If real parts of eigenvalues are positive, then the fixed point is unstable or repulsive. In this case, the direction of the flow is away from the fixed point. If the dynamical matrix has both positive and negative eigenvalues, then the fixed point represents a saddle point with both attractive and repulsive directions. If the eigenvalues have zero real parts, no statements regarding the stability of the respective fixed point can be made.

In the considered case, the dynamical matrix is defined through

$$\boldsymbol{M} = \left(\begin{array}{ccc} \dfrac{\partial(\partial_\ell \tilde{M}_\ell^2)}{\partial(\tilde{M}_\ell^2)} & \dfrac{\partial(\partial_\ell \tilde{M}_\ell^2)}{\partial \tilde{u}_\ell} & \dfrac{\partial(\partial_\ell \tilde{M}_\ell^2)}{\partial \tilde{x}_\ell} \\ \dfrac{\partial(\partial_\ell \tilde{u}_\ell)}{\partial(\tilde{M}_\ell^2)} & \dfrac{\partial(\partial_\ell \tilde{u}_\ell)}{\partial \tilde{u}_\ell} & \dfrac{\partial(\partial_\ell \tilde{u}_\ell)}{\partial \tilde{x}_\ell} \\ \dfrac{\partial(\partial_\ell \tilde{x}_\ell)}{\partial(\tilde{M}_\ell^2)} & \dfrac{\partial(\partial_\ell \tilde{x}_\ell)}{\partial \tilde{u}_\ell} & \dfrac{\partial(\partial_\ell \tilde{x}_\ell)}{\partial \tilde{x}_\ell} \end{array} \right) \Bigg|_{\tilde{M}_\ell^2, \tilde{u}_\ell, \tilde{u}_\ell \to \tilde{M}_{FP}^2, \tilde{u}_{FP}, \tilde{u}_{FP}} \tag{2.51}$$

where quantities $\tilde{M}_{FP}^2, \tilde{u}_{FP}$ and $\tilde{u}_{FP}$ denote the fixed point values of each parameter and partial derivatives must be thought of being applied to the right-hand side of corresponding equations. In the case considered here, the eigenvalues of the stability matrix at the Gaussian fixed point in $2 < D < 4$ are always positive. The Gaussian fixed point is thus completely repulsive. On the other hand, the eigenvalues of the stability matrix at the Wilson-Fisher fixed point have both positive and negative eigenvalues. Therefore, the Wilson-Fisher fixed point represents essentially a saddle point in the three dimensional parameter space. In Figure 2.1 we qualitatively show flows projected onto the set of orthogonal cross-section planes through each fixed point. We can clearly observe the saddle point-like behavior of the flow. Most importantly, in the $\{\tilde{x}_\ell, \tilde{M}_\ell\}-$plane both fixed points are repulsive which has some consequences for our investigation.

Pursuing the goal of calculating momentum dependent correlation functions close to criticality, we need to determine the full near critical flow of all coupling parameters. For this, we have to enforce the coupling constants to stay on the critical surface by carefully adjusting starting values for each of them. The fact that the Wilson-Fisher fixed point is strongly repulsive in the $\{\tilde{x}_\ell, \tilde{M}_\ell\}-$subspace of the parameter space makes it very difficult to find appropriate initial values.

The insufficiency of the sharp-cutoff regularization scheme for the estimation of the anomalous dimension close to the upper critical dimension and the rather cumbersome fine-tuning procedure of initial values for the coupling parameters were the main reasons why we gave this up and switched to an alternative scheme. In the next section we consider the same problem redefined by means of the additive regularization scheme.

2.3 Additive regularization scheme

The difficulties which are caused by using the sharp-cutoff regulator can be avoided if we use a smooth-cutoff procedure, which we implement via an additive regulator $R_\Lambda(\boldsymbol{k})$ in the inverse propagator [38]. The cutoff dependent propagator is then

$$G_\Lambda(\boldsymbol{k}) = \frac{1}{\boldsymbol{k}^2 + \Sigma_\Lambda(\boldsymbol{k}) + R_\Lambda(\boldsymbol{k})} \,. \tag{2.52}$$

At this point, it is not necessary to completely specify the cutoff function $R_\Lambda(\boldsymbol{k})$, except that we require it to be of the form

$$R_\Lambda(\boldsymbol{k}) = (1 - \delta_{\boldsymbol{k},0})\Lambda^2 Z_\ell^{-1} R(\boldsymbol{k}^2/\Lambda^2) \,, \tag{2.53}$$

where $R(x)$ is some dimensionless function satisfying $R(\infty) = 0$ and $R(0) = 1$. The factor of $1 - \delta_{\boldsymbol{k},0}$ in equation (2.53) is introduced to satisfy this condition. Without this factor the right-hand side of equation (2.10) would contain an additional term $\partial_\Lambda[R_\Lambda(0)M_\Lambda]$. Because the RG eliminates only modes with $\boldsymbol{k} \neq 0$, the projector $1 - \delta_{\boldsymbol{k},0}$ does not affect the RG-flow at any finite $\boldsymbol{k}$, while the fluctuation of the zero mode $\Delta\phi_{\boldsymbol{k}=0}$ can be ignored in the thermodynamic limit [14]. The introduction of Z_ℓ^{-1} in equation (2.53) is necessary to preserve the reparametrization invariance of physical quantities under a rescaling of the fields [38].

For explicit analytical calculations we shall use the Litim cutoff function [41],

$$R(x) = (1 - x)\Theta(1 - x) \,. \tag{2.54}$$

Sometimes, for some numerical calculations we shall also employ the regulator introduced in [12, 38]

$$R(x) = \frac{x}{e^x - 1} \,, \tag{2.55}$$

which has the advantage of being analytic, but leads to more complicated integrals.

We define the rescaled exact propagator,

$$\mathcal{G}_\ell(\boldsymbol{q}) = \frac{\Lambda^2}{Z_\ell} G_\Lambda(\boldsymbol{k}) = \frac{1}{Z_\ell \boldsymbol{q}^2 + \Gamma_\ell^{(2)}(\boldsymbol{q}) + R(\boldsymbol{q}^2)} \,, \tag{2.56}$$

and the corresponding single-scale propagator

$$\dot{\mathcal{G}}_\ell(\boldsymbol{q}) = \dot{R}_\ell(\boldsymbol{q})\mathcal{G}_\ell^2(\boldsymbol{q}), \tag{2.57}$$

where

$$\dot{R}_\ell(\boldsymbol{q}) = -\frac{Z_\ell}{\Lambda}\partial_\Lambda R_\Lambda(\boldsymbol{k}) = -(2 - \eta_\ell)R(\boldsymbol{q}^2) + 2\boldsymbol{q}^2 R'(\boldsymbol{q}^2). \tag{2.58}$$

Here $R'(x) = dR(x)/dx$ and η_ℓ is the flowing anomalous dimension defined in equation (2.27). For the Litim cutoff $R'(x) = -\Theta(1 - x)$, so that

$$\dot{R}_\ell(\boldsymbol{q}) = [-2 + \eta_\ell(1 - \boldsymbol{q}^2)]\Theta(1 - \boldsymbol{q}^2). \tag{2.59}$$

In contrast to the sharp-cutoff scheme, the leading term in the expansion of $\dot{\gamma}_\ell(\boldsymbol{q})$ (2.35) is proportional to $\boldsymbol{q}^2$, if the Litim regulator (2.54) or the analytic regulator (2.55) is employed. In this case, the expansion of the right-hand side of equation (2.35) for small $\boldsymbol{q}$ yields for the flowing anomalous dimension

$$\begin{aligned}\eta_\ell &= -\tilde{u}_\ell^2\tilde{M}_\ell^2\int_{\boldsymbol{q}}\dot{\mathcal{G}}_\ell(\boldsymbol{q})\Big\{\mathcal{G}_\ell^2(\boldsymbol{q})[1+R'(\boldsymbol{q}^2)]\\ &\quad+\frac{\boldsymbol{q}^2}{D}\left[2\mathcal{G}_\ell^2(\boldsymbol{q})R''(\boldsymbol{q}^2)-4\mathcal{G}_\ell^3(\boldsymbol{q})[1+R'(\boldsymbol{q}^2)]^2\right]\Big\},\end{aligned} \tag{2.60}$$

where $R''(x)=d^2R(x)/dx^2$. For the Litim cutoff $R''(x)=\delta(1-x)$.

In the simplest self-consistent approximation we expand the momentum dependent part $\gamma_\ell(\boldsymbol{q})$ of the two-point vertex on the right-hand side of our flow equations (2.30, 2.31, 2.34) to the first order in $\boldsymbol{q}^2$. Since by definition

$$Z_\ell = 1-\left.\frac{\partial\Gamma_\ell^{(2)}(\boldsymbol{q})}{\partial\boldsymbol{q}^2}\right|_{\boldsymbol{q}^2=0} = 1-\left.\frac{\partial\gamma_\ell(\boldsymbol{q})}{\partial\boldsymbol{q}^2}\right|_{\boldsymbol{q}^2=0}, \tag{2.61}$$

this enables us to approximate the propagator on the right-hand side of the flow equations (2.30, 2.31, 2.34) by

$$\mathcal{G}_\ell(\boldsymbol{q})\approx\frac{1}{\boldsymbol{q}^2+\tilde{r}_\ell+R(\boldsymbol{q}^2)}, \tag{2.62}$$

where

$$\tilde{r}_\ell=\Gamma_\ell^{(2)}(0)=\frac{\tilde{u}_\ell}{3}\tilde{M}_\ell^2, \tag{2.63}$$

see equation (2.29). The resulting system of flow equations for the coupling parameters $\tilde{M}_\ell^2$ and $\tilde{u}_\ell$ together with the flow equation $\partial_\ell Z_\ell=-\eta_\ell Z_\ell$ for Z_ℓ are equivalent to the quartic approximation for the effective potential with wave-function renormalization [38]. Using the Litim cutoff (2.54), equations (2.30) and (2.31) become

$$\partial_\ell\tilde{M}_\ell^2=(D-2+\eta_\ell)\tilde{M}_\ell^2-\frac{6(2+D-\eta_\ell)}{D(D+2)}\mathcal{G}_\ell^2(0), \tag{2.64}$$

$$\partial_\ell\tilde{u}_\ell=(4-D-2\eta_\ell)\tilde{u}_\ell-\frac{6(2+D-\eta_\ell)}{D(D+2)}\tilde{u}_\ell^2\mathcal{G}_\ell^3(0), \tag{2.65}$$

where $\mathcal{G}_\ell(0)\approx\left[1+\tilde{r}_\ell\right]^{-1}$ is the rescaled propagator at zero momentum. Moreover, with the Litim cutoff the flowing anomalous dimension (2.60) is simply

$$\eta_\ell=\frac{1}{D}\tilde{u}_\ell^2\tilde{M}_\ell^2\mathcal{G}_\ell^4(0). \tag{2.66}$$

Equations (2.64–2.66) form a closed system of differential equations for $\tilde{M}_\ell^2$, $\tilde{u}_\ell$ and η_ℓ which can easily be solved numerically. To find the flow along the critical surface we need to fine-tune carefully the initial values $\tilde{u}_0$ and $\tilde{M}_0^2$. A typical flow of the rescaled

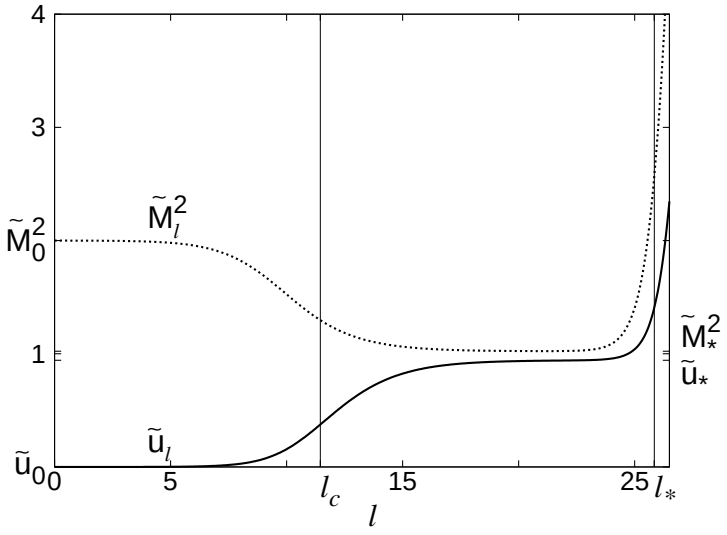

Figure 2.2: A typical near critical flow of the coupling parameters $\tilde{M}_\ell^2$ and $\tilde{u}_\ell$ obtained from equations (2.64) and (2.65) in $2 < D < 3$

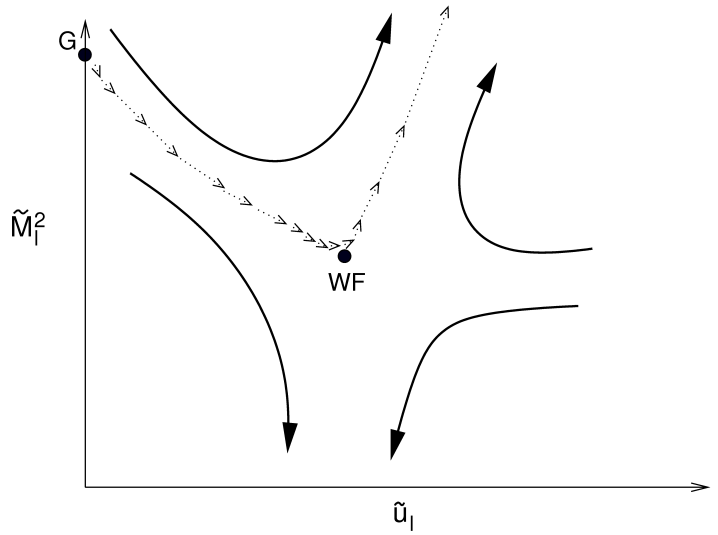

Figure 2.3: Qualitative flow diagram for the coupling parameters $\tilde{u}_\ell$ and $\tilde{M}_\ell^2$ corresponding to Figure 2.2. The size of the arrows represents the velocity of the flow. The dots mark the Gaussian fixed point (G) and the Wilson-Fisher fixed point (WF).

parameters as a function of ℓ is shown in Figure 2.2. In Figure 2.3 we show the flow schematically in the $\left\{\tilde{u}_\ell, \tilde{M}_\ell^2\right\}$ −plane.

The Wilson-Fisher fixed point in $D = 3$ is in this approximation at $\tilde{u}_\star \approx 0.942$ and $\tilde{M}_\star^2 \approx 1.022$. As can be seen in Figure 2.2, the coupling parameters initially flow very slowly and stay close to their initial values in the vicinity of the Gaussian fixed point. At a characteristic scale ℓ_c they are rapidly attracted by the Wilson-Fisher fixed point, where the flow is again almost stationary. Finally, at the scale $\ell_\star$ all non-critical RG trajectories rapidly move away from the Wilson-Fisher point attracted either by the ferromagnetic fixed point, which is characterized by infinite magnetization $\tilde{M}^2$, or by the paramagnetic fixed point with zero magnetization, where the symmetry of the system gets restored. In our case we chose the initial conditions for the coupling parameters slightly above the critical surface, so that the flow moves toward the ferromagnetic fixed point with the ℓ-dependence of the coupling parameters $\tilde{u}_\ell$ and $\tilde{M}_\ell^2$ determined by their scaling dimensions, $\tilde{u}_\ell \propto e^{\epsilon\ell}$, where $\epsilon = 4 - D$ and $\tilde{M}_\ell^2 \propto e^{(D-2)\ell}$; the flow of the unrescaled coupling parameters u_Λ and M_Λ^2 in this regime stops. Figure 2.4 shows flowing anomalous dimension η_ℓ as it follows from equation (2.66). The wave-function renormalization factor Z_ℓ calculated from

$$Z_\ell = \exp\left\{-\int_0^\ell dt\ \eta_t\right\} \tag{2.67}$$

is shown in Figure 2.5. The last graph shows very clearly that the both scales basically delimit the critical region, since Z_ℓ remains constant for both $\ell < \ell_c$ and $\ell > \ell_\star$.

What does determine the two characteristic scales ℓ_c and $\ell_\star$? The momentum scale $k_c = \Lambda_0 e^{-\ell_c}$ associated with ℓ_c measures the size of the Ginzburg critical region. For small initial values $\tilde{u}_0$ the logarithmic scale ℓ_c is given by [42, 59, 60, 61]

$$\ell_c \approx \frac{1}{\epsilon} \ln\left(\frac{\tilde{u}_\star}{\tilde{u}_0}\right), \tag{2.68}$$

where $\tilde{u}_\star$ is the value of $\tilde{u}_\ell$ at the Wilson-Fisher fixed point. This scale can be derived from equations (2.64) and (2.65) by approximating $\mathcal{G}_\ell(0) \approx 1$ and $\eta_\ell \approx 0$. In the intermediate regime $\ell_c \lesssim \ell \lesssim \ell_\star$ the flowing $\tilde{M}_\ell^2$ can then be replaced by a constant

$$\tilde{M}_\ell^2 \approx \tilde{M}_\star^2 = \frac{6}{D(D-2)}, \tag{2.69}$$

while for all ℓ the solution of equation (2.65) can be approximated by

$$\frac{\tilde{u}_\ell}{\tilde{u}_\star} \approx \frac{1}{e^{\epsilon(\ell_c - \ell)} + 1}, \tag{2.70}$$

where $\tilde{u}_\star = D\epsilon/6$. The numerically obtained flow shown in Figure 2.2 further reveals that the scale ℓ_c is also characteristic for the ℓ-dependence of $\tilde{M}_\ell^2$.

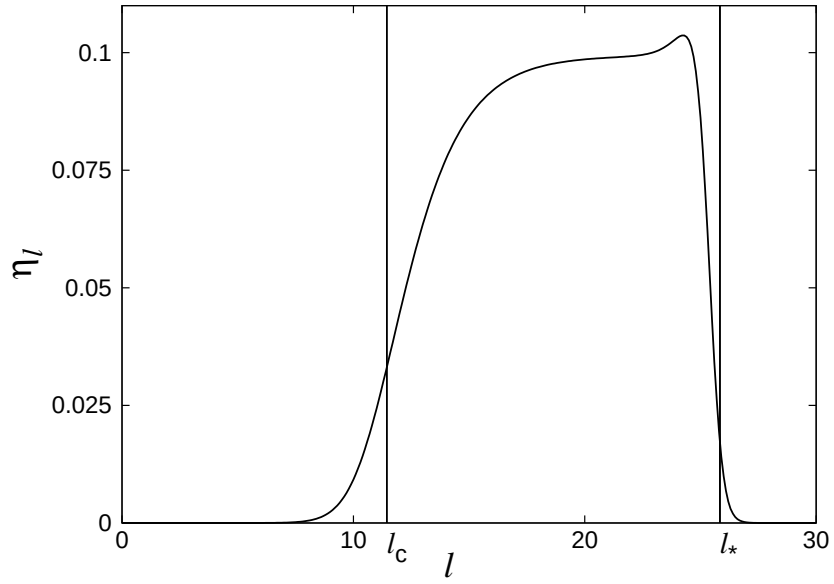

Figure 2.4: Nearly-critical flowing anomalous dimension η_ℓ calculated for $2 < D < 4$, corresponding to the flow from Figure 2.2.

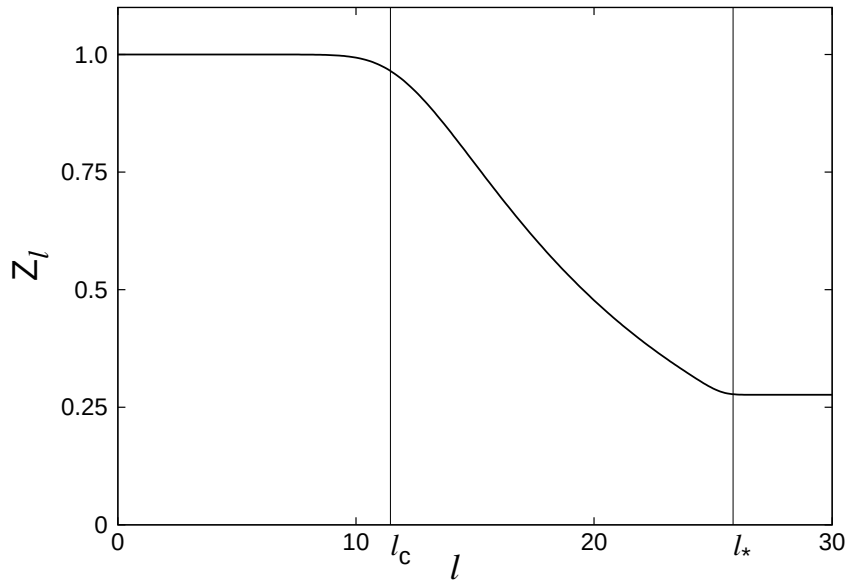

Figure 2.5: Wave-function renormalization factor Z_ℓ in $2 < D < 4$, corresponding to the flow from Figure 2.2.

Non-critical flows which describe the system at $T < T_c$ eventually obey

$$\frac{\tilde{M}_\ell^2}{\tilde{M}_\star^2} \gg \mathcal{G}_\ell^2(0), \tag{2.71a}$$

and

$$\frac{\tilde{u}_\star}{\tilde{u}_\ell} \gg \mathcal{G}_\ell^3(0). \tag{2.71b}$$

In this case the solutions for $\tilde{M}_\ell^2$ and $\tilde{u}_\ell$ depend exponentially on ℓ, corresponding to trivial scaling. The unrescaled variables u_Λ and M_Λ^2 then approach finite limits and also the physical correlation length ξ, which is defined via [45]

$$\xi^{-2} = \lim_{\Lambda\to 0}[Z_\Lambda \Sigma_\Lambda(0)], \tag{2.72}$$

remains finite. The scale $\ell_\star$ in Figures 2.2, 2.4 and 2.5 is related to ξ via $\xi^{-1} = \Lambda_0 e^{-\ell_\star}$ or equivalently

$$2\ell_\star = -\ln\left[\lim_{\ell\to\infty} e^{-2\ell}\Gamma_\ell^{(2)}(0)\right]. \tag{2.73}$$

Critical exponents may be obtained from the flow linearized around the Wilson-Fisher fixed point. The table below shows our results for critical exponents $\eta_\star$ and $\nu_\star$ calculated in different dimensions and compares them with the results from the exact calculation for $D = 2$ [7], Monte-Carlo simulation for $D = 3$ (chapter 4 in [38]) and ϵ-expansion to the leading order [24, 23]. Very similar results are obtained using the analytic cutoff (2.55).

	$D=2$	$D=3$	$D=4-\epsilon$		$D=2$	$D=3$	$D=4-\epsilon$
$\eta_\star$	0.462	0.0993	$\frac{\epsilon^2}{12}$	η	0.25	0.037	$\frac{\epsilon^2}{54}$
$\nu_\star$	0.403	0.553	$\left(2-\frac{\epsilon}{3}\right)^{-1}$	ν	1.00	0.64	$\left(2-\frac{\epsilon}{3}\right)^{-1}$

The poor comparison of our results to the established values can be traced to the low order truncation of our effective potential (2.13), see [51, 62, 63]. This clearly shows the limitations of a low-order effective potential approximation.

Of course, one could easily improve the approximations presented here. A straightforward extension would be to truncate the effective potential U_{eff} in equation (2.12) at some higher order $n > 2$,

$$U_{\text{eff}}[\tilde{\phi}^2] \approx \sum_{m=2}^{n} \frac{u_\Lambda^{(m)}}{(2m)!}\left[\tilde{\phi}^2 - M_\Lambda^2\right]^m. \tag{2.74}$$

To arrive at the flow equations of the parameters $u_\Lambda^{(2)}, \ldots, u_\Lambda^{(n)}$ one would need to take into account the flow equation of the lowest n vertices of a field expansion. We have done so up to $n = 5$; a significant improvement of the critical exponents $\eta_\star$ and $\nu_\star$ in the Ising model would however require approximately $n = 10$, as is known from previous investigations of the derivative expansion [62].

2.4 FRG-enhanced perturbation theory

So far we have truncated the self-energy retaining only its marginal and relevant parts. This is a good approximation for small momenta k. On the other hand, for large k this approximation cannot correctly reproduce the momentum dependence of the self-energy which arises from perturbation theory. To the leading order in the relevant dimensionless bare coupling $\bar{u}_0 = u_{\Lambda_0}\xi^{4-D}$, the perturbative momentum dependence of $\Sigma(\boldsymbol{k})$ in the broken symmetry phase is given by [45]

$$\Sigma(\boldsymbol{k}) - \Sigma(0) = \xi^{-2}\Delta\sigma_0^-(k\xi), \tag{2.75}$$

with

$$\Delta\sigma_0^-(x) = \frac{3\bar{u}_0}{2}[\chi(0) - \chi(x)] + O(\bar{u}_0^2), \tag{2.76}$$

where

$$\chi(p) = \int \frac{d^D p'}{(2\pi)^D} \frac{1}{[\boldsymbol{p}'^2 + 1][(\boldsymbol{p}' + \boldsymbol{p})^2 + 1]}. \tag{2.77}$$

Equations (2.75–2.77) are only accurate sufficiently far away from the critical point, where the correlation length ξ and the relevant dimensionless coupling $\bar{u}_0 = u_{\Lambda_0}\xi^{4-D}$ are small.

We now present an improved approximation for the momentum dependent self-energy which we call *FRG-enhanced perturbation theory*, since it embeds the perturbative expansion into a functional renormalization [64] such that it reproduces exactly the leading order perturbative behavior for large $\boldsymbol{k}$. However, in contrast to perturbation theory, FRG-enhanced perturbation theory does not suffer from any divergences; it yields an explicit description of the entire crossover to the critical regime and gives reasonable results even at the critical point.

Quite generally, the physical self-energy can be written as an integral over the entire RG trajectory [45],

$$\Sigma(\boldsymbol{k}) - \Sigma(0) = \Lambda_0^2 \int_0^\infty d\ell \; e^{-2\ell + \int_0^\ell d\tau \eta_\tau} \dot{\gamma}\big(e^\ell \boldsymbol{k}/\Lambda_0\big), \tag{2.78}$$

where $\Sigma(0) = Z^{-1}\xi^{-2}$, with Z denoting the wave-function renormalization at the end of the flow. In general, the expression for the inhomogeneity $\dot{\gamma}(\boldsymbol{q})$ will depend also on the momentum dependent parts of the three- and four-point irreducible vertices, as can be inferred from equation (2.8). To make progress we employ the truncation (2.11a-2.11c) which leads to the approximation (2.35) for the inhomogeneity $\dot{\gamma}(\boldsymbol{q})$. Only the momentum independent parts of the three- and four point vertices enter equation (2.78) and $\dot{\gamma}(\boldsymbol{q})$ is then completely determined by the self-energy and the order parameter alone. While this greatly simplifies the calculation of the self-energy since it leads to a closed set of equations, solving equation (2.78) remains non-trivial since the solution for the self-energy must be determined self-consistently. The FRG-enhanced perturbation theory provides for a non-self-consistent approximation to the solution of equation (2.78). In

the FRG-enhanced perturbation theory, the calculation of the subtracted inhomogeneity $\dot{\gamma}(\boldsymbol{q})$ via equation (2.35) is simplified by keeping only the first two terms in a momentum expansion of the self-energy. This amounts to the substitution

$$\Gamma_\ell^{(2)}(\boldsymbol{q}) \to \Gamma_\ell^{(2)}(0) + (1 - Z_\ell)\boldsymbol{q}^2 \tag{2.79}$$

and the approximation (2.62) for the propagator on the right-hand side of equation (2.35). Within this approximation, the flow of $\tilde{M}_\ell^2$, $\tilde{u}_\ell$, and η_ℓ are determined from equations (2.64–2.66). A similar truncation strategy has been adopted in [42] for the symmetric phase of the $O(2)$-model, and in [65] to calculate the spectral function of the Tomonaga-Luttinger model. A comparison with the completely self-consistently determined self-energy is presented at the end of this section where we show that the error arising from the non-self-consistency of the FRG solution is extremely small. Perturbation theory is recovered when the flow of the running coupling parameters is approximated by their trivial ℓ-dependence arising from their scaling dimensions. The self-energy can now be expressed in terms of a two-parameter scaling function,

$$\Sigma(\boldsymbol{k}) = k_c^2 \sigma^-(x, y), \tag{2.80}$$

with $x = k\xi$ and $y = k/k_c$. The ratio of these variables is then $x/y = e^{\ell_\star - \ell_c}$. If we introduce

$$\Delta\sigma^-(x, y) = \sigma^-(x, y) - k_c^2\Sigma(0) = \sigma^-(x, y) - y^2/Zx^2, \tag{2.81}$$

this leads to

$$\begin{aligned} \Delta\sigma^-(x, y) &= \int_0^\infty dl e^{-2(\ell-\ell_c)+\int_0^\ell d\tau\eta_\tau} \dot{\gamma}_\ell(e^{l-\ell_c}y) \\ &= y^2 \int_{ye^{-\ell_c}}^\infty dp\, p^{-3} Z^{-1}_{\ell_c+\ln(p/y)} \dot{\gamma}_{\ell_c+\ln(p/y)}(p), \end{aligned} \tag{2.82}$$

where we substituted $p = ye^{\ell-\ell_c}$ and used $Z_\ell = e^{-\int_0^\ell d\tau\eta_\tau}$. The asymptotic behavior of $\dot{\gamma}_\ell(\boldsymbol{q})$ for small q is $\dot{\gamma}_\ell(\boldsymbol{q}) \approx \eta_\ell \boldsymbol{q}^2$. For large q it approaches a constant which, using the Litim cutoff, is

$$\lim_{q\to\infty} \dot{\gamma}_\ell(\boldsymbol{q}) \approx 2u_\ell^2 \tilde{M}_\ell^2 \mathcal{G}_\ell^3(0) \frac{(2 + D - \eta_\ell)}{D(D + 2)}. \tag{2.83}$$

In $D = 3$ the function $\dot{\gamma}_\ell(\boldsymbol{q})$ can be calculated analytically for the Litim cutoff. Using the Litim cutoff [41] given in equation (2.54), we can rewrite the function $\dot{\gamma}_\ell(\boldsymbol{q})$ defined in equation (2.35) as

$$\dot{\gamma}_\ell(\boldsymbol{q}) = u_\ell^2 \tilde{M}_\ell^2 \mathcal{G}_\ell^3(0) \int_{\boldsymbol{q}'} \dot{R}_\ell(\boldsymbol{q}')\Theta\big(|\boldsymbol{q}' + \boldsymbol{q}|^2 - 1\big) \frac{1 - |\boldsymbol{q}' + \boldsymbol{q}|^2}{|\boldsymbol{q}' + \boldsymbol{q}|^2 + \tilde{r}_\ell}, \tag{2.84}$$

where $\dot{R}_\ell(\boldsymbol{q})$ is defined in equation (2.59). In $D = 3$ the integration in equation (2.84) can be performed exactly. We find

$$\dot{\gamma}_\ell(\boldsymbol{q}) = \Theta(2 - q)\dot{\gamma}_\ell^<(q) + \Theta(q - 2)\dot{\gamma}_\ell^>(q), \tag{2.85}$$

where the functions $\dot{\gamma}_\ell^<(q)$ and $\dot{\gamma}_\ell^>(q)$ are defined by

$$\begin{aligned}\dot{\gamma}_\ell^<(q) &= \tilde{M}_\ell^2 u_\ell^2 \mathcal{G}_\ell^3(0)\left\{A_\ell(q) + B_\ell(q)\ln\left[\frac{\tilde{r}_\ell + (1+q)^2}{\tilde{r}_\ell + 1}\right]\right. \\ &\quad \left. - C_\ell(q)\left[\arctan\left(\frac{1}{\sqrt{\tilde{r}_\ell}}\right) - \arctan\left(\frac{1+q}{\sqrt{\tilde{r}_\ell}}\right)\right]\right\}, \qquad (2.86)\\ \dot{\gamma}_\ell^>(q) &= \tilde{M}_\ell^2 u_\ell^2 \mathcal{G}_\ell^3(0)\left\{D_\ell(q) + E_\ell(q)\ln\left[\frac{\tilde{r}_\ell + (1+q)^2}{\tilde{r}_\ell + (1-q)^2}\right]\right. \\ &\quad \left. + C_\ell(q)\left[\arctan\left(\frac{1-q}{\sqrt{\tilde{r}_\ell}}\right) + \arctan\left(\frac{1+q}{\sqrt{\tilde{r}_\ell}}\right)\right]\right\}, \qquad (2.87)\end{aligned}$$

with

$$\begin{aligned}A_\ell(q) &= \frac{1}{480}\Big\{60\,[1+\tilde{r}_\ell]\,[4-\eta_\ell(1+\tilde{r}_\ell)] - 2\eta_\ell q^5 \\ &\quad -30q\left[4-\eta_\ell+4\tilde{r}_\ell(3-2\eta_\ell)-7\eta_\ell\tilde{r}_\ell^2\right] \\ &\quad +20\eta_\ell q^2\left[5+9\tilde{r}_\ell\right] - 5q^3\left[4+\eta_\ell(17+25\tilde{r}_\ell)\right]\Big\}, \qquad (2.88)\\ B_\ell(q) &= \frac{1+\tilde{r}_\ell}{16q}\Big\{4\big[q^2-\tilde{r}_\ell-1\big] \\ &\quad +\eta_\ell\big[\tilde{r}_\ell^2+2\tilde{r}_\ell(1-3q^2)+(q^2-1)^2\big]\Big\}, \qquad (2.89)\\ C_\ell(q) &= \frac{\sqrt{\tilde{r}_\ell}}{2}\big(1+\tilde{r}_\ell\big)\big[2-\eta_\ell(1+\tilde{r}_\ell-q^2)\big], \qquad (2.90)\\ D_\ell(q) &= \frac{\eta_\ell}{5} - \frac{1}{12}\big[\eta_\ell(5+\tilde{r}_\ell)-8\big] \\ &\quad -(1+\tilde{r}_\ell)\big[1-\frac{\eta_\ell}{4}(2+3\tilde{r}_\ell-q^2)\big], \qquad (2.91)\\ E_\ell(q) &= \frac{1+\tilde{r}_\ell}{16q}\Big\{\eta_\ell - 4 + \tilde{r}_\ell\big[\eta_\ell(2+\tilde{r}_\ell)-4\big] \\ &\quad -2q^2\big[3\eta_\ell\tilde{r}_\ell+\eta_\ell-2\big] + \eta_\ell q^4\Big\}. \qquad (2.92)\end{aligned}$$

At the critical point $x \to \infty$, since the correlation length diverges, so that the scaling function reduces to the usual one-parameter form

$$\Delta\sigma^-(\infty, y) = \sigma^-(\infty, y) = \sigma_\star(y). \qquad (2.93)$$

The asymptotic behavior of the scaling function for both very small and very large y follows directly from equation (2.82). For $y \ll 1$, i. e. in the critical long wavelength regime [45], the lower limit of integration may be replaced by zero and all coupling parameters may be replaced by their fixed point values. Then we find

$$\sigma_\star(y) \approx A_D y^{2-\eta}, \qquad (2.94)$$

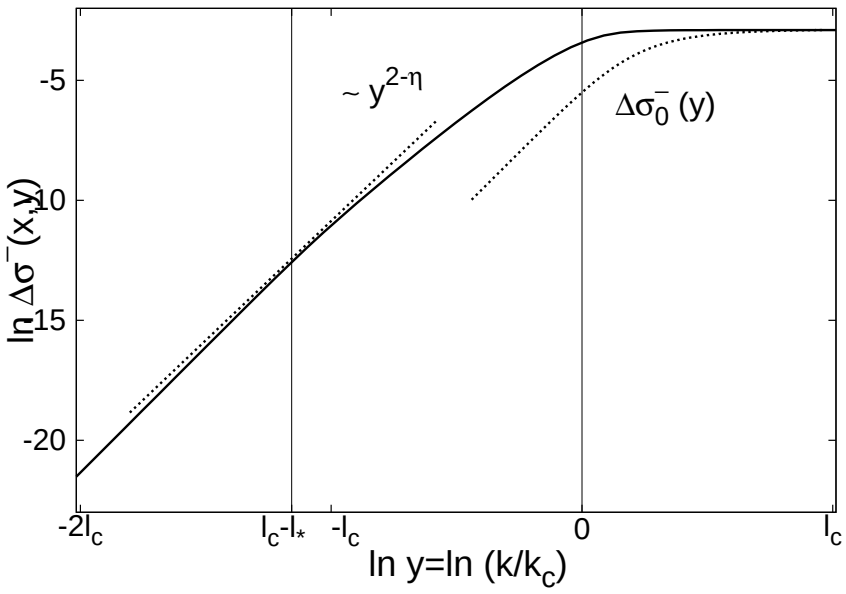

Figure 2.6: Typical behavior of the two-parameter scaling function $\Delta\sigma^-(x,y)$ defined in equation (2.82) for $x = e^{\ell_*-\ell_c}y$. The initial coupling parameters are $\tilde{u}_0 = 0.005$ and $M_0^2 = 1.9482092$, which yields $\ell_c \simeq 5.23$ and $\ell_\star \simeq 11.29$.

where η is the fixed point value of η_ℓ and

$$A_D = \int_0^\infty dp\, p^{\eta-3}\dot{\gamma}_\star(p), \tag{2.95}$$

with $\gamma_\star(p) = \lim_{\ell\to\infty}\gamma_\ell(p)$. In $D = 3$ we obtain numerically $A_3 \approx 1.075$. In the critical short wavelength regime $y \gg 1$ one may approximate all coupling parameters by their initial values. The scaling function then approaches the constant value

$$\sigma_\star(y) \approx \frac{2}{D}\tilde{u}_0^2\tilde{M}_0^2\mathcal{G}_0^3(0). \tag{2.96}$$

Such a constant plateau is expected from the structure of the truncation employed. In fact, for $k \gg k_c$ one expects that the momentum dependence of the self-energy is that of lowest order perturbation theory, see the discussion at the beginning of this subsection. However, an effective ultra-violet cutoff is now provided by k_c^{-1} which regularizes the theory in place of the correlation length ξ which is infinite at criticality. While this is indeed the leading order correction to the self-energy in an expansion in powers of the bare interaction strength, the correct form of the self-energy should further display a $\ln(k/k_c)$ dependence at large k with a prefactor which is quadratic in the bare interaction [42, 45]. The reason for the absence of such a term in the present approximation is that our truncation for the four-point vertex in equation (2.11c) does not take vertex corrections into account. In the macroscopically ordered regime $k\xi \ll 1$, we find that $\Sigma(\boldsymbol{k}) - \Sigma(0)$ vanishes as $\boldsymbol{k}^2$, as can be seen in Figure 2.6.

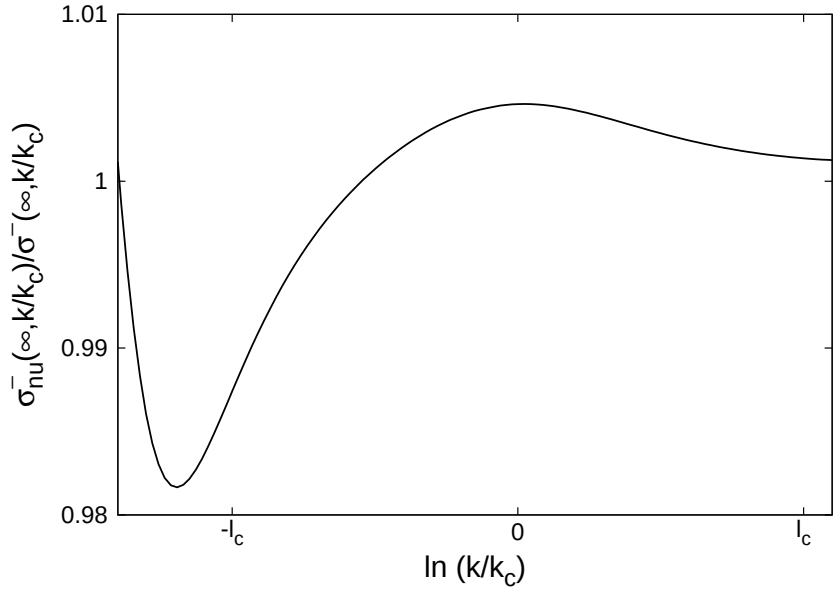

Figure 2.7: A comparison of two different approximations of the self-energy at criticality, as discussed in the text: self-consistent numerical solution $\sigma^-_{\mathrm{nu}}(\infty, k/k_c)$ of equations (2.14–2.16) and solution $\sigma^-(\infty, k/k_c)$ based on the substitution (2.79) on the right-hand sides of these flow equations.

For the present model it is of course possible to calculate the solution of the coupled integro-differential equations (2.14–2.16) exactly without any further approximations. One obtains completely self-consistent solutions for the flow of the self-energy $\Sigma_\Lambda(\boldsymbol{k})$ and the order parameter, if the truncation of the momentum dependence of Σ_Λ and G_Λ on the right-hand sides of equations (2.14–2.16) using the substitution (2.79) is omitted. A comparison of the completely self-consistent solution $\sigma^-_{\mathrm{nu}}(\infty, y)$ for the scaling function with the scaling function $\sigma^-(\infty, y)$ obtained within the FRG-enhanced perturbation theory, i. e. with the help of the substitution (2.79) on the right-hand sides of equations (2.14–2.16), is shown in Figure 2.7. Obviously, the relative error due to the substitution (2.79) is remarkably small, so that we conclude that our substitution (2.79) is quite accurate.

It is interesting to calculate the quantity

$$c_1 = -\frac{\alpha}{u_{\Lambda_0}} \int \frac{d^3k}{(2\pi)^3} \frac{\Sigma(\boldsymbol{k}) - \Sigma(0)}{\boldsymbol{k}^2 \left[\boldsymbol{k}^2 + \Sigma(\boldsymbol{k}) - \Sigma(0)\right]}. \tag{2.97}$$

For two-component fields, a similar expression is related to the interaction induced shift in the critical temperature of weakly interacting Bose gas [66]. The parameter α is defined as $\alpha = -256\pi^3\zeta(3/2)^{-4/3} \approx -2206.19$. Within our simple truncation, we obtain $c_1 \approx 0.705$, which is comparable with the field-theoretical result $c_1 \approx 1.07$ [67, 68] and FRG calculation with more sophisticated truncation $c_1 \approx 1.11$ [52, 53].

Note that our FRG-enhanced perturbation theory can also be adopted, if arbitrarily higher orders in n in the effective potential expansion (2.74) are included. This is because

within our approach the flow of the coupling parameters which parameterize the local potential depends only on the lowest order momentum expansion of the self-energy and can be calculated exactly as in the usual derivative expansion [62]. Once the flow of the local potential is known, the higher order momentum dependence of the self-energy can be determined. Of course, not all models have a structure as simple as the one discussed here which permits including arbitrarily high orders of the local potential. One may wonder whether our approach is also useful to describe more complicated systems. It is certainly expected to be useful in non-critical interacting systems, as e. g. interacting bosons in two or three dimensions, where a low order truncation of the effective action should suffice [46]. An accurate description of the momentum dependent self-energy of more complicated and possibly critical systems, such as e. g. frustrated spin models [69], is a very challenging task which we have not yet attempted. While including all orders of the local potentials would then be prohibitive, a low order truncation might yet be qualitatively correct.

2.5 Summary

In conclusion, we have applied the Functional Renormalization Group to the classical ϕ^4-model in the symmetry broken phase. Following the guideline of chapter 1 we derived RG-flow equation for the magnetization and self-energy. Restricting the consideration on the relevant coupling parameters we closed the system of flow equations. The truncation scheme which we employed combines lowest order local potential approximation with the lowest order derivative expansion. Hence, our approximation goes beyond the ones used in similar approaches [52, 53, 54, 62]. We recognized the insufficiency of the sharp-cutoff regularization scheme and performed calculations within the additive smooth-cutoff scheme. We calculated the near critical RG-flow of coupling parameters, which is determined by the interplay of two distinct length scales: the critical Ginzburg-scale, which depends on the strength of the interaction, and temperature dependent correlation length. We investigated how this scales affect the physical self-energy close to criticality. In order to do this, we developed an approximate approach which we call the FRG-enhanced perturbation theory. Finally we developed mathematical techniques which will be applied in next chapters to more sophisticated models.

3 Interacting bosons at $T = 0$

In this chapter, the FRG-formalism is applied to systems of interacting bosons at zero temperature in arbitrary spatial dimensions. The behavior of such systems is characterized by two exact relations: the Hugenholtz-Pines equality which states the absence of the energy gap in the spectrum of elementary excitations and the Nepomnyashchy-Nepomnyashchy relation which postulates the vanishing of the anomalous self-energy in the long wave length limit. We employ a new truncation scheme based on the non-locality of the interaction which satisfies both exact relations. We obtain RG-flow equations for the condensate and both normal and anomalous self-energies. These equations can be closed by means of the truncation scheme employed, which requires introducing additional coupling parameters. Flow equations for these, as well as for the interaction are also obtained. We investigate RG-flow of coupling parameters and calculate physical self-energies by taking account of this flow. Finally, the single-particle spectral density function of interacting bosons is calculated. The spectrum of elementary excitations and the damping of quasi-particles are extracted from the latter. Parts of this chapter were published in [71] and [70].

3.1 Introduction

The model of weakly interacting bosons have been studied with theoretical methods for more than half a century. Originally proposed as a toy-model for superfluid ^{4}He, the model attracted attention of several prominent physicists [4, 72, 73, 74, 75] [1]. The first qualitatively correct description of the excitation spectrum of the dilute Bose gas was given by Bogoliubov [4] within a mean-field theoretical approach. By separating zero-momentum modes of annihilation and creation operators, replacing them through the complex numbers and employing a suitable canonical transformation, Bogoliubov managed to diagonalize the quadratic part of the Hamiltonian and to calculate the spectrum of elementary excitations. The obtained spectrum was shown to have a gapless linear behavior at small momenta, which reflects the collective Goldstone-mode [15], and to approach the quadratic dispersion of free bosons at large momenta, where interaction effects become negligible. Despite the unquestionable success of the Bogoliubov theory, some points remained mysterious. As it was recognized by Bogoliubov himself, the crucial assumption of his theory, namely the replacement of annihilators and creators acting on particles in the condensate by usual complex numbers, violates the particle number conservation. This ambiguity seems to have been resolved only very recently [77, 78].

[1] For a nice historical overview see Griffin's review [76].

First applications of quantum field theoretical techniques to systems of interacting bosons were made by Beliaev already in the very early days of their history [79, 80] (see also standard text books [81, 82, 83, 84]). Again, a successful quantum field theoretical treatment of bosons at or close to zero temperature is only possible, if zero-momentum modes of field operators are considered separately from those with finite momenta. By using newly developed diagrammatic techniques, Beliaev was able not only to correctly reproduce Bogoliubov results, but also to calculate leading order corrections to the excitation spectrum. Furthermore, he was the first who managed to calculate the zero temperature damping of quasi-particles in three spatial dimensions. For the long wave length limit was shown that the quasi-particles damping increases with the fifth power of momenta and does not depend on the interaction. However, it turned out that diagrammatic series suffer from non-physical infrared (IR)-divergences [85]. Very soon after Beliaev work, Hugenholtz and Pines [16] reviewed his results and obtained an exact equality which is now commonly referred to as the Hugenholtz-Pines equality (HPE). HPE connects both normal and anomalous self-energies at zero momentum with the chemical potential and postulates the absence of the energy gap in the excitation spectrum of interacting bosons. Hugenholtz and Pines also proved that HPE holds to all orders in a perturbative expansion. The first extension to finite temperatures has been made by Popov [22] who proposed an alternative IR-divergence free effective field theory based on a hydrodynamic Hamiltonian. The extensive development of the subject was further continued in the work by Gavoret and Nozières [86] who derived low-energy asymptotic expressions for both normal and anomalous propagators. As last as at this stage, the problem of weak interacting bosons seemed to be satisfactorily solved.

The situation changed dramatically with the work by Nepomnyashchy and Nepomnyashchy [17, 87, 88] who showed by analyzing the skeleton diagram expansion of one-particle irreducible vertex functions that the anomalous self-energy must vanish at zero momenta. The obtained result is exact and cannot be reproduced by summing up perturbative series to any finite order. They also discussed infrared divergences of the normal self-energy and showed how this knowledge can be implemented to reproduce asymptotic formulas for propagators obtained by Gavoret and Nozières.

After the recent experimental breakthrough in creating Bose-Einstein condensates at extremely low temperatures [91], the field gained new attention by theorists, too. Recent measurements by using one-photon Bragg spectroscopy [92] confirmed spectacularly the Bogoliubov spectrum at all momenta. Furthermore, the transition from the weakly to strongly interacting regime in dilute Bose gases has been realized experimentally by employing Feshbach resonance techniques [93]. Since it is an essentially non-perturbative theory, the Functional Renormalization Group (FRG) offers a possible way to go beyond the description of the weak coupling regime. Recently, several authors showed how FRG can be applied to systems of interacting bosons at criticality [42, 43] and at zero temperature [95, 96, 97, 98] in spatial dimensions $1 \leqslant D \leqslant 3$. However, the efforts of these works were mainly concentrated on recovering thermodynamical observables. In this chapter we provide our view on the issue of interacting bosons. Our main interest lies in the investigation of dynamical single-particle properties which occur at finite momenta, such as the single-particle spectral density function. Surprisingly, no calculation of the

spectral density is known, which simultaneously takes both HPE and NNE into account. Our FRG-based calculation of the spectral function unifies both exact relations in one scheme in a natural way which does not require additional non- or badly-controllable assumptions.

3.2 Functional integral approach to interacting bosons

We consider a system of bosons with zero spin and mass m in an infinite $D+1-$ dimensional Euclidean volume which interact with each other through a non-local repulsive potential $u_{\Lambda_0}(X - X')$, where $X = (\boldsymbol{x}, \tau)$ with the imaginary time $\tau = it$, and Λ_0^{-1} denotes the short-distance cutoff which relates to the finite extent of interaction or, for hard-core bosons, to the size of particles. The bare Euclidean action of the model is given by the following expression

$$\begin{aligned} S[\bar{\psi}, \psi] &= \int_X \bar{\psi}_X \left(\partial_\tau - \frac{1}{2m} \partial_{\boldsymbol{x}}^2 - \mu \right) \psi_X + \frac{1}{2} \int_X \int_{X'} \bar{\psi}_X \bar{\psi}_{X'} u_{\Lambda_0} (X - X') \, \psi_X \psi_{X'} \\ &= -\int_K \bar{\psi}_K (i\omega - \epsilon_{\boldsymbol{k}} + \mu) \psi_K + \frac{1}{2} \int_K u_{\Lambda_0}(K) \rho_K \rho_{-K}, \end{aligned} \tag{3.1}$$

where $K = (\boldsymbol{k}, \omega)$ is a $D+1-$dimensional momentum with bosonic zero temperature Matsubara frequency ω and dispersion of free bosons

$$\epsilon_{\boldsymbol{k}} = \frac{k^2}{2m}. \tag{3.2}$$

The integration over K is defined by

$$\int_K \equiv \int \frac{d\omega}{2\pi} \int \frac{d^D k}{(2\pi)^D}. \tag{3.3}$$

The density operators which appear in the interaction part are given by

$$\rho_K = \int_Q \bar{\psi}_Q \psi_{Q+K} \tag{3.4}$$

and μ denotes the chemical potential.

The momentum-dependent interaction $u_{\Lambda_0}(K)$ has to obey following properties:

- It should remain finite at $K = 0$, i. e. $u_{\Lambda_0}(0) < \infty$;
- It should be symmetric with respect to the sign mirroring in the argument, i. e. $u_{\Lambda_0}(K) = u_{\Lambda_0}(-K)$. This requirement is in correspondence to the time reversal invariance of the action (3.1);

- It should be ultraviolet regularized by means of the cutoff Λ_0, i. e.

$$u_{\Lambda_0}(K) = \begin{cases} u(K) & \text{for } |\boldsymbol{k}| \leqslant \Lambda_0, \\ 0 & \text{else.} \end{cases} \tag{3.5}$$

  Hence, introducing of the ultraviolet cutoff Λ_0 essentially corresponds to the mapping of the continuous model onto the lattice with the lattice spacing Λ_0^{-1}.

The model (3.1) depends on two dimensionless parameters. First, there is a dimensionless chemical potential

$$\tilde{\mu}_0 \;=\; 2m\mu\Lambda_0^{-2}, \tag{3.6}$$

which gives the bare chemical potential μ in units of the cutoff energy $\Lambda_0^2/2m$. Secondly, there is a dimensionless interaction

$$\tilde{u}_0(K) = 2mk_\mu^{D-2}u_{\Lambda_0}(K), \tag{3.7}$$

which measures the bare interaction in units of the chemical potential related momentum $k_\mu \;=\; \sqrt{2m\mu}$, which is introduced in analogy to the Fermi-momentum in fermionic systems. Sometimes, the momentum k_μ is referred to as the inverse healing length [99].

Initially, action (3.1) remains invariant under the global gauge transformation

$$\psi_K \to e^{i\lambda}\psi_K, \tag{3.8a}$$
$$\bar{\psi}_K \to e^{-i\lambda}\bar{\psi}_K, \tag{3.8b}$$

with a real valued λ, which is known as $U(1)$-symmetry. In the $U(1)$ - symmetry broken phase, bosonic fields $\bar{\psi}$ and ψ acquire non-vanishing vacuum average values, i. e.

$$\psi_K = \Delta\psi_K + \delta_{K,0}\sqrt{\rho^0_{\Lambda_0}}, \tag{3.9a}$$
$$\bar{\psi}_K = \Delta\bar{\psi}_K + \delta_{K,0}\sqrt{\rho^0_{\Lambda_0}}, \tag{3.9b}$$

where we have assumed without loss of generality that the condensate density $\rho^0_{\Lambda_0} \in \mathbb{R}$. Setting fields (3.9a) and (3.9b) into the initial bare action (3.1) and performing some rearrangement we obtain

$$\begin{aligned} S[\Delta\bar{\psi},\Delta\psi] = &-\rho^0_{\Lambda_0}\left(\mu - \frac{1}{2}u_{\Lambda_0}\rho^0_{\Lambda_0}\right) - \sqrt{\rho^0_{\Lambda_0}}\left(\mu - u_{\Lambda_0}\rho^0_{\Lambda_0}\right)\left(\Delta\bar{\psi}_0 + \Delta\psi_0\right) \\ &-\frac{1}{2}\int\limits_K\int\limits_{K'}(\Delta\bar{\psi}_K, \Delta\psi_{-K})\begin{pmatrix} \Gamma^{(2,0)}_{\Lambda_0}(K,K') & \Gamma^{(1,1)}_{\Lambda_0}(K,K') \\ \Gamma^{(1,1)}_{\Lambda_0}(-K,-K') & \Gamma^{(0,2)}_{\Lambda_0}(K,K') \end{pmatrix}\begin{pmatrix} \Delta\bar{\psi}_{K'} \\ \Delta\psi_{-K'} \end{pmatrix} \\ &+\int\limits_{K_1}\int\limits_{K_2}\int\limits_{K_3}\left\{\Gamma^{(1,2)}_{\Lambda_0}(K_1;K_2,K_3)\Delta\bar{\psi}_{K_1}\Delta\psi_{K_2}\Delta\psi_{K_3} + \Gamma^{(2,1)}_{\Lambda_0}(K_1;K_2,K_3)\Delta\bar{\psi}_{K_3}\Delta\bar{\psi}_{K_2}\Delta\psi_{K_1}\right\} \\ &+\int\limits_{K_1}\int\limits_{K_2}\int\limits_{K_3}\int\limits_{K_4}\Gamma^{(2,2)}_{\Lambda_0}(K_1,K_2;K_3,K_4)\Delta\bar{\psi}_{K_1}\Delta\bar{\psi}_{K_2}\Delta\psi_{K_3}\Delta\psi_{K_4}, \end{aligned} \tag{3.10}$$

where $u_{\Lambda_0} = u_{\Lambda_0}(0)$. The condensate density is then fixed by demanding the vanishing of terms linear in fluctuating fields:

$$\rho^0_{\Lambda_0} = \frac{\mu}{u_{\Lambda_0}}. \tag{3.11}$$

In order to distinguish between the dilute and dense systems, it is convenient to introduce an inverse distance between particles in the condensate. We define it as [95]

$$k_{ip} \approx \frac{1}{2}\tilde{u}_{\Lambda_0}\left(\rho^0_{\Lambda_0}\right)^{1/D}, \tag{3.12}$$

where $\tilde{u}_{\Lambda_0} = \tilde{u}_{\Lambda_0}(0)$. We will call a system for which $k_{ip} \lesssim k_\mu$ dilute. A system for which $k_{ip} > k_\mu$ will be referred to as a dense system.

Irreducible vertex functions $\Gamma^{(i,j)}$ entering equation (3.10) can be extracted from this by taking functional derivatives with respect to fluctuating field parts $\Delta\bar{\psi}$ and $\Delta\psi$ at the point $\Delta\bar{\psi}, \Delta\psi = 0$. Proceeding this way we obtain for the two-point irreducible vertices following expressions:

$$\begin{aligned}
\Gamma^{(1,1)}_{\Lambda_0}(\pm K, \pm K') &= -\delta_{K,K'}\left[G_0^{-1}(\pm K) - \Sigma^N_{\Lambda_0}(\pm K)\right], && (3.13)\\
\Gamma^{(2,0)}_{\Lambda_0}(K, K') &= \Gamma^{(0,2)}_{\Lambda_0}(-K, -K') = \delta_{K,-K'}\Sigma^A_{\Lambda_0}(K), && (3.14)\\
\Gamma^{(2,0)}_{\Lambda_0}(-K, -K') &= \Gamma^{(0,2)}_{\Lambda_0}(K, K') = \delta_{K,-K'}\Sigma^A_{\Lambda_0}(-K), && (3.15)
\end{aligned}$$

where the normal inverse free propagator $G_0^{-1}(\pm K)$ is defined by

$$G_0^{-1}(\pm K) = \pm i\omega - \epsilon_{\boldsymbol{k}} + \mu, \tag{3.16}$$

while anomalous inverse free propagator does not exist. Note that both self-energies are symmetric functions regarding the sign mirroring in the argument, i. e. $\Sigma^N_{\Lambda_0}(K) = \Sigma^N_{\Lambda_0}(-K)$ and $\Sigma^A_{\Lambda_0}(K) = \Sigma^A_{\Lambda_0}(-K)$. They are found in the following form:

$$\begin{aligned}
\Sigma^N_{\Lambda_0}(\pm K) &= \rho^0_{\Lambda_0}[u_{\Lambda_0} + u_{\Lambda_0}(K)], && (3.17a)\\
\Sigma^A_{\Lambda_0}(\pm K) &= \rho^0_{\Lambda_0} u_{\Lambda_0}(K). && (3.17b)
\end{aligned}$$

For the bare vertices involving three fluctuating fields we obtain following expression

$$\begin{aligned}
&\Gamma^{(1,2)}_{\Lambda_0}(K_1; K_2, K_3) = \Gamma^{(2,1)}_{\Lambda_0}(K_1; K_2, K_3)\\
&= \delta_{K_1, K_2+K_3}\sqrt{\rho^0_{\Lambda_0}}\ \left[u_{\Lambda_0}(K_2) + u_{\Lambda_0}(K_3)\right],
\end{aligned} \tag{3.18}$$

and finally for the four-legged bare vertex

$$\Gamma^{(2,2)}_{\Lambda_0}(K_1, K_2; K_3, K_4) = \delta_{K_1+K_2;K_3+K_4}\left[u_{\Lambda_0}(K_1 - K_3) + u_{\Lambda_0}(K_1 - K_4)\right]. \tag{3.19}$$

The full propagator matrix can be obtained by inverting $2 \times 2-$matrix appearing in the second line of equation (3.10) in both Fourier- and field-space [79, 80]

$$\begin{aligned}\boldsymbol{G}_{\Lambda_0}(K) &= \begin{pmatrix} G^A_{\Lambda_0}(K) & G^N_{\Lambda_0}(K) \\ G^N_{\Lambda_0}(-K) & G^A_{\Lambda_0}(-K) \end{pmatrix} \\ &= \left[\begin{pmatrix} -\Sigma^A_{\Lambda_0}(K) & G_0^{-1}(K) - \Sigma^N_{\Lambda_0}(K) \\ G^{-1}_{\Lambda_0}(-K) - \Sigma^N_{\Lambda_0}(-K) & -\Sigma^A_{\Lambda_0}(-K) \end{pmatrix}^{-1} \right]^T \\ &= \frac{1}{\mathcal{D}(K)} \begin{pmatrix} \Sigma^A_{\Lambda_0}(-K) & G_0^{-1}(-K) - \Sigma^N_{\Lambda_0}(-K) \\ G_0^{-1}(K) - \Sigma^N_{\Lambda_0}(K) & \Sigma^A_{\Lambda_0}(K) \end{pmatrix}, \end{aligned} \tag{3.20}$$

where the denominator $\mathcal{D}(K)$ is given by

$$\mathcal{D}(K) = [i\omega + \epsilon_{\boldsymbol{k}} - \mu + \Sigma^N_{\Lambda_0}(-K)][i\omega - \epsilon_{\boldsymbol{k}} + \mu - \Sigma^N_{\Lambda_0}(K)] + \Sigma^A_{\Lambda_0}(K)\Sigma^A_{\Lambda_0}(-K). \tag{3.21}$$

Note that Green functions (3.20) are obtained without any assumption regarding the shape or strength of the interaction, i. e. they apply to any uniform Bose-condensed fluid, liquid or gas [85].

Elementary excitations in systems of interacting bosons are given by zero points of the expression (3.21) on the real axis. The absence of the energetic gap in the spectrum of elementary excitations follows from the condition

$$\mathcal{D}(0) = 0. \tag{3.22}$$

The solution of this equation for the only relevant positive value of the chemical potential is known as the Hugenholtz-Pines equality [16]:

$$\mu = \Sigma^N_{\Lambda_0}(0) - \Sigma^A_{\Lambda_0}(0). \tag{3.23}$$

By using explicit expressions for both normal and anomalous self-energies (3.17a), (3.17b), as well as the mean-field definition of the chemical potential (3.11), expression (3.21) reduces to

$$\mathcal{D}(K) = -\omega^2 - \epsilon_{\boldsymbol{k}} \left[\epsilon_{\boldsymbol{k}} + 2\rho^0_{\Lambda_0} u_{\Lambda_0}(K) \right] = -\left[\omega^2 + E_B^2(K) \right], \tag{3.24}$$

where the quantity

$$E_B(K) = \sqrt{\epsilon_{\boldsymbol{k}}[\epsilon_{\boldsymbol{k}} + 2\rho^0_{\Lambda_0} u_{\Lambda_0}(K)]} \tag{3.25}$$

represents the Bogoliubov spectrum [4]. It behaves linearly for small momenta, exhibits a roton-like minimum at some specific K given by the shape of the potential $u_{\Lambda_0}(K)$ [77] and approaches the free-particle dispersion at large K. Since in general, the interaction $u_{\Lambda_0}(K)$ may depend on the frequency ω, too, the elementary excitations may have a rather complex analytical structure for intermediate K. For small K, each physically relevant potential can be approximated by a constant in vicinity of the $K = 0-$point and hence, the Bogoliubov spectrum reduces to the sound wave-like excitation

$$E_B(K) \approx c_0 k, \tag{3.26}$$

where the velocity of the sound wave propagation is given by

$$c_0 = \sqrt{\frac{\rho^0_{\Lambda_0} u_{\Lambda_0}}{m}}. \tag{3.27}$$

Due to the Goldstone-theorem [15] which postulates the emergence of a gapless excitation mode in the systems with a broken continuous symmetry, the Bogoliubov spectrum can be associated with such a Goldstone-mode. Therefore, we will often call c_0 the velocity of the Goldstone-mode.

Below, we want to calculate the single-particle spectral density function of interacting bosons, which is proportional to the imaginary part of the real-frequency normal Green function [81, 82, 83]:

$$A(i\omega \to \omega + i0, \boldsymbol{k}) = -2\mathrm{Im}G^N(i\omega \to \omega + i0, \boldsymbol{k}). \tag{3.28}$$

In order to calculate the function $A(\omega, \boldsymbol{k})$, an analytical continuation to real frequencies has to be done. Apart from the few simplest cases, there is no established recipes how to perform this analytically. However, several numerical analytical continuation algorithms were proposed in the past. For instance, an analytical continuation technique based on the Padé-approximation is described in [100]. Another possibility is to employ the maximum-entropy approach developed in [101]. As an alternative way, the Keldysh formalism can be mentioned (see for instance [102]), where one works from the very beginning in the real-time space but doubles the number of fields.

After work by Popov [22] and more recent work by Castellani *et al.* [89, 90], it has become popular to redefine the problem sketched here by introducing new scalar bosonic fields, a longitudinal ψ^l and a transversal ψ^t ones, which relate to the original fields $\bar{\psi}$ and ψ via the unitary rotation

$$\psi^l_K = \frac{1}{\sqrt{2}}\left(\bar{\psi}_K + \psi_{-K}\right), \tag{3.29a}$$

$$\psi^t_K = -\frac{i}{\sqrt{2}}\left(\bar{\psi}_K - \psi_{-K}\right). \tag{3.29b}$$

The notation longitudinal and transversal refers to the corresponding fluctuations regarding the direction of the symmetry breaking. The introducing of the scalars ψ^l and ψ^t is equivalent to the mapping of the original $U(1)-$invariant action onto the quantum $O(2)-$model. The advantage of this choice becomes evident in the regime with the broken symmetry. As it reveals by setting expressions (3.9a) and (3.9b) into (3.29a) and (3.29b), only the longitudinal field acquires a non-vanishing vacuum expectation value, while the transversal field remains gapless. In appendix A we recapitulate the whole functional integral approach to Bose systems in the $O(2)-$basis.

3.3 Second order perturbation theory. Beliaev damping

In the weak coupling regime, the K-dependence of the interaction can be omitted. The full propagator matrix (3.20) then reduces to

$$\boldsymbol{G}(K) = \frac{1}{\omega^2 + E_{\boldsymbol{k}}^2} \begin{pmatrix} \Delta_{\Lambda_0} & -i\omega - \epsilon_{\boldsymbol{k}} - \Delta_{\Lambda_0} \\ i\omega - \epsilon_{\boldsymbol{k}} - \Delta_{\Lambda_0} & \Delta_{\Lambda_0} \end{pmatrix}, \tag{3.30}$$

where $\Delta_{\Lambda_0} = \rho^0_{\Lambda_0} u_{\Lambda_0}$ and

$$E_{\boldsymbol{k}} = \sqrt{\epsilon_{\boldsymbol{k}}^2 + 2\Delta_{\Lambda_0}\epsilon_{\boldsymbol{k}}} \tag{3.31}$$

denotes the Bogoliubov spectrum. These propagators suffice for setting up a perturbative expansion in small parameter u_{Λ_0}. In $D = 3$, the interaction is proportional to the $s-$wave scattering length a [85, 103] and perturbative expansion represents essentially an expansion in powers of a small dimensionless quantity ρa^3, where ρ denotes the density of bosons. In $D = 2$, the $s-$wave scattering length vanishes [35]. In this case, the quantity $1/\ln(\rho a^2)$ reveals itself as an appropriate small parameter for perturbative expansion [104], where a relates to the range of the potential.

Below we briefly sketch main ideas of the Beliaev theory. In order to calculate the damping of quasi-particles one has to go beyond the mean-field approximation. Here, we will only consider second order diagrams for both normal and anomalous self-energies and show these diagrams without derivation. For detailed derivation procedure we address the reader to the literature [79, 80, 85]. The second order diagrams for the normal self-energy are shown in Figure 3.1. Figure 3.2 shows the second order diagrams for the anomalous self-energy. Exploiting symmetries of propagators, corresponding algebraic expressions can be written as (here we skip the subscript Λ_0)

$$\begin{aligned} \Sigma_{II}^{(1,1)}(K) \;\approx\; & \frac{4\rho^0 u^2}{2!} \int\limits_Q \Big(G^{(1,1)}(Q) G^{(1,1)}(K-Q) + 2G^{(1,1)}(Q) \big[G^{(1,1)}(Q-K) \\ & + G^{(2,0)}(K-Q) \big] + 2G^{(2,0)}(Q) \big[G^{(1,1)}(Q-K) + G^{(2,0)}(K-Q) \big] \Big), \end{aligned} \tag{3.32}$$

$$\begin{aligned} \Sigma_{II}^{(2,0)}(K) \;\approx\; & \frac{4\rho^0 u^2}{2!} \int\limits_Q \Big(3G^{(2,0)}(Q) G^{(2,0)}(K-Q) + 2G^{(1,1)}(Q) G^{(1,1)}(Q-K) \\ & + 2G^{(1,1)}(Q) G^{(2,0)}(K-Q) + 2G^{(2,0)}(Q) G^{(1,1)}(K-Q) \Big), \end{aligned} \tag{3.33}$$

where $G^{(1,1)}$ denote the off-diagonal elements of matrix (3.30) and $G^{(2,0)}$ the diagonal ones, respectively. The loop Matsubara frequencies can now be integrated out. We obtain after performing some reordering and analytic continuation to real frequencies $\pm i\omega \to \omega \pm 0$ (we adopt here the notation used in [85])

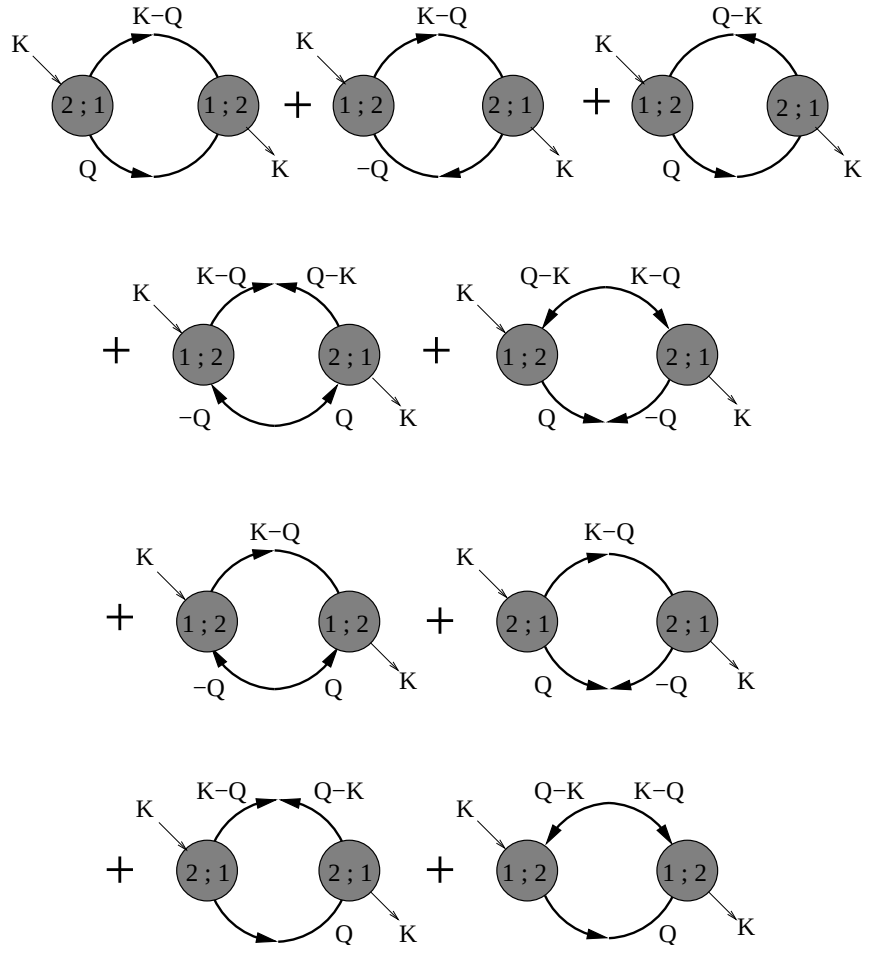

Figure 3.1: Second order diagrams for the normal self-energy

$$\Sigma_{II}^{(1,1)}(K) \approx \frac{1}{2}\rho^0 u^2 \int\limits_{\boldsymbol{q}} \frac{1}{E_1 E_2}\left(\frac{h(E_1,E_2)}{\omega - E_1 - E_2 + i0} - \frac{h(-E_1,-E_2)}{\omega + E_1 + E_2 - i0}\right), \quad (3.34)$$

$$\Sigma_{II}^{(2,0)}(K) \approx \frac{1}{2}\rho^0 u^2 \int\limits_{\boldsymbol{q}} \frac{1}{E_1 E_2}\left(\frac{g(E_1,E_2)}{\omega - E_1 - E_2 + i0} - \frac{g(-E_1,-E_2)}{\omega + E_1 + E_2 - i0}\right), \quad (3.35)$$

where the integration is to perform over the $D-$dimensional momentum space. Here, $E_1 = E_{\boldsymbol{q}}$, $E_2 = E_{\boldsymbol{q}-\boldsymbol{k}}$ and correspondingly for $\epsilon_1 = \epsilon_{\boldsymbol{q}}$ and $\epsilon_2 = \epsilon_{\boldsymbol{q}-\boldsymbol{k}}$. Both quantities $g(E_1,E_2)$ and $h(E_1,E_2)$ are defined as follows

$$g(E_1,E_2) = 3\epsilon_1\epsilon_2 + \Delta^2 - E_1E_2 + \Delta(\epsilon_1+\epsilon_2) - \Delta(E_1+E_2) + \epsilon_1E_2 + \epsilon_2E_1, \quad (3.36a)$$

$$h(E_1,E_2) = 2\epsilon_1\epsilon_2 + \Delta^2 - 2E_1E_2. \quad (3.36b)$$

Expressions (3.34) and (3.35) exhibit infrared divergences. Indeed, for vanishing external momenta K, the infrared behavior of both normal and anomalous self-energies is

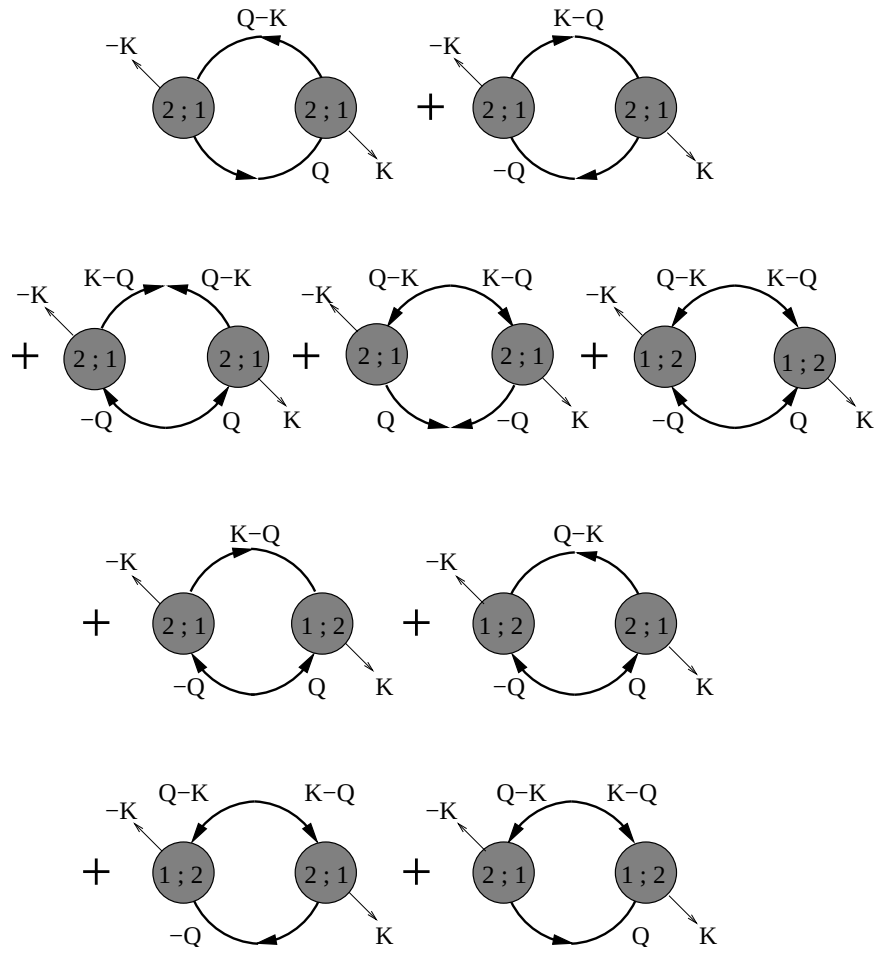

Figure 3.2: Second order diagrams for the anomalous self-energy

given by

$$\Sigma_{II}^{(1,1)}(0) \propto \Sigma_{II}^{(2,0)}(0) \propto \int_{\boldsymbol{k}} \frac{1}{E_k^3} \propto \int_0^{\Lambda_0} dk\; k^{D-4}, \tag{3.37}$$

and diverges as $k \to 0$ in all dimensions $D \leqslant 3$. For this reason, an explicit value for the upper integration bound Λ_0 is irrelevant. It is easy to see, that these divergences arise from the terms proportional to Δ^2 in both $g(E_1, E2)$ and $h(E_1, E_2)$. Although Beliaev does not mention these divergences in his work [79, 80], he seems to have been aware about their existence, since he does not consider divergent terms while calculating the damping of quasi-particles. As we will see below, the self-energies obtained within the FRG-framework do not exhibit any IR-divergences.

As shown by Beliaev [79, 80], the denominator of full Green-functions given by expression (3.21) may be rewritten in the following form:

$$\mathcal{D}(K) = \left[i\omega - E_{\boldsymbol{k}} - \Lambda^{+}(K)\right]\left[i\omega + E_{\boldsymbol{k}} + \Lambda^{-}(K)\right], \tag{3.38}$$

where $E_{\boldsymbol{k}}$ is given by equation (3.31). The Beliaev continuation $\Lambda^{\pm}(K)$ reads in our notation

$$\begin{aligned}\Lambda^{\pm}(K) &= \frac{\epsilon_{\boldsymbol{k}}}{2E_{\boldsymbol{k}}}\left[\Sigma_{II}^{(1,1)}(K)+\Sigma_{II}^{(1,1)}(-K)\right]\pm\frac{1}{2}\left[\Sigma_{II}^{(1,1)}(K)+\Sigma_{II}^{(1,1)}(-K)\right]\\ &\quad+\frac{\Delta}{2E_{\boldsymbol{k}}}\left[\Sigma_{II}^{(1,1)}(K)+\Sigma_{II}^{(1,1)}(-K)-2\Sigma_{II}^{(2,0)}(K)\right].\end{aligned} \tag{3.39}$$

The damping of quasi-particles represents the imaginary part of the Beliaev continuation at the resonance, i. e.

$$\gamma_{\boldsymbol{k}}^{(2)} = \operatorname{Im}\Lambda^{\pm}(K)\big|_{\omega=E_{\boldsymbol{k}}}. \tag{3.40}$$

By using expressions (3.34) and (3.35), we obtain from equations (3.40) and (3.39) to the leading order in interaction

$$\gamma_{\boldsymbol{q}}^{(2)} \approx -\frac{9\pi}{2}\rho^0 u_0^2\frac{\epsilon_{\boldsymbol{q}}}{E_{\boldsymbol{q}}}\int\limits_{\boldsymbol{k}}\frac{\epsilon_{\boldsymbol{k}}\epsilon_{\boldsymbol{q}-\boldsymbol{k}}}{E_{\boldsymbol{k}}E_{\boldsymbol{q}-\boldsymbol{k}}}\delta\left(E_{\boldsymbol{q}}-E_{\boldsymbol{k}}-E_{\boldsymbol{q}-\boldsymbol{k}}\right). \tag{3.41}$$

The argument of the delta function can be understood as a decay of a quasi-particle with the momentum $\boldsymbol{q}$ into two phonons with corresponding momenta $\boldsymbol{k}$ and $\boldsymbol{q}-\boldsymbol{k}$. Such a decay is only possible, if $k \approx q \ll \sqrt{2m\Delta}$ [83], i. e. the outgoing particles are emitted within a small spatial angle between them. For correct evaluation of the integral, it is necessary to expand the argument of the delta function to the third order in momenta, i. e.

$$E_{\boldsymbol{q}}-E_{\boldsymbol{k}}-E_{\boldsymbol{q}-\boldsymbol{k}} \approx \sqrt{\frac{\Delta}{m}}\left[q-k-|\boldsymbol{q}-\boldsymbol{k}|+\frac{1}{8m\Delta}\left(q^3-k^3-|\boldsymbol{q}-\boldsymbol{k}|^3\right)\right], \tag{3.42}$$

and to approximate

$$\begin{aligned}|\boldsymbol{q}-\boldsymbol{k}| &\approx (q-k)\left[1+\frac{qk}{(q-k)^2}\frac{\theta^2}{2}\right],\\ |\boldsymbol{q}-\boldsymbol{k}|^3 &\approx (q-k)^3,\end{aligned}$$

where θ is the spatial angle between momenta. Hence, for the delta function follows

$$\delta\left(E_{\boldsymbol{q}}-E_{\boldsymbol{k}}-E_{\boldsymbol{q}-\boldsymbol{k}}\right) \approx \frac{2m}{\sqrt{3}qk}\delta\left(\theta-\sqrt{\frac{3}{4m\Delta}}(q-k)\right).$$

Finally, after carrying out the D-dimensional integration, we obtain the expression for the damping of quasi-particles at $T=0$ in arbitrary dimensions (Beliaev 1958, Kreisel *et al.* 2008) [79, 80, 105]

$$\gamma_k^{(2)} \approx \alpha_0 k^{2D-1}, \tag{3.43}$$

where

$$\alpha_0 = 2^{-4}3^{\frac{D+1}{2}}K_{D-1}\frac{k_0^{3-D}}{2m\rho^0}\int\limits_0^1 dx\; x^{D-1}(1-x)^{D-1}, \tag{3.44}$$

and $k_0 = 2mc_0$. In $D = 3$ this expression reproduces the Beliaev result

$$\gamma_k^{(2)} = \frac{3k^5}{640\pi m\rho^0}, \tag{3.45}$$

and in $D = 2$ the recently published result by Chung and Bhattacherjee [106]

$$\gamma_k^{(2)} = \frac{\sqrt{3}c_0k^3}{32\pi\rho^0}. \tag{3.46}$$

The interaction enters equation (3.43) with the power $\epsilon = 3 - D$ and thus, in $D = 3$, the damping of the quasi-particles does not depend on the interaction at all. Since the stable condensed phase ρ^0 should be there in all dimensions at $T = 0$ we expect effects due to the renormalization of the interaction to be stronger in dimensions below three than in $D = 3$.

3.4 Anomalous self-energy at vanishing momenta

Gavoret and Nozières found that both normal and anomalous propagators have the same low-energy asymptotic behavior with the merely different sign [86, 94]

$$G^N(K) \sim -G^A(K) \sim \frac{\rho^0 mc_0^2}{\rho}\frac{1}{\omega^2 + c_0^2k^2}, \quad K \to 0, \tag{3.47}$$

where ρ^0 is the condensate density and ρ denotes the density of bosons. Note that expression (3.47) is an *exact* asymptotic result. However, as was mentioned by Gavoret and Nozières themselves, this asymptotic formulas were obtained by simply omitting divergent terms which appear in the diagrams for both self-energies. On the other hand, Gavoret and Nozières used truncation in which $\Sigma^A(0) \neq 0$. But this is not correct, as it was pointed out by Nepomnyashchy and Nepomnyashchy [17, 87, 94]. The Nepomnyashchy's argument is as follows: the anomalous self-energy can be represented as a sum of one-particle irreducible skeleton diagrams

$$\Sigma^A(K) = \Sigma^{A\prime}(K) + \Sigma^{A\prime\prime}(K), \tag{3.48}$$

where the first term on the right-hand side contains terms with a single closed line (the so-called tadpole graphs) and is thus regular in all $D > 1$, i. e. it vanishes as $K \to 0$. The second term in expression (3.48) is infrared divergent. In terms of skeleton diagrams this divergent part becomes

$$\begin{aligned}\Sigma^{A\prime\prime}(K) &= 2\sqrt{\rho^0}u\int\limits_Q \Gamma^{(1,2)}(Q, K, Q-K)G^N(Q)G^N(Q-K) \\ &+ 2\sqrt{\rho^0}u\int\limits_Q \Gamma^{(0,3)}(Q, K, Q-K)G^N(Q)G^A(K-Q),\end{aligned} \tag{3.49}$$

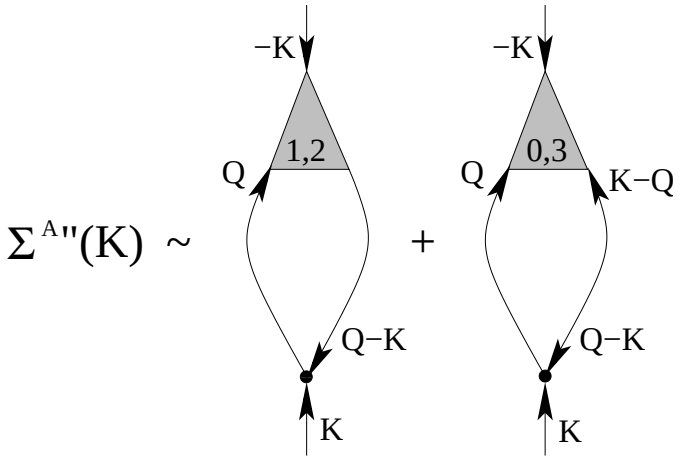

Figure 3.3: Diagrams corresponding to the IR-divergent terms from equation (3.48).

where $\Gamma^{(0,3)}$ and $\Gamma^{(1,2)}$ denote vertices with three ingoing, and two in- and one outgoing legs respectively. Note that they are different from the three-point vertices used in the perturbative expansion which are given by equation (3.18). The diagrammatic representation of equation (3.49) is shown in Figure 3.3. Here, black dots denote the bare vertices which coincide with the perturbative ones. In author's notation, equation (3.49) is exact up to an irrelevant constant factor. In the limit $K = 0$ and for small internal momenta Q, the use of the asymptotic formulas (3.47) is allowed and we obtain

$$\Sigma^A(0) = \left[\tilde{\Gamma}^{(1,2)}(0,0,0) - \tilde{\Gamma}^{(0,3)}(0,0,0)\right] \int_0^{\Lambda_0} dq\; q^{D-1} \int \frac{d\omega}{2\pi} \frac{2u\sqrt{\rho^0}}{(\omega^2 + c_0^2 q^2)^2}, \tag{3.50}$$

where the upper limit of the integration over momenta q does not need to be specified exactly, since we are only interested in recovering the infrared behavior of the anomalous self-energy. Taking into account the scaling behavior of the interaction $u \sim k^{2-D}/m$, we may guess that the expression in the brackets on the right-hand side of equation (3.50) can be further simplified by using following relation [17]

$$\tilde{\Gamma}^{(1,2)}(0,0,0) - \tilde{\Gamma}^{(0,3)}(0,0,0) \propto \frac{\Sigma^A(0)}{\sqrt{\rho^0}}, \tag{3.51}$$

which yields by setting expression (3.51) back into equation (3.50) an exact self-consistent equation for the anomalous self-energy. Since the integral on the right-hand side of equation (3.50) diverges power-law-like in $D < 3$ and logarithmic in $D = 3$, the only finite solution of this equation is

$$\Sigma^A(0) = 0, \tag{3.52}$$

which might be considered an exact result. As pointed out by Griffin in [94], in $D = 3$ the infrared behavior of the anomalous self-energy is inverse logarithmic:

$$\Sigma^A(K) \propto 1/\ln|\omega^2 + c^2\boldsymbol{k}^2|. \tag{3.53}$$

We will extend this result to arbitrary dimensions later on.

Furthermore, Nepomnyashchy and Nepomnyashchy pointed out that in leading order in momenta, corrections to both normal and anomalous self-energies coincide. This reads in the author's notation as

$$\Sigma^{(1,1)}(K) \approx \mu + i\omega + \Delta\Sigma(K) + a\epsilon_{\boldsymbol{k}} + b\omega^2 + \mathcal{O}(\boldsymbol{k}^3, \omega^3), \tag{3.54a}$$

$$\Sigma^{(2,0)}(K) \approx \Delta\Sigma(K) + a_1\epsilon_{\boldsymbol{k}} + b_1\omega^2 + \mathcal{O}(\boldsymbol{k}^3, \omega^3), \tag{3.54b}$$

where $\Delta\Sigma(K)$ denotes the non-analytical term. Therefore, the difference between both self-energies is analytic:

$$\sigma(K) \approx \mu + i\omega + (a - a_1)\epsilon_{\boldsymbol{k}} + (b - b_1)\omega^2 + \mathcal{O}(\omega^3, \boldsymbol{k}^3). \tag{3.55}$$

The truncation scheme which we will employ in order to close the hierarchy of RG-flow equations for irreducible vertex functions in next chapters is heavily influenced by equation (3.55).

3.5 Flowing effective action

In order to obtain RG-flow equations for the irreducible vertices we have to truncate the flowing effective action in some appropriate and physically reasonable way. We shall use the following non-local potential approximation for the flowing effective action given by equation (1.30)

$$\begin{aligned}\mathcal{L}_\ell\left[\bar{\phi}, \phi\right] &= -\int_K \bar{\phi}_K[i\omega - \epsilon_{\boldsymbol{k}} + \mu - R_\ell(\boldsymbol{k})]\phi_K \\ &\quad + \int_K \bar{\phi}_K \sigma_\ell(K)\phi_K + \frac{1}{2}\int_K u_\ell(K)\Delta\rho_K\Delta\rho_{-K}.\end{aligned} \tag{3.56}$$

Here, the cutoff function $R_\ell(\boldsymbol{k})$ is supposed to regulate momenta only. Again we shall use the Litim-regulator

$$R_\ell(\boldsymbol{k}) = (1 - \delta_{\boldsymbol{k},0})Z_\ell^{-1}(\epsilon_\Lambda - \epsilon_{\boldsymbol{k}})\Theta(\Lambda^2 - k^2), \tag{3.57}$$

where $\epsilon_\Lambda = \Lambda^2/2m$. The quantity

$$\Delta\rho_K = \int_Q \bar{\phi}_Q\phi_{K+Q} - \delta_{K,0}\rho_\ell^0 \tag{3.58}$$

denotes the Fourier-transform of the local density $\rho_X - \rho_\ell^0$, where $\rho_X = |\phi_X|^2$ and ρ_ℓ^0 denotes the flowing condensate density. The key quantity of our truncation $\sigma_\ell(K)$ is supposed to have the following low-energy behavior:

$$\sigma_\ell(K) \approx \Delta_{\Lambda_0} - \Delta_\ell + i\omega\,(1 - Y_\ell) + \epsilon_{\boldsymbol{k}}(Z_\ell^{-1} - 1) + \omega^2 V_\ell, \tag{3.59}$$

where the flowing *gap* is given by $\Delta_\ell = \rho_\ell^0 u_\ell(0) = \rho_\ell^0 u_\ell$. Note that expression (3.59) resembles in its shape equation (3.55) which follows from exact analysis.

At the beginning of the flow, i. e. at $\ell = 0$, the effective action $\mathcal{L}_\ell[\bar{\phi}, \phi]$ must reproduce the bare microscopic action (3.1). Therefore, the initial values of introduced dynamical coupling constants Y_ℓ, Z_ℓ and V_ℓ should be chosen as follows:

$$Y_0 = Y_{\Lambda_0} = 1, \tag{3.60a}$$
$$Z_0 = Z_{\Lambda_0} = 1, \tag{3.60b}$$
$$V_0 = V_{\Lambda_0} = 0. \tag{3.60c}$$

The flowing coupling parameters Y_ℓ, Z_ℓ and V_ℓ are always generated by the flow of the effective action. Since we are interested in the physics at low energies, we can take only terms to the quadratic order in both momenta and frequencies into account. The presence of the terms which are linear and quadratic in frequency in our truncation will enable us to study the crossover between the quasi-free regime, where $\omega \propto k^2$ and Goldstone-regime, where $\omega \propto k$. In the Renormalization Group language this means that the scaling dimension of the inverse imaginary time, the so-called *dynamical exponent* z, crosses over from the regime, where it equals 2, to the regime, where it eventually becomes 1.

At this point we can study coupling parameters entering the effective action (3.56) in order to reveal their scaling dimensions. Usually, one fixes scaling dimension of each spatial direction $[x] = -1$ and of the imaginary time $[\tau] = -z$. Scaling dimensions of the coupling parameters Y_ℓ and Z_ℓ are given by

$$[Y] = \eta_y, \tag{3.61a}$$
$$[Z] = \eta_z. \tag{3.61b}$$

If there were a critical point in the system, then the scaling dimension η_z would be identical with the anomalous dimension of the phase transition. Hence, we can find scaling dimensions of remaining quantities from the effective action (3.56)

$$[\phi] = \frac{1}{2}\left(D - \eta_y\right) = \frac{1}{2}\left(D + z + \eta_z - 2\right) = [Z^{1/2}\hat{\phi}], \tag{3.62a}$$
$$[V] = 2 - 2z - \eta_z, \tag{3.62b}$$
$$[u] = 4 - D - z - 2\eta_z = [Z^{-2}\hat{u}], \tag{3.62c}$$
$$[\rho^0] = D - 2 + z + \eta_z = [Z\hat{\rho}^0], \tag{3.62d}$$

where $\hat{\phi}$, $\hat{\rho}^0$ and $\hat{u}$ denote bare fields, condensate and interaction with the corresponding scaling dimensions $(D+z-2)/2$, $D-2+z$ and $4-D-z$. Finally, from equation (3.62a) follows expression for the dynamical exponent:

$$z = 2 - \eta_z - \eta_y. \tag{3.63}$$

Equation (3.56) implies the following form of the generating functional of one-particle irreducible vertex functions

$$\Gamma_\ell[\bar{\phi}, \phi] = \int_K \bar{\phi}_K \sigma_\ell(K) \phi_K + \frac{1}{2} \int_K u_\ell(K) \Delta\rho_K \Delta\rho_{-K}. \tag{3.64}$$

From equation (3.64) we can extract the corresponding expressions for the flowing normal and anomalous self-energies

$$\Sigma_\ell^N(\pm K) = \sigma_\ell(\pm K) + \rho_\ell^0[u_\ell + u_\ell(K)], \tag{3.65a}$$
$$\Sigma_\ell^A(\pm K) = \rho_\ell^0 u_\ell(K). \tag{3.65b}$$

At finite momenta, the difference between both self-energies reproduces exactly the low-energy behavior (3.55) obtained by Nepomnyashchy and Nepomnyashchy and reduces in limit $K = 0$ to the Hugenholtz-Pines equality (3.23)

$$\Sigma_\ell^N(0) - \Sigma_\ell^A(0) = \Delta_{\Lambda_0} \equiv \mu, \tag{3.66}$$

which thus is fulfilled for all values of the flowing parameter ℓ.

3.6 RG-flow equations for interacting bosons

Irreducible vertices can be found by analyzing the effective action

$$\tilde{\mathcal{L}}_\ell[\bar{\phi}, \phi] = \mathcal{L}_\ell[\bar{\phi}, \phi] - \frac{1}{2}\int_K \bar{\phi}_K R_\ell(\boldsymbol{k})\phi_K, \tag{3.67}$$

where $\mathcal{L}[\bar{\phi}, \phi]$ is given by equation (3.56) and fields are supposed to have finite flowing vacuum expectation values $\sqrt{\rho_\ell^0}$. Then, taking functional derivatives with respect to the fluctuating fields $\Delta\bar{\phi}_K$ and $\Delta\phi_K$ at the point $\Delta\bar{\phi}_K, \Delta\phi_K = 0$, we obtain expressions for the flowing two-point vertices

$$\Gamma_\ell^{(1,1)}(\pm K, \pm K') = -\delta_{K,K'}\left[G_0^{-1}(\pm K) - \Sigma_\ell^N(\pm K)\right], \tag{3.68}$$
$$\Gamma_\ell^{(2,0)}(K, K') = \Gamma_\ell^{(0,2)}(K, K') = \delta_{K,-K'}\Sigma_\ell^A(K), \tag{3.69}$$

as well as for the flowing three-point vertices

$$\Gamma_\ell^{(2,1)}(K_1; K_2, K_3) = \Gamma_\ell^{(1,2)}(K_1; K_2, K_3) = \delta_{K_1,K_2+K_3}\sqrt{\rho_\ell^0}\left[u_\ell(K_2) + u_\ell(K_3)\right]. \tag{3.70}$$

Note that for $\Gamma_\ell^{(2,1)}$ the momentum K_1 is associated with the ingoing field, while for $\Gamma_\ell^{(1,2)}$ with the outgoing one. Finally we obtain the expression for the flowing four-point vertex

$$\Gamma_\ell^{(2,2)}(K_1, K_2; K_3, K_4) = \delta_{K_1+K_2,K_3+K_4}\left[u_\ell(K_1 - K_3) + u_\ell(K_1 - K_4)\right]. \tag{3.71}$$

Here, momenta K_3 and K_4 are associated with ingoing fields, while momenta K_1 and K_2 with the outgoing ones. Formally these expressions are entirely analogous to expressions (3.13-3.19). In order to simplify the evaluation we will neglect the momentum dependence of vertices entering right-hand sides of each flow equation. We thus follow the guideline of the perturbative approach, where the locality of interaction is assumed

from the very beginning. We will also neglect anomalous vertices involving more than two fields of the same sort. In another words we will neither take the RG-flow of vertices $\Gamma^{(3,0)}$ and $\Gamma^{(0,3)}$ in account, nor the RG-flow of vertices $\Gamma^{(4,0)}$, $\Gamma^{(3,1)}$, $\Gamma^{(1,3)}$ and $\Gamma^{(0,4)}$.

Following the guideline of chapter 1.5 and using expressions (3.68-3.71) for the one-particle irreducible vertices we obtain RG-flow equations for the flowing condensate ρ_ℓ^0, as well as for both normal and anomalous self-energies $\Sigma_\ell^N(K)$ and $\Sigma_\ell^A(K)$. Below we give a detailed explanation for this procedure.

3.6.1 RG-flow equation for the condensate

Associating the only external leg α_1 in the diagram shown in Figure 1.6 for the flow of the condensate with an outgoing particle, i. e. with the field $\Delta\bar{\phi}$, we realize that the combinatorics for the left-hand side of this equation consists of two possible terms, the one with an in- ($\Gamma^{(1,1)}\bar{\phi}\dot{\phi}^0$) and another one with an outgoing ($\Gamma^{(2,0)}\bar{\phi}\dot{\bar{\phi}}^0$) condensed particle. Corresponding diagrams are shown in the figure below.

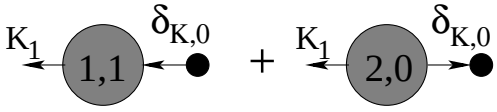

Here, the numbers inside the shadowed circles correspond to the number of in- or outgoing particles. The ingoing particle is identified with the arrow pointing to the circle, the outgoing one with the arrow pointing from the circle away, respectively. Analytically we obtain:

$$\begin{aligned}
&\int_K \left[\Gamma_\ell^{(1,1)}(K_1,K)+\Gamma_\ell^{(2,0)}(K_1,K)\right]\delta_{K,0}\,\partial_\Lambda\sqrt{\rho_\ell^0}\\
&= -\int_K \delta_{K_1,K}\left[G_0^{-1}(K)-\Sigma_\ell^N(K)\right]\delta_{K,0}\,\partial_\Lambda\sqrt{\rho_\ell^0}+\int_K \delta_{K_1,-K}\Sigma_\ell^A(K)\delta_{K,0}\,\partial_\Lambda\sqrt{\rho_\ell^0}\\
&= 2\delta_{K_1,0}u_\ell\rho_\ell^0\,\partial_\Lambda\sqrt{\rho_\ell^0}=\delta_{K_1,0}u_\ell\sqrt{\rho_\ell^0}\,\partial_\Lambda\rho_\ell^0. \qquad (3.72)
\end{aligned}$$

In the last line we used expressions (3.65a) and (3.65b).

The combinatorics for the right-hand side of diagrammatic equation shown in Figure 1.6 includes four possible terms corresponding to following field combinations: $\Gamma^{(2,1)}\bar{\phi}\bar{\phi}\phi$, $\Gamma^{(2,1)}\bar{\phi}\phi\bar{\phi}$, $\Gamma^{(3,0)}\bar{\phi}\bar{\phi}\bar{\phi}$ and $\Gamma^{(1,2)}\bar{\phi}\phi\phi$. Since in our truncation the vertex $\Gamma^{(3,0)}=0$, the right-hand side of the flow equation for the condensate has following diagrammatic expression:

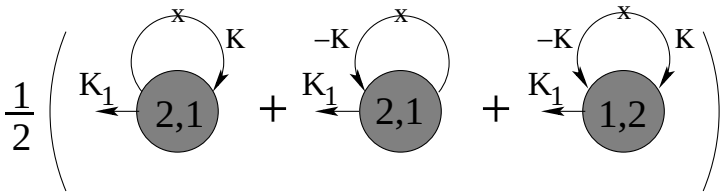

Thus, the right-hand side of the RG-flow equation for the condensate reads

$$\begin{aligned}
&\frac{1}{2}\int\limits_K \Big(\Gamma_\ell^{(2,1)}(K;K_1,K)\dot{G}_\ell^N(K) + \Gamma_\ell^{(2,1)}(-K;K_1,-K)\dot{G}_\ell^N(-K) \\
&\qquad\qquad + \Gamma_\ell^{(1,2)}(K_1;K,-K)\dot{G}_\ell^A(K)\Big) \\
= \;& \delta_{K_1,0}\frac{1}{2}\sqrt{\rho_\ell^0}\int\limits_K \Big\{[u_\ell + u_\ell(K)]\left(\dot{G}_\ell^N(K) + \dot{G}_\ell^N(-K)\right) + 2u_\ell(K)\dot{G}_\ell^A(K)\Big\}, \quad (3.73)
\end{aligned}$$

where we used expressions for three-point vertices (3.70) and symmetry of the potential with respect to the sign mirroring in the argument. Equating expressions (3.72) and (3.73) we finally obtain the flow equation for the condensate

$$\partial_\Lambda \rho_\ell^0 = \frac{1}{2u_\ell}\int\limits_K \Big\{[u_\ell + u_\ell(K)]\left(\dot{G}_\ell^N(K) + \dot{G}_\ell^N(-K)\right) + 2u_\ell(K)\dot{G}_\ell^A(K)\Big\}. \quad (3.74)$$

The same equation can be obtained, if we associate the only external leg with the ingoing field $\Delta\phi$. Omitting the momentum dependence of the interaction we finally arrive at the following equation

$$\partial_\Lambda \rho_\ell^0 \approx \int\limits_K \Big\{\dot{G}_\ell^N(K) + \dot{G}_\ell^N(-K) + \dot{G}_\ell^A(K)\Big\}. \quad (3.75)$$

Explicit expressions for both normal and anomalous single-scale propagators $\dot{G}_\ell^N$ and $\dot{G}_\ell^A$ will be given later on.

3.6.2 Flow equation for the normal self-energy

Now we derive the flow equation for the normal two-point vertex function $\Gamma_\ell^{(1,1)}(K_1, K_2)$. By using equation (3.68) is not difficult to see that the left-hand side of this equation is given by

$$\partial_\Lambda \Gamma_\ell^{(1,1)}(K_1, K_2) = \delta_{K_1,K_2}\partial_\Lambda \Sigma_\ell^N(K_1). \quad (3.76)$$

Due to the diagrammatic expression shown in Figure 1.7, the right-hand side of the flow equation for the normal self-energy Σ_ℓ^N contain graphs which belong to three topologic classes. Below we only consider graphs which provide a non-vanishing contribution in our truncation, i. e. such diagrams which do not contain higher order anomalous vertices like $\Gamma^{(3,0)}$, $\Gamma^{(0,3)}$, $\Gamma^{(3,1)}$ and $\Gamma^{(1,3)}$. Contributions from the first class diagrams are shown below:

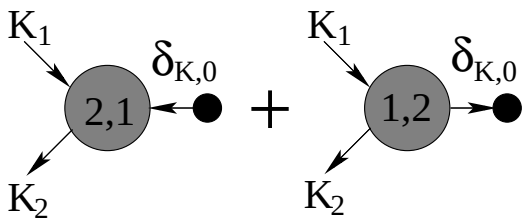

Analytically these diagrams can be written as

$$\begin{aligned}
&\partial_\Lambda \sqrt{\rho_\ell^0} \int\limits_K \delta_{K,0} \left(\Gamma_\ell^{(1,2)}(K_2; K_1, K) + \Gamma_\ell^{(2,1)}(K_1; K_2, K) \right) \\
= \;& \delta_{K_1,K_2} \partial_\Lambda \rho_\ell^0 \left[u_\ell + u_\ell(K_1) \right] = \delta_{K_1,K_2} \frac{1}{2} \left(1 + \frac{u_\ell(K_1)}{u_\ell} \right) \times \\
\times \;& \int\limits_K \left\{ \left[u_\ell + u_\ell(K) \right] \left(\dot{G}_\ell^N(K) + \dot{G}_\ell^N(-K) \right) + 2 u_\ell(K) \dot{G}_\ell^A(K) \right\}. \qquad (3.77)
\end{aligned}$$

Note that we used equation (3.74) in the second line of this expression.

The non-vanishing contributions arising from the second class of diagrams are as follows:

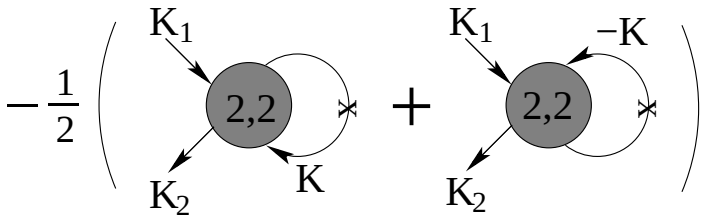

which analytically yields

$$\begin{aligned}
&-\frac{1}{2} \int\limits_K \left\{ \Gamma_\ell^{(2,2)}(K_2, K; K_1, K) \dot{G}_\ell^N(K) + \Gamma_\ell^{(2,2)}(K_2, -K; K_1, -K) \dot{G}_\ell^N(-K) \right\} \\
= \;& -\delta_{K_1,K_2} \frac{1}{2} \int\limits_K \left\{ \left[u_\ell + u_\ell(K_1 - K) \right] \dot{G}_\ell^N(K) + \left[u_\ell + u_\ell(K_1 + K) \right] \dot{G}_\ell^N(-K) \right\}. \qquad (3.78)
\end{aligned}$$

If we omit the momentum dependence of the interaction, then contribution from the first-order terms given by expressions (3.77) and (3.78) becomes

$$\delta_{K_1,K_2} u_\ell \int\limits_K \left\{ \dot{G}_\ell^N(K) + \dot{G}_\ell^N(-K) + 2 \dot{G}_\ell^A(K) \right\}. \qquad (3.79)$$

Non-vanishing contributions arising from the second-order diagrams are shown in Figure 3.4. The symmetrization operator S which appears in front of the corresponding term in Figure 1.7 yields in this case the value $S_{\alpha_1,\alpha_2} = 2!/(1!1!) = 2$. These diagrams can be further subdivided into three subclasses: three diagrams where both three-legged vertices are connected with each other by normal propagators only, two diagrams containing anomalous propagators only and four diagrams with a mixed combination of propagators. Topologically these diagrams are entirely analogous to the perturbative diagrams shown in Figure 3.1, which thus provide the initial condition for the RG-flow of the momentum dependent part of the normal self-energy.

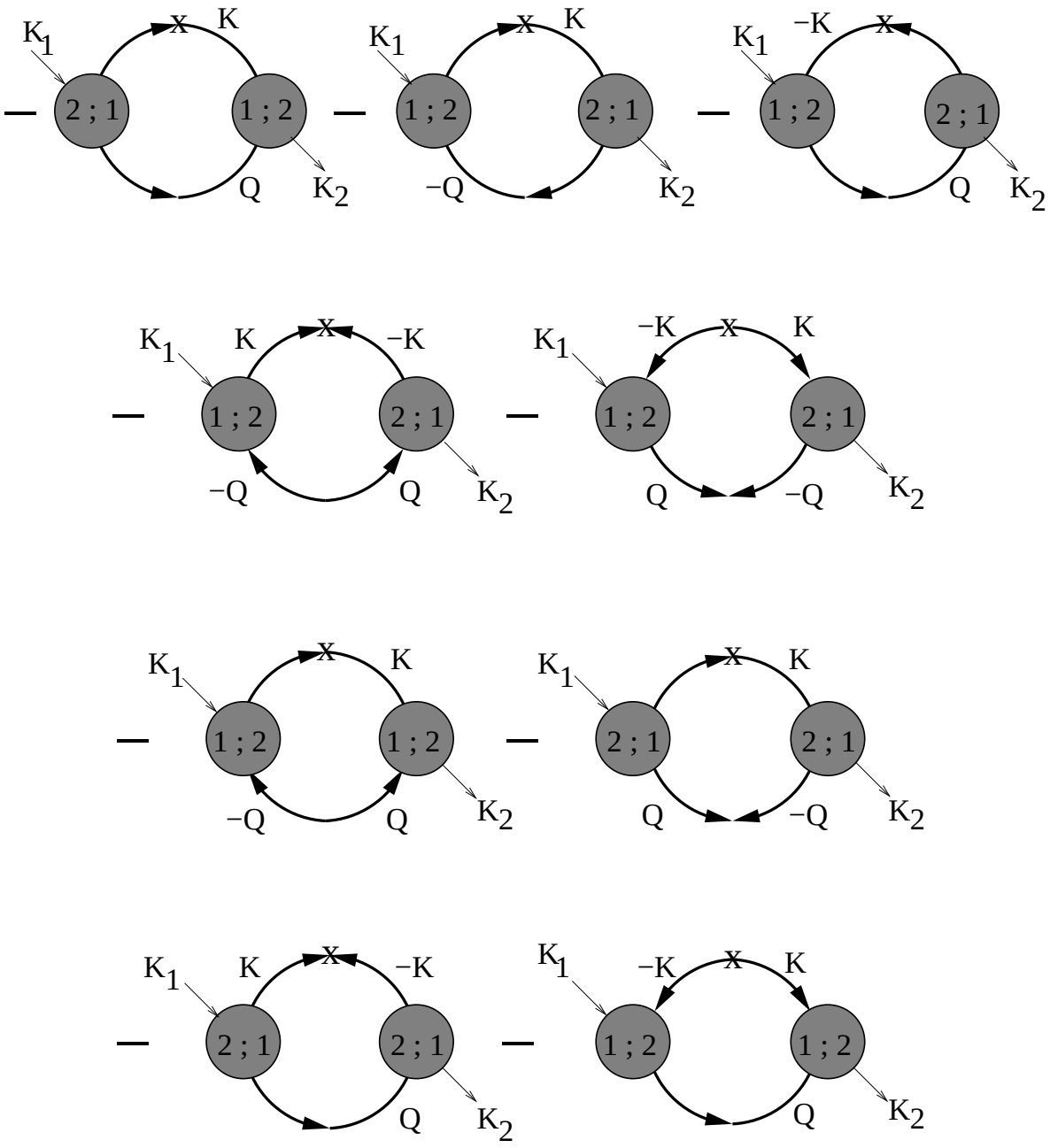

Figure 3.4: Second order diagrams for the flow of the normal self-energy

Algebraically, the expression corresponding to the diagrams shown in Figure (3.4) can be written down as follows (not in the order in which the diagrams are depicted)

$$
\begin{aligned}
&-\int_K\int_Q \Gamma_\ell^{(1,2)}(Q;K_1,-K)\Gamma_\ell^{(2,1)}(K;K_2,-Q)\dot{G}_\ell^A(K)G_\ell^A(Q)\\
&-\int_K\int_Q \Gamma_\ell^{(2,1)}(K_1;K,Q)\dot{G}_\ell^N(K)\left\{\Gamma_\ell^{(1,2)}(K_2;K,Q)G_\ell^N(Q)+\Gamma_\ell^{(2,1)}(K;K_2,-Q)G_\ell^A(Q)\right\}\\
&-\int_K\int_Q \Gamma_\ell^{(1,2)}(K;K_1,-Q)\dot{G}_\ell^N(K)\left\{\Gamma_\ell^{(2,1)}(K;K_2,-Q)G_\ell^N(-Q)+\Gamma_\ell^{(1,2)}(K_2;K,Q)G_\ell^A(Q)\right\}\\
&-\int_K\int_Q \Gamma_\ell^{(1,2)}(Q;K_1,-K)\left\{\Gamma_\ell^{(2,1)}(Q;K_2,-K)\dot{G}_\ell^N(-K)+\Gamma_\ell^{(1,2)}(K_2;Q,K)\dot{G}_\ell^A(K)\right\}G_\ell^N(Q)\\
&-\int_K\int_Q \Gamma_\ell^{(2,1)}(Q;K_2,-K)\dot{G}_\ell^A(K)\left\{\Gamma_\ell^{(1,2)}(K;K_1,-Q)G_\ell^A(Q)+\Gamma_\ell^{(2,1)}(K_1;K,Q)G_\ell^N(Q)\right\}
\end{aligned}
$$

This expression can be further simplified by integrating out the loop momenta Q. Then it reduces to

$$
\begin{aligned}
&-\delta_{K_1,K_2}\rho_\ell^0\int_K\Big\{\left[u_\ell(K)+u_\ell(K_1)\right]^2\dot{G}_\ell^N(-K)G_\ell^N(K_1-K)+\left[u_\ell(K)+u_\ell(K_1-K)\right]^2\\
&\times\dot{G}_\ell^N(K)\left\{G_\ell^N(K_1-K)+G_\ell^N(K-K_1)+2G_\ell^A(K_1-K)\right\}+2\dot{G}_\ell^A(K)\left[u_\ell(K)+u_\ell(K_1)\right]\\
&\qquad\times\left[u_\ell(K)+u_\ell(K_1-K)\right]\left[G_\ell^A(K_1-K)+G_\ell^N(K_1-K)\right]\Big\} \qquad (3.80)\\
&\approx-\delta_{K_1,K_2}4\rho_\ell^0u_\ell^2\int_K\Big\{\dot{G}_\ell^N(-K)G_\ell^N(K_1-K)+2\dot{G}_\ell^A(K)\left[G_\ell^A(K_1-K)+G_\ell^N(K_1-K)\right]\\
&\qquad+\dot{G}_\ell^N(K)\left[G_\ell^N(K_1-K)+G_\ell^N(K-K_1)+2G_\ell^A(K_1-K)\right]\Big\}. \qquad (3.81)
\end{aligned}
$$

In equation (3.81) we omitted the momentum dependence of the interaction. Finally, equating expression (3.76) to (3.79) and (3.81) and renaming variables $K\to Q$ and $K_1\to K$, we obtain the RG-flow equation for the normal self-energy:

$$
\begin{aligned}
\partial_\Lambda\Sigma_\ell^N(K)\approx u_\ell\int_Q&\left[\dot{G}_\ell^N(Q)+\dot{G}_\ell^N(-Q)+2\dot{G}_\ell^A(Q)\right]\\
-4\rho_\ell^0u_\ell^2\int_Q&\Big\{2\dot{G}_\ell^A(Q)\left[G_\ell^N(K-Q)+G_\ell^A(K-Q)\right]+\dot{G}_\ell^N(-Q)G_\ell^N(K-Q)\\
&+\dot{G}_\ell^N(Q)\left[G_\ell^N(K-Q)+G_\ell^N(Q-K)+2G_\ell^A(K-Q)\right]\Big\}. \qquad (3.82)
\end{aligned}
$$

3.6.3 Flow equation for the anomalous self-energy

Our next task is to obtain the RG-flow equation for the anomalous self-energy. In this case we associate both external legs of diagrammatic equation shown in Figure 1.7 with the outgoing particles. Hence, it is obvious that the left-hand side of this equation reduces due to equation (3.69) to

$$\partial_\Lambda \Gamma_\ell^{(2,0)}(K_1, K_2) = \delta_{K_1,-K_2} \Sigma_\ell^A(K_1). \tag{3.83}$$

The only non-vanishing contribution from the first term on the right-hand side of Figure (1.7) corresponds to the following diagram

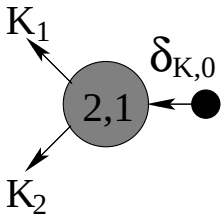

and has the following algebraic representation:

$$\begin{aligned}\partial_\Lambda \sqrt{\rho_\ell^0} \int\limits_K \delta_{K,0} \Gamma_\ell^{(2,1)}(K; K_1, K_2) &= \delta_{0,K_1+K_2} \partial_\Lambda \sqrt{\rho_\ell^0}\, \sqrt{\rho_\ell^0}\, [u_\ell(K_1) + u_\ell(K_2)] \\ = \delta_{K_1,-K_2} \partial_\Lambda \rho_\ell^0\, u_\ell(K) &\approx \delta_{K_1,-K_2}\, u_\ell \int\limits_K \left\{ \dot{G}_\ell^N(K) + \dot{G}_\ell^N(-K) + \dot{G}_\ell^A(K) \right\}. \end{aligned} \tag{3.84}$$

In the last line of equation (3.84) we omitted the momentum dependence of the interaction and used equation (3.75).

The combinatorics for the second term from Figure 1.7 also consists of the single diagram which is shown below:

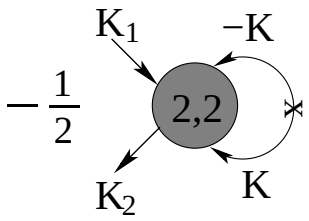

Algebraically we obtain for this contribution

$$\begin{aligned} -\frac{1}{2} \int\limits_K \Gamma_\ell^{(2,2)}(K_1, K_2; K, -K) \dot{G}_\ell^A(K) \\ = -\int\limits_K \delta_{K_1+K_2;K-K} u_\ell(K) \dot{G}_\ell^A(K) \approx -\delta_{K_1,-K_2}\, u_\ell \int\limits_K \dot{G}_\ell^A(K). \end{aligned} \tag{3.85}$$

Summing up expressions (3.84) and (3.85) yields the Hartree-Fock-like contribution to the flow of the anomalous self-energy:

$$\delta_{K_1,-K_2}\, u_\ell \int\limits_K \left\{ \dot{G}_\ell^N(K) + \dot{G}_\ell^N(-K) \right\}. \tag{3.86}$$

Again, the non-vanishing diagrams arising from the third term on the right-hand side of Figure 1.7 can be subdivided into three subclasses: two diagrams connected by normal propagators only, three diagrams connected by anomalous propagators only, as well as four diagrams containing both normal and anomalous propagators. These diagrams are shown in Figure 3.5. The topology of these diagrams reproduces the topology of the perturbative diagrams shown in Figure 3.2. Hence, perturbative series represents the starting value for the flowing momentum-dependent part of the anomalous self-energy, too. The symmetrization operator $S_{\alpha_1;\alpha_2}$ yields again the additional factor 2.

In algebraic form, diagrams shown in Figure 3.5 can be written as follows:

$$\begin{aligned}
&-\int\limits_K \int\limits_Q \Gamma_\ell^{(2,1)}(-Q;K_1,K)\Gamma_\ell^{(2,1)}(Q;K_2,-K)\dot{G}_\ell^A(K)G_\ell^A(Q) \\
&-\int\limits_K \int\limits_Q \Gamma_\ell^{(2,1)}(-K;K_1,Q)\left\{\Gamma_\ell^{(2,1)}(Q;K_2,-K)\dot{G}_\ell^N(-K) + \Gamma_\ell^{(1,2)}(K_2;K,Q)\dot{G}_\ell^A(K)\right\} G_\ell^N(Q) \\
&-\int\limits_K \int\limits_Q \Gamma_\ell^{(2,1)}(-Q;K_1,K)\dot{G}_\ell^N(K)\left\{\Gamma_\ell^{(2,1)}(K;K_2,-Q)G_\ell^N(-Q) + \Gamma_\ell^{(1,2)}(K_2;Q,K)G_\ell^A(Q)\right\} \\
&-\int\limits_K \int\limits_Q \Gamma_\ell^{(1,2)}(K_1;-K,-Q)\left\{\Gamma_\ell^{(1,2)}(K_2;K,Q)\dot{G}_\ell^A(K) + \Gamma_\ell^{(2,1)}(Q;K_2,-K)\dot{G}_\ell^N(-K)\right\} G_\ell^A(Q) \\
&-\int\limits_K \int\limits_Q \Gamma_\ell^{(2,1)}(-K;K_1,Q)\dot{G}_\ell^A(K)\Gamma_\ell^{(2,1)}(K;K_2,-Q)G_\ell^A(Q) \\
&-\int\limits_K \int\limits_Q \Gamma_\ell^{(1,2)}(K_1;-K,-Q)\dot{G}_\ell^A(K)\Gamma_\ell^{(2,1)}(K;-Q,K_2)G_\ell^N(-Q),
\end{aligned}$$

or, after integrating out the loop momenta Q,

$$\begin{aligned}
-\delta_{K_1,-K_2}\rho_\ell^0 \int\limits_K \Big\{ &[u_\ell(K_1)+u_\ell(K_1+K)][u_\ell(K_1)+u_\ell(K)]\Big[\dot{G}_\ell^N(K)\left\{G_\ell^N(K_1+K)+G_\ell^A(K_1+K)\right\} \\
&+\dot{G}_\ell^N(-K)\left\{G_\ell^N(-K_1-K)+G_\ell^A(K_1+K)\right\}\Big] \\
&+\dot{G}_\ell^A(K)G_\ell^A(K_1+K)\left([u_\ell(K_1)+u_\ell(K)]^2+[u_\ell(K_1)+u_\ell(K_1+K)]^2\right. \\
&+[u_\ell(K_1)+u_\ell(K_1+K)][u_\ell(K)+u_\ell(K_1+K)]) \\
&+[u_\ell(K)+u_\ell(K_1+K)][u_\ell(K_1)+u_\ell(K_1+K)] \\
&\times\dot{G}_\ell^A(K_1)\left[G_\ell^N(K_1+K)+G_\ell^N(-K_1-K)\right]\Big\}.
\end{aligned}$$

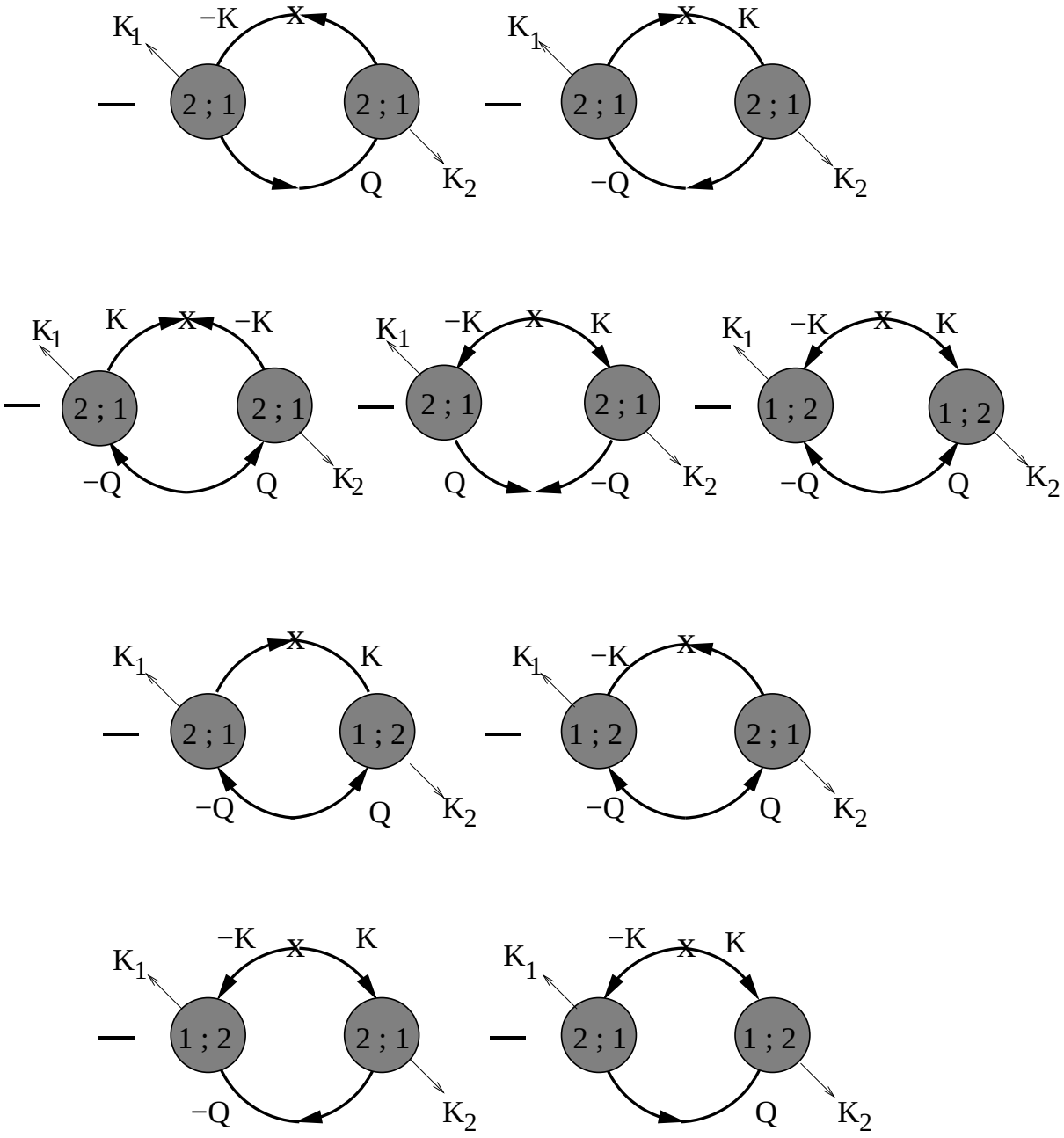

Figure 3.5: Second order diagrams for the flowing anomalous self-energy

If we omit the momentum dependence of the interaction and rename momenta $K \to Q$, $K_1 \to -K$, then the flow equation for the anomalous self-energy becomes

$$\partial_\Lambda \Sigma^A_\ell(K) = u_\ell \int\limits_Q \left[\dot{G}^N_\ell(Q) + \dot{G}^N_\ell(-Q)\right] - 4\rho^0_\ell u^2_\ell \int\limits_Q \Big\{ \dot{G}^N_\ell(Q) \left[G^N_\ell(Q-K) + G^A_\ell(Q-K)\right] + \dot{G}^A_\ell(Q) \left[G^N_\ell(Q-K) + G^N_\ell(K-Q) + 3G^A_\ell(Q-K)\right] + \dot{G}^N_\ell(-Q) \left[G^N_\ell(K-Q) + G^A_\ell(K-Q)\right] \Big\}. \tag{3.87}$$

The same equation can be obtained, if we associate both external legs in Figure (1.7) with ingoing fields.

3.6.4 Flow equations for the interaction and dynamical parameters

In order to close the system of differential equations we need in addition to equations (3.74), (3.82) and (3.87) flow equations for the interaction u_ℓ and for the dynamical two-field coupling parameter $\sigma_\ell(K)$ defined in equation (3.59). The RG-flow for the interaction can be extracted from the flow equation for the anomalous self-energy (3.87) in the limit $K \to 0$

$$\partial_\Lambda u_\ell = -\frac{u_\ell}{\rho^0_\ell}\partial_\Lambda \rho^0_\ell + \frac{1}{\rho^0_\ell}\partial_\Lambda \Sigma^A_\ell(0). \tag{3.88}$$

Using flow equation for the condensate (3.74) we arrive at the flow equation for the interaction

$$\partial_\Lambda u_\ell = -\frac{u_\ell}{\rho^0_\ell} \int\limits_Q \dot{G}^A_\ell(Q) - 4u^2_\ell \int\limits_Q \Big\{ \dot{G}^A_\ell(Q) \left[G^N_\ell(Q) + G^N_\ell(-Q) + 3G^A_\ell(Q)\right] + \dot{G}^N_\ell(Q) \left[G^N_\ell(Q) + G^A_\ell(Q)\right] + \dot{G}^N_\ell(-Q) \left[G^N_\ell(-Q) + G^A_\ell(Q)\right] \Big\}. \tag{3.89}$$

with the initial condition $u_{\ell=0} = u_{\Lambda_0}$.

In order to obtain the flow equation for the dynamical coupling parameter $\sigma_\ell(K)$ we have to consider the difference between the normal and anomalous self-energies:

$$\partial_\Lambda \sigma_\ell(K) + \partial_\Lambda \Delta_\ell = \partial_\Lambda \left[\Sigma^N_\ell(K) - \Sigma^A_\ell(K)\right]. \tag{3.90}$$

The Hugenholtz-Pines theorem [16] manifests itself in the vanishing of equation (3.90) in the limit $K \to 0$, i. e.

$$\partial_\Lambda \left[\sigma_\ell(0) + \Delta_\ell\right] = 0 = \partial_\Lambda \left[\Sigma^N_\ell(0) - \Sigma^A_\ell(0)\right]. \tag{3.91}$$

This is true, since the chemical potential μ is not a flowing parameter. The fulfillment of the Nepomnyashchy-Nepomnyashchy equality (3.52) can only be achieved if the flowing gap vanishes in the large $\ell-$limit, i. e.

$$\Delta_{\ell\to\infty} \to 0. \tag{3.92}$$

Recalling our truncation (3.59) for the coupling parameter $\sigma_\ell(K)$ we may obtain flow equations for coupling parameters Z_ℓ, Y_ℓ and V_ℓ by expanding right-hand side of expression (3.90) in powers of momentum and frequency. It is convenient to introduce derivatives with respect to the logarithmic cutoff ℓ which are related to the derivatives with respect to Λ through $\partial_\ell = -\Lambda\partial_\Lambda$. The RG-flow for the three coupling parameters are thus determined by following expressions:

$$\partial_\ell Z_\ell = -mZ_\ell^2 \frac{\partial^2}{\partial k^2}\partial_\ell \sigma_\ell(\boldsymbol{k},0)\Big|_{k=0}, \tag{3.93a}$$

$$\partial_\ell Y_\ell = -\frac{\partial}{\partial(i\omega)}\partial_\ell \sigma_\ell(0,i\omega)\Big|_{\omega=0}, \tag{3.93b}$$

$$\partial_\ell V_\ell = \frac{1}{2}\frac{\partial^2}{\partial\omega^2}\partial_\ell \sigma_\ell(0,i\omega)\Big|_{\omega=0}. \tag{3.93c}$$

Flowing scaling dimensions η_z and η_y of the parameters Z_ℓ and Y_ℓ can be found from equations

$$\eta_z = -\partial_\ell \ln Z_\ell, \tag{3.94a}$$

$$\eta_y = -\partial_\ell \ln Y_\ell. \tag{3.94b}$$

RG-flow equations for the condensate ρ_ℓ^0, for the interaction u_ℓ, as well as for the dynamical parameters V_ℓ, Z_ℓ and Y_ℓ form a closed system of differential equations. In order to solve them we need to specify the propagators entering right-hand sides of each flow equation.

3.6.5 Flowing propagators

Below we discuss flowing propagators entering RG-flow equations for the coupling parameters and self-energies. Without any loss of generality flowing full Beliaev-Green functions can be given in the following form:

$$G_\ell^N(\pm K) = \frac{-\left[G_{0,\ell}^{-1}(\mp K) - \Sigma_\ell^N(\mp K)\right]}{[G_{0,\ell}^{-1}(K) - \Sigma_\ell^N(K)][G_{0,\ell}^{-1}(-K) - \Sigma_\ell^N(-K)] - \Sigma_\ell^A(K)\Sigma_\ell^A(-K)}, \tag{3.95a}$$

$$G_\ell^A(\pm K) = \frac{\Sigma_\ell^A(\mp K)}{[G_{0,\ell}^{-1}(K) - \Sigma_\ell^N(K)][G_{0,\ell}^{-1}(-K) - \Sigma_\ell^N(-K)] - \Sigma_\ell^A(K)\Sigma_\ell^A(-K)}, \tag{3.95b}$$

where $G_{0,\ell}^{-1}(\pm K) = \pm i\omega - \epsilon_{\boldsymbol{k}} + \mu - R_\ell(\boldsymbol{k})$. Within our truncation propagators (3.95a) and (3.95b) reduce to

$$G_\ell^N(\pm K) = \frac{\Delta_\ell \pm iY_\ell\omega + \bar{\epsilon}_\ell(\boldsymbol{k}) + V_\ell\omega^2}{Y_\ell^2\omega^2 + (\bar{\epsilon}_\ell(\boldsymbol{k}) + V_\ell\omega^2)(2\Delta_\ell + \bar{\epsilon}_\ell(\boldsymbol{k}) + V_\ell\omega^2)}, \tag{3.96a}$$

$$G_\ell^A(K) = -\frac{\Delta_\ell}{Y_\ell^2\omega^2 + (\bar{\epsilon}_\ell(\boldsymbol{k}) + V_\ell\omega^2)(2\Delta_\ell + \bar{\epsilon}_\ell(\boldsymbol{k}) + V_\ell\omega^2)}, \tag{3.96b}$$

with $\bar{\epsilon}_\ell(\boldsymbol{k}) = Z_\ell^{-1}\epsilon_{\boldsymbol{k}} + R_\ell(\boldsymbol{k})$. Propagators in this form will be used in order to evaluate flow equations for coupling constants and self-energies.

Within the additive regularization scheme, the single scale propagators (1.74) can be written as follows:

$$\dot{G}^N_\ell(\pm K) = -\partial_\Lambda R_\ell(\boldsymbol{k}) \left\{ [G^N_\ell(\pm K)]^2 + [G^A_\ell(K)]^2 \right\}, \tag{3.97}$$

$$\dot{G}^A_\ell(K) = -\partial_\Lambda R_\ell(\boldsymbol{k}) G^A_\ell(K) \left\{ G^N_\ell(K) + G^N_\ell(-K) \right\}. \tag{3.98}$$

The hierarchy of RG-flow equations is now closed and can be solved.

3.7 Evaluation of the flow equations for coupling parameters

Below we shall evaluate flow equations for the interaction, the condensate density, and dynamical coupling parameters Y_ℓ, Z_ℓ and V_ℓ. If we choose the Litim regularization scheme [41], then momentum integrals can by carried out analytically by using the identity

$$\int \frac{d^D k}{(2\pi)^D} \partial_\Lambda R_\Lambda(\boldsymbol{k}) \mathcal{F}_\ell(k^2) = \kappa_\ell \frac{\Lambda^{D+1}}{m Z_\ell} \mathcal{F}_\ell(\epsilon_\ell), \tag{3.99}$$

where

$$\kappa_\ell = K_D \frac{(2 + D - \eta_z)}{D(D+2)},$$

with

$$K_D = \frac{2^{1-D}}{\pi^{D/2}\Gamma\left[\frac{D}{2}\right]} \tag{3.100}$$

and

$$\epsilon_\ell = \frac{\Lambda^2}{2 m Z_\ell}. \tag{3.101}$$

From equation (3.74) we obtain for the condensate density

$$\partial_\ell \rho^0_\ell = -2\kappa_\ell \frac{\Lambda^{D+2}}{m Z_\ell} \int \frac{d\omega}{2\pi} \sum_{i=0}^{2} \frac{c^{(\rho)}_{2i} \omega^{2i}}{\mathcal{D}^2(\epsilon_\ell, \omega)}, \tag{3.102}$$

where $\mathcal{D}(\epsilon_\ell, \omega)$ denotes the denominator of the Green functions (3.96a)-(3.96b) and

$$\begin{aligned} c^{(\rho)}_0 &= \epsilon^2_\ell + \epsilon_\ell \Delta_\ell + \Delta^2_\ell, \\ c^{(\rho)}_2 &= V_\ell(2\epsilon_\ell + \Delta_\ell) - Y^2_\ell, \\ c^{(\rho)}_4 &= V^2_\ell. \end{aligned}$$

The flow equation for the interaction equation (3.89) becomes

$$\partial_\ell u_\ell = -2u_\ell^2 \kappa_\ell \frac{\Lambda^{D+2}}{mZ_\ell} \int \frac{d\omega}{2\pi} \sum_{i=0}^{3} \frac{c_{2i}^{(g)} \omega^{2i}}{\mathcal{D}^3(\epsilon_\ell, \omega)}, \tag{3.103}$$

where

$$\begin{aligned} c_0^{(u)} &= 5\epsilon_\ell^3 + 3\epsilon_\ell^2 \Delta_\ell + 6\epsilon_\ell \Delta_\ell^2 + 4\Delta_\ell^3, \\ c_2^{(u)} &= 3V_\ell \left(5\epsilon_\ell^2 + 2\epsilon_\ell \Delta_\ell + 2\Delta_\ell^2\right) - Y_\ell^2 \left(7\Delta_\ell + 11\epsilon_\ell\right), \\ c_4^{(u)} &= V_\ell \left(3V_\ell \left(5\epsilon_\ell + \Delta_\ell\right) - 11Y_\ell^2\right), \\ c_6^{(u)} &= 5V_\ell^3. \end{aligned}$$

From equation (3.93a) we obtain the flow equation for the parameter Z_ℓ:

$$\partial_\ell Z_\ell = -2\rho_\ell^0 u_\ell^2 \Lambda^{D+2} \frac{K_D}{mD} \int \frac{d\omega}{2\pi} \frac{1}{\mathcal{D}^2(\epsilon_\ell, \omega)}. \tag{3.104}$$

In the same manner, from equation (3.93b) follows the flow equation for the parameter Y_ℓ:

$$\partial_\ell Y_\ell = 4\rho_\ell^0 u_\ell^2 Y_\ell \kappa_\ell \frac{\Lambda^{D+2}}{mZ_\ell} \int \frac{d\omega}{2\pi} \sum_{i=0}^{2} \frac{c_{2i}^{(y)} \omega^{2i}}{\mathcal{D}^3(\epsilon_\ell, \omega)}, \tag{3.105}$$

where

$$\begin{aligned} c_0^{(y)} &= \epsilon_\ell^2 - 2\epsilon_\ell \Delta_\ell - 2\Delta_\ell^2, \\ c_2^{(y)} &= Y_\ell^2 + 2(\epsilon_\ell - \Delta_\ell) V_\ell, \\ c_4^{(y)} &= V_\ell^2. \end{aligned}$$

Using equation (3.93c), the flow equation for the parameter V_ℓ can be rewritten as follows:

$$\partial_\ell V_\ell = -4\rho_\ell^0 u_\ell^2 \kappa_\ell \frac{\Lambda^{D+2}}{mZ_\ell} \int \frac{d\omega}{2\pi} \sum_{i=0}^{2} \frac{c_{2i}^{(v)} \omega^{2i}}{\mathcal{D}^3(\epsilon_\ell, \omega)}, \tag{3.106}$$

where

$$\begin{aligned} c_0^{(v)} &= -Y_\ell^2(\epsilon_\ell + \Delta_\ell) - \epsilon_\ell(\epsilon_\ell + 2\Delta_\ell) V_\ell, \\ c_2^{(v)} &= 2V_\ell[Y_\ell^2 + V_\ell(\epsilon_\ell + \Delta_\ell)], \\ c_4^{(v)} &= 3V_\ell^3. \end{aligned}$$

Figures 3.6 and 3.7 demonstrate solutions of equations (3.102)-(3.106) in $D = 2$ calculated for the initial values of dimensionless quantities $\tilde{\mu}_0 = 2m\mu\Lambda_0^{-2} = 0.4$ and $\tilde{u}_0 = 2mu_0 k_\mu^{D-2} = 4$. Figures 3.8 and 3.9 show solutions in $D = 3$ for $\tilde{\mu}_0 = 0.4$ and $\tilde{u}_0 \approx 2.53$. In both cases the condensate ρ_ℓ^0 approaches some finite limit $\rho_\star^0$ corresponding to the real physical condensate which is always present at $T = 0$. The crossover between

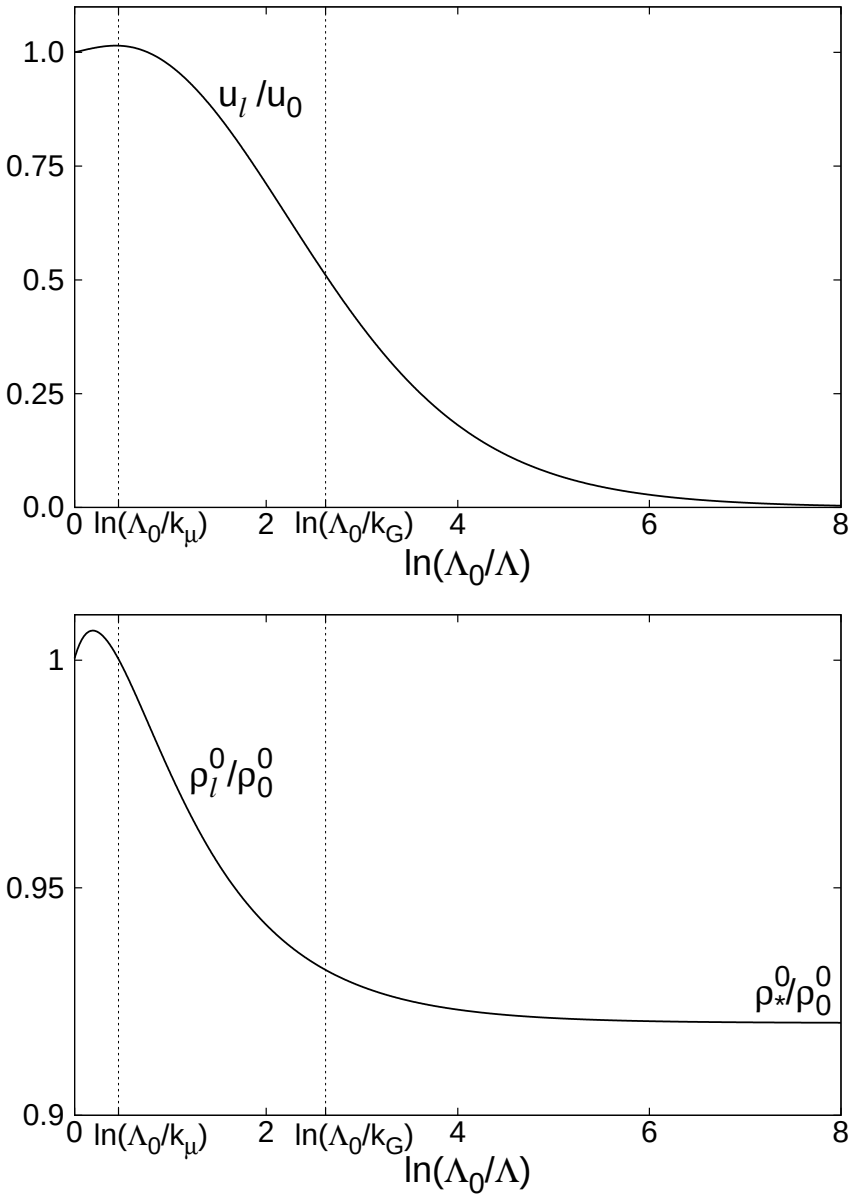

Figure 3.6: Typical RG-flows for the interaction u_ℓ and condensate density ρ_ℓ^0 in $D = 2$ calculated with initial values for the dimensionless chemical potential $\tilde{\mu}_0 = 2m\mu\Lambda_0^{-2} = 0.4$ and dimensionless interaction $\tilde{u}_0 = 2mu_0k_\mu^{D-2} = 4$. The vertical dashed lines illustrate both scales which influence flows of coupling parameters. The momentum k_G will be calculated in section 3.9.

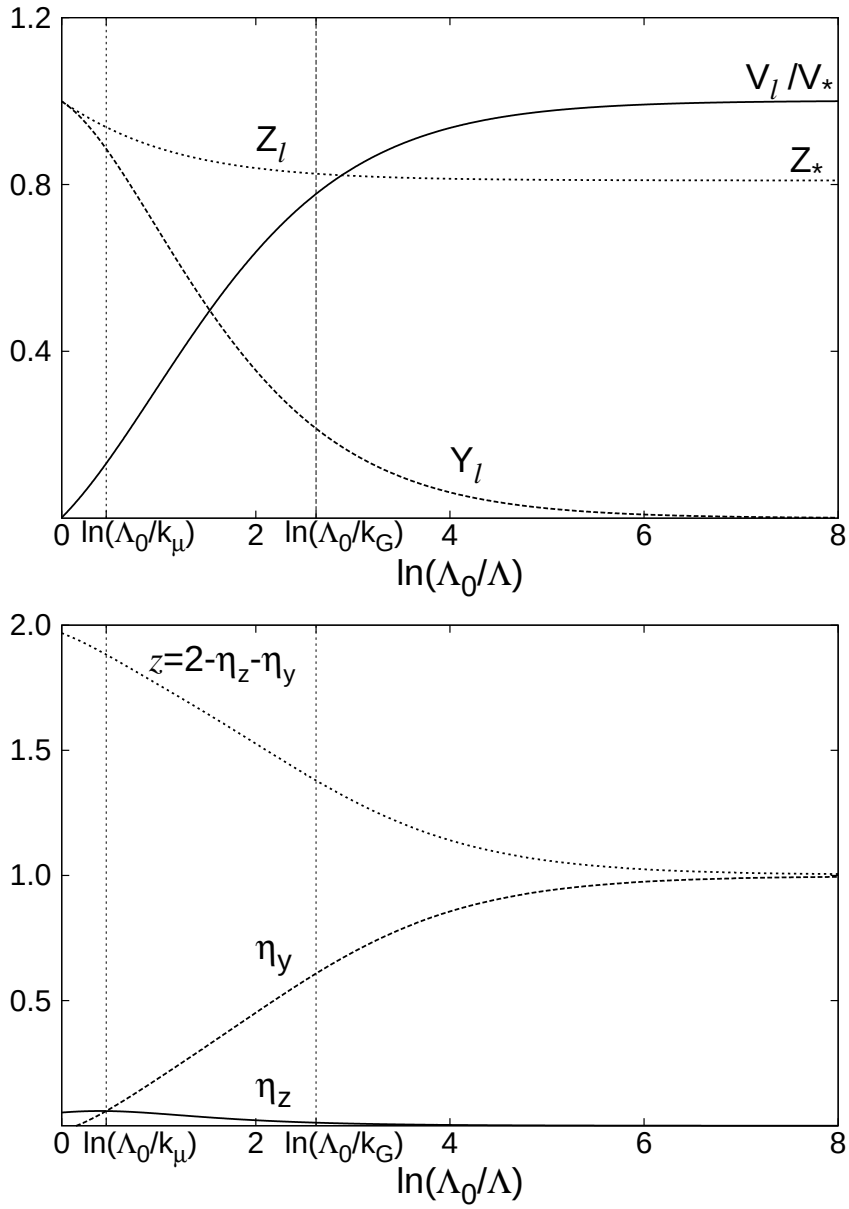

Figure 3.7: Typical RG-flows for the coupling parameters Y_ℓ, Z_ℓ and V_ℓ, as well as for the dynamical exponent z and both anomalous dimensions η_z and η_y in $D = 2$ calculated with initial values for the dimensionless chemical potential $\tilde{\mu}_0 = 2m\mu\Lambda_0^{-2} = 0.4$ and dimensionless interaction $\tilde{u}_0 = 2mu_0k_\mu^{D-2} = 4$. The vertical dashed lines illustrate both scales influencing flows of coupling parameters.

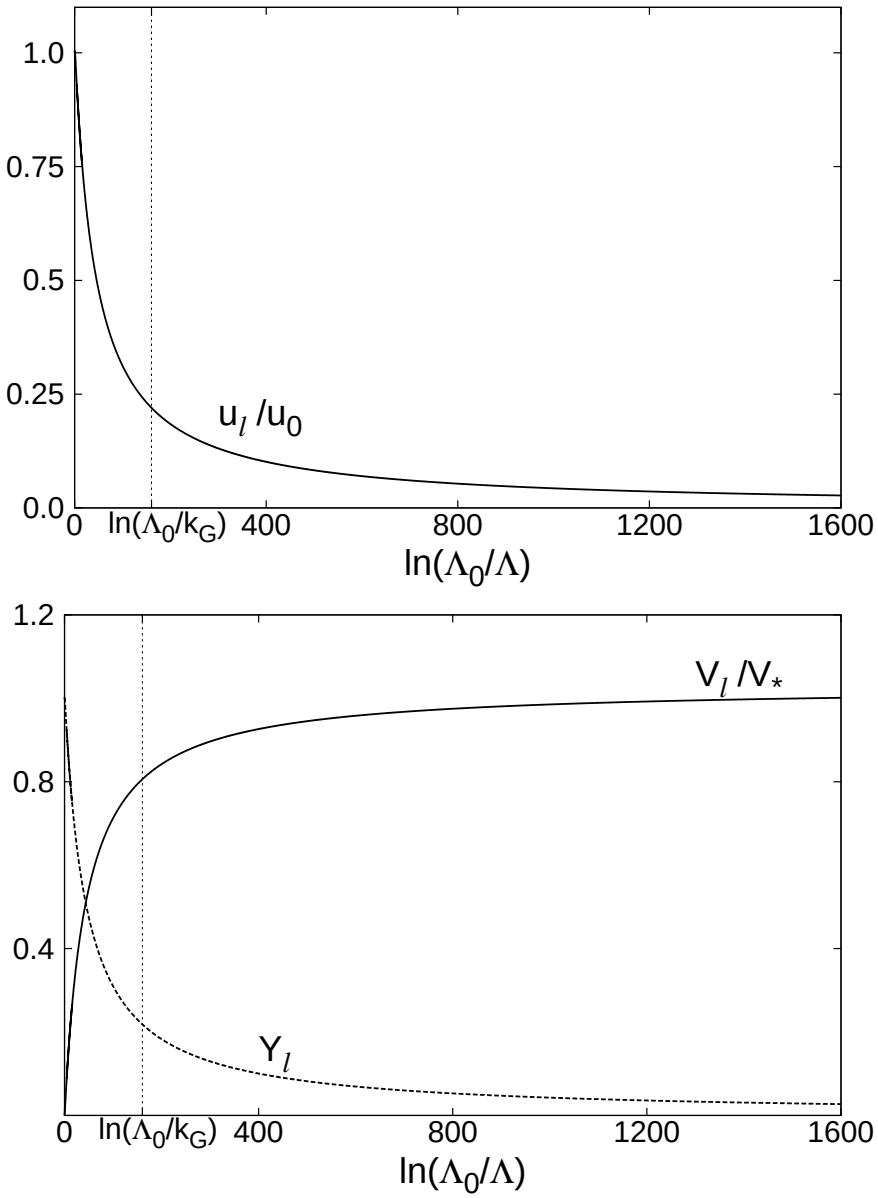

Figure 3.8: Typical RG-flows for the interaction u_ℓ (above), as well as for the parameters Y_ℓ and V_ℓ in $D = 3$ calculated with initial values for the dimensionless chemical potential $\tilde{\mu}_0 = 2m\mu\Lambda_0^{-2} = 0.4$ and dimensionless interaction $\tilde{u}_0 = 2mu_0k_\mu^{D-2} \approx 2.53$. The vertical dashed line corresponds to our estimation for the crossover scale k_G, which will be obtained in section 3.9. Note the difference in the saturation scale for the parameter V_ℓ compared to the $D = 2-$ case.

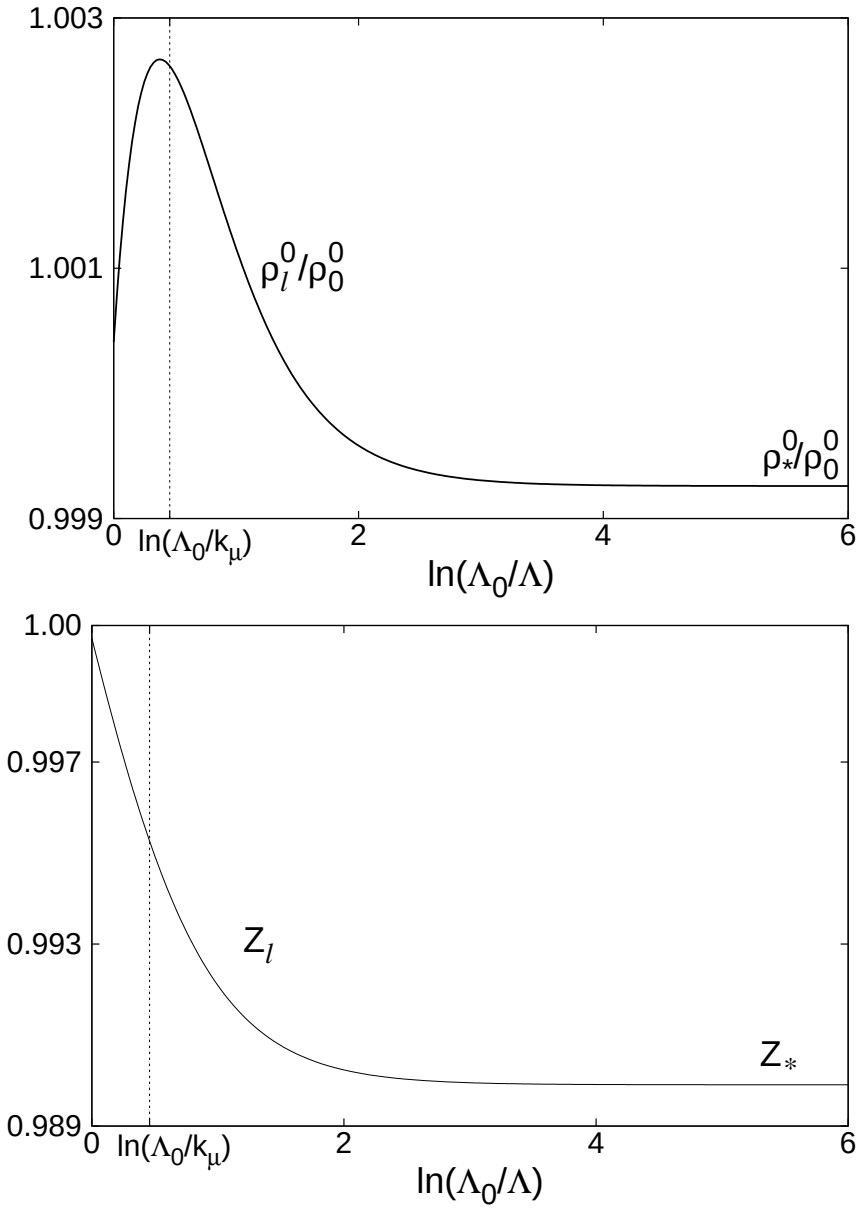

Figure 3.9: Typical RG-flows for the coupling parameters ρ_ℓ^0 and Z_ℓ in $D = 3$ calculated with initial values for the dimensionless chemical potential $\tilde{\mu}_0 = 0.4$ and dimensionless interaction $\tilde{u}_0 \approx 2.53$. Remarkably, the flow stops at arguments which are much smaller than the crossover scale k_G. The only relevant scale for these parameters corresponds to the momentum k_μ.

the $z = 2-$ and $z = 1-$scaling regimes determines the behavior of the RG-flow. This crossover is nicely illustrated by the dynamical exponent z, as shown in Figure 3.7 for the $D = 2-$case. The flow of coupling parameters is governed by two scales. The first scale corresponds to the characteristic momentum $k_\mu = \sqrt{2m\mu}$ and is the only scale affecting the flow of the condensate ρ_ℓ^0 and wave function renormalization parameter Z_ℓ. The second scale corresponding to the inverse characteristic length k_G is responsible for the crossover between the $z = 2-$ and $z = 1-$scaling regimes. At this scale the non-trivial fixed point corresponding to the Goldstone regime [89, 90] strongly attracts the flow of the interaction. The discussion of the flow in the vicinity of the fixed point and calculation of the momentum k_G will be made in section 3.9.

The reason why flow of anomalous dimensions η_z and η_y differs from zero at the beginning is due to the fact that the flow of both dynamical parameters Y_ℓ and Z_ℓ depends directly on the condensate and interaction. Therefore, for any finite u_0 and ρ_0^0, an infinitesimal change of the flowing parameter $\ell = \ln(\Lambda_0/\Lambda)$ close to $\ell = 0$ gives rise to a finite change of both dynamical parameters, which is essentially responsible for the finite starting values of both anomalous dimensions.

For large ℓ, the flow of both coupling parameters Y_ℓ and u_ℓ approaches zero, while the parameter V_ℓ becomes finite. In $D = 3$ this process is very slow. The saturation scale for the parameter V_ℓ for chosen initial conditions lies at $\ell \approx 1600$, while in $D = 2$ at merely $\ell \approx 8$. We shall explore the reason for such a behavior in chapter 3.9.

3.8 Renormalized velocity of the Goldstone-mode

The poles of propagators (3.96a) and (3.96b) lie on the imaginary axis and can be found by solving the quartic equation

$$Y_\ell^2\Omega_\ell^2 + (\bar{\epsilon}_\ell(\boldsymbol{k}) + V_\ell\Omega_\ell^2)(2\Delta_\ell + \bar{\epsilon}_\ell(\boldsymbol{k}) + V_\ell\Omega_\ell^2) = 0,$$

which has the following positive valued solutions

$$i\Omega_\ell^\pm = \sqrt{\frac{1}{2V_\ell^2}\left[Y_\ell^2 + 2V_\ell\left[\bar{\epsilon}_\ell(\boldsymbol{k}) + \Delta_\ell\right] \pm \sqrt{Y_\ell^4 + 4\left[\bar{\epsilon}_\ell(\boldsymbol{k}) + \Delta_\ell\right]Y_\ell^2V_\ell + 4\Delta_\ell^2V_\ell^2}\right]}. \quad (3.107)$$

At $\ell = 0$, i. e. for $V_0 = 0$, $Y_0 = 1$ and $\Delta_0 = \mu$, the only solution which reproduces the Bogoliubov spectrum is $i\Omega_\ell^-$. The solution Ω_ℓ^+ diverges in this limit and thus disappears from the spectrum [97]. On the other hand, both the interaction and dynamical parameter $Y_{\ell\to\infty} \to 0$ vanish in the Goldstone-regime, while parameters V_ℓ and Z_ℓ approach constant values $V_\star$ and $Z_\star$. In this case, assuming $k \leqslant \Lambda$, solution $i\Omega_\ell^-$ reduces to a phonon-like form

$$i\Omega_{\ell\to\infty}^- = \sqrt{\frac{\bar{\epsilon}_\ell(\boldsymbol{k})}{V_\star}} = ck, \quad (3.108)$$

where the fully renormalized velocity of the Goldstone-mode is given by

$$c = \frac{1}{\sqrt{2mZ_\star V_\star}}. \quad (3.109)$$

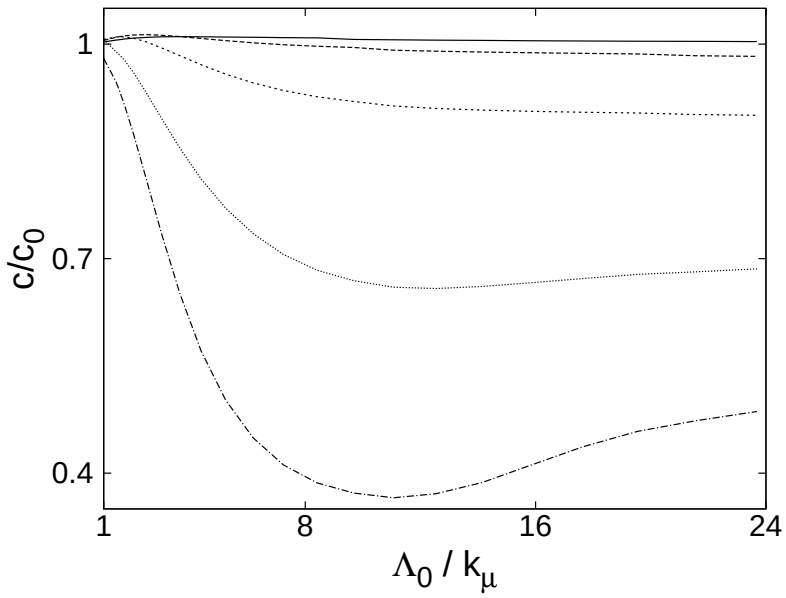

Figure 3.10: Results of numerical studies on equations (3.102)-(3.106) in $D = 2$. The chemical potential μ is kept constant, the condensate density is fixed by the mean-field condition $\rho_0^0 = \mu/u_0$. The plotted curves are calculated for the following values of $\tilde{u}_0$, from above: $\tilde{u}_0 = 1, 2, 4, 8, 12$. The corresponding values for the ratio $k_{ip}/k_\mu = 0.5, 0707, 1, 1.414, 1.732$, where $k_{ip} = mu\sqrt{\rho_0^0}$ denotes the inverse inter-particle distance in the condensate.

The velocity of the Goldstone-mode c is directly measurable. Recent experiments [92] have shown that the mean-field velocity c_0 provides a good estimation only for extremely dilute systems. As a Bose system becomes dense, the measured value of c deviates strongly from the mean-field value. In order to study the crossover from the dilute to the dense regime we keep the bare chemical potential constant and vary the dimensionless interaction $\tilde{u}_0 = 2mu_0k_\mu^{D-2}$, where $k_\mu = \sqrt{2m\mu}$ is also constant. The condensate ρ_0^0 is fixed by the mean-field condition $\rho_0^0 = \mu/u_0$. The ratio k_{ip}/k_μ, where k_{ip} corresponds to the inverse distance between particles in the condensate and is introduced by equation (3.12), is varied from sufficiently far below to sufficiently far above the unity. The first limit corresponds to the dilute and the second one to the dense regime.

Figure 3.10 demonstrates the plot of the ratio c/c_0, where c and c_0 are the renormalized and mean-field velocities of the Goldstone-mode, correspondingly, depicted versus the ratio Λ_0/k_μ, where Λ_0 denotes the interaction range in the Fourier-space. The calculation has been made in $D = 2$. Since the ratio $\Lambda_0/k_\mu = 1/\sqrt{\tilde{\mu}_0}$, where $\tilde{\mu}_0 = 2m\mu\Lambda_0^{-2}$ denotes another dimensionless parameter characterizing the bare action, this calculation takes both characteristic parameters of the bare model into account.

We observe a strong dependence of the renormalized velocity of the Goldstone-mode c on both the interaction strength $\tilde{u}_0$ and ultraviolet-cutoff Λ_0. For small values of $\tilde{u}_0$ which corresponds here to the dilute regime, the renormalized velocity c does not change

considerably and takes nearly the same value as the mean-field velocity c_0 independent from the choice of Λ_0. In this limit the mean-field theory yields satisfactory results. As the interaction and thus the ratio k_{ip}/k_μ increases, the velocity of the Goldstone-mode is stronger renormalized. The deviation from the mean-field value can achieve more than 50%. The velocity c becomes also dependent on the infrared cutoff Λ_0, i. e. on the lattice spacing. In the dense regime the depicted functions exhibit minima due to the finite lattice spacing. In order to obtain a finite and cutoff-independent value of the velocity c, the UV-cutoff Λ_0 should be extended to infinity which is analogous to taking continuous limit. Transfered into the real space this means that the finite range interaction potential of the lattice model collapses to a point-like interaction in the continuous limit since $\Lambda_0^{-1} \to 0$.

3.9 Interaction close to the fixed point. Crossover scale

The shape of the flows which we obtained numerically in section 3.7 enables us to recover their analytical structure for large ℓ. Close to the fixed point we may replace $Z_\ell \approx Z_\star$, $V_\ell \approx V_\star$, $\eta_z \approx 0$, and $\rho_\ell^0 \approx \rho_\star^0$ and only retain flows of u_ℓ and Y_ℓ. Assuming $\omega \leqslant c\Lambda$, where c denotes the renormalized velocity of the Goldstone mode defined in equation (3.109), we recognize the large$-\ell$ behavior of the denominator in the propagators (3.96a) and (3.96b)

$$\begin{aligned} Y_\ell^2\omega^2 + (\epsilon_\ell + V_\ell\omega^2)(2\Delta_\ell + \epsilon_\ell + V_\ell\omega^2) &\approx 2\Delta_\ell\left(\epsilon_\ell + V_\star\omega^2\right) \\ &= 2V_\star\Delta_\ell(\omega^2 + c^2\Lambda^2). \end{aligned} \tag{3.110}$$

For large ℓ, the leading contribution in the numerator of equation (3.103) arises from the term which is proportional to Δ_ℓ^3 in $c_0^{(u)}$. The integration over Matsubara frequencies can be carried out and the flow equation of the interaction (3.103) simplifies to

$$\partial_\ell u_\ell \approx -\frac{u_\ell^2}{A_D}\Lambda^{D-3}, \tag{3.111}$$

where

$$A_D = \frac{4}{3mk_c\kappa_D}\left(\frac{\rho}{\rho_\star^0}\right)^2 = \frac{A_D'}{mk_c}, \tag{3.112}$$

with $\kappa_D = K_D/D$, $k_c = 2mc$ and $\rho_\star^0 = Z_\star\rho$, where ρ denotes the density of bosons and

$$A_D' = \frac{4}{3\kappa_D}\left(\frac{\rho}{\rho_\star^0}\right)^2. \tag{3.113}$$

One has to distinguish between the $D \neq 3$ and $D = 3$ cases. In the first case, the general solution of equation (3.111) can be found in the form

$$u_\ell \approx \frac{u_{\Lambda_0}\Lambda^\epsilon}{\Lambda^\epsilon + \dfrac{mk_c u_{\Lambda_0}}{\epsilon A_D'}\left[1 - \left(\dfrac{\Lambda}{\Lambda_0}\right)^\epsilon\right]}, \tag{3.114}$$

where $\epsilon = 3 - D$. This solution has following properties:

- At $\Lambda = \Lambda_0$ it yields the initial value u_{Λ_0} in all dimensions. The choice of the initial conditions is a delicate matter. Since we consider the flow of the interaction in the $z = 1-$regime, the initial value u_0 should be different from the interaction of the bare model. However, as it becomes clear from below, the flow of the interaction in the $z = 1-$regime in $D < 3$ neither depends on the chosen initial interaction u_0 nor on the starting value for the cutoff-parameter Λ directly, but only through the fully renormalized quantities entering the momentum k_c and factor A'_D. Therefore, we can identify starting value of the cutoff-parameter with the UV-cutoff Λ_0 and the initial value for the interaction with the bare interaction u_{Λ_0}.

- For positive ϵ, i. e. for $D < 3$, it approaches zero as $\Lambda \to 0$. The asymptotical expression for the interaction in this limit is given by

$$u_{\Lambda\to 0} \sim \frac{\epsilon A'_D}{m k_c} \Lambda^{\epsilon}, \tag{3.115}$$

  i. e. it does not depend on the initial value u_{Λ_0} which characterizes the $z = 1-$regime.

- For negative ϵ, i. e. for $D > 3$ and small Λ, it approaches the constant value

$$u_{\Lambda\to 0} \sim \frac{u_{\Lambda_0}}{1 + \dfrac{m k_c u_{\Lambda_0} \Lambda_0^{-\epsilon}}{(D-3)A'_D}} \approx \frac{(D-3)A'_D}{m k_c \Lambda_0^{D-3}}, \tag{3.116}$$

  where Λ_0 should be associated with some inverse length scale relevant in $D > 3$.

For positive ϵ, the crossover from the $z = 2-$ to the $z = 1-$regime is governed by the generalized Ginzburg-scale, with the characteristic momentum k_G [90, 108, 99]. The flow of the interaction for $\Lambda < k_G$ does not depend on the initial condition directly. The Ginzburg-scale related momentum k_G can be found from the denominator of equation (3.114)

$$k_G^{\epsilon} \approx \frac{m k_c u_{\Lambda_0}}{\epsilon A'_D} \left[1 - \left(\frac{k_G}{\Lambda_0} \right)^{\epsilon} \right]. \tag{3.117}$$

Resolving equation (3.117) with respect to k_G, we obtain

$$k_G \approx \left[\frac{\dfrac{m k_c u_{\Lambda_0}}{\epsilon A'_D}}{1 + \dfrac{m k_c u_{\Lambda_0}}{\epsilon A'_D \Lambda_0^{\epsilon}}} \right]^{\frac{1}{\epsilon}} \approx \left[\frac{m k_c u_{\Lambda_0}}{\epsilon A'_D} \right]^{\frac{1}{\epsilon}}. \tag{3.118}$$

For weak coupled regime, where $k_c \sim k_\mu$, this expression coincides up to a constant factor with the one introduced by Dupuis in [99]. If one assumes $k_c \approx k_{c_0}$ and $\rho \approx \rho_\star \approx \rho_0$,

then this expression may be rewritten in the form similar to the one, which was obtained by Castellani *et al.* [89, 90] and Kreisel *et al.* [108]

$$k_G \approx \left(\frac{3\kappa_D}{16\epsilon}\right)^{\frac{1}{\epsilon}} \; k_{c_0} \; \left(\frac{k_{c_0}^D}{\rho_0}\right)^{\frac{1}{\epsilon}}. \tag{3.119}$$

The corresponding flowing parameter ℓ_G is then found to be

$$\ell_G \approx \frac{1}{\epsilon} \ln\left(\Lambda_0^\epsilon \frac{\epsilon A'_D}{m k_c u_{\Lambda_0}}\right). \tag{3.120}$$

For the flows shown in Figures 3.6 and 3.7 we find $\ell_G \approx 2.62$.

In $D = 3$, the only non-trivial solution of equation (3.111) is

$$u_\ell \approx \frac{u_{\Lambda_0}}{1 + \dfrac{m k_c u_{\Lambda_0}}{A'_3} \ln\left(\dfrac{\Lambda_0}{\Lambda}\right)}. \tag{3.121}$$

Solution (3.121) explains large ℓ-scales in the numerical result shown in Figure 3.8. As $\Lambda \approx \Lambda_0$, the interaction stays close to the initial value u_{Λ_0} and vanishes logarithmically as $\Lambda \to 0$. The cross-over scale between the two asymptotes can be easily found as

$$k_G \approx \Lambda_0 \exp\left(-\frac{A'_3}{m k_c u_{\Lambda_0}}\right). \tag{3.122}$$

For flows shown in Figure 3.8, we obtain $\ell_G = A'_3/m k_c u_{\Lambda_0} \approx 160$.

In the dilute regime, expression (3.122) reduces to

$$k_G \approx \Lambda_0 \exp\left(-\frac{8\pi^2 \rho_0}{k_{c_0}^3}\right). \tag{3.123}$$

Since equation (3.122) represents solution of the RG-flow equation in the Goldstone-regime, which is observable for $k \ll k_{c_0}$, the effective IR-cutoff Λ_0 can identified with the scale k_{c_0}. Therefore we obtain for the Ginzburg-scale

$$k_G \approx k_{c_0} \exp\left(-\frac{8\pi^2 \rho_0}{k_{c_0}^3}\right), \tag{3.124}$$

which is also consistent with the result represented in [89, 90] and [108].

Solutions (3.114) and (3.121) thus guarantee the vanishing of the interaction for large ℓ in all dimensions $D \leqslant 3$. Since the interaction connects to the anomalous self-energy via equation (3.65b), solutions (3.114) and (3.121) also explain why and how the anomalous self-energy vanishes at zero external momenta in accordance with the Nepomnyashchy's equality [17]. Strictly speaking, the validity of the Nepomnyashchy's equality in our truncation is insured only in $D \leqslant 3$. Whether taking flows of marginal and irrelevant

vertex functions into account can guarantee the fulfillment of Nepomnyashchy's equality in spatial dimensions larger than three remains unclear. But, since the model becomes non-renormalizable in the RG-sense in $D > 3$ [18, 21], the answer is probably no.

Analogously we can proceed with equation (3.105):

$$\partial_\ell Y_\ell \approx -\frac{u_\ell Y_\ell}{A_D}\Lambda^{D-3}, \tag{3.125}$$

which has completely the same form as equation (3.111), if we assume $Y_\ell \propto u_\ell$, which is obvious from the numerical calculations.

3.10 Exact asymptotic propagators in the infrared limit

Recalling the truncation for the anomalous self-energy given by equation (3.65b) we might expect for this the following low-energy behavior:

$$\Sigma^A_\ell(K) = \rho^0_\ell u_\ell(K) \approx \rho^0_\ell \left(u_\ell + \alpha_\ell \epsilon_{\boldsymbol{k}} + \beta_\ell \omega^2\right). \tag{3.126}$$

Note that non-analytic terms proportional to $|\boldsymbol{k}|$ and $|\omega|$ disappear from the expansion (3.126). This is because the corresponding coupling parameters vanish after averaging with respect to the angular coordinate. We can estimate the importance of each coupling parameter in the Goldstone regime by analyzing respective scaling dimensions. We find the scaling dimensions of coupling parameters α_ℓ and β_ℓ to be

$$[\alpha] = 2 - D - z, \tag{3.127a}$$
$$[\beta] = 4 - D - 3z. \tag{3.127b}$$

In $D = 2$ and in the Goldstone regime with $z = 1$, expressions for the scaling dimensions yield $[\alpha] = [\beta] = -1$ and we might expect that both introduced dynamical parameters α_ℓ and β_ℓ diverge $\propto \Lambda^{-1}$. Hence, for $k \leqslant \Lambda$ the leading order behavior of the interaction for small K should be proportional to $|\boldsymbol{k}|$ or, correspondingly, to $|\omega|$. In $D = 3$ the dimensional analysis predicts the constant behavior of the anomalous self-energy for small k and ω, but this is not true, as it becomes clear from below.

The flow equations for α_ℓ and β_ℓ follow from equation (3.126):

$$\partial_\ell \alpha_\ell = -\frac{\alpha_\ell}{\rho^0_\ell}\partial_\ell \rho^0_\ell + \frac{m}{\rho^0_\ell}\partial_\ell \left(\frac{\partial^2}{\partial k^2}\Sigma^A_\ell(\boldsymbol{k}, 0)\bigg|_{k=0}\right), \tag{3.128a}$$
$$\partial_\ell \beta_\ell = -\frac{\beta_\ell}{\rho^0_\ell}\partial_\ell \rho^0_\ell + \frac{1}{2\rho^0_\ell}\partial_\ell \left(\frac{\partial^2}{\partial \omega^2}\Sigma^A_\ell(0, \omega)\bigg|_{\omega=0}\right). \tag{3.128b}$$

The initial conditions of α_ℓ and β_ℓ should be chosen as $\alpha_{\ell=0} = 0$ and $\beta_{\ell=0} = 0$. For the parameter α_ℓ we obtain:

$$\partial_\ell \alpha_\ell = -\frac{\alpha_\ell}{\rho^0_\ell}\partial_\ell \rho^0_\ell - \frac{2u^2_\ell K_D}{mDZ^2_\ell}\Lambda^{D+2}\int \frac{d\omega}{2\pi}\sum_{i=0}^{4}\frac{c^{(\alpha)}_{2i}\omega^{2i}}{\mathcal{D}^4(\epsilon_\ell, \omega)}, \tag{3.129}$$

where

$$\begin{aligned}
c_0^{(\alpha)} &= -\epsilon_\ell^4 - 2\epsilon_\ell^2\Delta_\ell^2 - 4\epsilon_\ell\Delta_\ell^3 - 2\Delta_\ell^4, \\
c_2^{(\alpha)} &= 6\epsilon_\ell^2 Y_\ell^2 - 4\epsilon_\ell^3 V_\ell + 4\Delta_\ell^2(Y_\ell^2 - \Delta_\ell V_\ell) - 4\epsilon_\ell\Delta_\ell(-2Y_\ell^2 + \Delta_\ell V_\ell), \\
c_4^{(\alpha)} &= -Y_\ell^4 + 4(3\epsilon_\ell + 2\Delta_\ell)Y_\ell^2 V_\ell - 2(3\epsilon_\ell^2 + \Delta_\ell^2)V_\ell^2, \\
c_6^{(\alpha)} &= 2V_\ell^2(3Y_\ell^2 - 2\epsilon_\ell V_\ell), \\
c_8^{(\alpha)} &= -V_\ell^4,
\end{aligned}$$

and flow of the condensate is given by equation (3.102). The flow equation for the parameter β_ℓ becomes

$$\partial_\ell\beta_\ell = -\frac{\beta_\ell}{\rho_\ell^0}\partial_\ell\rho_\ell^0 - \frac{4u_\ell^2}{mZ_\ell}\kappa_\ell\Lambda^{D+2}\int\frac{d\omega}{2\pi}\sum_{i=0}^{6}\frac{c_{2i}^{(\beta)}\omega^{2i}}{\mathcal{D}^5(\epsilon_\ell,\omega)}, \tag{3.130}$$

where

$$\begin{aligned}
c_0^{(\beta)} &= -\epsilon_\ell(\epsilon_\ell + 2\Delta_\ell)(\epsilon_\ell^3 Y_\ell^2 + \epsilon_\ell^4 V_\ell + 2\epsilon_\ell^2\Delta_\ell^2 V_\ell + \Delta_\ell^3(Y_\ell^2 + 2\Delta_\ell V_\ell) \\
&\quad +\epsilon_\ell\Delta_\ell^2(Y_\ell^2 + 4\Delta_\ell V_\ell)), \\
c_2^{(\beta)} &= (-2\epsilon_\ell^5 V_\ell^2 - 10\epsilon_\ell^4 V_\ell(-2Y_\ell^2 + \Delta_\ell V_\ell) + 3\Delta_\ell^3(Y_\ell^2 + 2\Delta_\ell V_\ell)^2 \\
&\quad +2\epsilon_\ell^3(5Y_\ell^4 + 26\Delta_\ell Y_\ell^2 V_\ell + 2\Delta_\ell^2 V_\ell^2) + \epsilon_\ell^2\Delta_\ell(20Y_\ell^4 + 71\Delta_\ell Y_\ell^2 V_\ell + 12\Delta_\ell^2 V_\ell^2) \\
&\quad +\epsilon_\ell\Delta_\ell^2(15Y_\ell^4 + 46\Delta_\ell Y_\ell^2 V_\ell + 20\Delta_\ell^2 V_\ell^2)),
\end{aligned}$$

$$\begin{aligned}
c_4^{(\beta)} &= (5\epsilon_\ell^4 V_\ell^3 + 10\epsilon_\ell^3 V_\ell^2(5Y_\ell^2 - 2\Delta_\ell V_\ell) + \epsilon_\ell^2 V(-5Y_\ell^4 + 88\Delta_\ell Y_\ell^2 V_\ell + 24\Delta_\ell^2 V_\ell^2) \\
&\quad +\Delta_\ell(-2Y_\ell^6 - 5\Delta_\ell Y_\ell^4 V + 13\Delta_\ell^2 Y_\ell^2 V_\ell^2 + 30\Delta_\ell^3 V_\ell^3) \\
&\quad +\epsilon_\ell(-5Y_\ell^6 - 10\Delta_\ell Y_\ell^4 V_\ell + 61\Delta_\ell^2 Y_\ell^2 V_\ell^2 + 48\Delta_\ell^3 V_\ell^3)), \\
c_6^{(\beta)} &= V_\ell(-2Y_\ell^6 - 2(10\epsilon_\ell + 7\Delta_\ell)Y_\ell^4 V_\ell + (20\epsilon_\ell^2 + 12\epsilon_\ell\Delta_\ell - 11\Delta_\ell^2)Y_\ell^2 V_\ell^2 \\
&\quad +4(5\epsilon_\ell^3 - 5\epsilon_\ell^2\Delta_\ell + 7\epsilon_\ell\Delta_\ell^2 + 7\Delta_\ell^3)V_\ell^3), \\
c_8^{(\beta)} &= V_\ell^3(-5Y_\ell^4 - (25\epsilon_\ell + 22\Delta_\ell)Y_\ell^2 V_\ell + 5(5\epsilon_\ell^2 - 2\epsilon_\ell\Delta_\ell + 2\Delta_\ell^2)V_\ell^2), \\
c_{10}^{(\beta)} &= 2V_\ell^5(-8Y_\ell^2 + 7\epsilon_\ell V_\ell - \Delta_\ell V_\ell), \\
c_{12}^{(\beta)} &= 3V_\ell^7.
\end{aligned}$$

The flow of both parameters α_ℓ and β_ℓ in $D = 2$ is shown in Figure 3.11. The divergence of both parameters is evident. To reveal the qualitative behavior of this divergence, we may only retain leading terms in the limit $\ell \to \infty$. For the denominator of the propagators we use the asymptotic formula (3.110), while leading order terms in the numerators are

$$\begin{aligned}
c_0^{(\alpha)} &\approx -2\Delta_\ell^4, \\
c_0^{(\beta)} &\approx -4\epsilon_\ell V_\star\Delta_\ell^5.
\end{aligned}$$

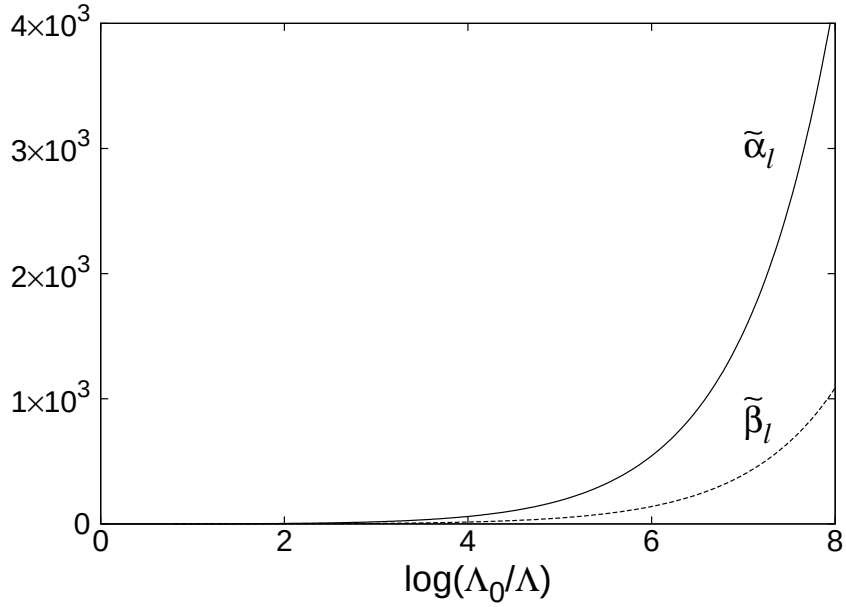

Figure 3.11: RG-flow of the dimensionless flowing parameters $\tilde{\alpha}_\ell = \Lambda_0^D \alpha_\ell$ and $\tilde{\beta}_\ell = 2m\Lambda_0^{D+2z-2}\beta_\ell$, calculated in $D = 2$ for the initial values of the dimensionless chemical potential $\tilde{\mu}_0 = 2m\mu\Lambda_0^{-2} = 0.4$ and dimensionless interaction $\tilde{u}_0 = 2mu_0 k_\mu^{D-2} = 4$.

In this case, both equations reduce to the same form

$$\partial_\ell \alpha_\ell \propto \partial_\ell \beta_\ell \propto u_\ell^2 \Lambda^{D-5}. \tag{3.131}$$

In $D < 3$, where $u_\ell \propto \Lambda^{3-D}$, the solution of equations (3.131) has the following large$-\ell$ behavior

$$\alpha_\ell \propto \beta_\ell \propto \Lambda^{1-D}, \tag{3.132}$$

which explains the Λ^{-1} divergence of the curves depicted in Figure 3.11 and confirms the statement of the simple dimensional analysis. In $D = 3$, the large$-\ell$ behavior of the interaction is proportional to ℓ^{-1} and solutions of equations (3.131) become

$$\alpha_\ell \propto \beta_\ell \propto \int_{\tilde{\ell}}^{\ell} dt\ t^{-2}\ e^{2t} \propto \frac{e^{2\ell}}{\ell} \text{ for large } \ell. \tag{3.133}$$

The lower integration boundary $\tilde{\ell}$ can be chosen arbitrarily, since we are interested in $\ell \gg \tilde{\ell}-$regime. The integral on the right-hand side diverges for $\ell \to \infty$, but weaker than Λ^{-2} as it follows from the dimensional analysis. Hence, we obtain the analytical behavior of the physical anomalous self-energy in the low-energy limit in $1 < D < 3$

$$\Sigma^A(K)\big|_{D<3} \propto C_D\left[(c|\boldsymbol{k}|)^\epsilon + |\omega|^\epsilon\right] \approx C_D(c^2\boldsymbol{k}^2 + \omega^2)^{\frac{\epsilon}{2}}, \tag{3.134}$$

where $\epsilon = 3 - D$ and

$$C_D \approx -\frac{5}{8}\frac{K_D\epsilon^2}{D(\epsilon-2)}\left(\frac{\rho_\star^0}{\rho}\right)^2 \rho_\star^0 m k_c c^{-\epsilon} A_D^2 = \frac{5}{6}\frac{\epsilon^2}{2-\epsilon}\frac{A'_D\rho_\star^0}{m k_c c^\epsilon}, \tag{3.135}$$

$k_c = 2mc$, and A_D and A'_D are defined in equations (3.112) and (3.113).

In $D = 3$, the leading order of the anomalous self-energy is logarithmic in $|\boldsymbol{k}|$ and $|\omega|$

$$\Sigma^A(K)\big|_{D=3} \propto C_3\left[\frac{1}{\ln\left(\dfrac{c\Lambda_0}{c|\boldsymbol{k}|}\right)} + \frac{1}{\ln\left(\dfrac{c\Lambda_0}{|\omega|}\right)}\right] \approx \frac{C_3}{\ln\left(\dfrac{c\Lambda_0}{\sqrt{c^2\boldsymbol{k}^2+\omega^2}}\right)}, \tag{3.136}$$

where

$$C_3 = -\frac{5}{48\pi^2}\left(\frac{\rho_\star^0}{\rho}\right)^2 \rho_\star^0 m k_c A_3^2 = -\frac{5}{9}\frac{A'_3\rho_\star^0}{m k_c}. \tag{3.137}$$

Expression (3.136) reproduces the leading order behavior of the anomalous self-energy obtained by Griffin (see chapter 6.3 in [94]).

We are now in the position to recover the low-energy behavior of the Green functions (3.20). By taking equations (3.65a), (3.65b) and (3.126) into account, expressions for the flowing normal and anomalous full propagators become

$$G_\ell^N(\pm K) = \frac{1}{\mathcal{D}_\ell(K)}\left(\Delta_\ell \pm iY_\ell\omega + (1+\rho_\ell^0\alpha_\ell)\epsilon_{\boldsymbol{k}} + R_\ell(\boldsymbol{k}) + (V_\ell + \rho_\ell^0\beta_\ell)\omega^2\right), \tag{3.138}$$

$$G_\ell^A(K) = -\frac{1}{\mathcal{D}_\ell(K)}\left(\Delta_\ell + \rho_\ell^0\alpha_\ell\epsilon_{\boldsymbol{k}} + \rho_\ell^0\beta_\ell\omega^2\right), \tag{3.139}$$

$$\begin{aligned}\mathcal{D}_\ell(K) = {} & Y_\ell^2\omega^2 + (\epsilon_{\boldsymbol{k}} + R_\ell(\boldsymbol{k}) + V_\ell\omega^2) \\ & \times((1+2\rho_\ell^0\alpha_\ell)\epsilon_{\boldsymbol{k}} + R_\ell(\boldsymbol{k}) + (V_\ell + 2\rho_\ell^0\beta_\ell)\omega^2).\end{aligned} \tag{3.140}$$

The divergence of the parameters α_ℓ and β_ℓ enables us to expand equations (3.138) and (3.139) in powers of the small quantity α_ℓ^{-1} under assumption $\beta_\ell/\alpha_\ell \to const$. For momenta $k \leqslant \Lambda$, we obtain in the leading order of the expansion

$$\begin{aligned}G^N(\pm K) &= -G^A(K) = \frac{1}{2V_\star(\omega^2 + (2mZ_\star V_\star)^{-1}k^2)} \\ &= \frac{m\rho_\star^0 c^2}{\rho}\frac{1}{\omega^2 + c^2k^2},\end{aligned} \tag{3.141}$$

where the introduced velocity of the Goldstone mode

$$c = \frac{1}{\sqrt{2mV_\star Z_\star}} \tag{3.142}$$

reproduces expression (3.109). Equation (3.141) reproduces exactly the infrared asymptote of the propagators (3.47), which was first obtained by Gavoret and Nozières [86].

3.11 Hard-core limit

We are now in the position to make contact with the work of Schick [104] who investigated the hard-core Bose gas in two dimensions perturbatively. As we will see below, in $D = 2$ the vanishing of the interaction for $\ell \to \infty$ in the initial $z = 2$ regime is logarithmic in Λ/Λ_0, which reflects the vanishing of the s-wave scattering length [107]. This requires a modified perturbative approach in terms of the new small parameter $1/\ln(\rho a^2)$, where ρ denotes the density of bosons and a is related to the size of the hard-core disc. In the $z = 2$ regime, it suffices only to investigate the flow of the interaction, while setting all remaining flowing quantities to their initial values. Performing the summation over the Matsubara-frequencies we then obtain

$$\partial_\ell u_\ell \;=\; -u_\ell^2 \kappa_D \frac{\Lambda^{D+2}}{2m} \frac{\epsilon_\ell^3 - 5\epsilon_\ell^2 \Delta_\ell + \epsilon_\ell \Delta_\ell^2 + 3\Delta_\ell^3}{E_\ell^5}, \tag{3.143}$$

where $E_\ell = \sqrt{\epsilon_\ell(\epsilon_\ell + 2\Delta_\ell)}$ and $\kappa_D = K_D/D$.

In the $z = 2-$regime, the Bogoliubov-spectrum approaches the free particle dispersion, i. e. $\epsilon_\ell \gg \Delta_l$. In this case we may simplify equation (3.143) as follows

$$\partial_\ell u_\ell^{-1} \approx 2m\kappa_D \Lambda^{D-2}. \tag{3.144}$$

Again, we have to distinguish between the $D = 2$ and $D \neq 2$ cases. In the latter case, solution of this equation is found in the form

$$u_\ell = \frac{u_{\Lambda_0}}{1 + \dfrac{2m u_{\Lambda_0} \kappa_D}{D-2} \left(\Lambda_0^{D-2} - \Lambda^{D-2}\right)}. \tag{3.145}$$

If $D > 2$, then the interaction flows to a finite value

$$u_{\ell\to\infty} \approx \frac{u_{\Lambda_0}}{1 + \dfrac{2m u_{\Lambda_0} \kappa_D}{D-2} \Lambda_0^{D-2}} \approx \frac{(D-2) a^{D-2}}{2m\kappa_D}, \tag{3.146}$$

where we replaced the UV-cutoff Λ_0 by the inverse $s-$wave scattering length a. In $D = 3$ we obtain for the physical interaction

$$u \approx \frac{3\pi^2}{m} a, \tag{3.147}$$

which is slightly larger than the scattering theory prediction for the $T-$matrix $8\pi a/m$ (see for instance [85]). However, the accuracy can be improved by adjusting the UV-cutoff to $\Lambda_0 = 3\pi/8a$. Due to equation (3.145), the $s-$wave scattering length is finite in all dimensions above two.

On the other hand, expression (3.145) approaches zero as $\Lambda \to 0$ in dimensions below two. This behavior is power-law-like, i. e.

$$u_{\ell\to\infty} \approx \frac{2-D}{2m\kappa_D} \Lambda^{2-D}. \tag{3.148}$$

Hence, the $s-$wave scattering length vanishes in all dimensions $D < 2$. From equation (3.148) follows an interesting consequence for the anomalous self-energy at zero frequency and momenta, which thus vanishes also in the $z = 2-$regime.

Below we concentrate on the two dimensional case. In $D = 2$, the only solution of equation (3.144) has the form

$$u_\Lambda \approx \frac{u_0}{1 + \frac{mu_0}{2\pi} \ln\left(\frac{\Lambda_0}{\Lambda}\right)}. \tag{3.149}$$

In the regime $1 \gg \frac{mu_0}{2\pi} \ln\left(\frac{\Lambda_0}{\Lambda}\right)$ the interaction does not flow and the Bogoliubov theory remains correct. The opposite case $1 \ll \frac{mu_0}{2\pi} \ln\left(\frac{\Lambda_0}{\Lambda}\right)$ corresponds to the limit of hard-core bosons, where the flow does not depend on the initial value of the interaction. In this case we may write

$$u_\Lambda \approx \frac{2\pi}{m \ln\left(\frac{\Lambda_0}{\Lambda}\right)}, \tag{3.150}$$

which reproduces the result obtained by Fisher and Hohenberg [107].

If we now define the cross-over scale as $\epsilon_{\Lambda_\star} \approx 2\rho^0 u_{\Lambda_\star} \approx 2\rho u_{\Lambda_\star}$, where the scaling character of the Bogoliubov spectrum is expected to change, then we find up to logarithmic accuracy $\ln(\Lambda_0/\Lambda_\star)^2 \approx 1$ and thus

$$\Lambda_\star^2 \approx 16\pi\rho. \tag{3.151}$$

Hence, the corresponding energy cross-over scale is given by,

$$\Delta_{\Lambda_*} \approx \rho u_{\Lambda_*} \approx -\frac{8\pi\rho}{m \ln(\rho a^2)}, \tag{3.152}$$

which is nothing but Schick's cross-over scale for hard-core bosons [104], where a is the diameter of the hard-core disc and UV-cutoff is chosen such that $\Lambda_0 = \sqrt{16\pi/a^2}$. The velocity of the Goldstone mode in the hard-core regime thus becomes

$$c = \sqrt{\frac{\Delta_\star}{2m}} \approx \sqrt{-\frac{4\pi\rho}{m^2 \ln(\rho a^2)}}. \tag{3.153}$$

In conclusion, we have shown that the FRG-flow equations are able to correctly describe the hard-core limit, too. A new small parameter for the perturbative expansion in $D \leqslant 2$ emerges naturally from these equations.

3.12 Spectral density function

In this section we shall investigate dynamical properties of interacting bosons which occur at finite external momenta. The main goal is to calculate the single-particle spectral density function. We can extract from the spectral density function both the damping of quasi-particles as width of the spectral peaks at half maximum [85] and the

spectrum of elementary excitations as positions of resonances. Therefore, it is sufficient to calculate the spectral density function in order to obtain the full spectral line-shape of interacting bosons.

As is well known, the quasi-particle damping can be calculated perturbatively by analyzing second-order diagrams [79, 80]. The sketch of Beliaev theory of the damping was given in section 3.3. Extended to arbitrary dimensions, Beliaev damping is given by equation (3.43). Since in $D = 3$, Beliaev damping does not depend on the interaction directly, but only weakly through the condensate, we expect the renormalization effects in $D = 3$ to be not very strong. Moreover, as pointed out by Andersen [103] (see also [109]), Beliaev result (3.43) in $D = 3$ is valid for any non-relativistic superfluid with the broken $U(1)$-symmetry in the long-wavelength limit. On the other hand, Beliaev damping directly depends on the interaction in all dimensions $D < 3$. Therefore, we restrict our consideration to the systems in $D = 2$. Nonetheless, the approach presented here is completely general and applicable with less modification to whatever dimensions.

In order to obtain momentum dependent self-energies in the FRG-framework we need to resolve the flow-equations (3.82) and (3.87). Without any loss of generality, a momentum dependent physical vertex $\Gamma(K)$ can be found from the respective flow equation by integrating out the cutoff momentum Λ:

$$\Gamma(K) = \Gamma_{\Lambda_0}(K) - \int_0^{\Lambda_0} d\Lambda \; \dot{\gamma}_\Lambda(K), \tag{3.154}$$

where $\dot{\gamma}_\Lambda(K)$ denotes the right-hand side of the corresponding flow equation and $\Gamma_{\Lambda_0}(K)$ denotes the vertex at the beginning of the flow. In order to calculate real-time quantities, one has to perform an analytical continuation to the real frequencies $\pm i\omega \to \omega \pm i0^+$, which then allows the separation of the real and imaginary parts of the Green function by means of the Dirac identity

$$\frac{1}{\omega - E \pm i0^+} = \mathcal{P}\frac{1}{\omega - E} \mp i\pi\delta\left(\omega - E\right), \tag{3.155}$$

where $\mathcal{P}$ denotes the principle value operator. However, since the structure of the single-scale propagators given by equations (3.97) and (3.98) implies double poles, i. e.

$$\dot{\boldsymbol{G}}_\Lambda = -\boldsymbol{G}_\Lambda \cdot [\partial_\Lambda \boldsymbol{R}_\Lambda] \cdot \boldsymbol{G}_\Lambda, \tag{3.156}$$

this conventional procedure of analytical continuation leads to ambiguities. Therefore, we decided to abandon attempts to find an analytical expression for the damping of quasi-particles and concentrated on the purely numerical solution of the problem.

Instead of attempting to find a completely self-consistent solution, we use a non-self-consistent approach proposed in chapter 2 (see also [44]). As pointed out in [44], the full solution is expected to appreciably deviate from the non-self-consistent solution only for large momenta (at the order of Λ_0) or at strong coupling. We approximate self-energies entering Green functions on the right-hand side of corresponding RG-flow

equation by using truncation (3.65a), (3.65b) and (3.59), inserting in the place of the coupling parameters ρ_ℓ^0, u_ℓ, V_ℓ, Y_ℓ and Z_ℓ the corresponding flows.

The calculation of the real-time vertex functions was made in two distinct steps. First, the imaginary-frequency self-energies were calculated for discrete constant values of the momentum as functions of the Matsubara frequency. Secondly, the analytical continuation of calculated normal Green function to the real frequencies was made. For this we employed the Padé-approximant algorithm described in [100].

Numerical evaluation of equations (3.82) and (3.87) requires integrations over respectively internal Matsubara frequencies, two dimensional internal momenta, and finally the logarithmic flowing parameter ℓ. For the immediate integration we used well established routines from [110]. Nonetheless, it turned out to be a highly complicated and a very time consuming task.

The determined imaginary-frequency vertex functions exhibit all demanded properties. For small external momenta and frequencies, the physical dynamical two-field coupling parameter introduced by equation (3.59) should exhibit the following asymptotic behavior:

$$\begin{aligned} \sigma(\boldsymbol{k}, i\omega) &= \Sigma^N(\boldsymbol{k}, i\omega) - \Sigma^A(\boldsymbol{k}, i\omega) \\ &\approx -i\omega(Y_\star - 1) + \frac{1 - Z_\star}{2mZ_\star}k^2 + V_\star\omega^2 \\ &\approx i\omega + \frac{1 - Z_\star}{2mZ_\star}k^2 + V_\star\omega^2, \end{aligned} \tag{3.157}$$

as predicted by equation (3.59). These asymptotes are plotted in Figure 3.12 in comparison to our numerical calculation. The asymptotical region becomes more narrow, if we vary initial conditions of the flowing coupling parameters in order to achieve $2mc \ll \Lambda_0$, where $c = 1/\sqrt{2mZ_\star V_\star}$ denotes the renormalized velocity of the Goldstone-mode.

As predicted by equation (3.134), the leading order behavior of the imaginary-frequency anomalous self-energy in $D = 2$ is expected to be proportional to $|\boldsymbol{k}|$ and $|\omega|$. The results of our numerical calculation are demonstrated in Figures 3.13 and 3.14. The slope values of the linear asymptotes predicted by equations (3.134) and (3.135) deviate a little from the values obtained by fitting the numerical data (see the Figure legend). However, if we think of approximations which have been made while deriving our result (3.134) and (3.135), it might be considered quite satisfactory. The striking resemblance of functions shown in Figures 3.13 and 3.14 is due to the kind how frequency and momenta enter equation (3.134).

As pointed out by Shi and Griffin in [85], self-energies calculated within the usual perturbation theory suffer from infrared divergences at zero external momentum. Since our vertices vanish at $K = 0$, our theory is free of any IR-divergences.

In Figure 3.15 we show real and imaginary parts of both normal $G^N(K)$ and anomalous $-G^A(K)$ imaginary-frequency Green functions calculated for the small external momentum $k = 0.1mc$. This calculation has been done in order to demonstrate that our numerics correctly reproduces asymptotic equality $G^N(K) \approx -G^A(K)$ for small K. Noticeable is that the position of the minimum of the imaginary part of the normal Green function is found at the predicted resonance frequency $\omega \approx ck$.

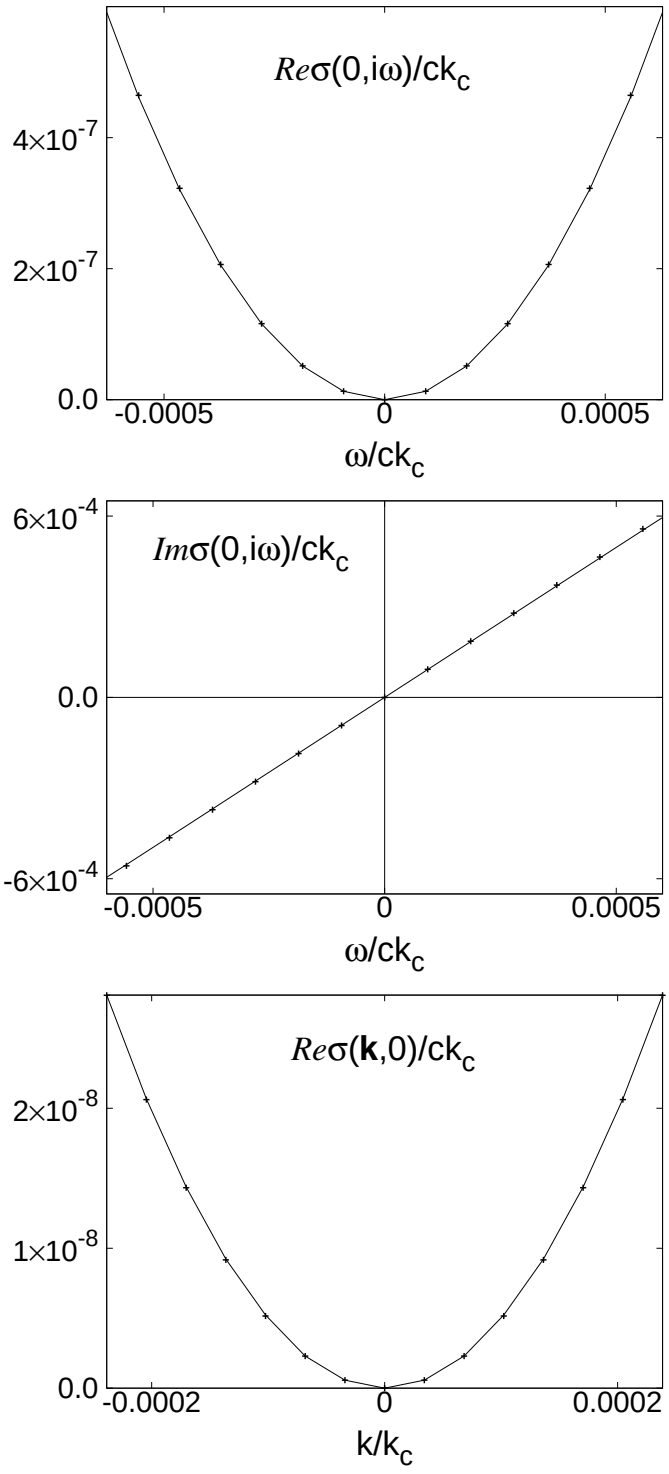

Figure 3.12: Infrared behavior of the dynamical two-fields coupling parameter $\sigma(\boldsymbol{k}, i\omega) = \Sigma^N(\boldsymbol{k}, i\omega) - \Sigma^A(\boldsymbol{k}, i\omega)$ calculated with $\tilde{\mu}_0 = 0.15$ and $\tilde{u}_0 = 15$. Here, the solid lines correspond to the numerical evaluation of equations (3.82) and (3.87), while the crosses come from the asymptotic formula (3.157). The first plot demonstrates $\mathrm{Re}\{\sigma(0, i\omega)\} \approx V_\star \omega^2$. The plot in the middle demonstrates $\mathrm{Im}\{\sigma(0, i\omega)\} \approx i\omega$. Finally, the last plot shows $\mathrm{Re}\{\sigma(k, 0)\} \approx (Z_\star^{-1} - 1)k^2/2m$. All quantities are plotted in units of the momentum $k_c = 2mc$.

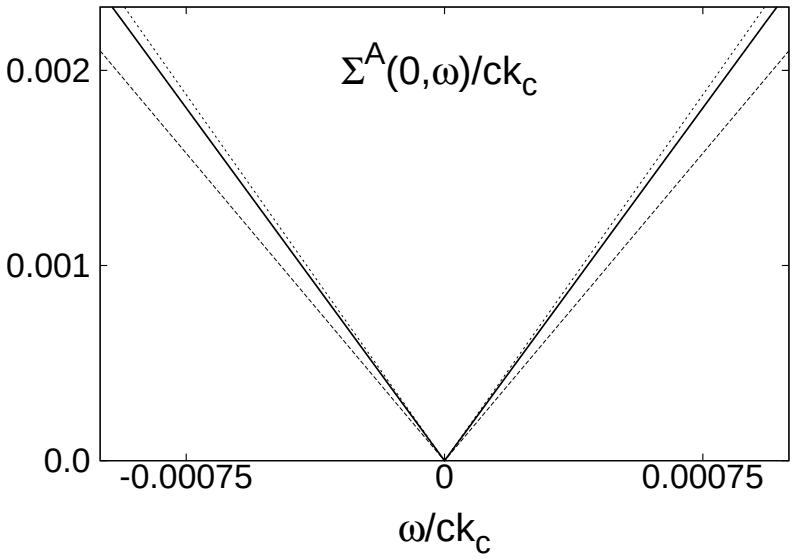

Figure 3.13: Infrared behavior of the physical anomalous imaginary-frequency self-energy $\Sigma^A(0,\omega)$ in $D = 2$ calculated with the initial conditions $\tilde{\mu}_0 = 0.15$ and $\tilde{u}_0 = 15$. The thin dashed line follows from equation (3.134). Its slope value is ≈ 2.1, while the fitting of the numerical data yields the value ≈ 2.5 (dotted line).

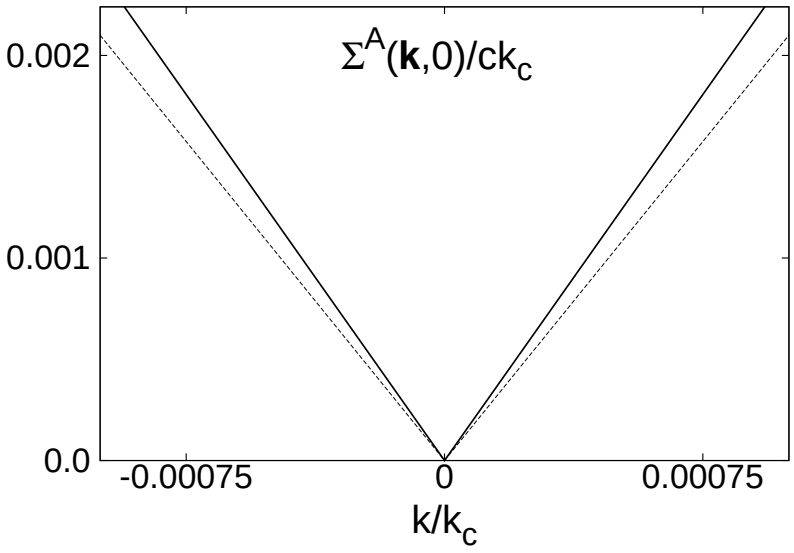

Figure 3.14: Infrared behavior of the physical anomalous self-energy in $D = 2$ calculated with the initial conditions $\tilde{\mu}_0 = 0.15$ and $\tilde{u}_0 = 15$. Here, the anomalous self-energy at zero frequency $\Sigma^A(\boldsymbol{k}, 0)$ is shown. The thin dashed line shows the asymptote $\approx 0.74|\boldsymbol{k}|$ as it follows from equation (3.134). All quantities are measured in units of $k_c = 2mc$.

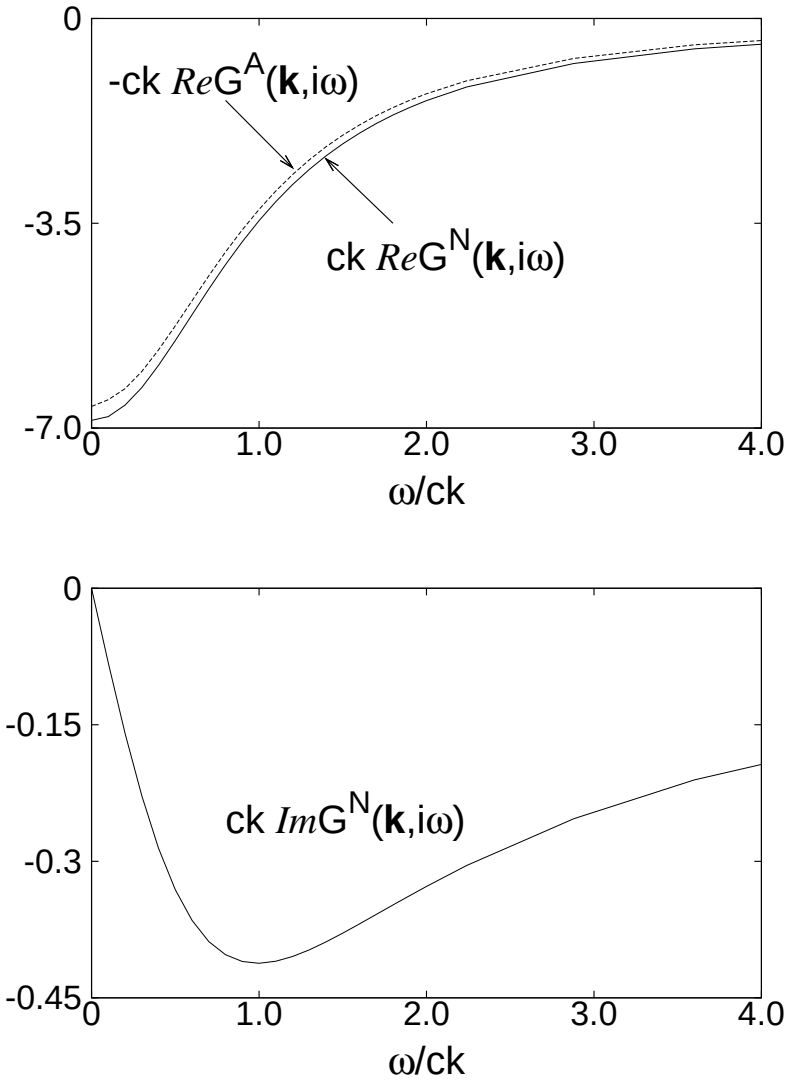

Figure 3.15: A typical shape of both normal and anomalous imaginary-frequency Green functions in the limit $\ell \to \infty$. The curves were calculated with the initial conditions $\tilde{\mu}_0 = 0.15$ and $\tilde{u}_0 = 15$ at fixed external momentum $k = 0.1mc$. The little deviation of both real parts is due to the asymptotic formulas (3.141). Note the position of the minimum of the imaginary part of the normal Green function which lies at the resonance in the Goldstone-regime, as well as the linear behavior for small frequencies which is in accordance to the truncation employed. The imaginary part of the anomalous Green function equals zero.

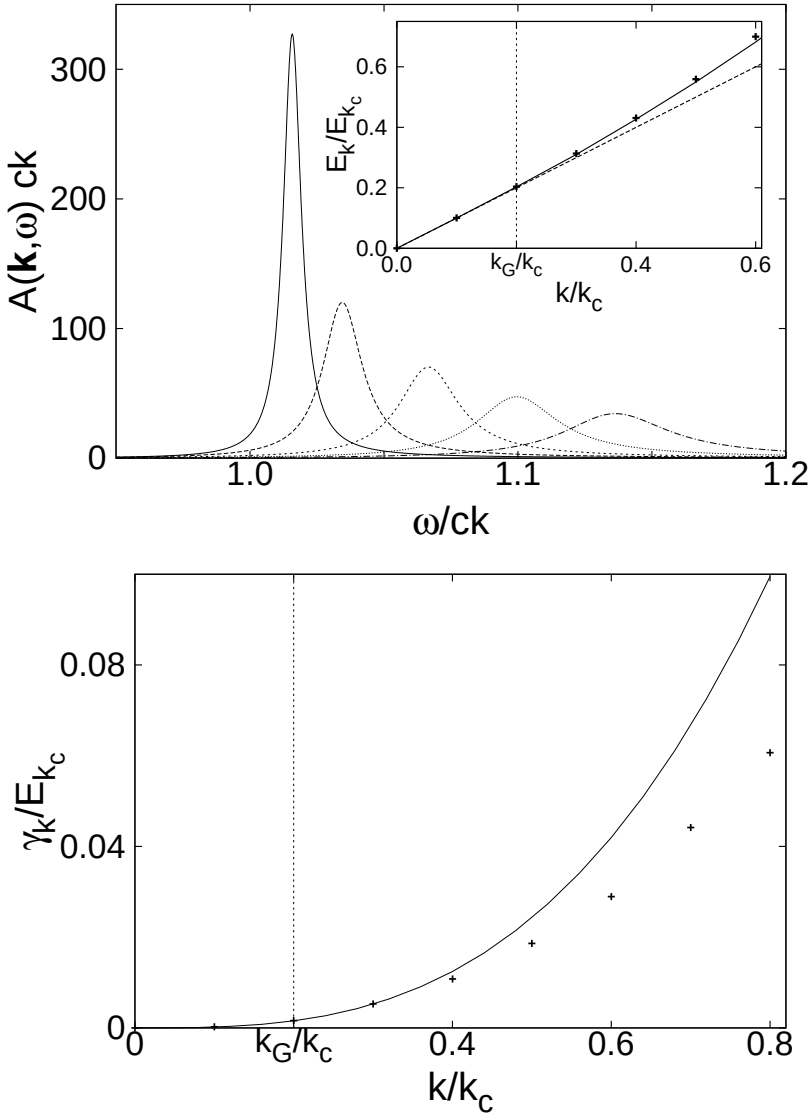

Figure 3.16: Single-particle spectral density $A(\boldsymbol{k}, \omega)$ as a function of the real frequency ω for different values of k, calculated for $\tilde{\mu}_0 = 0.15$ and $\tilde{u}_0 = 15$ (on the top), and FRG result for the quasi-particle damping γ_k (below). The inset in the plot on the top shows the quasi-particle dispersion E_k which deviates at large k from linearity but is well described by a Bogoliubov type expression $E_k = \sqrt{\epsilon_k^2 + c^2 k^2}$ with renormalized velocity $c = (2mV_* Z_*)^{-1/2}$ (black dots). The peaks of the spectral function correspond to (from left to right) $k/k_c = 0.2$, 0.3, 0.4, 0.5 and 0.6, where $k_c = 2mc$. In the plot below, black dots are extracted from the spectral density, while the solid line fits them as $\gamma_k \approx 0.194 k^3/2mk_c$. The deviation of the spectrum from linearity and of the damping from cubic behavior becomes visible at the Ginzburg-scale calculated from equation (3.118).

We are ultimately interested in the real-time dynamical quantities, such as spectral density function. In order to calculate it, we have to perform an analytical continuation of imaginary-frequency self-energies to real frequencies. In the recent decades, several analytical continuation techniques were proposed [100, 101]. However, all of them suffer from their own specific disadvantages. We chose the Padé-approximant technique, which has the advantage to be relatively easy to implement numerically. The routine we used, implemented the algorithm described in [100]. Although it was originally proposed for dealing with systems at finite temperatures, it can also be used for zero-temperature calculations, if input functions are resolved sufficiently well. Taking the normalization condition of the spectral density function

$$\int_{-\infty}^{\infty} \frac{d\omega}{2\pi} A(\boldsymbol{k}, \omega) = 1 \tag{3.158}$$

as a criterion for the accuracy of the calculation, we observe a tendency toward the higher accuracy as both, the order of Padé approximation and the range of the calculated imaginary-frequency Green function increase. However, the price to pay for the accuracy consists of an enormous increase of the computational time. The results which we present here were calculated within the $N = 200$ Padé approximation. The imaginary-frequency Green functions were calculated for $\omega \in [0, 100ck)$ for each momentum k. The achieved deviation in the norm of the spectral density from the unity is in this case less than 5%. It is obvious that an exact fulfillment of the condition (3.158) is only possible, if the imaginary-frequency Green functions are determined for all frequencies from zero to infinity. This limit is however not achievable numerically. A typical shape of the spectral density function of a bosonic system obtained by implementing the Padé approximant technique is shown in Figure 3.16 for $\omega \geqslant 0$. One clearly observes a finite peak broadening which grows with increasing momenta. The broadening arises from Beliaev damping [79, 80]. Both quantities which can be extracted from the spectral density are also demonstrated in this figure. The extracted spectrum of elementary excitations is always well fitted by a Bogoliubov-like expression $E_k = \sqrt{\epsilon_k^2 + c^2 k^2}$. On the other hand, the damping of quasi-particles always reveals a k^3-behavior for small momenta, which is in accordance with the predictions of the perturbative analysis, compare equation (3.43). However, the weight α_0 in equation (3.43) should be replaced by a function $\alpha(\tilde{\mu}_0, \tilde{u}_0)$ of the relevant dimensionless parameters $\tilde{\mu}_0$ and $\tilde{u}_0$ of the model (3.1). For small values of both dimensionless parameters we nearly reproduce the perturbative result given by equation (3.46). For instance, for $\tilde{\mu}_0 = 0.008$ and $\tilde{u}_0 = 0.8$ we obtain $c/c_0 \approx 1.0054$ and $\alpha(\tilde{\mu}_0, \tilde{u}_0)/\alpha_0 \approx 0.967$. As both parameters increase (keeping UV-cutoff Λ_0 constant), we observe deviation of both velocity of the Goldstone mode (see Figure 3.10) and function $\alpha(\tilde{\mu}_0, \tilde{u}_0)$ from the prediction of the perturbation theory. For instance, for $\tilde{\mu}_0 = 0.4$ and $\tilde{u}_0 = 4$ we obtain $c/c_0 \approx 1.01$ and $\alpha(\tilde{\mu}_0, \tilde{u}_0)/\alpha_0 \approx 0.915$, while the results for $\tilde{\mu}_0 = 0.15$ and $\tilde{u}_0 = 15$ are $c/c_0 \approx 0.669$ and $\alpha(\tilde{\mu}_0, \tilde{u}_0)/\alpha_0 \approx 0.526$. The first example corresponds to the weak-interacting regime, where effects due to the renormalization are expected not to play an important role, while the last choice of the initial conditions corresponds to the strong coupling regime, because of the considerable difference in our

results compared to that predicted by the perturbation theory.

The deviation of the Bogoliubov-spectrum from linearity becomes visible at the Ginzburg-scale determined in equation (3.118). The same scale is also visible in the deviation of the Beliaev-damping from the cubic behavior, as it is clearly seen from Figure 3.16. The Ginzburg-scale is here illustrated by the vertical straight dashed line.

3.13 Summary

In conclusion, we have successfully applied Functional Renormalization Group to interacting bosons at zero temperature. The employed truncation scheme is based on the non-local character of the interaction, which reveals itself crucial for correct prediction of the low-energy asymptotical behavior of both self-energies and Green functions. In contrast to the previous approaches [89, 90, 95, 96, 98] we go beyond the description of the asymptotic regime near zero temperature and calculate the entire spectral line-shape of interacting bosons. Our approach takes both Hugenholtz-Pines and Nepomnyashchy-Nepomnyashchy exact relations into account. To the best of our knowledge, this is the first successful attempt to imbed both relations in one scheme in order to study the true dynamics. Both dynamical quantities, the spectrum of elementary excitations and the damping of quasi-particles obey qualitatively the same behavior as predicted by the perturbation theory. In comparison to the mean-field prediction, the velocity of the Goldstone-mode, as well as the weight of the damping in reduced spatial dimensions are strongly renormalized. The absolute value of this renormalization reveals dependence on the initial interaction and condensate. The obtained results can be directly compared with experimental data.

4 Summary

The main issue of this thesis consists in the application of the Functional Renormalization Group to interacting bosons with broken symmetry. The physics of Bose systems in the broken symmetry phase is very different from the physics in the symmetric phase, because of the long-range order which emerges in the system below the critical temperature. This ordered fraction is taken into account by introducing an order parameter which can be considered a mean-field background. However, the efficiency of the mean-field theory in description of phase transitions is restricted, since it does not take fluctuations into account which become important if the system approaches the critical point. Perturbative corrections to the mean-field results often fail to provide appreciable improvements in exploring the critical behavior of the system. Since it is a non-perturbative approach [9, 10, 12, 13, 18, 27], the Renormalization Group (RG) as a whole, and Functional RG in particular, offers a possible way to go beyond the mean-field theoretical level in description of the ordered phase physics. Applied to the many body systems in the disordered phase, FRG always yields very accurate results and sometimes represents the only way to treat systems, which are not achievable by using usual techniques [37]. For this reason, an extension of the FRG-formalism for dealing with the symmetry breaking is urgent. The necessary modification of the FRG-formalism has only very recently been done [14] and less is known about the specifics of the FRG-treatment of the ordered phase. This fact is the main motivation for the investigations which we present in this work.

In this thesis we consider two well-known models. As first, the behavior of the classical one-component scalar field model close to criticality is studied. In such a system, a spontaneous magnetization emerges below the critical temperature. In contrast to the disordered phase, where the phase transition is governed by the interaction [43, 61], an additional length scale, the temperature dependent correlation length, strongly affects the behavior of the model as it approaches the critical point of the phase transition from the ordered phase. The main objective of this part consists in revealing how the interplay between effects due to the interaction and temperature reflects itself in the critical behavior of the model. It turns out that a qualitatively correct description of this physics is possible already on the simplest approximate level, where only parameters relevant in the RG-sense are taken into account. It suffices to consider only the flow of the magnetization and interaction, in order to study effects due to the competition between the two scales. This competition becomes especially visible in the vicinity of the non-trivial fixed point, since the interaction dependent Ginzburg-length is characteristic for the attractive direction of the fixed point, while the temperature dependent correlation length corresponds to the repulsive one. Due to the competition between the two scales, two different scenarios for the behavior of the system are possible, as it can be seen

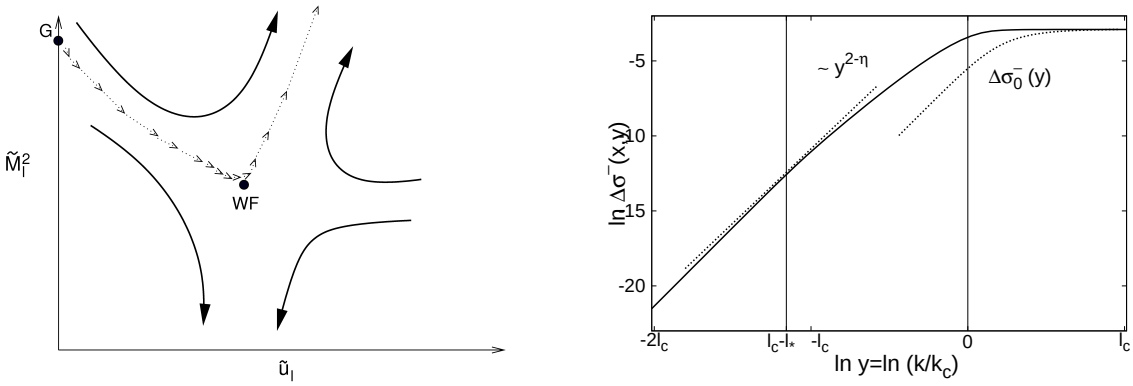

Figure 4.1: Left: The nearly-critical RG-flow of the rescaled interaction $\tilde{u}_\ell$ and magnetization $\tilde{M}_\ell^2$ in the parameter space for $2 < D < 4$. The expansion of the system toward a stable ferromagnetic phase is shown. Right: The nearly-critical scaling function of the self-energy for $\xi \gg l_G$, where ξ denotes the correlation length and l_G the critical Ginzburg length. The crossover area is clearly visible around $y \approx \ell_c - \ell_\star$, where $\ell_c = \ln(\Lambda_0 l_G)$ and $\ell_\star = \ln(\Lambda_0 \xi)$ and Λ_0 is the ultraviolet momentum cutoff.

from Figure 4.1, where the RG-flow of the rescaled interaction and magnetization is shown in the parameter space. In the first scenario, the symmetry of the system gets restored, as the magnetization vanishes. In the second scenario, which is illustrated in Figure 4.1, the system expands toward the stable ferromagnetic phase. The scenario chosen by the system only depends on the choice of initial conditions of the model. Both scales determine the behavior of the physical self-energy close to the scaling regime (see Figure 4.1), where an intermediate area between the critical regime with $\Sigma(\boldsymbol{k}) \propto k^{2-\eta}$ with the anomalous dimension η, and non-critical one with $\Sigma(\boldsymbol{k}) \propto k^2$ emerges.

Quantitatively, our results can be improved by taking irrelevant coupling parameters into account, which is equivalent to employing of a higher order local potential approximation. However, this requires an extension of the flow equations hierarchy in order to imbed all coupling parameters. This procedure becomes very cumbersome already on the level of the four-point vertex function.

In the second part of this thesis we consider systems of interacting bosons with condensate at zero temperature. In this case, the continuous $U(1)-$symmetry group is spontaneously broken. Due to the Goldstone theorem [15], this implies the emergence of the gapless excitation spectrum with the linear behavior at small momenta. Mathematically the absence of the energetic gap in the spectrum of elementary excitations is predicted by the Hugenholtz-Pines equality (HPE)

$$\mu = \Sigma^N(0) - \Sigma^A(0), \tag{4.1}$$

where $\Sigma^N(0)$ and $\Sigma^A(0)$ are normal and anomalous self-energies at zero momenta. The HPE is known to hold to any order in perturbative expansion. To any order of perturbative expansion too, the anomalous self-energy always has a non-vanishing value

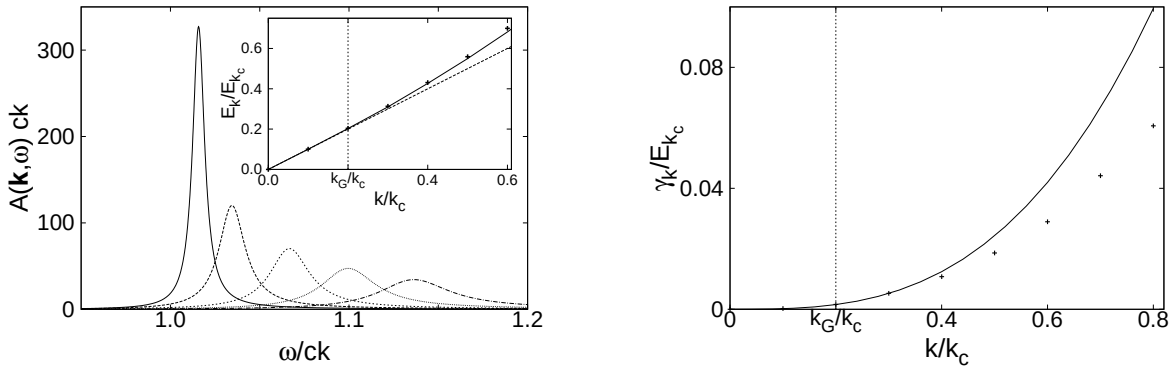

Figure 4.2: Left: A typical single-particle spectral density function of interacting bosons. The inset shows the spectrum of elementary excitations extracted from the spectral function. Black dots refer to the analytical Bogoliubov-like spectrum $E_k = \sqrt{\epsilon_k^2 + c^2k^2}$ with the renormalized velocity of the Goldstone-mode c. Right: The damping of the quasi-particles extracted from the spectral function (black dots). The solid line qualitatively reproduces the perturbative results for small momenta. The dashed vertical line marks the Ginzburg-scale, at which the deviation of the spectrum from linearity becomes visible.

in the long wavelength limit, which is a contradiction to the exact Nepomnyashchy-Nepomnyashchy equality (NNE), which postulates its vanishing, i. e.

$$\Sigma^A(0) = 0. \tag{4.2}$$

The perturbative approach to interacting bosons has several disadvantages. There is no uniform expansion parameter for an arbitrary spatial dimension. Both HPE and NNE cannot be simultaneously taken into account by neither of the perturbative approaches. From this point of view, no calculations of dynamical quantities which kept track of both relations had been previously done. Furthermore, the perturbation theory for interacting bosons suffers from non-physical infrared divergences [85]. Finally, the strong coupling regime is not achievable for the perturbation theory.

Most of these difficulties are avoided in the FRG-framework. All quantities obtained within the FRG scheme are finite, i. e. no divergences occur. The non-perturbative nature of the Renormalization Group makes it a possible candidate for treating strong coupling regime. The FRG-resumation of the perturbative series enables one to imbed both HPE and NNE in one scheme, since the RG-flow of the anomalous self-energy is shown to vanish in the infrared limit in all dimensions $D \leqslant 3$. Hence, the correct description of the dynamics of interacting bosons at finite momenta becomes possible. In particular we managed to calculate the single-particle spectral density function in $D = 2$, which is shown in Figure 4.2.

In conclusion, we believe that the objectives of our investigation have been successfully achieved. We believe that we managed to clearly demonstrate the efficiency of the FRG-approach to the symmetry broken phase. We think RG is a most promising way to

approach the physics of strong correlated systems with broken symmetry. We hope that further development in the Renormalization Group science will one day bring us into the position, where it becomes possible to unveil the mystery of superfluid Helium and high temperature superconductors.

A Bosonic FRG in the real field basis

In this appendix we consider an alternative parametrization of the model described in chapter 3. In this parametrization we map the $U(1)-$invariant Euclidean action onto the quantum $O(2)-$model. The both field components of the latter correspond to the longitudinal and transversal fluctuations with respect to the direction of the broken symmetry [61, 89, 90, 95, 98]. We derive RG-flow equations for the vertex functions in the real field basis. Of course, all results obtained by employing this basis are identical with the ones obtained in the previous chapter. Partially, the material presented here has been published in [70].

A.1 Functional integral approach in the real field basis

The starting point is the same $U(1)-$invariant Euclidean action which served us as the initial action in the previous chapter. However we omit the momentum dependence of the interaction for reasons of simplicity. We consider a system of spinless Bose particles with mass m at zero temperature interacting with each other via a repulsive contact potential u_{Λ_0}

$$\begin{aligned} S[\bar{\psi},\psi] &= -\int_K \bar{\psi}_K(i\omega-\epsilon_{\boldsymbol{k}}+\mu)\psi_K \\ &+ \frac{u_{\Lambda_0}}{2}\int_{K_1'}\int_{K_2'}\int_{K_2}\int_{K_1}\delta_{K_1'+K_2',K_2+K_1}\bar{\psi}_{K_1'}\bar{\psi}_{K_2'}\psi_{K_2}\psi_{K_1}. \end{aligned} \tag{A.1}$$

In the $U(1)$-symmetry broken phase, both scalar fields are introduced through the expressions

$$\bar{\psi}_K = \delta_{K,0}\sqrt{\rho^0_{\Lambda_0}}+\frac{1}{\sqrt{2}}\left(\psi^l_K+i\psi^t_K\right), \tag{A.2a}$$

$$\psi_K = \delta_{K,0}\sqrt{\rho^0_{\Lambda_0}}+\frac{1}{\sqrt{2}}\left(\psi^l_{-K}-i\psi^t_{-K}\right), \tag{A.2b}$$

where the fluctuating field $\langle\psi^l_K\rangle$ and $\langle\psi^t_K\rangle$ correspond to the longitudinal and transversal quantum fluctuations above the mean-field $\rho^0_{\Lambda_0}$. Mathematically, such a change of the basis corresponds to the mapping of the initially $U(1)-$invariant action onto the $O(2)-$model. The suitable dimensionless parameters $\tilde{\mu}_0$ and $\tilde{u}_0$ of the bare model remain the same as given in equations (3.6) and (3.7). The initial action (A.1) may be

rewritten after some algebra in the following form:

$$
\begin{aligned}
S\left[\psi^l,\psi^t\right] &= \tilde{S}_0 + \sqrt{2\rho^0_{\Lambda_0}}(u_{\Lambda_0}\rho^0_{\Lambda_0}-\mu)\psi^l_0 \\
&+\frac{1}{2}\int\limits_K \left(\psi^l_K,\ \psi^t_K\right)\begin{pmatrix}\epsilon_{\boldsymbol{k}}+\Sigma^{ll}_{\Lambda_0}(K)-\mu & -\omega \\ \omega & \epsilon_{\boldsymbol{k}}+\Sigma^{tt}_{\Lambda_0}(K)-\mu\end{pmatrix}\begin{pmatrix}\psi^l_{-K}\\ \psi^t_{-K}\end{pmatrix} \\
&+\int\limits_{K_1}\int\limits_{K_2}\int\limits_{K_3}\delta_{K_1+K_2+K_3,0}\left(\frac{1}{3!}\Gamma^{lll}_{\Lambda_0}(K_1,K_2,K_3)\psi^l_{K_1}\psi^l_{K_2}\psi^l_{K_3}+\frac{1}{2!}\Gamma^{ltt}_{\Lambda_0}(K_1,K_2,K_3)\psi^l_{K_1}\psi^t_{K_2}\psi^t_{K_3}\right) \\
&+\int\limits_{K_1}\int\limits_{K_2}\int\limits_{K_3}\int\limits_{K_4}\delta_{K_1+K_2+K_3+K_4,0}\left(\frac{1}{4!}\Gamma^{llll}_{\Lambda_0}(K_1,K_2,K_3,K_4)\psi^l_{K_1}\psi^l_{K_2}\psi^l_{K_3}\psi^l_{K_4}\right. \\
&+\frac{1}{(2!)^2}\Gamma^{lltt}_{\Lambda_0}(K_1,K_2,K_3,K_4)\psi^l_{K_1}\psi^l_{K_2}\psi^t_{K_3}\psi^t_{K_4} \\
&\left.+\frac{1}{4!}\Gamma^{tttt}_{\Lambda_0}(K_1,K_2,K_3,K_4)\psi^t_{K_1}\psi^t_{K_2}\psi^t_{K_3}\psi^t_{K_4}\right),
\end{aligned}
\tag{A.3}
$$

where

$$
\tilde{S}_0 = -\rho^0_{\Lambda_0}\left(\mu-\frac{1}{2}u_{\Lambda_0}\rho^0_{\Lambda_0}\right) \tag{A.4}
$$

denotes the classical part of the action. Using the notation $\Delta_{\Lambda_0}=\rho^0_{\Lambda_0}u_{\Lambda_0}$ we obtain for two-legged vertices,

$$
\begin{aligned}
\Sigma^{ll}_{\Lambda_0}(K) &= 3\Delta_{\Lambda_0}, && \text{(A.5a)}\\
\Sigma^{tt}_{\Lambda_0}(K) &= \Delta_{\Lambda_0}, && \text{(A.5b)}\\
\Sigma^{lt}_{\Lambda_0}(K) &= 0. && \text{(A.5c)}
\end{aligned}
$$

By demanding the vanishing of the term which is linear in longitudinal fields ψ^l_0 we obtain the usual mean-field estimation for the condensate $\rho^0_{\Lambda_0}=\mu/u_{\Lambda_0}$. Thus, three-legged vertices become proportional to $\sqrt{u_{\Lambda_0}}$, i. e.

$$
\begin{aligned}
\Gamma^{lll}_{\Lambda_0}(K_1,K_2,K_3) &= 6u_{\Lambda_0}\sqrt{\frac{\rho^0_{\Lambda_0}}{2}}=\sqrt{18u_{\Lambda_0}\mu}, && \text{(A.6a)}\\
\Gamma^{ltt}_{\Lambda_0}(K_1,K_2,K_3) &= u_{\Lambda_0}\sqrt{2\rho^0_{\Lambda_0}}=\sqrt{2u_{\Lambda_0}\mu}, && \text{(A.6b)}
\end{aligned}
$$

and four-legged vertices are proportional to u_{Λ_0}:

$$
\begin{aligned}
\Gamma^{llll}_{\Lambda_0}(K_1,K_2,K_3,K_4) &= 3u_{\Lambda_0}, && \text{(A.7a)}\\
\Gamma^{tttt}_{\Lambda_0}(K_1,K_2,K_3,K_4) &= 3u_{\Lambda_0}, && \text{(A.7b)}\\
\Gamma^{lltt}_{\Lambda_0}(K_1,K_2,K_3,K_4) &= u_{\Lambda_0}. && \text{(A.7c)}
\end{aligned}
$$

At this point we define correlation functions between fields in the $O(2)-$basis:

$$\langle \psi^l_K \psi^l_{K'} \rangle = \delta_{K,-K'} G^{ll}_{\Lambda_0}(K) \tag{A.8a}$$
$$\langle \psi^l_K \psi^t_{K'} \rangle = \delta_{K,-K'} G^{lt}_{\Lambda_0}(K) \tag{A.8b}$$
$$\langle \psi^t_K \psi^l_{K'} \rangle = \delta_{K,-K'} G^{tl}_{\Lambda_0}(K) \tag{A.8c}$$
$$\langle \psi^t_K \psi^t_{K'} \rangle = \delta_{K,-K'} G^{tt}_{\Lambda_0}(K), \tag{A.8d}$$

where $\langle XY \rangle$ denotes the time ordered grand canonical functional average of complex numbers X and Y. Let us derive relations between Green functions in the both bases. The correlation functions between field fluctuating parts in the initially $U(1)-$invariant basis are given by the following expressions

$$\langle \psi_K \psi^\dagger_{K'} \rangle = \delta_{K,K'} G^N_{\Lambda_0}(K), \tag{A.9a}$$
$$\langle \psi^\dagger_K \psi_{K'} \rangle = \delta_{K,K'} [G^N_{\Lambda_0}(K)]^\star = \delta_{K,K'} G^N_{\Lambda_0}(-K), \tag{A.9b}$$

for normal propagators, and

$$\langle \psi^\dagger_K \psi^\dagger_{K'} \rangle = \delta_{K,-K'} G^A_{\Lambda_0}(K), \tag{A.10a}$$
$$\langle \psi_{-K} \psi_{-K'} \rangle = \delta_{K,-K'} G^A_{\Lambda_0}(K), \tag{A.10b}$$

for anomalous ones. Then one can easily obtain relations between correlation functions in both basis:

$$G^{ll}_{\Lambda_0}(K) = \frac{1}{2}\left\{ G^N_{\Lambda_0}(K) + G^N_{\Lambda_0}(-K) + 2G^A_{\Lambda_0}(K) \right\}, \tag{A.11a}$$
$$G^{tt}_{\Lambda_0}(K) = \frac{1}{2}\left\{ G^N_{\Lambda_0}(K) + G^N_{\Lambda_0}(-K) - 2G^A_{\Lambda_0}(K) \right\}, \tag{A.11b}$$
$$G^{lt}_{\Lambda_0}(K) = \frac{i}{2}\left\{ G^N_{\Lambda_0}(K) - G^N_{\Lambda_0}(-K) \right\} = -G^{tl}_{\Lambda_0}(K). \tag{A.11c}$$

It follows that correlation functions of two identical scalar fields are symmetric under momentum-reversal, i. e. $K \to -K$, while correlation functions of two different fields are antisymmetric. Resolving the Dyson-Beliaev matrix equation [79, 80, 85]

$$\mathbf{G}^{-1}_{\Lambda_0} = \mathbf{G}^{-1}_0 - \mathbf{\Sigma}_{\Lambda_0}, \tag{A.12}$$

where all matrices dwell on both, field and energy-momentum space, we obtain explicit expressions for the propagators (A.11a)-(A.11c)

$$G^{ll}_{\Lambda_0}(K) = \frac{\epsilon_{\boldsymbol{k}} + \Sigma^{tt}_{\Lambda_0}(K) - \mu}{[i\omega + \tilde{E}^+_{\Lambda_0}(K)][i\omega + \tilde{E}^-_{\Lambda_0}(K)]}, \tag{A.13a}$$
$$G^{tt}_{\Lambda_0}(K) = \frac{\epsilon_{\boldsymbol{k}} + \Sigma^{ll}_{\Lambda_0}(K) - \mu}{[i\omega + \tilde{E}^+_{\Lambda_0}(K)][i\omega + \tilde{E}^-_{\Lambda_0}(K)]}, \tag{A.13b}$$
$$G^{lt}_{\Lambda_0}(K) = \frac{i[\Sigma^{lt}_{\Lambda_0}(K) + i\omega]}{[i\omega + \tilde{E}^+_{\Lambda_0}(K)][i\omega + \tilde{E}^-_{\Lambda_0}(K)]}. \tag{A.13c}$$

where the poles of the Green functions (A.13a)-(A.13c) are given by

$$\tilde{E}^{\pm}_{\Lambda_0}(K) = \Sigma^{lt}_{\Lambda_0}(K) \pm \sqrt{[\epsilon_{\boldsymbol{k}} + \Sigma^{ll}_{\Lambda_0}(K) - \mu][\epsilon_{\boldsymbol{k}} + \Sigma^{tt}_{\Lambda_0}(K) - \mu]} \tag{A.14}$$

There exist unique relations between self-energies expressed in both bases:

$$\Sigma^{N}_{\Lambda_0}(\pm K) = \frac{1}{2}\left[\Sigma^{ll}_{\Lambda_0}(K) + \Sigma^{tt}_{\Lambda_0}(K) \mp 2\Sigma^{lt}_{\Lambda_0}(K)\right], \tag{A.15a}$$

$$\Sigma^{A}_{\Lambda_0}(K) = \frac{1}{2}\left[\Sigma^{ll}_{\Lambda_0}(K) - \Sigma^{tt}_{\Lambda_0}(K)\right], \tag{A.15b}$$

or by inverting these expressions

$$\Sigma^{ll}_{\Lambda_0}(K) = \frac{1}{2}\left[\Sigma^{N}_{\Lambda_0}(K) + \Sigma^{N}_{\Lambda_0}(-K) + 2\Sigma^{A}_{\Lambda_0}(K)\right] \tag{A.16a}$$

$$\Sigma^{tt}_{\Lambda_0}(K) = \frac{1}{2}\left[\Sigma^{N}_{\Lambda_0}(K) + \Sigma^{N}_{\Lambda_0}(-K) - 2\Sigma^{A}_{\Lambda_0}(K)\right] \tag{A.16b}$$

$$\Sigma^{lt}_{\Lambda_0}(K) = \frac{1}{2}\left[\Sigma^{N}_{\Lambda_0}(K) - \Sigma^{N}_{\Lambda_0}(-K)\right]. \tag{A.16c}$$

These expressions are entirely general and apply to any uniform Bose systems.

A.2 Flow equations for self-energies and coupling parameters

Approximating flowing momentum-dependent self-energies of the scalar basis in the spirit of the truncation scheme (3.65a) and (3.65b), i. e.

$$\Sigma^{ll}_{\ell}(K) \approx \Delta_{\Lambda_0} + 2\Delta_{\ell} + (Z_{\ell}^{-1} - 1)\epsilon_{\boldsymbol{k}} + V_{\ell}\omega^2, \tag{A.17a}$$

$$\Sigma^{tt}_{\ell}(K) \approx \Delta_{\Lambda_0} + (Z_{\ell}^{-1} - 1)\epsilon_{\boldsymbol{k}} + V_{\ell}\omega^2, \tag{A.17b}$$

$$\Sigma^{tt}_{\ell}(\pm K) \approx \mp i\omega(1 - Y_{\ell}), \tag{A.17c}$$

we obtain for the full inverse propagator matrix

$$\left[\mathbf{G}_{\ell}^{-1}\right]_{K,K'} = \delta_{K+K',0} \begin{pmatrix} \bar{\epsilon}_{\ell}(\boldsymbol{k}) + V_{\ell}\omega^2 + 2\Delta_{\ell} & -Y_{\ell}\omega \\ Y_{\ell}\omega & \bar{\epsilon}_{\ell}(\boldsymbol{k}) + V_{\ell}\omega^2 \end{pmatrix}, \tag{A.18}$$

where the regularized free particle dispersions is given by

$$\bar{\epsilon}_{\ell}(\boldsymbol{k}) = (2mZ_{\ell})^{-1}\left(k^2 + \Lambda^2 R(\boldsymbol{k}/\Lambda)\right) \tag{A.19}$$

with the dimensionless regulator function $R(\boldsymbol{k}/\Lambda)$. Because the set of the flowing coupling parameters remains precisely the same as considered in chapter 3 we do not discuss them at this point again. The three dynamical coupling parameters Z_{ℓ}, V_{ℓ} and Y_{ℓ} can

now be conveniently expressed in terms of the derivative expansion of the self-energies in the scalar field basis:

$$Z_\ell^{-1} = 1 + m\frac{\partial^2\Sigma_\ell^{tt}(\boldsymbol{k},0)}{\partial k^2}\bigg|_{k=0}, \tag{A.20a}$$

$$Y_\ell = 1 + \frac{\partial\Sigma_\ell^{lt}(0,i\omega)}{\partial(i\omega)}\bigg|_{\omega=0}, \tag{A.20b}$$

$$V_\ell = \frac{1}{2}\frac{\partial^2\Sigma_\ell^{tt}(0,i\omega)}{\partial\omega^2}\bigg|_{\omega=0}. \tag{A.20c}$$

By using truncation of the flowing higher vertices based on expressions (A.5a)-(A.7c), flow equations for the condensate, as well as for the three self-energies can be easily obtained. The flow equation for the condensate reads

$$\partial_\Lambda\rho_\ell^0 = \frac{1}{2}\int_K\left[\dot{G}_\ell^{tt}(K) + 3\dot{G}_\ell^{ll}(K)\right], \tag{A.21}$$

and equations for the self-energies read

$$\begin{aligned}\partial_\Lambda\Sigma_\ell^{tt}(Q) &= u_\ell\int_K\left[\dot{G}_\ell^{ll}(K) - \dot{G}_\ell^{tt}(K)\right] - 2\rho_\ell^0u_\ell^2\int_K\Big[\dot{G}_\ell^{ll}(K)G_\ell^{tt}(Q-K)\\ &+ \dot{G}_\ell^{tt}(K)G_\ell^{ll}(Q-K) + 2\dot{G}_\ell^{lt}(K)G_\ell^{tl}(Q-K)\Big],\end{aligned} \tag{A.22}$$

$$\begin{aligned}\partial_\Lambda\Sigma_\ell^{ll}(Q) &= u_\ell\int_K\left[\dot{G}_\ell^{tt}(K) + 3\dot{G}_\ell^{ll}(K)\right] - 2\rho_\ell^0u_\ell^2\int_K\Big[9\dot{G}_\ell^{ll}(K)G_\ell^{ll}(Q-K)\\ &+ \dot{G}_\ell^{tt}(K)G_\ell^{tt}(Q-K) + 6\dot{G}_\ell^{lt}(K)G_\ell^{lt}(Q-K)\Big],\end{aligned} \tag{A.23}$$

$$\begin{aligned}\partial_\Lambda\Sigma_\ell^{lt}(Q) &= -\rho_\ell^0u_\ell^2\int_K\Big\{\Big(\dot{G}_\ell^{tt}(K) + 3\dot{G}_\ell^{ll}(K)\Big)G_\ell^{lt}(Q-K)\\ &+ \dot{G}_\ell^{lt}(K)\left(G_\ell^{tt}(Q-K) + 3G_\ell^{ll}(Q-K)\right)\Big\}.\end{aligned} \tag{A.24}$$

The flow equation for the interaction may be obtained from the flow of the longitudinal self-energy in the limit $K \to 0$:

$$\partial_\Lambda u_\ell = -u_\ell^2\int_K\Big(9\dot{G}_\ell^{ll}(K)G_\ell^{ll}(-K) + \dot{G}_\ell^{tt}(K)G_\ell^{tt}(-K) + 6\dot{G}_\ell^{lt}(K)G_\ell^{lt}(-K)\Big). \tag{A.25}$$

The single-scale propagators appearing in equations (A.21-A.25) are defined as follows:

$$\dot{G}_\ell^{ll}(K) = -\partial_\Lambda R_\ell(\boldsymbol{k})\left\{[G_\ell^{ll}(K)]^2 + G_\ell^{lt}(K)G_\ell^{tl}(K)\right\}, \tag{A.26}$$

$$\dot{G}_\ell^{tt}(K) = -\partial_\Lambda R_\ell(\boldsymbol{k})\left\{[G_\ell^{tt}(K)]^2 + G_\ell^{lt}(K)G_\ell^{tl}(K)\right\}, \tag{A.27}$$

$$\dot{G}_\ell^{lt,tl}(K) = -\partial_\Lambda R_\ell(\boldsymbol{k})\left\{G_\ell^{ll}(K) + G_\ell^{tt}(K)\right\}G^{lt,tl}(K). \tag{A.28}$$

Finally, the flow equations for coupling parameters Z_ℓ, Y_ℓ and V_ℓ follow from equations (A.20a)-(A.20c) and equations (A.22) and (A.24):

$$\partial_\ell Z_\ell = -mZ_\ell^2 \frac{\partial^2}{\partial k^2} \partial_\ell \Sigma_\ell^{tt}(\boldsymbol{k}, 0)\Big|_{k=0}, \tag{A.29a}$$

$$\partial_\ell Y_\ell = \frac{\partial}{\partial(i\omega)} \partial_\ell \Sigma_\ell^{lt}(0, i\omega)\Big|_{\omega=0}, \tag{A.29b}$$

$$\partial_\ell V_\ell = \frac{1}{2} \frac{\partial^2}{\partial \omega^2} \partial_\ell \Sigma_\ell^{tt}(0, i\omega)\Big|_{\omega=0}. \tag{A.29c}$$

Equations (A.22)-(A.29c) are completely analogous to (3.75), (3.82), (3.87), (3.89) and (3.93a)-(3.93c) and describe precisely the same physics. Therefore, we do not consider them any further.

B Deutsche Zusammenfassung

In der vorliegenden Arbeit wird der mathematische Apparat der Funktionalen Renormierungsgruppe (FRG) auf bosonische Systeme in der symmetriegebrochener Phase angewandt. Bei der kritischen Temperatur T_c findet in einem bosonischen System ein Phasenübergang statt. Unterhalb der kritischen Temperatur entsteht im so einem System eine neue makroskopische Substanz, die allgemeinhin als das Bose-Einstein Kondensat bezeichnet wird [1, 2]. In nichtwechselwirkenden Bose-Systemen entsteht das Kondensat in Folge der Überlappung der Wellenpackete einzelner Teilchen, wodurch eine effektive Anziehung zwischen den Bosonen zustande kommt. Oberhalb der kritischen Temperatur wird das Kondensat durch thermische Fluktuationen zerstört.

Das Entstehen des Kondensats in den wechselwirkenden Bose-Systemen ist durch die Wechselwirkung zwischen den Teilchen verursacht [4]. Es kann durch die Einführung eines Ordnungsparameters berücksichtigt werden, welcher eine makroskopische Grösse darstellt, die nur unterhalb der kritischen Temperatur von Null verschieden ist. Die Phase unterhalb der kritischen Temperatur wird daher als geordnet bezeichnet im Unterschied zu der ungeordneten Phase oberhalb der kritischen Temperatur. Da das Entstehen einer langreichweitigen Ordnung immer mit der Reduzierung der Symmetrie des mathematischen Modells [5] verbunden ist, nennt man die geordnete Phase auch die Phase mit gebrochener Symmetrie. Je nach dem Verhalten des Systems in der Nähe des kritischen Punktes unterscheidet man zwischen den Phasenübergängen erster und zweiter Ordnung. Bei dem übergang zweiter Ordnung verschwindet der Ordnungsparameter am kritischen Punkt kontinuierlich und weist dabei ein nicht analytisches Verhalten auf. Einige thermodynamische Observablen divergieren am kritischen Punkt mit Potenzgesetzen. Diese Potenzen nennt man kritische Exponenten. Sie sind universell für Systeme mit derselben Symmetrie, selbst wenn sich diese Systeme physikalisch stark voneinander unterscheiden. Modelle mit denselben kritischen Exponenten gehören derselben Universalitätsklassen an.

Die genaue Berechnung der kritischen Exponenten beschäftigte Physiker über mehrere Jahrzehnte hindurch. Die Landau phänomenologische Theorie der Phasenübergänge zweiter Ordnung [6] (und die Molekularfeldtheorie im breiteren Sinne) wurde lange Zeit als die richtige Theorie des Phänomens angesehen. Es stellte sich jedoch heraus, dass sie nur bedingt befriedigende Ergebnisse liefert. Wie der Vergleich mit wenigen bekannten exakten Lösungen (wie z. B. im Falle der Ising-Universalitätsklasse [7]), sagt die Molekularfeldtheorie falsche Ergebnisse für die kritischen Exponenten voraus. Der Grund hierfür liegt darin, das die Molekularfeldtheorie die Fluktuationen vernachlässigt, welche am kritischen Punkt wichtig werden [8]. Deswegen besteht ein akuter Bedarf bei der Beschreibung der Physik der geordneten Phase über die Molekularfeldnäherung hinaus zu gehen. Die Abhilfe wurde von Kenneth Wilson in der Form seines

Renormierungsverfahrens [9, 10] geschaffen. Übersetzt in die Sprache der erzeugenden Funktionale [12, 13] stellt die funktionale Renormierungsgruppe (FRG) eine äußerst leistungsvolle und vielversprechende Untersuchungsmethode dar, deren Möglichkeiten weit über die Bestimmung von kritischen Exponenten hinaus gehen.

Strukturell gliedert sich diese Arbeit wie folgt auf:

1. Im Kapitel 1 stellen wir den formalen Rahmen der Theorie vor. Wir führen das Konzept der erzeugenden Funktionale ein, leiten für diese die exakten Renormierungsgruppen- (RG)-Flussgleichungen ab und erweitern diese um die Flussgleichung des Ordnungsparameters. Ein kurzer Überblick über die Grundlagen der Wilsonschen Renormierungsgruppe vervollständigt diese Einführung und legt die begriffliche Basis fest.

2. Im Kapitel 2 erfolgt die erste Anwendung des entwickelten Formalismus auf das klassische ϕ^4-Modell. Wir leiten RG-Flussgleichungen für den Ordnungsparameter und die irreduzible Selbstenergie ab, extrahieren aus der letzteren die Flussgleichung für die Wechselwirkung und erhalten somit ein geschlossenes Differentialgleichungssystem, welches dann numerisch gelöst wird. Wir untersuchen das fast kritische Verhalten des Modells, ermitteln seine kritischen Exponenten und berechnen seine impulsabhängige Selbstenergie mit Hilfe des Verfahrens, welches wir die FRG-erweiterte Störungstheorie nennen. Es stellt sich heraus, dass die Selbstenergie in der Nähe des kritischen Punktes durch das Zwischenspiel von mehreren unterschiedlichen Skalen geprägt ist.

3. Im Kapitel 3 wird der FRG-Formalismus auf Systeme der wechelwirkenden Bosonen bei $T = 0$ angewandt. Das Verhalten eines solchen Systems im Limes langer Wellenlängen ist durch zwei exakte Relationen bestimmt: Zum einen durch das Hugenholtz-Pines (HP)-Theorem [16], welches in diesem Grenzfall eine Beziehung zwischen dem chemischen Potential und beiden Selbstenergien (normaler und anomaler) herstellt und damit die Abwesenheit der energetischen Lücke in dem Anregungsspektrum postuliert. Zum anderen gibt es die Nepomnyashchy-Nepomnyashchy (NN)-Relation [17], welche das Verschwinden der anomalen Selbstenergie bei langen Wellenlängen vorhersagt. Während HP bereits aus der niedrigsten Ordnung in der Störungstheorie ersichtlich ist, folgt NN nicht aus der *naiven* Störungstheorie. Durch die Resummierung der Störungsreihe mittels der funktionalen Renormierungsgruppe können wir die beiden exakten Relationen berücksichtigen. Wir benutzen ein Trunkierungsschema für die effektive Wirkung mit nichtlokaler Wechselwirkung, leiten daraus die Flussgleichungen für die relevanten Kopplungsparameter her und lösen diese numerisch. Während die Störungstheorie infrarotdivergent ist, sind unsere Ergebnisse frei von jeglichen Divergenzen. Wir ermitteln die Crossoverskala zwischen dem quasifreien und dem kollektiven Regime. Wir reproduzieren korrektes Verhalten der beiden Selbstenergien im Infraroten, sowie das der normalen und anomalen Green Funktionen. Anschließend wird die Spektralfunktion der wechselwirkenden Bosonen berechnet. Aus ihr werden dann das Spektrum der elementaren Anregungen, sowie die

Dämpfung der Quasiteilchen extrahiert. Für schwache Wechselwirkung wird das Ergebnis der Störungstheorie reproduziert. Jedoch besteht die wahre stärke unserer Theorie darin, dass sie in der Lage ist, kontrollierte Rechenergebnisse für beliebig starke Wechselwirkung zwischen den Teilchen zu liefern.

4. Im Appendix A wird eine alternative Parametrisierung für die wechselwirkenden Bosonen vorgestellt. Sie zeichnet sich durch die Einführung von zwei skalaren Feldern aus, welche in Richtung transversal und longitudinal zur Symmetriebrechung fluktuieren. Die Wahl dieser Parametrisierung bringt gewisse ästhetische Vorteile mit sich, so erhält z. B. nur das longitudinale Feld einen nicht verschwindenden Vakuumerwartungswert, während das transversale Feld lückenfrei bleibt. Selbstverständlich beeinflusst diese Wahl in keiner Weise die Rechenergebnisse, welche in der üblichen Darstellung erhalten werden.

Im Folgenden fassen wir den Inhalt der Doktorarbeit kurz zusammen.

Exakte FRG-Flussgleichung

Kapitel 1 befasst sich mit dem Formalismus der funktionalen Renormierungsgruppe. Die Darstellung des Formalismus richtet sich im Wesentlichen nach [18]. Der Ausgangspunkt für die Herleitung der exakten RG-Flussgleichung stellt das erzeugende Funktional der zusammenhängenden Greenschen Funktionen

$$e^{\mathcal{G}_c[\boldsymbol{J}]} = \frac{1}{Z_0} \int \mathcal{D}\boldsymbol{\Phi}\ e^{-S[\boldsymbol{\Phi}]+\boldsymbol{J}\cdot\boldsymbol{\Phi}} \tag{B.1}$$

dar, wobei der Vektor $\boldsymbol{\Phi} = (\bar{\boldsymbol{\phi}}, \boldsymbol{\phi})^T$ für das Quantensuperfeld steht, während $\boldsymbol{J} = (\boldsymbol{j}, \bar{\boldsymbol{j}})^T$ für den Vektor der Superquellen. Das Quantenfeld $\boldsymbol{\phi}$ kann beliebig viele Komponenten enthalten, wobei jede von ihnen einer konkreten Teilchensorte entspricht. Die Komponenten können sowohl Fermionen, wie auch Bosonen oder Teilchen mit jeder anderen Statistik beschreiben. Das Skalarprodukt zweier Supervektoren ist wie folgt definiert:

$$\boldsymbol{J}\cdot\boldsymbol{\Phi} = \int\limits_{\alpha} J_\alpha \Phi_\alpha, \tag{B.2}$$

wobei das Symbol α einen Multiindex darstellt, welcher für die Teilchensorte, seinen Impuls, Frequenz, Spin, etc. steht und die Integration darüber dementsprechend die Spurbildung über die Definitionsräume der diskreten Variablen (wie z. B. die Teilchensorte oder -spin) und die Integration über die kontinuierlichen Variablen bedeutet.

Die großkanonische Zustandssumme des wechselwirkungsfreien Systems ist durch den Ausdruck

$$Z_0 = \int \mathcal{D}\boldsymbol{\Phi}\ e^{-S_0[\boldsymbol{\Phi}]} \tag{B.3}$$

gegeben und die großkanonische Zustandssumme des wechselwirkenden Systems durch $Z = \exp\{\mathcal{G}_c[0]\}$. Die Euklidische Wirkung des Modells $S[\boldsymbol{\Phi}]$ besteht demnach aus einem wechselwirkungsfreien Anteil

$$S_0[\boldsymbol{\Phi}] = -\frac{1}{2}\boldsymbol{\Phi}\cdot\boldsymbol{G}_0^{-1}\cdot\boldsymbol{\Phi}, \tag{B.4}$$

welcher quadratisch in den Feldern $\boldsymbol{\Phi}$ ist und einem Wechselwirkungsterm, der eine beliebige, mit den Symmetrien des Models verträgliche Anzahl der Felder enthält. Die zusammenhängenden Greenschen Funktionen ergeben sich durch die wiederholte Ableitung des Funktionals $\mathcal{G}_c$ nach den Quellen $\boldsymbol{J}$ an der Stelle $\boldsymbol{J} = 0$.

Es ist bequem ein weiteres Funktional einzuführen, welches allgemein als effektive Wirkung bezeichnet wird. Es ist als Legendre-Transformierte von $\mathcal{G}_c$ bezüglich der Quellen $\boldsymbol{J}$

$$\mathcal{L}[\tilde{\boldsymbol{\Phi}}[\boldsymbol{J}]] = \boldsymbol{J}\cdot\tilde{\boldsymbol{\Phi}}[\boldsymbol{J}] - \mathcal{G}_c[\boldsymbol{J}] \tag{B.5}$$

definiert, wobei

$$\tilde{\boldsymbol{\Phi}}[\boldsymbol{J}] = \frac{\delta}{\delta\boldsymbol{J}}\mathcal{G}_c[\boldsymbol{J}] \tag{B.6}$$

für das gemittelte Feld steht. Für das Funktional $\mathcal{L}$ wird die Existenz einer unendlichen Entwicklung nach den Feldern $\tilde{\boldsymbol{\Phi}}$

$$\mathcal{L}[\tilde{\boldsymbol{\Phi}}] = \mathcal{L}[0] + S_0[\tilde{\boldsymbol{\Phi}}] + \sum_{n=1}^{\infty}\frac{1}{n!}\int_{\alpha_1}\cdots\int_{\alpha_n}\Gamma^{(n)}_{\alpha_1,\ldots,\alpha_n}\tilde{\Phi}_{\alpha_1}\cdots\tilde{\Phi}_{\alpha_n} \tag{B.7}$$

vorausgesetzt, wobei Elemente $\Gamma^{(n)}_{\alpha_1,\ldots,\alpha_n}$ dieser Reihe als Ein-Teilchen-irreduziblen Vertexfunktionen bezeichnet werden. Manchmal führt man ein weiteres Funktional ein, das sogenannte erzeugende Funktional der Ein-Teilchen-irreduziblen Vertexfunktionen $\Gamma[\tilde{\boldsymbol{\Phi}}]$, welches mit der effektiven Wirkung über die Beziehung

$$\Gamma[\tilde{\boldsymbol{\Phi}}] = \mathcal{L}[\tilde{\boldsymbol{\Phi}}] - S_0[\tilde{\boldsymbol{\Phi}}] \tag{B.8}$$

zusammenhängt.

Die Herleitung der exakten funktionalen RG-Flussgleichung benötigt die Erweiterung der mikroskopischen Wirkung um den zusätzlichen quadratischen Abschneide-Term

$$\Delta S_\Lambda[\boldsymbol{\Phi}] = -\frac{1}{2}\boldsymbol{\Phi}\cdot\boldsymbol{R}_\Lambda\cdot\boldsymbol{\Phi}, \tag{B.9}$$

wobei $\boldsymbol{R}_\Lambda$ eine quadratische Matrix darstellt. Sie enthält die Abschneidefunktionen (auch Cutoff- oder Regulatorfunktionen genannt) für die zu renormierende Teilchensorte als Matrixelemente. Die Regulatorfunktionen hängen explizit von dem Impuls $0 \leqslant \Lambda < \Lambda_0$ ab, wobei Λ_0 einen passenden Abschneide-Impuls im Ultravioletten bezeichnet. Gewöhnlich wird Λ_0 so gewählt, dass es viel größer als eine charakteristische inverse Länge des Systems ist. Das Einführen der Regulatorfunktion entspricht der Einführung eines zusätzlichen Massenterms, so dass die Fluktuationen im Ultravioletten

unterdrückt werden. Wenn der Cutoff entfernt, d. h. der physikalische Limes $\Lambda \to 0$ ausgeführt wird, werden Fluktuationen nach und nach berücksichtigt. Deswegen müssen die Regulatorfunktion für die i-te Teilchensorte $R_{i,\Lambda}(K)$, $K = (\boldsymbol{k}, \omega)$, unabhängig von ihrer Form folgenden Forderungen genügen:

- Sie müssen positiv semidefinit, d. h. $R_{i,\Lambda}(K) \geqslant 0$, $\forall\, \Lambda$, K und mindestens einfach nach dem Cutoffimpuls Λ differenzierbar sein.
- Im ultravioletten Limes müssen sie divergieren, d. h. $R_{i,\Lambda\to\Lambda_0}(K) \to \infty$, $\forall\, K$. Diese Forderung gewährleistet die Unterdrückung von Fluktuationen im Grenzfall kleiner Wellenlängen.
- Im physikalischen Limes $\Lambda \to 0$ müssen sie verschwinden, d. h. $R_{i,\Lambda\to 0}(K) \to 0$, $\forall\, K$. Dies garantiert, dass die physikalischen Größen am Ende des Flusses unabhängig von der Wahl der Regulatorfunktion sind.
- Schließlich müssen sie die Bedingung $\lim_{|K|\to 0} R_{i,\Lambda}(K) > 0$, $\forall\, \Lambda$ erfüllen, welche die Abwesenheit von Infrarotdivergenzen gewährleistet.

Leitet man das erzeugende Funktional der zusammenhängenden Greenschen Funktionen $\mathcal{G}_c[\boldsymbol{J}]$ nach dem Cutoffimpuls Λ ab, drückt diese Ableitung durch die effektive Wirkung

$$\tilde{\mathcal{L}}[\tilde{\boldsymbol{\Phi}}] = \mathcal{L}[\tilde{\boldsymbol{\Phi}}] - \frac{1}{2}\tilde{\boldsymbol{\Phi}} \cdot [\boldsymbol{R}_\Lambda] \cdot \tilde{\boldsymbol{\Phi}} \tag{B.10}$$

aus, so erhält man nach einigen Rechenschritten die exakte Flussgleichung für das Funktional $\tilde{\mathcal{L}}$:

$$\partial_\Lambda \tilde{\mathcal{L}}_\Lambda[\tilde{\boldsymbol{\Phi}}] = \partial_\Lambda \ln Z_{0,\Lambda} - \frac{1}{2}\mathrm{Tr}\left\{ \boldsymbol{Z} \cdot \left(\frac{\delta^{(2)}\Gamma_\Lambda}{\delta\tilde{\boldsymbol{\Phi}}\delta\tilde{\boldsymbol{\Phi}}} - [\boldsymbol{G}_{0,\Lambda}^{-1}]^T \right)^{-1} \cdot [\partial_\Lambda \boldsymbol{R}_\Lambda]^T \right\}. \tag{B.11}$$

Hier bedeutet der Operator Tr die Spur über sämtliche diskreten und Integration über sämtliche kontinuierlichen Variablen. Die Matrix $[\boldsymbol{G}_{0,\Lambda}^{-1}]$ bedeutet die Matrix der Greenschen Funktionen des wechselwirkungsfreien Systems, und die Matrix $\boldsymbol{Z}$ berücksichtigt unterschiedliche Statistik für die bosonischen, fermionischen, Majorana, etc. Komponenten des Quantenfeldes $\boldsymbol{\phi}$. Entwickelt man das Funktional Γ auf beiden Seiten der Gleichung (B.11) nach Potenzen von $\tilde{\boldsymbol{\Phi}}$ und macht einen Koeffizientenvergleich, so entsteht eine unendliche Hierarchie von Flussgleichungen für Ein-Teilchen-irreduziblen Vertexfunktionen. Es handelt sich dabei um eine nicht geschlossene Gleichungshierarchie, da die rechte Seite jeder Gleichung Vertexfunktionen höherer Ordnung enthält, als die linke. Damit ist man bei der Behandlung von diesen Gleichungen auf Näherungen und Trunkierungen angewiesen. Es gibt keine einheitlichen Vorschriften dafür, wie diese zu machen sind. Für gewöhnlich verhilft eine qualitative molekularfeldtheoretische Analyse zur passenden Trunkierung des Funktionals Γ.

Bekommt mindestens eine der Komponenten des Quantenfelds $\boldsymbol{\phi}$ den nicht verschwindenden Vakuumerwartungswert, d. h. wird mindestens eine der Symmetrien des Modells spontan gebrochen, so kann die Flussgleichung für diesen Erwartungswert aus der Forderung nach dem Verschwinden des Flusses vom linearen Term aus der Entwicklung (B.7) gewonnen werden.

Klassisches Skalarfeldmodell

Im Kapitel 2 wird der oben dargestellte Formalismus auf das klassische einkomponentige Skalarfeldmodell angewandt, welches allgemein als ϕ^4-Modell bezeichnet wird. Seine Wirkung ist durch den Ausdruck

$$S[\phi] = \int d^D r \left[\frac{1}{2}(\boldsymbol{\nabla}\phi)^2 + \frac{r_{\Lambda_0}}{2}\phi^2 + \frac{u_{\Lambda_0}}{4!}\phi^4\right] \tag{B.12}$$

gegeben, wobei die Größe

$$r_{\Lambda_0} = \frac{1}{a^2}\frac{T - T_c^{MF}}{T_c^{MF}} \tag{B.13}$$

den Abstand zur kritischen Temperatur angibt. Hier bedeutet T_c^{MF} den Molekularfeldwert für die kritische Temperatur des Phasenübergangs, a die Gitterkonstante und u_{Λ_0} die Wechselwirkung im nackten Modell. Das Integral in der Gleichung (B.12) wird im Integrationsbereich $0 \leqslant |r| \leqslant \Lambda_0^{-1}$ mit einem passend gewählten Λ_0^{-1} ausgeführt. Da die Wirkung unter der Spiegelung von Feldern $\phi \to -\phi$ invariant bleibt, gehört das Modell der Ising-Universalitätsklasse an, und ist somit eines der am besten studierten und verstandenen Modellen überhaupt. In der symmetriegebrochenen Phase erhält das skalare Feld ϕ den nichtverschwindenden Vakuumerwartungswert M, welcher mit der Magnetisierung identifiziert werden kann. Es muss betont werden, dass es sich bei der gebrochenen Symmetrie um eine diskrete Symmetrie handelt. Aus der molekularfeldtheoretischen Analyse folgen Beziehungen zwischen der Magnetisierung M_{Λ_0} und den Parametern r_{Λ_0} und u_{Λ_0}

$$M_{\Lambda_0} = \begin{cases} 0 & \text{for } r_{\Lambda_0} > 0 \\ \sqrt{-\dfrac{6r_{\Lambda_0}}{u_{\Lambda_0}}} & \text{for } r_{\Lambda_0} < 0 \end{cases} , \tag{B.14}$$

sowie für die Selbstenergie

$$\Sigma_{\Lambda_0}(\boldsymbol{k}) = r_{\Lambda_0} + \frac{u_{\Lambda_0}}{2}M_{\Lambda_0}^2 = \frac{u_{\Lambda_0}}{3}M_{\Lambda_0}^2 = -2r_{\Lambda_0} , \tag{B.15}$$

welche zum einen die Anfangsbedingungen für die jeweiligen fließenden Größen liefern, zum anderen aber ein natürliches Trunkierungsschema festlegen.

Folgt man dem im Kapitel 1 skizzierten Formalismus, so erhält man unter Berücksichtigung der Gleichung (B.15) die Flussgleichungen für die Magnetisierung

$$\partial_\Lambda M_\Lambda^2 = -3\int \frac{d^D k}{(2\pi)^D}\dot{G}_\Lambda(\boldsymbol{k}), \tag{B.16}$$

für die Selbstenergie

$$\partial_\Lambda \Sigma_\Lambda(\boldsymbol{k}) = -u_\Lambda \int \frac{d^D k'}{(2\pi)^D}\dot{G}_\Lambda(\boldsymbol{k}') - u_\Lambda^2 M_\Lambda^2 \int \frac{d^D k'}{(2\pi)^D}\dot{G}_\Lambda(\boldsymbol{k}')G_\Lambda(\boldsymbol{k}'+\boldsymbol{k}), \tag{B.17}$$

und aus dem letzten Ausdruck im Limes $\boldsymbol{k} = 0$ die Flussgleichung für die Wechselwirkung u_Λ:

$$\partial_\Lambda u_\Lambda = -3u_\Lambda^2 \int \frac{d^D k}{(2\pi)^D} \dot{G}_\Lambda(\boldsymbol{k}) G_\Lambda(\boldsymbol{k}), \tag{B.18}$$

wobei in diesen Gleichungen $G_\Lambda(\boldsymbol{k})$ für die renormierte Greensche Funktion steht, deren Form von dem konkreten Regulator abhängt, während

$$\dot{G}_\Lambda(\boldsymbol{k}) = -\partial_\Lambda [G_{0,\Lambda}^{-1}(\boldsymbol{k})] G_\Lambda^2(\boldsymbol{k}) \tag{B.19}$$

den sogenannten *single scale* Propagator bezeichnet.

Da wir an der Physik im Grenzfall langer Wellenlängen interessiert sind, können wir die Selbstenergie nur zur führenden Ordnung in $\boldsymbol{k}$ berücksichtigen, d. h.

$$\begin{aligned} \Sigma_\Lambda(\boldsymbol{k}) &\approx \Sigma_\Lambda(0) + \frac{\boldsymbol{k}^2}{2} \left. \frac{\partial^2 \Sigma_\Lambda(\boldsymbol{k})}{\partial \boldsymbol{k}^2} \right|_{\boldsymbol{k}=0} \\ &= \frac{1}{3} u_\Lambda M_\Lambda^2 + \boldsymbol{k}^2 \left(Z_\ell^{-1} - 1 \right), \end{aligned} \tag{B.20}$$

wobei hier der Wellenfunktionsrenormierungsfaktor

$$Z_\ell^{-1} = 1 + \frac{1}{2} \left. \frac{\partial^2 \Sigma_\Lambda(\boldsymbol{k})}{\partial \boldsymbol{k}^2} \right|_{\boldsymbol{k}^2=0}, \tag{B.21}$$

und logarithmischer Flussparameter $\ell = \ln(\Lambda_0/\Lambda)$ eingeführt wurden. Für das Weitere müssen wir das Regularisierungsschema festlegen.

Es stellt sich heraus, dass das sogenannte Regularisierungsschema mit der scharfen Abschneidefunktion inakzeptable Ergebnisse für die kritischen Exponenten in der Nähe der oberen kritischen Dimension des Modells liefert. Deswegen muss dieses Schema verworfen werden, trotz seines beachtlichen Erfolgs bei der Anwendung auf kritische Systeme aus der ungeordneten Phase [42, 43]. Wir entscheiden uns für das additive Regularisierungsschema. Bei dieser Wahl lässt sich die Greensche Funktion wie folgt schreiben:

$$G_\Lambda(\boldsymbol{k}) = \frac{1}{\boldsymbol{k}^2 + R_\Lambda(\boldsymbol{k}) + \Sigma_\Lambda(\boldsymbol{k})}, \tag{B.22}$$

wobei die Regulatorfunktion nur Moden mit $\boldsymbol{k} \neq 0$ regularisiert:

$$R_\Lambda(\boldsymbol{k}) = (1 - \delta_{\boldsymbol{k},0}) \Lambda^2 Z_\ell^{-1} R(\boldsymbol{k}^2/\Lambda^2). \tag{B.23}$$

Die dimensionslose Funktion $R(x)$ muss den Bedingungen $R(\infty) = 0$ und $R(0) = 1$ genügen. Für die konkrete Rechnung benutzen wir die Litim-Regulatorfunktion [41]

$$R(x) = (1 - x)\Theta(1 - x), \tag{B.24}$$

wobei hier $\Theta(1 - x)$ die Heavisidesche Stufenfunktion bedeutet. Mit dieser Wahl lassen sich Integrale in den Gleichungen (B.16)-(B.18) analytisch auswerten. Zur Ermittlung

ihrer Skalendimensionen ist es bequem sämtliche fließenden Größen zu reskalieren:

$$\Sigma_\Lambda(\boldsymbol{k}) = \frac{\Lambda^2}{Z_\ell}\Gamma_\ell(\boldsymbol{q}), \tag{B.25}$$

$$u_\Lambda = \frac{\Lambda^{4-D}}{K_D Z_\ell^2}\,\tilde{u}_\ell, \tag{B.26}$$

$$M_\Lambda^2 = Z_\ell K_D \Lambda^{D-2}\tilde{M}_\ell^2, \tag{B.27}$$

wobei $K_D^{-1} = 2^{D-1}\pi^{D/2}\Gamma[D/2]$. Die beiden Kopplungsparameter u_Λ und M_Λ^2 sind somit relevant in den Dimensionen $2 < D < 4$. Die Dimension $D = 2$, in welcher Magnetisierung M_Λ^2 marginal wird, ist die untere kritische Dimension des Modells und $D = 4$, in welcher Wechselwirkung u_Λ marginal wird, heißt die obere kritische Dimension. Berücksichtigt man auch die Flussgleichung für die Wellenfunktionsrenormierung $\partial_\ell Z_\ell = -\eta_\ell Z_\ell$, so zieht unsere Trunkierung *alle* relevanten Parameter in $2 < D < 4$ mit in Betracht.

Drücken wir die Flussgleichung für den $\boldsymbol{k}$-abhängigen Anteil der Selbstenergie $\gamma_\ell(\boldsymbol{k}) = \Gamma_\ell^{(2)}(\boldsymbol{k}) - \Gamma_\ell^{(2)}(0)$ durch die reskalierten Größen aus, so erhalten wir für ihn folgende inhomogene Differentialgleichung

$$\partial_\ell\gamma_\ell(\boldsymbol{k}) = (2 - \eta_\ell - \boldsymbol{k}\cdot\nabla_{\boldsymbol{k}})\gamma_\ell(\boldsymbol{k}) + \dot{\gamma}_\ell(\boldsymbol{k})\;, \tag{B.28}$$

mit der Inhomogenität

$$\dot{\gamma}_\ell(\boldsymbol{k}) = \tilde{u}_\ell^2\tilde{M}_\ell^2 \int\limits_{\boldsymbol{q}} \dot{\mathcal{G}}_\ell(\boldsymbol{q})[\mathcal{G}_\ell(\boldsymbol{k}+\boldsymbol{q}) - \mathcal{G}_\ell(\boldsymbol{q})], \tag{B.29}$$

und den normierten Integralen

$$\int\limits_{\boldsymbol{q}} = \frac{1}{K_D(2\pi)^D}\int d^Dq. \tag{B.30}$$

Aus der Gleichung (B.28) kann die anomale Dimension η_ℓ gewonnen werden:

$$\eta_\ell = \frac{1}{2}\,\frac{\partial^2\dot{\gamma}_\ell(\boldsymbol{k})}{\partial\boldsymbol{k}^2}\bigg|_{\boldsymbol{k}=0}. \tag{B.31}$$

Setzt man den Litim-Cutoff ein, so vereinfacht sich Gleichung (B.31) zu

$$\eta_\ell = \frac{1}{D}\tilde{u}_\ell^2\tilde{M}_\ell^2\mathcal{G}_\ell^4(0) \tag{B.32}$$

mit $\mathcal{G}_\ell(0) \approx \left[1 + \tilde{u}_\ell\tilde{M}_\ell^2/3\right]^{-1}$.

Für die reskalierten Wechselwirkung und Magnetisierung erhalten wir nach dem Ausintegrieren der internen Impulse die korrespondierenden Flussgleichungen:

$$\partial_\ell\tilde{M}_\ell^2 = (D - 2 + \eta_\ell)\tilde{M}_\ell^2 - \frac{6(2+D-\eta_\ell)}{D(D+2)}\mathcal{G}_\ell^2(0), \tag{B.33}$$

$$\partial_\ell\tilde{u}_\ell = (4 - D - 2\eta_\ell)\tilde{u}_\ell - \frac{6(2+D-\eta_\ell)}{D(D+2)}\tilde{u}_\ell^2\mathcal{G}_\ell^3(0), \tag{B.34}$$

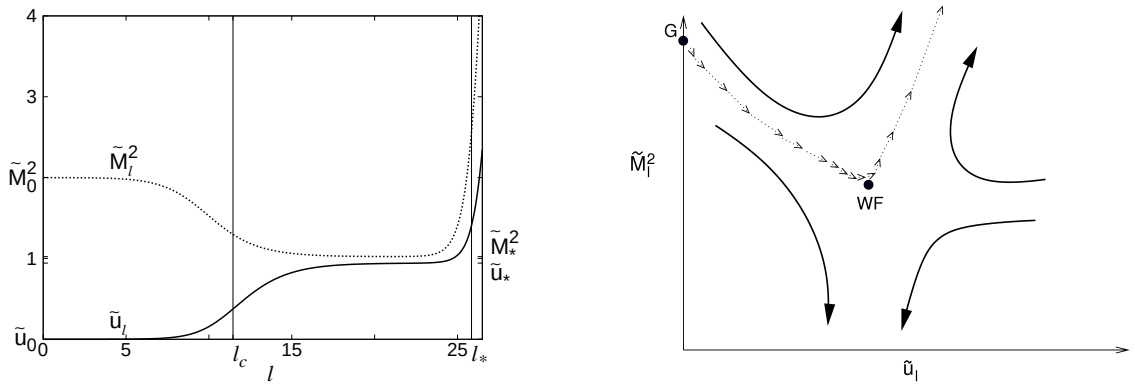

Figure B.1: Typischer fast kritischer Fluss der reskalierten Kopplungsparameter $\tilde{M}_\ell^2$ und $\tilde{u}_\ell$ in $2 < D < 4$, wie er aus der Auflösung von Gleichungen (B.32-B.34) folgt (links) und seine qualitative Darstellung im $\left\{\tilde{u}_\ell, \tilde{M}_\ell^2\right\}$-Parameterraum (rechts). Die Pfeile veranschaulichen den fast kritischen Fluss entlang der kritischen Oberfläche, wobei die Pfeildichte zur inversen Flussgeschwindigkeit korrespondiert. Die beiden fett markierten Punkte bezeichnen den Gaußschen (G) und den Wilson-Fisher (WF) Fixpunkt.

welche zusammen mit der Gleichung (B.32) ein geschlossenes Gleichungssystem darstellen und gelöst werden können. Der fast kritische Fluss der beiden Parameter ist durch das Wechselspiel zweier charakteristischen Längenskalen ℓ_c und $\ell_\star$ geprägt, wie es die Abbildung (B.1) veranschaulicht. Die Skala $\ell_c = -\ln(k_c/\Lambda_0)$ misst die Breite des wechselwirkungsabhängigen kritischen Ginzburg-Bereichs. Sie kann aus der Gleichung (B.34) im Limes $\mathcal{G}_\ell(0) \approx 1$ und $\eta_\ell \approx 0$ gefunden werden. Man erhält für diese Skala

$$\ell_c \approx \frac{1}{4-D} \ln\left(\frac{\tilde{u}_\star}{\tilde{u}_0}\right), \tag{B.35}$$

wobei $\tilde{u}_\star$ für den Wert der reskalierten Wechselwirkung am Wilson-Fisher (WF)-Fixpunkt und $\tilde{u}_0$ für den angepassten Startwert der Wechselwirkung steht. Wenn sich der fließende Parameter ihrem Wert nähert, d. h. $\ell \approx \ell_c$, wird der Fluss der Wechselwirkung vom WF-Fixpunkt stark angezogen. Über die internen Zusammenhänge ist ℓ_c auch für die Magnetisierung $\tilde{M}_\ell^2$ charakteristisch. In der unmittelbaren Nähe des WF-Fixpunkts bleibt der Fluss der beiden Parameter sehr langsam, bis er sich schließlich bei $\ell \approx \ell_\star$ sehr schnell vom Fixpunkt entfernt. Diese zweite Skala folgt aus der Bedingung für die Endlichkeit der Korrelationslänge unterhalb der kritischen Temperatur. Definiert man die physikalische Korrelationslänge als

$$\xi^{-2} = \lim_{\Lambda \to 0} [Z_\Lambda \Sigma_\Lambda(0)], \tag{B.36}$$

so erhält man mit $\xi^{-1} = \Lambda_0 e^{-\ell_\star}$ für die Skala $\ell_\star$ den Ausdruck

$$2\ell_\star = -\ln\left[\lim_{\ell \to \infty} e^{-2\ell} \Gamma_\ell^{(2)}(0)\right]. \tag{B.37}$$

Als ein quantitatives Maß für die Abschätzung, wie gut unsere Trunkierung ist, können wir den Wert für die anomale Dimension des Phasenübergangs benutzen. Sie kann aus dem linearisierten RG-Fluss der Kopplungsparameter in der Nähe des WF-Fixpunktes gewonnen werden. Wir erhalten $\eta = 0.0993$ in $D = 3$ und $\eta = \epsilon^2/12$ in der Entwicklung nach dem kleinen Parameter $\epsilon = 4 - D$. Diese beiden Werte weichen zwar stark von der etablierten ab, für welche $\eta = 0.0334$ in $D = 3$ [38] und $\eta = \epsilon^2/54$ [24, 23] in ϵ-Entwicklung im Allgemeinen anerkannt sind. Sie können jedoch verbessert werden, falls irrelevante Kopplungen mit berücksichtigt werden, vgl. [51, 62, 63].

Die beiden Skalen beeinflussen das Verhalten der impulsabhängigen physikalischen Selbstenergie. Sie kann nämlich in der Form eines Integrals über die gesamte RG-Trajektorie

$$\Sigma(\boldsymbol{k}) - \Sigma(0) = \Lambda_0^2 \int_0^\infty d\ell \; e^{-2\ell + \int_0^\ell d\tau \eta_\tau} \dot{\gamma}\big(e^\ell \boldsymbol{k}/\Lambda_0\big), \tag{B.38}$$

dargestellt werden, wobei hier $\Sigma(0) = Z^{-1}\xi^{-2}$. In unserer Trunkierung ist die Inhomogenität $\dot{\gamma}\big(e^\ell \boldsymbol{k}/\Lambda_0\big)$ durch die Gleichung (B.29) gegeben. Da dieser Ausdruck die Störungsentwicklung mit der funktionaler Renormierungsgruppe verknüpft, nennen wir dieses Verfahren die FRG-erweiterte Störungstheorie (zu Englisch: *FRG-enhanced perturbation theory*). Im Allgemeinen kann die Selbstenergie in der Form einer zweiparametrigen Skalenfunktion

$$\Sigma(\boldsymbol{k}) = k_c^2 \sigma^-(x, y), \tag{B.39}$$

mit $x = k\xi$ und $y = k/k_c$ ausgedrückt werden. Führt man die Größe

$$\Delta\sigma^-(x, y) = \sigma^-(x, y) - k_c^2 \Sigma(0) = \sigma^-(x, y) - y^2/Zx^2 \tag{B.40}$$

ein, so erhält man für sie

$$\begin{aligned} \Delta\sigma^-(x, y) &= \int_0^\infty dl e^{-2(\ell - \ell_c) + \int_0^\ell d\tau \eta_\tau} \dot{\gamma}_\ell(e^{l - \ell_c} y) \\ &= y^2 \int_{y e^{-\ell_c}}^\infty dp \, p^{-3} Z^{-1}_{\ell_c + \ln(p/y)} \dot{\gamma}_{\ell_c + \ln(p/y)}(p), \end{aligned} \tag{B.41}$$

wobei $p = y e^{\ell - \ell_c}$ und $Z_\ell = e^{-\int_0^\ell d\tau \eta_\tau}$.

Am kritischen Punkt können wir $x \to \infty$ setzen, da die Korrelationslänge divergiert. In diesem Fall reduziert sich die Skalenfunktion $\sigma^-(x, y)$ auf die übliche einparametrige Form

$$\Delta\sigma^-(\infty, y) = \sigma^-(\infty, y) = \sigma_\star(y). \tag{B.42}$$

Im kritischen langwelligen Regime, d. h. für $y \ll 1$, können wir die untere Integrationsgrenze in (B.41) durch Null und alle fließenden Größen durch ihre Fixpunktwerte ersetzen. Dann findet man

$$\sigma_\star(y) \approx A_D y^{2-\eta}, \tag{B.43}$$

wobei η den Wert der anomalen Dimension am Wilson-Fisher Fixpunkt bedeutet, und

$$A_D = \int_0^\infty dp \; p^{\eta - 3} \dot{\gamma}_\star(p), \tag{B.44}$$

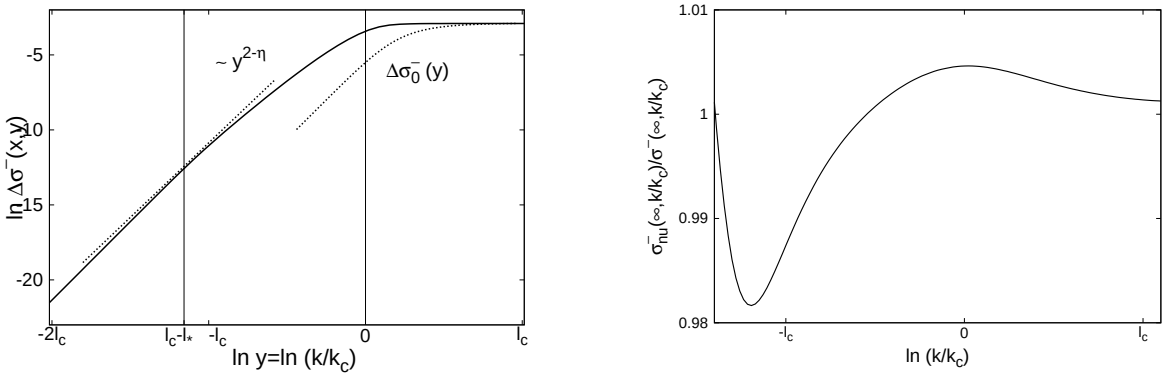

Figure B.2: Links: Typisches Verhalten der zwei-parametrigen Skalenfunktion $\Delta\sigma^-(x,y)$ nach Gleichung (B.41). Die gewählten Anfangsbedingungen $\tilde{u}_0 = 0.005$ und $M_0^2 = 1.9482092$ liefern für $\ell_c \approx 5.23$ und $\ell_\star \approx 11.29$. Unsere Rechnung reproduziert das störungstheoretische Ergebnis $\Delta\sigma_0^-(y)$ für große y. Das fast kritische Verhalten offenbart sich in dem Annäheren der Skalenfunktion an das kritische $y^{2-\eta}-$Verhalten um $y = \exp(\ell_c - \ell_\star)$. Rechts: Der Vergleich zwischen der selbstkonsistenten Rechnung für die Selbstenergie mit der Molekularfeld-ähnlichen Trunkierung (B.15). Hier bezeichnet $\sigma^-_{\mathrm{nu}}(\infty, k/k_c)$ das Ergebnis der numerischen selbstkonsistenten Rechnung, während $\sigma^-(\infty, k/k_c)$ das Ergebnis der im Text beschriebenen Rechnung. Man sieht deutlich, dass der Unterschied in der Größenordnung von 2% liegt.

mit $\gamma_\star(p) = \lim_{\ell\to\infty}\gamma_\ell(p)$. Im anderen Limes, d. h. für $y \gg 1$, nähert sich die Skalenfunktion dem konstanten Wert

$$\sigma_\star(y) \approx \frac{2}{D}\tilde{u}_0^2\tilde{M}_0^2\mathcal{G}_0^3(0). \tag{B.45}$$

Die Ergebnisse unserer Rechnung sind in Abbildung (B.2) gezeigt. Um $y = \exp(\ell_c - \ell_\star)$ sieht man klar den Crossover vom fast kritischen Verhalten der Selbstenergie mit der asymptotischen Form $\Delta\sigma_\star(y) \propto y^{2-\eta}$ zum nicht kritischen, wo $\Delta\sigma_\star(y) \propto y^2$.

Zusammenfassend haben wir am Beispiel eines einfachen einkomponentigen skalaren Modells gezeigt, wie die funktionale Renormierungsgruppe zur Beschreibung vom fast kritischen Verhalten des Systems von symmetriegebrochener Phase aus angewandt werden kann. Unter Verwendung des durch die Molekularfeldanalyse festgelegten Trunkierungsschemas kann die Differentialgleichungshierarchie auf dem Niveau der Zweipunktvertexfunktion geschlossen werden. Das fast kritische Verhalten des Systems wird durch das Wechselspiel mehrerer Skalen geprägt, wobei diese Skalen qualitativ wie quantitativ aus den Flussgleichungen extrahiert werden können. Schließlich haben wir die impuls-abhängige physikalische Selbstenergie berechnet und den Einfluss beider relevanten Skalen auf die fast kritische Physik des Modells nachgewiesen.

Wechselwirkende Bosonen bei $T = 0$

Im Kapitel 3 wenden wir den Formalismus der funktionalen Renormierungsgruppe auf die wechselwirkenden Bosonen bei $T = 0$ an. Die mikroskopische Euklidische Wirkung des Modells ist durch

$$S[\bar{\psi}, \psi] = -\int_K \bar{\psi}_K (i\omega - \epsilon_{\boldsymbol{k}} + \mu)\psi_K + \frac{1}{2}\int_K u_{\Lambda_0}(K)\rho_K \rho_{-K}, \tag{B.46}$$

gegeben, wobei $K = (\boldsymbol{k}, \omega)$ den $D+1-$dimensionalen Impuls mit der imaginären Matsubara Frequenz ω bezeichnet. Des Weiteren bezeichnet hier $\epsilon_{\boldsymbol{k}} = k^2/(2m)$ die Dispersion der freien Bosonen mit Masse m, μ das chemische Potential, $u_{\Lambda_0}(K) = u_{\Lambda_0}(-K)$ die nicht-lokale Wechselwirkung und $\rho_K = \int_Q \bar{\psi}_Q \psi_{Q+K}$ die Fourier-Transformierte der lokalen Dichte. Die Integration über den Impuls K ist als

$$\int_K \equiv \int \frac{d\omega}{2\pi} \int \frac{d^D k}{(2\pi)^D} \tag{B.47}$$

definiert. Die Regularisierung des Wechselwirkungsterms durch einen Abschneideimpuls Λ_0 im Ultravioletten ist vorausgesetzt. Im Falle der Hard-Core-Bosonen bezieht sich Λ_0 auf den Durchmesser der Bosonen und sonst auf die Reichweite der Wechselwirkung. Die Wirkung (B.46) bleibt invariant unter der globalen Eichtransformation $\psi_K \to e^{i\lambda}\,\psi_K$, $\bar{\psi}_K \to e^{-i\lambda}\,\bar{\psi}_K$ mit reellem λ, d. h. das Modell gehört der $U(1)$-Invarianzklasse an. Es hängt von zwei dimensionslosen Parametern ab: Zum einen ist es $\tilde{\mu}_0 = 2m\mu\Lambda_0^{-2}$, welches das chemische Potential in Einheiten der Abschneideenergie $\Lambda_0^2/2m$ angibt, zum anderen die dimensionslose Wechselwirkung $\tilde{u}_0(K) = 2mk_\mu^{D-2}u_{\Lambda_0}(K)$ in Einheiten des charakteristischen Impulses $k_\mu = \sqrt{2m\mu}$, welcher in Analogie zum Fermiimpuls fermionischer Systeme eingeführt wird.

Wird die $U(1)$-Symmetrie gebrochen, so erhalten Quantenfelder einen nicht verschwindenden Vakuumerwartungswert

$$\psi_K = \Delta\psi_K + \delta_{K,0}\sqrt{\rho^0_{\Lambda_0}}, \tag{B.48a}$$

$$\bar{\psi}_K = \Delta\bar{\psi}_K + \delta_{K,0}\sqrt{\rho^0_{\Lambda_0}}. \tag{B.48b}$$

Setzt man Ausdrücke (B.48a) und (B.48b) in die Wirkung (B.46) ein und separiert diese nach den Potenzen von fluktuierenden Feldern um, so erhält man

$$S[\Delta\bar{\psi},\Delta\psi] = \tilde{S}[\Delta\bar{\psi},\Delta\psi]$$

$$- \quad \frac{1}{2}\int_K (\Delta\bar{\psi}_K, \Delta\psi_{-K}) \begin{pmatrix} -\Sigma^A_{\Lambda_0}(K) & G_0^{-1}(K) - \Sigma^N_{\Lambda_0}(K) \\ G_0^{-1}(-K) - \Sigma^N_{\Lambda_0}(-K) & -\Sigma^A_{\Lambda_0}(-K) \end{pmatrix} \begin{pmatrix} \Delta\bar{\psi}_{-K} \\ \Delta\psi_K \end{pmatrix}$$

$$+ \int_{K_1}\int_{K_2}\int_{K_3} \left(\Gamma^{(1,2)}_{\Lambda_0}(K_1;K_2,K_3)\Delta\bar{\psi}_{K_1}\Delta\psi_{K_2}\Delta\psi_{K_3} + \Gamma^{(2,1)}_{\Lambda_0}(K_1;K_2,K_3)\Delta\bar{\psi}_{K_3}\Delta\bar{\psi}_{K_2}\Delta\psi_{K_1}\right)$$

$$+ \int_{K_1}\int_{K_2}\int_{K_3}\int_{K_4} \Gamma^{(2,2)}_{\Lambda_0}(K_1,K_2;K_3,K_4)\Delta\bar{\psi}_{K_1}\Delta\bar{\psi}_{K_2}\Delta\psi_{K_3}\Delta\psi_{K_4}, \tag{B.49}$$

wobei $\tilde{S}[\Delta\bar{\psi},\Delta\psi]$ Terme zu nullter und linearer Ordnung in den fluktuierenden Feldern enthält. Das Kondensat wird aus der Forderung nach dem Verschwinden des linearen Terms fixiert:

$$\rho^0_{\Lambda_0} = \frac{\mu}{u_{\Lambda_0}}, \tag{B.50}$$

wobei $u_{\Lambda_0} = u_{\Lambda_0}(0)$. Die beiden hier eingeführten nackten Selbstenergien, die normale $\Sigma^N_{\Lambda_0}(\pm K)$ und die anomale $\Sigma^A_{\Lambda_0}(\pm K)$ ergeben sich in der folgenden Form:

$$\Sigma^N_{\Lambda_0}(\pm K) = \rho^0_{\Lambda_0}[u_{\Lambda_0} + u_{\Lambda_0}(K)], \tag{B.51a}$$

$$\Sigma^A_{\Lambda_0}(\pm K) = \rho^0_{\Lambda_0} u_{\Lambda_0}(K). \tag{B.51b}$$

Zum anderen erhalten wir für die höheren Vertizes:

$$\Gamma^{(1,2)}_{\Lambda_0}(K_1;K_2,K_3) = \Gamma^{(2,1)}_{\Lambda_0}(K_1;K_2,K_3)$$

$$= \delta_{K_1,K_2+K_3}\sqrt{\rho^0_{\Lambda_0}}[u_{\Lambda_0}(K_1+K_2) + u_{\Lambda_0}(K_1+K_3)], \tag{B.52}$$

$$\Gamma^{(2,2)}_{\Lambda_0}(K_1,K_2;K_3,K_4) = \delta_{K_1+K_2,K_3+K_4}[u_{\Lambda_0}(K_1+K_3) + u_{\Lambda_0}(K_1+K_4)]. \tag{B.53}$$

Schließlich ist die Greensche Funktion des freien Systems durch

$$G_0^{-1}(\pm K) = \pm i\omega - \epsilon_{\boldsymbol{k}} + \mu \tag{B.54}$$

gegeben. Mit wenigen Änderungen werden diese Ausdrücke als Trunkierung für die Renormierungsgruppenanalyse dienen.

Die Matrix der vollen Propagatoren können wir durch das Invertieren des quadratischen Terms aus der Wirkung (B.49) ermitteln. Man beachte, dass diese Invertierung in den beiden Räumen, dem Fourier- und dem Quantenfeldraum ausgeführt werden muss. Wir erhalten den Beliaev-Propagator [79, 80, 85]

$$\boldsymbol{G}_{\Lambda_0}(K) = \begin{pmatrix} G^A_{\Lambda_0}(-K) & G^N_{\Lambda_0}(K) \\ G^N_{\Lambda_0}(-K) & G^A_{\Lambda_0}(K) \end{pmatrix}$$

$$= \frac{1}{\mathcal{D}(K)} \begin{pmatrix} \Sigma^A_{\Lambda_0}(-K) & G_0^{-1}(-K) - \Sigma^N_{\Lambda_0}(-K) \\ G_0^{-1}(K) - \Sigma^N_{\Lambda_0}(K) & \Sigma^A_{\Lambda_0}(K) \end{pmatrix}, \tag{B.55}$$

wobei der Nenner durch

$$\mathcal{D}(K) = [i\omega + \epsilon_{\boldsymbol{k}} - \mu + \Sigma^N_{\Lambda_0}(-K)][i\omega - \epsilon_{\boldsymbol{k}} + \mu - \Sigma^N_{\Lambda_0}(K)] + \Sigma^A_{\Lambda_0}(K)\Sigma^A_{\Lambda_0}(-K) \quad \text{(B.56)}$$

gegeben ist. Die Nullstellen des Nenners (B.56) geben die elementaren Anregungen an. Die Abwesenheit der Energielücke im Spektrum der elementaren Anregungen folgt aus der Bedingung $\mathcal{D}(0) = 0$, welche nach Umstellung die Hugenholtz-Pines-Beziehung [16]

$$\mu = \Sigma^N_{\Lambda_0}(0) - \Sigma^A_{\Lambda_0}(0). \quad \text{(B.57)}$$

liefert. Setzt man Ausdrücke (B.51a) und (B.51b) in (B.56) ein, so erhält man

$$\mathcal{D}(K) \propto \left(\omega^2 + E_B^2(K)\right), \quad \text{(B.58)}$$

wobei $E_B(K) = \sqrt{\epsilon_{\boldsymbol{k}}[\epsilon_{\boldsymbol{k}} + 2\rho^0_{\Lambda_0} u_{\Lambda_0}(K)]}$ das Bogoliubov-Spektrum bezeichnet.

Beliaev untersuchte das Modell (B.49) störungstheoretisch und leitete den Ausdruck für die Dämpfung der Quasiteilchen ab. In beliebiger Dimension kann man die Beliaev-Dämpfung wie folgt schreiben: [79, 80, 105]

$$\gamma_k^{(2)} \approx \alpha_0 k^{2D-1}, \quad \text{(B.59)}$$

wobei

$$\alpha_0 = 2^{-4} 3^{\frac{D+1}{2}} K_{D-1} \frac{k_0^{3-D}}{2m\rho^0_{\Lambda_0}} \int_0^1 dx\; x^{D-1}(1-x)^{D-1} \quad \text{(B.60)}$$

und $k_0 = 2mc_0$, wobei $c_0 = \sqrt{\rho^0_{\Lambda_0} u_{\Lambda_0}/m}$ die Geschwindigkeit der lückenlosen Goldstone-Mode [15] bezeichnet.

In einer Reihe von Arbeiten [17, 87, 88] wiesen Nepomnyashchy und Nepomnyashchy exakt nach, dass die anomale Selbstenergie im Limes langer Wellenlängen verschwindet. Hierfür untersuchten sie die Skeletondiagramme für die anomale Selbstenergie. Unter Verwendung der exakten asymptotischen Propagatoren [86]

$$G^N(\pm K) = -G^A(K) \propto \frac{1}{\omega^2 + c_0^2 k^2}, \quad \text{(B.61)}$$

und Vernachlässigung der Impulsabhängigkeit der Dreipunktvertizes erhalten sie eine Integralgleichung, welche als eine *exakte* Selbstkonsistenzgleichung angesehen werden kann. Die einzige physikalisch relevante Lösung dieser Gleichung lautet

$$\Sigma^A(0) = 0. \quad \text{(B.62)}$$

Diese Tatsache kann zu keiner Ordnung in der Störungsentwicklung reproduziert werden. Sie kann allerdings mittels der RG-theoretischen Resummierung der Störungsreihe bewiesen werden.

Für unseren FRG-Zugang zu den wechselwirkenden Bosonen benutzen wir folgende Trunkierung des erzeugenden Funktionals der Ein-Teilchen-irreduziblen Vertexfunktionen mit der nicht-lokalen Wechselwirkung:

$$\Gamma_\ell[\bar{\phi},\phi] = \int\limits_K \bar{\phi}_K \sigma_\ell \phi_K + \int\limits_K \Delta\rho_\ell u_\ell(K) \Delta\rho_{-K}, \tag{B.63}$$

wobei der Wechselwirkungsteil durch die fluktuierende Dichte

$$\Delta\rho_K = \int\limits_Q \bar{\phi}_Q \phi_{K+Q} - \delta_{K,0}\rho_\ell^0 \tag{B.64}$$

ausgedrückt ist, mit dem fließenden Kondensat ρ_ℓ^0. Die Größe

$$\sigma_\ell(K) \approx \mu\left(1 - \frac{\Delta_\ell}{\mu}\right) + i\omega\,(1 - Y_\ell) + \epsilon_{\boldsymbol{k}}(Z_\ell^{-1} - 1) + \omega^2 V_\ell, \tag{B.65}$$

welche den Crossover vom $\omega \propto k^2-$Regime zum $\omega \propto k-$Regime beschreibt, wird nur durch den RG-Fluss erzeugt und muss dementsprechend am Anfang des Flusses verschwinden. Diese Forderung legt die Anfangsbedingungen für die fließende Lücke Δ_ℓ und Kopplungsparameter Y_ℓ, Z_ℓ und V_ℓ auf $\Delta_0 = \rho_0^0 u_0 = \mu$, $Y_0 = Z_0 = 1$ und $V_0 = 0$ fest. Für die fließenden Selbstenergien finden wir

$$\Sigma_\ell^N(\pm K) = \sigma_\ell(K) + \rho_\ell^0(u_\ell + u_\ell(K)), \tag{B.66a}$$
$$\Sigma_\ell^A(\pm K) = \rho_\ell^0 u_\ell(K), \tag{B.66b}$$

wogegen die fließenden Dreipunkt- und Vierpunktvertizes die Form (B.52) und (B.53) beibehalten, mit dem Unterschied, dass die nackten Kopplungskonstanten durch die fließenden ersetzt werden müssen. Diese Ausdrücke verwenden wir als Trunkierung für die Vertizes auf der rechten Seite der jeweiligen Flussgleichung. Bei der Herleitung von RG-Flussgleichungen für das Kondensat und die beiden Selbstenergien verwenden wir erneut das Litim-Regularisierungsschema [41]

$$R_\ell(\boldsymbol{k}) = (1 - \delta_{\boldsymbol{k},0})\frac{Z_\ell^{-1}}{2m}(\Lambda^2 - k^2)\Theta(\Lambda^2 - k^2). \tag{B.67}$$

Die wichtigste Vereinfachung besteht dabei in der Vernachlässigung der Impulsabhängigkeit der Wechselwirkung auf der rechten Seite der RG-Flussgleichungen, so dass wir

$$\partial_\Lambda \rho_\ell^0 = \int_Q \left[\dot{G}_\ell^N(Q) + \dot{G}_\ell^N(-Q) + \dot{G}_\ell^A(Q)\right], \tag{B.68}$$

$$\begin{aligned}\partial_\Lambda \Sigma_\ell^N(\pm K) = {} & u_\ell \int_Q \left[\dot{G}_\ell^N(Q) + \dot{G}_\ell^N(-Q) + 2\dot{G}_\ell^A(Q)\right] \\ & -4\rho_\ell u_\ell^2 \int_Q \Big\{2\dot{G}_\ell^A(Q)\left[G_\ell^N(\pm K - Q) + G_\ell^A(\pm K - Q)\right] \\ & +\dot{G}_\ell^N(Q)\left[G_\ell^N(\pm K - Q) + G_\ell^N(Q \mp K) + 2G_\ell^A(\pm K - Q)\right] \\ & + \dot{G}_\ell^N(-Q) G_\ell^N(\pm K - Q)\Big\},\end{aligned} \tag{B.69}$$

$$\begin{aligned}\partial_\Lambda \Sigma_\ell^A(K) = {} & u_\ell \int_Q \left[\dot{G}_\ell^N(Q) + \dot{G}_\ell^N(-Q)\right] \\ & -4\rho_\ell u_\ell^2 \int_Q \Big\{\dot{G}_\ell^N(Q)\left[G_\ell^N(Q - K) + G_\ell^A(Q - K)\right] \\ & +\dot{G}_\ell^A(Q)\left[G_\ell^N(Q - K) + G_\ell^N(K - Q) + 3G_\ell^A(Q - K)\right] \\ & + \dot{G}_\ell^N(-Q)\left[G_\ell^N(K - Q) + G_\ell^A(K - Q)\right]\Big\}\end{aligned} \tag{B.70}$$

erhalten. Gleichung (B.68) beschreibt den Fluss des Kondensats, während Gleichungen (B.69) und (B.70) den Fluss der normalen und anomalen Selbstenergie. In unserer Trunkierung ergibt sich für die Propagatoren

$$G_\ell^N(\pm K) = \frac{\Delta_\ell \pm i Y_\ell \omega + \bar{\epsilon}_\ell(\boldsymbol{k}) + V_\ell \omega^2}{Y_\ell^2 \omega^2 + (\bar{\epsilon}_\ell(\boldsymbol{k}) + V_\ell \omega^2)(2\Delta_\ell + \bar{\epsilon}_\ell(\boldsymbol{k}) + V_\ell \omega^2)}, \tag{B.71a}$$

$$G_\ell^A(K) = -\frac{\Delta_\ell}{Y_\ell^2 \omega^2 + (\bar{\epsilon}_\ell(\boldsymbol{k}) + V_\ell \omega^2)(2\Delta_\ell + \bar{\epsilon}_\ell(\boldsymbol{k}) + V_\ell \omega^2)}, \tag{B.71b}$$

wobei $\bar{\epsilon}_\ell(\boldsymbol{k}) = Z_\ell^{-1}\epsilon_{\boldsymbol{k}} + R_\ell(\boldsymbol{k})$. Die single scale Propagatoren werden aus den Beziehungen

$$\dot{G}_\ell^N(\pm K) = -\partial_\Lambda R_\ell(\boldsymbol{k})\left\{[G_\ell^N(\pm K)]^2 + [G_\ell^A(K)]^2\right\}, \tag{B.72}$$

$$\dot{G}_\ell^A(K) = -\partial_\Lambda R_\ell(\boldsymbol{k}) G_\ell^A(K)\left\{G_\ell^N(K) + G_\ell^N(-K)\right\}. \tag{B.73}$$

erhalten. Somit wird das Hugenholtz-Pines-Theorem für alle Werte von Λ erfüllt, wie es aus der Beziehung

$$\partial_\Lambda\left(\Sigma_\ell^N(0) - \Sigma_\ell^A(0)\right) = 0 \tag{B.74}$$

ersichtlich ist.

Schließlich erhalten wir die RG-Flussgleichungen für die Wechselwirkung

$$\partial_\ell u_\ell = -\frac{u_\ell}{\rho_\ell}\partial_\ell \rho_\ell + \frac{1}{\rho_\ell}\partial_\ell \Sigma_\ell^A(0), \tag{B.75}$$

und die Flussgleichungen für die Parameter Y_ℓ, Z_ℓ und V_ℓ

$$\partial_\ell Z_\ell = -mZ_\ell^2 \frac{\partial^2}{\partial k^2}\partial_\ell \sigma_\ell(\boldsymbol{k},0)\Big|_{k=0}, \tag{B.76a}$$

$$\partial_\ell Y_\ell = -\frac{\partial}{\partial(i\omega)}\partial_\ell \sigma_\ell(0,i\omega)\Big|_{\omega=0}, \tag{B.76b}$$

$$\partial_\ell V_\ell = \frac{1}{2}\frac{\partial^2}{\partial \omega^2}\partial_\ell \sigma_\ell(0,i\omega)\Big|_{\omega=0}. \tag{B.76c}$$

Die Skalendimensionen η_z und η_y der beiden Parameter Z_ℓ und Y_ℓ erhält man aus

$$\eta_z = -\partial_\ell \ln Z_\ell, \tag{B.77a}$$

$$\eta_y = -\partial_\ell \ln Y_\ell. \tag{B.77b}$$

Sie entsprechen den anomalen Dimensionen des Modells. Die Skalendimension der temporären Variable z, die auch dynamischer Exponent genannt wird, hängt mit den beiden anomalen Dimensionen über die Beziehung

$$z = 2 - \eta_z - \eta_y \tag{B.78}$$

zusammen und stellt ein nützliches Instrument zur Veranschaulichung des Crossovers zwischen dem quasifreien ($z = 2$) und dem Goldstone-Regime ($z = 1$) dar.

In der Abbildung (B.3) zeigen wir die Ergebnisse der numerischen Lösung der Gleichungen (B.68), (B.75) und (B.76a)-(B.76c) in $D = 2$. Wie erwartet fließt das Kondensat gegen einen konstanten Wert $\rho_\star^0$. Der Crossover zwischen dem quasifreien und dem Goldstone-Regime offenbart sich im Verschwinden des Parameters Y_ℓ für große ℓ mit der gleichzeitigen Saturierung des Flusses von V_ℓ. Diese Tatsache äußert sich auch in der Änderung des dynamischen Exponenten z von $z = 2$ am Anfang des Flusses zu $z = 1$ für große ℓ. Schließlich verschwindet die Wechselwirkung u_ℓ im physikalischen Limes. Ähnliches Verhalten der Flüsse wurde auch in $D = 3$ gefunden, mit dem Unterschied, dass die relevanten ℓ-Skalen um ein Mehrfaches größer sind. Der Grund dafür liegt in dem unterschiedlichen asymptotischen Verhalten der Kopplungsparameter für $\ell \to \infty$. In diesem Limes kann man in Gleichungen (B.68), (B.75) und (B.76a)-(B.76c) ρ_ℓ^0, Z_ℓ und V_ℓ durch ihre Fixpunktwerte ersetzen. Dann erhalten wir für die Wechselwirkung

$$u_\ell \approx \begin{cases} \dfrac{u_{\Lambda_0}\Lambda^\epsilon}{\Lambda^\epsilon + \dfrac{mk_c u_{\Lambda_0}}{\epsilon A'_D}\left[1 - \left(\dfrac{\Lambda}{\Lambda_0}\right)^\epsilon\right]}, & D < 3, \\ \dfrac{A_3 u_0}{A_3 + u_0 \ln\left(\dfrac{\Lambda}{\Lambda_0}\right)}, & D = 3, \end{cases} \tag{B.79}$$

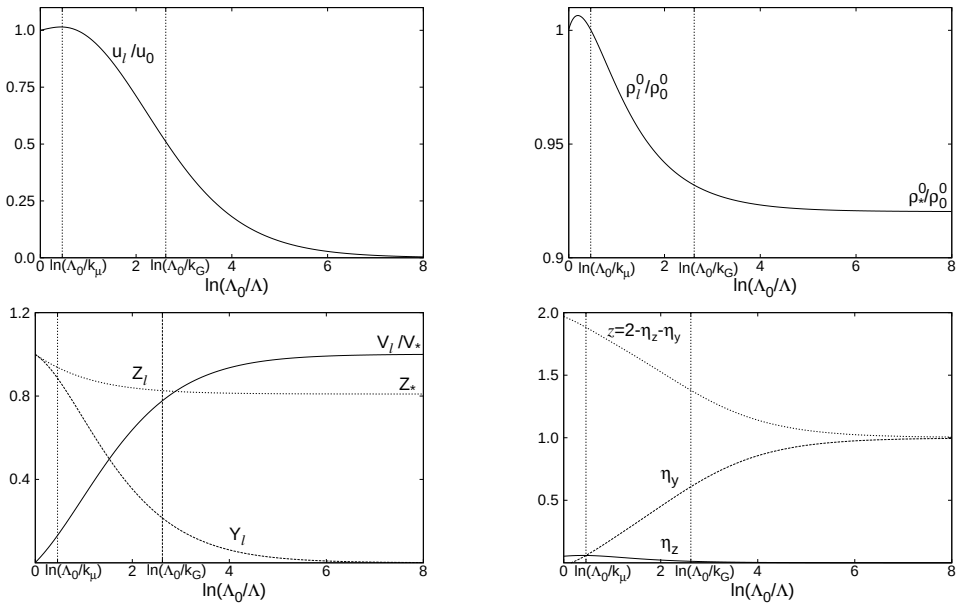

Figure B.3: Typischer RG-Fluss der Kopplungsparameter u_ℓ (oben links), ρ_ℓ^0 (oben rechts), Y_ℓ, Z_ℓ und V_ℓ (unten links), sowie des dynamischen Exponenten und der anomalen Dimensionen η_z und η_y (unten rechts) in $1 < D < 3$. Die gewählten Anfangsbedingungen sind $\tilde{\mu}_0 = 2m\mu\Lambda_0^{-2} = 0.4$ und $\tilde{u}_0 = 2mu_0k_\mu^{D-2} = 4$ mit $D = 2$.

mit $\epsilon = 3 - D$,

$$A_D = \frac{4}{3c\kappa_D}\left(\frac{\rho}{m\rho_\star^0}\right)^2 = \frac{A'_D}{mk_c}, \tag{B.80}$$

$k_c = 2mc$, $\kappa_D = K_D/D$, $\rho_\star^0 = Z_\star\rho$, wobei ρ die Dichte der Bosonen bedeutet, und der renormierten Geschwindigkeit der Goldstone-Mode

$$c = \frac{1}{\sqrt{2mV_\star Z_\star}}, \tag{B.81}$$

wobei $V_\star$ und $Z_\star$ die Fixpunktwerte entsprechender Parameter bezeichnen. Die Crossoverskala vom $z = 2-$ zum $z = 1-$Regime lässt sich aus der Gleichung (B.79) finden:

$$k_G \approx \begin{cases} \left[\dfrac{mk_cu_{\Lambda_0}}{\epsilon A'_D}\right]^{\frac{1}{\epsilon}} & \text{for} \quad D < 3, \\ \Lambda_0 \exp\left(\dfrac{mk_cu_{\Lambda_0}}{A'_3}\right) & \text{for} \quad D = 3. \end{cases} \tag{B.82}$$

Analoges Ergebnis kann man auch für den Kopplungsparameter Y_ℓ erhalten. Da die anomale Selbstenergie von der Wechselwirkung abhängt, verschwindet sie ebenfalls im Limes $\ell \to \infty$, was genau der Aussage der Nepomnyashchy-Nepomnyashchy-Relation entspricht.

Als ein wichtiges Zwischenergebnis haben wir die exakte asymptotische Form der Propagatoren (vgl. [86]) reproduziert. Für ihre Herleitung ist die Impulsabhängigkeit der Wechselwirkung von entscheidender Bedeutung. Zur führenden Ordnung in $\boldsymbol{k}$ und ω kann $u_\ell(K)$ wie folgt entwickelt werden:

$$u_\ell(K) \approx u_\ell + \alpha_\ell \boldsymbol{k}^2 + \beta_\ell \omega^2 + \mathcal{O}(K^3). \tag{B.83}$$

Es stellt sich heraus, dass die Flüsse der beiden neueingeführten Parametern α_ℓ und β_ℓ im Limes $\ell \to \infty$ divergieren, und zwar wie

$$\alpha_\ell \propto \beta_\ell \propto \begin{cases} e^{(D-1)\ell}, & D < 3, \\ \\ \ell^{-1} e^{2\ell}, & D = 3. \end{cases} \tag{B.84}$$

Wichtig ist, dass die Divergenz in $D = 3$ schwächer ist, als $\exp(2\ell)$, denn dies besagt das asymptotische Verschwinden der anomalen Selbstenergie im Limes $\boldsymbol{k} \to 0,\ \omega \to 0$ in $D = 3$. Wenn wir jetzt die Entwicklung (B.83) in den Ausdruck für die Greenschen Funktionen (B.55) einsetzen, so finden wir zur führenden Ordnung in der Entwicklung nach dem kleinen Parameter α_ℓ^{-1}

$$\begin{aligned} G^N(\pm K) &= -G^A(K) = \frac{1}{2V_\star(\omega^2 + (2mZ_\star V_\star)^{-1}k^2)} \\ &= \frac{m\rho_\star^0 c^2}{\rho} \frac{1}{\omega^2 + c^2 k^2}. \end{aligned} \tag{B.85}$$

Das ist exakt das Ergebnis von Gavoret und Nozières [86].

Als nächstes können wir die Schick-Skala für das entartete Gas von Hard-Core-Bosonen [104] in $D = 2$ aus den Flussgleichungen extrahieren. Während die Störungstheorie in $D = 3$ im Wesentlichen als Entwicklung nach der kleinen Größe $u_0 \propto \rho a^3$ [79, 85, 103] definiert ist, wobei a für die s-Wellenstreulänge steht, ist es in $D = 2$ anders. In $D = 2$ und bei $T = 0$ verschwindet nämlich die s-Wellenstreulänge, die Störungsentwicklung kann aber in der relevanten kleinen Größe $1/\ln(\rho a^2)$, $\rho a^2 \ll 1$ definiert werden, wobei ρ die Dichte der Bosonen und a die Reichweite des Potentials sind. Setzt man den Parameter Y_ℓ, Z_ℓ und V_ℓ und ρ_ℓ auf ihre Anfangswerte und löst die Gleichung für die Wechselwirkung (B.75) im Grenzfall langer Wellenlängen auf, so erhält man für sie

$$u_\Lambda = \frac{u_0}{1 + \dfrac{m u_0}{2\pi} \ln\left(\dfrac{\Lambda_0}{\Lambda}\right)}. \tag{B.86}$$

Im Limes $1 \gg m u_0/(2\pi) \ln(\Lambda_0/\Lambda)$ fließt die Wechselwirkung nicht und die Bogoliubov-Theorie bleibt korrekt. Der andere Limes $1 \ll m u_0/(2\pi) \ln(\Lambda_0/\Lambda)$ entspricht dem Hard-Core-Limes. Man erhält nach kurzer Zwischenrechnung für die Geschwindigkeit der Goldstone-Mode in diesem Regime

$$c = \sqrt{-\frac{4\pi\rho}{m^2 \ln(\rho a^2)}}, \tag{B.87}$$

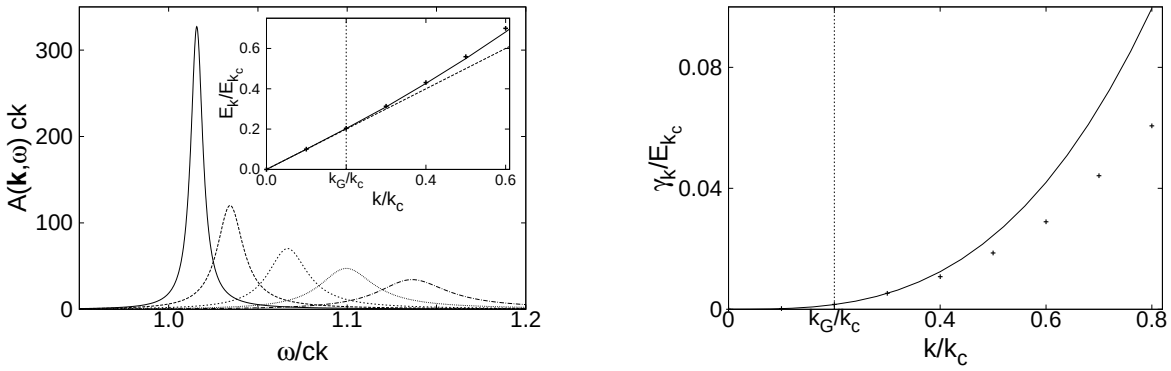

Figure B.4: Links: Einteilchenspektralfunktion $A(\boldsymbol{k}, \omega)$ für $D = 2$ in Abhängigkeit von der reellen Frequenz ω. Die gewählten Anfangsbedingungen sind $\tilde{\mu}_0 = 0.15$ und $\tilde{u}_0 = 15$. Die Peaks sind mit $k/k_c = 0.2,\ 0.3,\ 0.4, 0.5$ und 0.6 berechnet, wobei $k_c = 2mc$, $c = (2mV_\star Z_\star)^{-1/2}$. Die eingefügte Grafik zeigt das extrahierte Spektrum der Elementaranregungen im Vergleich mit dem Bogoliubov-ähnlichen Spektrum $E_k^2 = \epsilon_k^2 + c^2k^2$ (schwarze Punkte). Rechts: Die Dämpfung der Quasiteichen extrahiert aus der Spektralfunktion $A(\boldsymbol{k}, \omega)$ (schwarze Punkte). Die durchgezogene Linie stellt die Asymptote $\gamma_k \approx 0.194k^3/2mk_c$ dar.

wobei wir hier den Wert von Λ_0 auf $\Lambda_0 = \sqrt{16\pi/a^2}$ festgelegt haben. Gleichung (B.87) reproduziert das Ergebnis von Schick.

Schließlich wollen wir die Einteilchenspektralfunktion der wechselwirkenden Bosonen berechnen. Sie ist durch den Imaginärteil der normalen reellzeitigen Greenschen Funktion wie folgt definiert

$$A(i\omega \to \omega + i0, \boldsymbol{k}) = -2\mathrm{Im}G^N(i\omega \to \omega + i0, \boldsymbol{k}). \tag{B.88}$$

Wir berechnen die Spektralfunktion numerisch. Dafür müssen wir zuerst Gleichungen (B.69) und (B.70) zusammen mit den Gleichungen (B.68), (B.75) und (B.76a)-(B.76c) im Imaginärzeit-Formalismus auswerten, und dann die ermittelten Selbstenergien mittels Padé-Approximanten zur reellen Achse analytisch fortsetzen. Hat man die Spektralfunktion berechnet, so können aus ihr das Spektrum der Elementaranregungen als Position der Peaks, sowie die Beliaev-Dämpfung als ihre Halbwertsbreite extrahiert werden. Wir zeigen Ergebnisse unserer Rechnung für $D = 2$ in der Abbildung (B.4).

Unsere Rechnung ergibt das richtige qualitative Verhalten sowohl für das Anregungsspektrum, wie auch für die Dämpfung der Quasiteichen (siehe den Text unter der Abbildung B.4). Quantitativ beobachten wir eine Abweichung von dem Bogoliubov-Spektrum, bzw. von der Beliaev-Dämpfung (B.59), wobei diese Abweichung stark mit der Wahl der Anfangsbedingungen zusammenhängt. Wir erhalten eine sehr gute Übereinstimmung unserer Ergebnisse mit der Störungstheorie für schwache Wechselwirkungen. Wählen wir als Anfangsbedingungen $\tilde{\mu}_0 = 0.008$ und $\tilde{u}_0 = 0.8$, so erhalten wir $c/c_0 \approx 1.0054$ und $\alpha(\tilde{\mu}_0, \tilde{u}_0)/\alpha_0 \approx 0.967$. Für stärkere Wechselwirkungen wird

die Abweichung von den Vorhersagen der Störungstheorie deutlicher. So finden wir für $\tilde{\mu}_0 = 0.4$ und $\tilde{u}_0 = 4$ für die Renormierung der Geschwindigkeit der Goldstone-Mode $c/c_0 \approx 1$ und für die Renormierung des α-Faktors aus der Gleichung (B.59) $\alpha(\tilde{\mu}_0, \tilde{u}_0)/\alpha_0 \approx 0.92$. Auf der anderen Seite erhalten wir mit $\tilde{\mu}_0 \approx 0.15$ und $\tilde{u}_0 \approx 15$ für $c/c_0 \approx 0.67$ und für $\alpha(\tilde{\mu}_0, \tilde{u}_0)/\alpha_0 \approx 0.53$. Dabei bleibt unsere Theorie voll kontroliert selbst im Bereich sehr starken Wechselwirkungen. Ein direkter Vergleich mit dem Experiment bietet sich daher an [93].

Zusammenfassend haben wir den mathematischen Apparat der funktionalen Renormierungsgruppe erfolgreich auf wechselwirkende Bosonen angewandt. Wir benutzen ein Trunkierungsschema mit der nicht lokalen Wechselwirkung, welches über die derivative Trunkierung der effektiven Wirkung hinaus geht, die in den früheren FRG-Zugängen zu diesem Thema [89, 90, 95, 96, 98] benutzt wurde. Die Nichtlokalität der Wechselwirkung erweist sich als entscheidend, um exaktes asymptotisches Verhalten der Selbstenergien und Propagatoren zu garantieren. Die Selbstenergien in unserer Näherung genügen beiden exakten Beziehungen: Der Hugenholtz-Pines- und der Nepomnyashchy-Nepomnyashchy-Relation. Wir berechnen die Eintelchenspektraldichte unter der Berücksichtigung der beiden Relationen und extrahieren daraus das Spektrum der elementaren Anregungen, sowie die Beliaev-Dämpfung.

Bibliography

[1] S. N. Bose, Z. Phys. **26**, 178 (1924).

[2] A. Einstein, *Sitzungsberichte der Preussischen Akademie der Wissenschaften, Physikalisch-mathematische Klasse*, p. 261 (1924); p. 3 (1925).

[3] C. J. Pethrick and H. Smith, *Bose-Einstein condensation in dilute gases*, Cambridge University Press, Cambridge, UK, (2002).

[4] N. N. Bogoliubov, J. Phys. (USSR) **11**, 23 (1947).

[5] L. D. Landau and E. M. Lifschitz, *Course on Theoretical Physics: Statistical Physics Pt. 1, V 5*, Addison-Wesley, Reading, (1958).

[6] L. D. Landau, Phys. Z. der Sowjet Union **11**, 26 (1937).

[7] L. Onsager, Phys. Ref. **65**, 117 (1944).

[8] V. L. Ginzburg, Sov. Phys. Sol. State **2**, 1824 (1960).

[9] K. G. Wilson, Phys. Rev. B **4**, 3174 (1971).

[10] K. G. Wilson, Phys. Rev B **4**, 3184 (1971).

[11] F. J. Wegner and A. Houghton, Phys. Rev. A **8**, 401 (1973).

[12] C. Wetterich, Phys. Lett. B **301**, 90 (1993).

[13] T. R. Morris, Int. J. Mod. Phys. A **9**, 2411 (1994).

[14] F. Schütz and P. Kopietz, J. Phys. A **39**, 8205 (2006).

[15] J. Goldstone, Nuovo Cim. **19**, 154 (1961).

[16] N. M. Hugenholtz and D. Pines, Phys. Rev. **116**, 489 (1959).

[17] A. A. Nepomnyashchy and Yu. A. Nepomnyashchy, JETP Lett. **21**, 1 (1975).

[18] P. Kopietz, *Theorie der Renormierungsgruppe (in German)*, lectures script, Frankfurt, (2006).

[19] P. Kopietz, L. Bartosch, and F. Schütz, *Lectures on the Renormalization Group*, to appear at Springer, Berlin, (2009).

[20] J. W. Negele and H. Orlando, *Quantum many particle systems*, Addison-Wesley, Redwood City, (1988).

[21] J. Zinn-Justin, *Quantum field theory and critical phenomena (4th edition)*, Claredon Press, Oxford, UK, (2002).

[22] V. N. Popov, *Functional integrals in quantum field theory and statistical physics*, Reidel Publishing Company, Dorbrecht, (1983).

[23] K.G. Wilson, Phys. Rev. Lett. **28**, 548 (1972).

[24] K. G. Wilson and M. E. Fisher, Phys. Rev. Lett. **28**, 240 (1972).

[25] K. G. Wilson and J. Kogut, Phys. Rep. **12**, 75 (1974).

[26] S.-K. Ma, Rev. Mod. Phys. **45**, 589 (1973).

[27] S.-K. Ma, *Modern theory of critical phenomena*, Westview Press, Cumnor Hill, (1976).

[28] N. Goldenfeld, *Lectures on phase transitions and the renormalization group*, Addison-Wesley, Redwood City, (1992).

[29] J. Cardy, *Scaling and renormalization in the statistical physics*, Cambridge University Press, Cambridge, UK, (1996).

[30] D. J. Amit, *Field theory, the renormalization group, and critical phenomena*, World Scientific, Singapore, (1984).

[31] P. M. Chaikin and T. C. Lubensky, *Pinciples of condensed matter physics*, Cambridge University Press, Cambridge, UK, (1995).

[32] J. J. Binney, N. J. Dowrick, A. J. Fisher, and M. E. J. Newman, *The theory of critical phenomena*, Claredon Press, Oxford, UK, (1992).

[33] F. J. Wegner, Phys. Rev. B **5**, 4529 (1972).

[34] F. J. Wegner, Phys. Rev. B **6**, 1891 (1972).

[35] M. E. Fisher, Rev. Mod. Phys. **70**, 653 (1998).

[36] B. Delamotte, *Preprint* cond-mat/0702365 (2007).

[37] K. G. Wilson, Rev. Mod. Phys. **47**, 773 (1975).

[38] J. Berges, N. Tetradis, and C. Wetterich, Phys. Rep. **363**, 223 (2002).

[39] C. Bagnuls and C. Bervillier, Phys. Rep. **348**, 91 (2001).

[40] F. Schütz, L. Bartosch, and P. Kopietz, Phys. Rev. B **72**, 035107 (2005).

[41] D. F. Litim, Phys. Rev. D **64**, 105007 (2001).

[42] S. Ledowski, N. Hasselmann, and P. Kopietz, Phys. Rev. A **69**, 061601(R) (2004)

[43] N. Hasselmann, S. Ledowski, and P. Kopietz, Phys. Rev. A **70**, 063621 (2004).

[44] A. Sinner, N. Hasselmann, and P. Kopietz, J. Phys.: Cond. Mat. **20**, 075208 (2008).

[45] N. Hasselmann, A. Sinner and P. Kopietz, Phys. Rev. E **76**, 040101(R) (2007).

[46] A. Sinner, N. Hasselmann, and P. Kopietz, in *Path Integrals - New Trends and Perspectives*, ed. by W. Janke and A. Pelster, World Scientific, Singapore, (2008).

[47] E. Ising, Z. Phys. **31**, 253 (1925).

[48] K. Huang, *Statistical Mechanics*, Willey, New York, (1987).

[49] C. N. Yang, Phys. Rev. **85**, 809 (1952).

[50] A. B. Zamalodchikov, Int. J. Mod. Phys. A **4**, 4235 (1989).

[51] K. I. Aoki, K. Morikawa, W. Souma, J. L. Sumi, and H. Terao, Prog. Theor. Phys. **99**, 451 (1998).

[52] J.-P. Blaizot, M. Méndez-Galain, and N. Wschebor, Phys. Rev. E **74**, 051116 (2006).

[53] J.-P. Blaizot, M. Méndez-Galain, and N. Wschebor, Phys. Rev. E **74**, 051117 (2006).

[54] J.-P. Blaizot, M. Méndez-Galain, and N. Wschebor, Phys. Lett. B **632**, 571 (2006).

[55] J.-P. Blaizot, M. Méndez-Galain, and N. Wschebor, Eur. Phys. J. B **58**, 297 (2007).

[56] D. Guerra, R. Méndez-Galain, and N. Wschebor, Eur. Phys. J. B **59**, 357 (2007).

[57] H. K. Khalil, *Nonlinear Systems (3rd Edition)*, Prentice Hall, New Jersey, (2002).

[58] M. Vidyasagar, *Nonlinear Systems Analysis*, Prentice Hall, New Jersey, (1993).

[59] D. J. Amit, J. Phys. C **7**, 3369 (1974).

[60] A. Pelissetto and E. Vicari, Phys. Rep. **368**, 549 (2002).

[61] G. Baym, J.-P. Blaizot and J. Zinn-Justin, Europhys. Lett. **49**, 150 (2000).

[62] L. Canet, B. Delamotte, D. Mouhanna, and J. Vidal, Phys. Rev. D **67**, 065004 (2003).

[63] N. Dupuis and K. Sengupta, *Preprint* arXiv:0806.4257 (2008).

[64] C. Wetterich, Mod. Phys. Lett. A **14**, 2573 (1996).

[65] T. Busche, L. Bartosch, and P. Kopietz, J. Phys.: Cond. Mat. **14**, 8513 (2002).

[66] G. Baym, J.-P. Blaizot, M. Holzmann, F. Laloe and D. Vautherin, Eur. Phys. J. B **24**, 107 (2001).

[67] B. Kastening, Phys. Rev. A **68**, 061601(R) (2003).

[68] B. Kastening, Phys. Rev. A **69**, 043613 (2004).

[69] B. Delamotte B, D. Mouhanna, and M. Tissier, Phys. Rev. B **69**, 134413 (2004).

[70] A. Sinner, N. Hasselmann, and P. Kopietz, *Proceedings of the 25th International Conference on Low Temperature Physics*, Journal of Physics: Conference Series **150**, 032097 (2009).

[71] A. Sinner, N. Hasselmann, and P. Kopietz, Phys. Rev. Lett. **102**, 120601 (2009).

[72] L. D. Landau, J. Phys. (USSR) **5**, 71 (1941).

[73] L. D. Landau, J. Phys. (USSR) **11**, 91 (1947).

[74] R. P. Feynman, Phys. Rev. **94**, 262 (1954).

[75] R. P. Feynman and M. Cohen, Phys. Rev. **102**, 1189 (1956).

[76] A. Griffin, *Bose-Einstein Condensation in Atomic Gases*, ed. by M. Inguscio, S. Stringari, and C. Wieman, Italian Physical Society, Roma, (1999). Also in *Preprint* cond-mat/9901123.

[77] V. A. Zagrebnov and J.-B. Bru, Phys. Rep. **350**, 291 (2001).

[78] V. I. Yukalov, Laser Phys. **16**, 511 (2006).

[79] S. T. Beliaev, JETP **7**, 289 (1958).

[80] S. T. Beliaev, JETP **7**, 299 (1958).

[81] A. A. Abrikosov, L. P. Gorkov, and I. E. Dzyaloshinski, *Methods of quantum field theory in statistical physics*, Prentice Hall, New Jersey, (1963).

[82] A. L. Fetter and J. D. Walecka, *Quantum theory of many-particle systems*, McGraw-Hill, New York, (1971).

[83] L. P. Pitaevskii and E. M. Lifschitz, *Course on Theoretical Physics: Statistical Physics Pt. 2, V 9*, Butterworth-Heinemann, Oxford, UK, (1981).

[84] P. Nozières and D. Pines, *The Theory of Quantum Liquids, Vol. 2*, Addison-Wesley, Redwood City, (1990).

[85] H. Shi and A. Griffin, Phys. Rev. **304**, 1 (1998).

[86] J. Gavoret and P. Nozières, Ann. Phys. **28**, 349 (1964).

[87] Yu. A. Nepomnyashchy and A. A. Nepomnyashchy, JETP **48**, 493 (1978).

[88] Yu. A. Nepomnyashchy, JETP **58**, 722 (1983).

[89] C. Castellani, C. Di Castro, F. Pistolesi, and G. C. Strinati, Phys. Rev. Lett. **78**, 1612 (1997).

[90] F. Pistolesi, C. Castellani, C. Di Castro, and G. C. Strinati, Phys. Rev. B **69**, 024513 (2004).

[91] K. B. Davis, M.-O. Mewes, M. R. Andrews, N. J. van Druten, D. S. Durfee, D. M. Kurn, and W. Ketterle, Phys. Rev. Lett. **75**, 3969 (1995).

[92] J. Steinhauer, R. Ozeri, N. Katz, amd N. Davidson, Phys. Rev. Lett. **88**, 120407 (2002).

[93] S. B. Papp, J. M. Pino, R. J. Wild, S. Ronen, C. E. Wieman, D. S. Jin, and E. A. Cornell, Phys. Rev. Lett. **101**, 135301 (2008).

[94] A. Griffin, *Excitations in a Bose-condensed liquid*, Cambridge University Press, Cambridge, UK, (1993).

[95] C. Wetterich, Phys. Rev. B **77**, 064504 (2008).

[96] S. Floerchinger and C. Wetterich, Phys. Rev. A **77**, 053603 (2008).

[97] S. Floerchinger and C. Wetterich, Phys.Rev. A **79**, 013601 (2009).

[98] N. Dupuis and K. Sengupta, Europhys. Lett. **80**, 50007 (2007).

[99] N. Dupuis, *Preprint*, arXiv:0901.4631 (2009).

[100] H. J. Vidberg and J. W. Serene, J. Low Temp. Phys. **29**, 179 (1977).

[101] J. E. Gubernatis, M. Jarrell, R. N. Silver, and D. S. Sivia, Phys. Rev. B **44**, 6011 (1991);

[102] A. Kamenev, *Preprint*, cond-mat/0412296 (2004).

[103] J. O. Andersen, *Preprint* cond-mat/0209243, (2002).

[104] M. Schick, Phys. Rev. A **3**, 1067 (1971).

[105] A. Kreisel, F. Sauli, N. Hasselmann, and P. Kopietz, Phys. Rev. B **78**, 035127 (2008).

[106] M.-C. Chung and A. B. Bhattacherjee, *Preprint*, arXiv:0809.3632 (2008).

[107] D. S. Fisher and P. C. Hohenberg, Phys. Rev. B **37**, 10 (1988).

[108] A. Kreisel, N. Hasselmann, and P. Kopietz, Phys. Rev. Lett. **98**, 067203 (2007).

[109] W. V. Liu, Phys. Rev. Lett. **79**, 4056 (1997).

[110] W. H. Press, S. A. Teukolsky, W. T. Vetterling, and B. P. Flannary, *Numerical Recipes in Fortran 77*, Cambridge Univercity Press, Cambridge, UK, (2003).

Veröffentlichungen

1. Andreas Sinner, Florian Schütz, and Peter Kopietz, *Landau function for noninteracting bosons*, Phys. Rev. A **74**, 023608 (2006).

2. Nils Hasselmann, Andreas Sinner, and Peter Kopietz, *Two parameter scaling of correlation function near continuous phase transitions*, Phys. Rev. E **76**, 040101(R) (2007).

3. Andreas Sinner, Nils Hasselmann, and Peter Kopietz, *Functional renormalization group in the broken symmetry phase: momentum dependence and two-parameter scaling of the self-energy*, J. Phys.: Condens. Matter **20**, 075208 (2008).

4. Andreas Sinner, Nils Hasselmann, and Peter Kopietz, *Functional renormalization group in the broken symmetry phase*, Proceedings of the 9th International Conference *Path Integrals - New Trends and Perspectives*, edited by W. Janke and A. Pelster, World Scientific, Singapour, (2008).

5. Andreas Sinner, Nils Hasselmann, and Peter Kopietz, *Functional renormalization group approach to the two dimensional Bose gas*, Proceedings of the 25th International Conference on Low Temperature Physics, Journal of Physics: Conference Series **150**, 032097 (2009).

6. Andreas Sinner, Nils Hasselmann, and Peter Kopietz, *Spectral function and quasiparticle damping of interacting bosons in two dimensions*, Phys. Rev. Lett. **102**, 120601 (2009).

Tagungen

- 9th International Conference *Path Integrals - New Trends and Perspectives*, September 2007, Dresden, Germany. Teilnahme mit dem Poster: *Functional renormalization group in the broken symmetry phase.*

- DPG-Frühjahrstagung, Februar 2008, Berlin, Germany. Teilnahme mit dem Vortrag: *Functional Renormalization Group analysis of the interacting Bose gas in the symmetry broken phase.*

Lebenslauf

Allgemeine Informationen

Name	Andreas Sinner
Geburtsdatum	07. Oktober 1974
Geburtsort	Kuibyschew (UdSSR), heutiges Samara
Familienstand	ledig
Nationalität	deutsch / russisch

Ausbildung und beruflicher Werdegang

Nov. 2005 - Mär. 2009	Doktorand am Institut für Theoretische Physik, Goethe-Universität Frankfurt. Betreuer: Prof. Dr. Peter Kopietz. Promotion am 6. Juli 2009.
Okt. 2001 - Mär. 2005	Studium der Physik an der TU Braunschweig. Abschluss: Diplom-Physiker. Gesamtnote: sehr gut. Thema der Diplomarbeit: Squashed Entanglement für symmetrische Zustände. Betreuer: Prof. Dr. R. F. Werner.
Jul. 2000 - Jul. 2001	Gastwissenschaftler am Institut für Elektrische Maschinen, Antriebe und Bahnen, Technische Universität Braunschweig.
Februar 2000	Einwanderung nach Deutschland.
Sep. 1996 - Dez. 1999	Assistent am Lehrstuhl für Allgemeine Elektrotechnik und Elektroantriebe, Staatsuniversität für Technologie Kasan, Russland. DAAD-Stipendium WS97-SS98. Kandidatur in Elektrotechnik am 8. Juni 1999.
Sep. 1991 - Jun. 1996	Studium der Elektrotechnik an der Staatsuniversität für Technologie Kasan, Russland. Abschluss: Diplom-Ingenieur. Gesamtnote: mit Auszeichnung.
Juni 1991	Reifezeugnis, Mittelschule Nr. 110, Kasan, Russland. Gesamtnote: gut.

Danksagung

Es ist jetzt an der Zeit all denen zu danken, die diese Arbeit maßgeblich beeinflusst haben.

Mein tiefster Dank gehört meinem Lehrer Herrn Prof. Dr. Peter Kopietz. Ohne jeden Zweifel kann ich behaupten, dass ich es nie mit einer Promotion soweit gebracht hätte, hätte er mich nicht seinerzeit in seine Arbeitsgruppe aufgenommen, wo mir selbst elementare Begriffe der Feskörperphysik, geschweige denn der funktionalen Renormierungsgruppe ein Geheimnis waren. Seine Bereitschaft Leuten wie mich eine Chance zu geben, habe ich immer bewundert. Als Theoretiker verfügt er über eine glänzende Rechentechnik, von der ich nicht einmal träumen kann, die mich allerdings immer motivierte. Für diese Motivation, sowie für die Möglichkeit von seinen umfangreichen und vielseitigen Kenntnissen direkt wie indirekt profitieren zu dürfen, möchte ich mich noch einmal aufs Herzlichste bedanken.

Herrn Prof. Dr. Nils Hasselmann danke ich für die fast dreijährige fruchtbare Zusammenarbeit. Seine intuitive und auf mich irgendwie geheimnisvoll wirkende Art Physik zu machen, inspirierte mich zutiefst die ganze Zeit über. Manchmal reichte diese Inspiration auch bis zum Verzweifeln, gerade wenn er mit einem flüchtigen Satz all meine mühsam erarbeiteten und scheinbar unerschüttert festen Argumente dementierte.

Herrn Prof. Dr. Walter Hoffstetter möchte ich für die Übernahme der Begutachtung dieser Arbeit danken, sowie für die vielen anregenden Diskussionen über die Physik während des gemeinsamen Seminars. Von seiner Art eine Prüfung zu gestalten bin ich sehr beeindruckt.

Einen besonderen Dank möchte ich Herrn Andreas Kreisel für die jahrelange Betreuung und Beratung in allen Fragen betreffend Linux und Computer im breiteren Sinne, sowie für seine Hilfsbereitschaft in allen Bereichen des universitären Lebens.

Herrn Dr. Lorentz Bartosch danke ich für seine stets hilfsbereite und freundliche Haltung.

Für ihre Freundschaft, sowie die Möglichkeit aus ihrem Wissen und Erfahrungen zu schöpfen möchte ich mich bei Herrn Dr. Miodrag Kulic und Herrn Dr. Markus Kasner bedanken.

Meinem Büropartner Herrn Dr. Jose J. Ramos Cardenias danke ich für die nette Arbeitsatmosphäre, die in unserem Büro herrschte und für die mehreren aufschlussreichen Erzählungen über sein Heimatland Mexico. Darauf knüpfend danke ich Herrn Dr. Hermann Freire für seine Freundschaft.

Herrn Christopher Eichler danke ich für seine sehr mitreißende und motivierende Art bis zum Umfallen zu arbeiten, wie auch für die schöne Zeit in Brasilia wo wir gemeinsam ein Zimmer bewohnten.

Meinen Eltern, Herrn Prof. Dr. Lew Sinner und Frau Soja Sinner, sowie meiner Schwester Frau Tatjana Babak und meiner Nichte Emilia danke ich für die Unterstützung und Rückenhalt, die ich über all die Jahre genoss. Niemals hätte ich es geschafft, wäre nicht die Wärme des Elternhauses immer für mich da.

Herrn Dr. Harald O. Jeschke danke ich für die freundliche Genehmigung seine Routine zur Implementierung des approximativen Padé-Algorithmus zu benutzen.

Frau Dr. Charlotte Boecken danke ich vom Herzen für ihre Teilnahme an meinem Leben, sowie für nicht zu unterschätzende finanzielle Unterstützung.

Für zahlreiche lustigen sowie aufmunternden Gesprächen bei der einen oder anderen Zigarette über die Musik, den Fußball, worüber auch immer, bedanke ich mich bei Herrn Joe Laperal-Gomez.

Schließlich danke ich allen Mitgliedern des Arbeitskreises um Prof. Peter Kopietz, namentlich: Florian Schütz, Francesca Sauli, Charlotte Dinges, Peyman Pirooznia, Nils Lerch, Thomas Kloss für die nette Arbeitsatmosphäre in der Arbeitsgruppe. Derselbe Dank gebührt ebenfalls allen Mitgliedern des Instituts für Theoretische Physik.